University of Nottingham

UK | CHINA | MALAYSIA

Transcriptome Alterations Following Loss of PIP5K1α Function in Prostate Cancer Cells

Ryan D Morris, BSc, MSc

Thesis submitted to the University of Nottingham for the degree of Doctor of Philosophy

Abstract

The human genome encodes three membrane-targeted phosphatidylinositol-4-phosphate 5-kinases (PIP5K1α, PIP5K1β and PIP5K1γ) that generate the signalling molecule phosphatidylinositol 4,5-bisphosphate [$PI(4,5)P_2$]. These lipid kinases target the 5^{th} position of the inositol ring structure located on phosphatidylinositol 4-phosphate [PI(4)P]. $PI(4,5)P_2$ acts as a key second messenger in cells, involved in regulation of many cellular processes, a major aspect of which is through the activation of PI3K/AKT and PKC signalling pathways. Dysregulation of these pathways through gene alterations is commonly associated with oncogenesis, resulting in sustained cell proliferation, aberrant cell migration, evasion of apoptosis and increased angiogenic potential. In the context of prostate cancer, inactivation of the tumour suppressor gene PTEN occurs in ~50% of advanced malignancies, with this a main driver in oncogenesis. More recently, it has been identified that PIP5K1A gene amplifications are found in ~10% of advanced prostate cancers, however the role that this kinase exerts in prostate tumorigenesis has been less studied.

This research project has set out to explore whether altered expression of PIP5K1α may be associated with transcriptome changes in cancer cells, using human LNCaP C4-2 cells as a model for castration-resistant prostate cancer. Two previously generated CRISPR edited cell lines were used in this work (ΔN and KO) which have abrogated or severely reduced PIP5K1α protein expression. Targeting of Exon 1 in ΔN LNCaP C4-2 cells impaired PIP5K1α protein expression, with translation initiation pursuing from downstream AUG codons. In KO C4-2 cells, both Exons 1 and 6 in PIP5K1A were targeted through CRISPR editing, which heavily impacted protein expression. Exon 1 and Exon 6 encode the N terminus and part of the PIP5K1A kinase domain respectively.

RNA-Sequencing the CRISPR clones relative to WT LNCaP C4-2 revealed significant transcriptome alterations. Approximately 2 fold more differentially expressed genes were observed in ΔN-WT in comparison to KO-WT. However enrichment analysis revealed that both CRISPR clones were associated with genes upregulated with androgen signalling and cell cycle progression. In regards to the former,upon rescuing PIP5K1A depleted cells with a PIP5K1α-mVenus-N1 construct, this negatively regulated the expression of KLK3, a classical androgen regulated gene. This suggests that the expression of PIP5K1α is needed to coordinate the expression of KLK3.

With enrichment analysis suggesting that both cell lines undergo increased expression of genes implicated with cell cycle progression, it was interesting to observe that both ΔN and KO C4-2 cells showed defects in cell proliferation. Through BrdU incorporation assays it was observed that both clones exhibited G1 arrest, with this coupled with increased formation of γ-H2AX foci, indicative of double stranded DNA breaks. Furthermore, both ΔN and KO LNCaP C4-2 cells showed increased p21 levels, a protein which triggers cell cycle arrest. Collectively, this suggests that PIP5K1α is necessary in orchestrating progression through the cell cycle.

Another unexpected observation was that activation of AKT phosphorylation was increased in the ΔN clone compared to WT or KO, despite reduced expression of PIP5K1α. The levels of AKT activating phosphoinositides were not elevated in this clone, with this assayed using fluorescent biosensors. Upon further scrutinising the DEGs from ΔN LNCaP C4-2 cells, a loss of PIK3R1 expression was observed. Subsequently the role of PIK3R1 in regulating AKT phosphorylation in ΔN C4-2 cells underwent preliminary exploration in this work. In this, ΔN cells were rescued with a fluorescent PIK3R1 construct with phospho-AKT levels assayed by flow cytometry.

These assays suggested that rescuing PIK3R1 expression in clone ΔN may reduce levels of phosphorylated AKT, albeit with these results being statistically insignificant. Overall, the elevations in AKT phosphorylation in ΔN cells may be linked to loss of PIP5K1α expression, implying that this kinase may be influencing PI3K/AKT signalling at a transcriptional level.

Declaration

Except where cited in text, I declare this PhD thesis as my own work. This is research which was conducted by me in the Gene Regulation and RNA Biology Laboratories, School of Pharmacy, University of Nottingham, United Kingdom.

Acknowledgments

I arrived at the University of Nottingham with a deep interest into signal transduction pathways; by joining Professor David Heery's lab, this proved to be the catalyst for harnessing this enthusiasm. I will be forever grateful for the opportunities David has provided me through my time in his laboratory, and his willingness to discuss my results. Often, I would arrive unannounced to his office with some preliminary findings and David would always find time to talk about these data. In the position as my primary supervisor David has taught me so many valuable lessons regarding the rigor which is needed to conduct robust research. These lessons will stay with me for eternity. I would also like to thank my secondary supervisor, Dr Hilary Collins for all the help, training, and support throughout my PhD project. I certainly could not have done any of my confocal microscopy work without your guidance and tutelage, for which I am extremely grateful for.

With Professor David Heery's lab being based in the Gene Regulation and RNA Biology Laboratories (GRRB) this provided the backdrop to meet so many wonderful people. When I started my PhD, the friendless and helpfulness I was greeted to by latter year PhD students (Hannah, Poppy, AJ, Aalam, Kat , Declan and Nicole) was never unnoticed. Thank you for making me so welcome. I joined the GRRB labs at the same time as many new PhD students: Athena, Max, Arnelle, Steven, Michael, Chloe and Paulyna. This naturally developed a strong sense of community and an indelible spirit. I will be forever grateful for the technical support and moral support you have given me throughout the last several years. Additionally, the GRRB lab has been fortunate enough to be joined by experienced postdocs: Angie, Shruti and Sasha. You have all helped me on numerous occasions with technical expertise, I greatly appreciate the insights you have shared with me. A significant proportion of the work conducted in the GRRB laboratories is funded by the Biotechnology and Biological Sciences Research Council (BBSRC) and I am no exception. As such I would like to acknowledge the BBSRC for the financial support throughout my time of study.

I would also like to acknowledge the past and present Heery group members throughout my time: Mitchell, Ruby, Jonas, Chris ,Yi and Luc. Thank you for the humour, guidance and support throughout my PhD studies, it will never be forgotten. Chris, I am indebted to you for the tuition and patience you provided me over the last several years. You taught how to clone and to appreciate molecular biology to its truest form. Ruby, you were always on hand to help me with optimising experiments, most notably western blots! Luc, thank you for the kind gift you gave me expressing the gratitude for my teachings. I have been so lucky to receive such great tutelage, I am glad I have been able to reciprocate this for you.

Finally, to my Mother and Father, thank you for everything. You motivate me to become the best version of myself and have provided me immense amounts of motivation throughout my time as a PhD student. I cannot thank you enough for support you have given me, I love you both and hope to make you as proud as possible.

Contents Page

List of Figures

List of Tables

List of Abbreviations

17β-HSD6	17β-hydroxysteroid dehydrogenase 6
4E-BP1	Eukaryotic translation initiation factor 4E-binding protein 1
5-AR	5α-reductase
ABD	Adaptor binding domain
ADT	Androgen Deprivation Therapy
AF-1/2	Activation Function-1/2
AGC	Protein kinase A, Protein Kinase G, and Protein Kinase C Related
AKT	RAC-alpha serine/threonine-protein kinase
AP-1	Activator Protein 1
APS	Ammonium Persulphate
AR	Androgen Receptor
ARE	Androgen Response Elements
ARF6	ADP Ribosylation Factor 6
AR-V7	Androgen Receptor Splice Variant 7
ATM	Ataxia-telangiectasia mutated
ATR	Ataxia telangiectasia and Rad3-related
BP	Base Pair
BH	Breakpoint cluster region-homology
BrdU	Bromodeoxyuridine
BTG2	B-cell translocation gene 2
BSA	Bovine serum albumin
BTK	Burtons tyrosine kinase
CAMK	Ca^{2+}/Calmodulin-Dependent Kinase

CAMK2N1	Calcium/Calmodulin Dependent Protein Kinase II Inhibitor
CAMKK2	Calcium/calmodulin-dependent protein kinase kinase 2
cAMP	Cyclic adenosine monophosphate
Cas9n	Cas9 nickase
CBP	CREB Binding Protein
CD26	Cluster of Differentiation 26
Cdc42	Cell division control protein 42
CDK	Cyclin-dependent kinase
CDKN1A	Cyclin dependent kinase inhibitor 1A
CK1	Casein Kinase 1
CMGC	Cdk, MAPK, GSK, Cdk-like related
CMV	Cytomegalovirus
Complete Medium	10% FBS (v/v) , 1% Sodium Pyruvate (v/v) , 1%(v/v) , Penicillin/Streptomycin and 1% L-glutamine in RPMI-1640 medium
CPM	Counts per million
CRISPR	Clustered regularly interspaced short palindromic repeats
CRKL	CRK Like Proto-Oncogene, Adaptor Protein
CTD	c-terminal regulatory domain
Ct	Cycle Threshold
DAG	Diacylglycerol
ddH_2O	Double distilled water
DEGs	Differentially expressed genes
DEPTOR protein	DEP domain-containing mTOR-interacting
DESeq2	Differential gene expression analysis based on the negative binomial distribution.

DH	Dbl homology
DHT	Dihydrotestosterone
diH_2O	Deionised water
DMSO	Dimethyl sulfoxide
DNA-PK	DNA-dependent protein kinase
DYRK1A	Dual specificity tyrosine phosphorylation regulated kinase 1A
E.coli	*Escherichia coli*
EGFR	Epidermal Growth Factor Receptor
eIF4A	Eukaryotic initiation factor-4A
eIF4B	Eukaryotic translation initiation factor 4B
eIF4E	Eukaryotic translation initiation factor 4E
EMT	Epithelial-mesenchymal transition
ENTH	Epsin N-terminal homology
ER	Endoplasmic reticulum
ERK1/2	Extracellular signal-regulated kinases-1/2
FACS	Fluorescence-activated Cell Sorting
FAK	Focal Adhesion Kinase
FBS	Fetal bovine serum
FDR	False Discovery Rate
FOXO	Forkhead Transcription Factors
FPKM	Fragments per kilobase of exon per million mapped fragments
FUT	Fucosyltransferase
FYVE	Fab-1, YGL023, Vps27, and EEA1
Gab2	GRB2-associated-binding protein 2
Grp1	general receptor for phosphoinositides isoform 1

GRTH	Gonadotropin-Regulated Testicular RNA Helicase
GSK3β	Glycogen synthase kinase-3β
H3K9me3	Histone H3 Lysine 9 Trimethylation
HA	Hemagglutinin
HCl	Hydrochloric Acid
HGF	Hepatocyte Growth Factor
HM	Hydrophobic Motif
HO-1	Haem oxygenase-1
HP1-α	Heterochromatin Protein 1α
HSPs	Heat shock proteins
IDEP	Integrated web application for differential expression and pathway analysis
IGF-1	Insulin-like growth factor 1
INPP4s	Inositol polyphosphate-4-phosphatases
INPP5s	Inositol polyphosphate-5-phosphatases
IP_3	Inositol triphosphate
JNK	c-Jun N-terminal kinase
KLK3	Kallikrein related peptidase 3
KO	LNCaP C4-2 PIP5K1A-KO
KRAS	Kirsten rat sarcoma viral oncogene homolog
LB	Luria-Bertani
LBD	Ligand Binding Domain
LH	Luteinizing Hormone
limma	Linear Models for Microarray Data
Log2FC	Log2 Fold Change
LPA	Lysophosphatidic acid
MCS	Multiple Cloning Site

MIT	Massachusetts Institute of Technology
mLST8	Mammalian target of rapamycin complex subunit
MRN	MRE11-RAD50-NBS1
MsigDB	Molecular Signatures Database
mSIN1	Mammalian stress-activated protein kinase-interacting protein
MTMs	Myotubularins
mTOR	Mammalian target of rapamycin
mTORC1/2	Mammalian target of rapamycin complexes 1 and 2
MTT	3-(4,5-Dimethylthiazol-2-yl)-2,5-Diphenyltetrazolium Bromide)
Myc	MYC proto-oncogene, bHLH transcription factor
NTD	N terminal domain
NaCl	Sodium Chloride
NaOH	Sodium Hydroxide
NCBI	National Centre for Biotechnology Information
NEB	New England Biolabs
ORM1	Orosomucoid 1
p300	Histone acetyltransferase p300
PA	Phosphatidic acid
PAK6	P21-Activated Kinase 6
PBD	p110γ binding domain
PBS	Phosphate-buffered saline
PBST	Phosphate buffered saline with Tween
PCA	Principle component analysis

PCR	Polymerase Chain Reaction
PDCD4	Programmed cell death 4
PDGF	Platelet derived growth factor
PDK1	Phosphoinositide-dependent kinase-1
PEG10	Paternally Expressed 10
PFA	Paraformaldehyde
PH	Pleckstrin Homology
PI	Phosphatidylinositol
PI(3)P	Phosphatidylinositol 3-phosphate
$PI(3,4)P_2$	Phosphatidylinositol (3,4)-bisphosphate
$PI(3,4,5)P_3$	Phosphatidylinositol (3,4,5)-trisphosphate
$PI(3,5)P_2$	Phosphatidylinositol (3,5)-bisphosphate
PI(4)P	Phosphatidylinositol 4-phosphate
$PI(4,5)P_2$	Phosphatidylinositol 4,5-bisphosphate
PI(5)P	Phosphatidylinositol 5-phosphate
PIK3C	Phosphatidylinositol-4,5-Bisphosphate 3-Kinase catalytic subunit
PIK3R	Phosphatidylinositol 3-kinase regulatory subunit
PIKfyve	Type III phosphatidylinositol-4-phosphate 5-kinase
PIP	Phosphatidylinositol Phosphate
PIP4Ks	Type II phosphatidylinositol-5-phosphate 4-kinases
PIP5Ks	Type I phosphatidylinositol-4-phosphate 5-kinases
PKA	Protein Kinase A
PKC	Protein Kinase C
PKIB	cAMP-Dependent Protein Kinase Inhibitor Beta

PLA2G2A	Phospholipase A2 Group IIA
PLC	Phospholipase C
PMA	Phorbol 12-myristate 13-acetate
PP1	Protein Phosphatase 1
PP2A	Protein Phosphatase 2A
PRAS40	Proline-rich AKT substrate of 40 kDa
pRB	Retinoblastoma protein
PSA	Prostate Specific Antigen
PTEN	Phosphatase and tensin homolog
PTM	Post translational modifications
PX	Phox Homology
Rac1	Rac Family Small GTPase 1
Raptor	Regulatory-associated protein of mTOR
RAS	Rat sarcoma virus
RBD	Ras binding domain
RBM10	RNA Binding Motif Protein 10
RGC	Receptor Guanylyl Cyclase
RhoA	Ras homolog family member A
Rictor	Rapamycin-insensitive companion of mammalian target of rapamycin
RIPA	Radioimmunoprecipitation assay
RNAi	RNA interference
RNA-Seq	RNA-Sequencing
RPMI	Roswell Park Memorial Institute
RTK	Receptor tyrosine kinase
RT-qPCR	Reverse transcription quantitative polymerase chain reaction
S6K1	Ribosomal protein S6 kinase β-1

SDF1α	Stromal Cell-Derived Factor 1α
SDS	Sodium Dodecyl Sulphate
SDS-PAGE	SDS Polyacrylamide
SGK	Serum and glucocorticoid-inducible kinase
SH2	Central Src Homology 2
SH3	Central Src Homology 3
siRNA	small interfering RNAs
SLC30A7	Solute Carrier Family 30 Member 7
SPINK1	serine protease inhibitor Kazal-type 1
SOB	Super Optimal Broth
SOC	Super Optimal broth with Catabolite repression
SRA	Short Read Archive
Src	Proto-oncogene tyrosine-protein kinase Src
SRC-1/2/3	Steroid Receptor Coactivators-1/2/3
Star-PAP	Nuclear speckle targeted PIPKIα regulated-poly(A) polymerase
STAT	Signal transducer and activator of transcription
STE	STE20, STE11 and STE7 related
SUMO	Small ubiquitin-related modifier
SWI/SNF	Switching defective/Sucrose nonfermenting
SXN	Sorting Nexins
TAPP1	Pleckstrin Homology Domain Containing A1
TBE	Tris/Borate/EDTA
TBS	Tris buffered saline
TBST	Tris buffered saline with Tween
Tel2	Telomere length regulation protein TEL2 homolog
TEMED	Tetramethylethylenediamine

TGS	Tris-Glycine-SDS
TIF2	Transcriptional Intermediary Factor 2
TK	Tyrosine Kinase
TKL	Tyrosine Kinase-Like
TM	Turn Motif
TSC1/2	Tuberous sclerosis proteins 1 and 2
Tti1	ELO2 Interacting Protein 1
TWIST1	Twist Family BHLH Transcription Factor 1
UGT2B	UDP-glucuronosyltransferase
VEGF	Vascular endothelial growth factor
VEGFR	Vascular Endothelial Growth Factor Receptor
WT	Wildtype
γ-H2AX	Gamma H2A Histone Family Member X
ΔN	LNCaP C4-2 PIP5K1A-ΔN

Chapter 1
Introduction

1.1. The Structure and Function of the Prostate

The prostate is the male reproductive gland responsible for the production and storage of seminal fluid and consists of two main compartments. The stromal compartment maintains the appropriate microenvironment for the prostate epithelium, which is responsible for prostatic secretions *(Verze, et al., 2016).* Key constituents of prostatic fluid from the epithelium includes prostatic acid phosphatase and albumin which maintains the longevity and motility of spermatozoa *(Kumar and Majumder, 1995).* However, the secretion which is ubiquitously associated with the prostate is the prostate specific antigen (PSA), which is a member of the kallikrein-related peptidase family of serine proteases *(Hong, 2014).* The principle function of PSA is to degrade semenogelins, proteins which inhibit the motility of spermatozoa *(Young et al., 1995).*

The prostate can succumb to a range of diseases which can be benign or malignant in nature, such as prostatitis, benign prostatic hyperplasia and prostate cancer *(Verze et al., 2016).* Behind lung cancer, prostate cancer is the second most frequently diagnosed malignancy in the male population *(Rawla, 2019)* with approximately 1.5 million diagnoses per annum *(Pernar et al., 2018).* Prostate adenocarcinoma can arise from 3 distinct cell types which reside in the prostate epithelium: luminal, basal and neuroendocrine cells.

1.2. Cellular Biology of the Prostate

Luminal cells *(Figure 1.1)* mediate PSA secretions in the epithelium and require the presence of androgens for their growth and survival *(Zhang et al., 2018).* Luminal cells are the most abundant cell type in epithelium (~60%) and have been postulated to act as the major cell type for the origin of prostate cancer *(Packer et al., 2016).* The Shen laboratory demonstrate this by using lineage tracing in 6 different mice models of prostate cancer *(Wang et al., 2014b).* For example, when mice were

treated with both testosterone and 17β-estradiol for 4 months (with this inducing low grade neoplasms) this is associated with clusters of luminal cell populations relative to the rare abundance of basal cells *(Wang et al., 2014b).* Due to luminal cells dependence on androgens and their role in prostate cancer initiation, androgen deprivation therapy (ADT) is the first line therapy for prostate cancer *(Sharifi et al., 2005).*

Basal cells *(Figure 1.1)* are androgen insensitive which are situated between the basement membrane and luminal cells *(Long et al., 2005).* This cell type has been postulated to form a barrier, sequestering luminal cells away from oncogenic stresses *(Xin, 2012).* Consequently, basal cells are characterised by higher levels of Gamma H2A Histone Family Member X (γ-H2AX) relative to luminal cells which is a marker for DNA damage *(Jaamaa et al., 2010).* Indeed, the histological subtype of prostate cancer considered to be the most common is acinar type adenocarcinomas (~90% prevalence) which are characterised by a severe reductions of basal cell populations *(Stoyanova et al., 2013).* Comparatively, basal cell carcinomas are extremely rare, with a prevalence of ~0.01% *(Ninomiya et al., 2018).*

However, an additional property of basal cells is their ability to ability to undergo self-renew, proliferate and differentiate into luminal cells *(Bonkhoff, et al., 1994).* Therefore, oncogenic transformation of basal cells may initiate malignancy. *Stoyanova et al., (2013)* demonstrated this by expressing the oncogenes RAC-alpha serine/threonine-protein kinase (AKT) and MYC proto-oncogene, bHLH transcription factor (Myc) in prostate basal cells and implanting these immune deficient mice. As little as 10,000 transformed basal cells could initiate tumours which were characterised by the expression of acinar type adenocarcinoma protein markers such as cluster of differentiation 26 (CD26) and the androgen receptor (AR) *(Stoyanova et al., 2013).* Consequently, the proliferation and differentiation of basal cells into luminal cells has been suggested to act as a rate limiting step for prostate cancer initiation and progression *(Choi et al., 2012).*

The most diffuse cell type within the prostate epithelium are neuroendocrine cells *(Figure 1.1)* whose physiological function is not completely clarified. The current understanding is that neuroendocrine cells can secrete mediators such as serotonin, somatostatin and bombesin *(Szczyrba et al., 2016).* These molecules are thought to influence the proliferation and differentiation of both basal and luminal cells *(Szczyrba et al., 2016).* Like basal cells, neuroendocrine cells are androgen insensitive as they lack the expression of AR *(Krijnen et al., 1993).* Due to limited populations of neuroendocrine cells within the prostate epithelium, primary neuroendocrine tumours are rare with a prevalence of less than 1% *(Aggarwal et al., 2014).*

Interestingly when androgen responsive LNCaP prostate cancer cells are cultured in the absence of androgens, this can induce neuroendocrine differentiation. Work by *Yuan et al., (2006)* found culturing LNCaP cells with media lacking androgens resulted in the establishment of 20 subclone cell lines. These cell lines were associated with the increased expression of neuroendocrine markers such as Enolase 2 and chromogranin B, with reduced expression of AR *(Yuan et al., 2006)*. In prostate cancer patients the expression of chromogranin B is commonly elevated in advanced disease which assume a neuroendocrine-like phenotype *(Schmid et al., 1994).* Collectively, these data suggest that more advanced prostate cancer can acquire a neuroendocrine-like phenotype possibly as a means of resisting ADT.

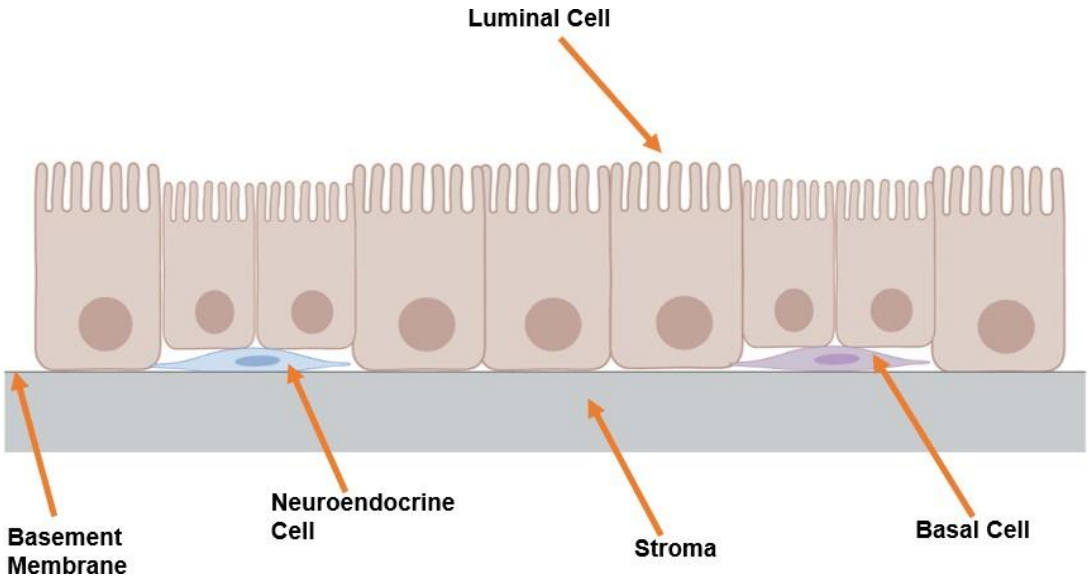

Figure 1.1. Cell types that comprise the prostate. The prostate epithelium consists of three principle cell types: luminal, basal and neuroendocrine. Luminal cells are androgen responsive and mediate PSA secretions *(Zhang et al., 2018).* Basal cells are believed to sequester luminal cells away from oncogenic stresses *(Xin, 2012).* Neuroendocrine cells secrete a spectrum of mediators which positively regulates the growth of basal and luminal cells *(Szczyrba et al., 2016).* A basement membrane separates these cell types from the stroma, which supports the cellular microenvironment. Figure adapted from *Verze et al., (2016)* and created with BioRender.com.

1.3. Signal Transduction by the AR

Androgens in the form of testosterone and dihydrotestosterone (DHT) can interact with the AR to stimulate gene transcription. The production of testosterone is stimulated by the pituitary gonadotropin luteinizing hormone (LH) which interacts with cognate receptors expressed by Leydig cells in the testes *(Oh, 2014).* LH stimulation increases cyclic adenosine monophosphate (cAMP) levels in Leydig cells, resulting in the activation of Protein Kinase A (PKA) which stimulates testosterone biosynthesis via the mobilisation of cholesterol *(Oh, 2014).* The activities of 5*α*-reductases (5-AR) are responsible for the reduction of testosterone to generate DHT. There are three 5-AR isozymes (5-AR1, 5-AR2,

5-AR3) all of which are expressed in the prostate *(Niu et al., 2014).* In comparison to testosterone, DHT is around a 10 fold more potent agonist for the AR *(Deslypere et al., 1992).*

The domain structure of AR *(Figure 1.2)* characterises it as a member of the nuclear receptor superfamily for which there are 48 members. The nuclear receptor superfamily is divided into seven subfamilies, on the basis of sequence homology and the ligands the receptors interact with *(Weikum et al., 2018).* It must be noted however that over half of the proteins comprising the nuclear receptor superfamily do not have known endogenous ligand *(Frigo et al., 2021).* The AR is part of subfamily 3 which comprises additional steroid receptors, such as oestrogen receptors, the progesterone receptor, the mineralocorticoid receptor, and the glucocorticoid receptor *(Weikum et al., 2018).*

The ligand binding domain (LBD) of the AR consists of ~250 amino acids *(Figure 1.2).* Upon ligand binding this releases AR from inhibitory heat shock proteins (HSPs) leading to dimerization and nuclear translocation *(Figure 1.3).* The DNA binding domain of AR *(Figure 1.2)* is responsible for binding to genes which present regulatory sequences in their regulatory or enhancer regions known as androgen response elements (AREs) *(Wilson., 2016).* Classically these sequences are palindromic and comprises of 15 base pairs (bps) and are arranged as two hexametric half sites (5'-AGAACA-3') separated by a 3bp spacer *(Horie-Inoue et al., 2004).* However, AREs can also exist as single half sites, but can still undergo regulation by androgens. An example of this mode of regulationis exhibited by the Gonadotropin-Regulated Testicular RNA Helicase (GRTH) gene. This gene is particularly expressed by Leydig cells and encodes an RNA helicase that is essential for spermatogenesis *(Villar etal., 2012).* GRTH contains two ARE half sites (ARE1 and ARE2), whilst ARE1 is not functional, mutagenesis of ARE2 suppressed GRTH expression after DHT treatment *(Villar et al., 2012).*

Following recruitment of AR dimers to genomic target sites additional components of the transcriptional machinery (cofactors) are recruited to modulate gene expression. Recruitment of transcriptional co-factors to nuclear receptors is mediated via LXXLL motifs which permit binding to the Activation Function-2 (AF-2) region of the C terminal ligand binding domain *(Heery et al., 1997).* Amongst the major known cofactors which harbour LXXLL motifs includes Steroid Receptor coactivators-1/2/3 (SRC-1/2/3) which recruits the histone acetyltransferase CREB binding protein (CBP) and p300 *(Sheppard et al., 2001)* to modulate gene expression. Additional LXXLL motif containing co-factors which are recruited to AR ligand binding domain include Transcriptional Intermediary Factor 2 (TIF2) *(Coulthard et al., 2003 ; Fancher et al., 2016).* TIF2 possesses a CBP interaction domain which also contributes to the recruitment of CBP/p300 to promote gene transcription *(Yin et al., 2007).* It is also suggested that TIF2 binding to AR enhances receptor stability and promotes ligand binding (*Fancher et al., 2016).*

To ensure tight regulation of gene expression, co-repressors which antagonise transcription can also be recruited to the AF-2 region via LXXLL motifs such as B-cell translocation gene 2 (BTG2). The BTG2 protein harbours an intact LXXLL motif (located between residues 92 and 96), when this motif is mutated this abrogated interaction to the AR *(Huet al., 2011).* Conversely, overexpression of wildtype BTG2 in LNCaP cells inhibited downstream PSA/KLK3 expression, highlighting the role this protein has on AR activity *(Hu et al., 2011).* Additionally the AF-2 domain can also interact with co-regulators harbouring FXXLY, FXXLF , WXXLF, FXXFF and FXXMF motifs *(He et al., 2000 ; van de Wijngaart et al., 2006).* For instance, the proteins gelsolin and P21-Activated Kinase 6 (PAK6) can interact with the LBD of AR through harbouring FXXFF and FXXMF motifs respectively (*van de Wijngaart et al., 2006).* Additionally, the N terminal domain (NTD) *(Figure 1.2)* of the AR harbours a FXXLF motif which can interact with its own LBD *(Dubbink et al., 2004).*

In summary the AF-2 domain of AR, and more broadly nuclear receptors, is responsible for mediating core transcriptional functions. Due to this, there is strong sequence conservation between nuclear receptor family members for the AF-2 domain *(Danielian et al., 1992 ; Bevan et al., 1999).* However, the NTD harbouring the AF-1 domain is poorly conserved between nuclear receptors *(Wärnmark et al., 2003)* which accounts for receptor specific functions each protein exerts. In the case of AR, the NTD is one of the largest in the nuclear receptor subfamily, with a size of spanning over 550 amino acids *(Figure 1.2)*. This NTD facilitates further protein-protein interactions and residues in this domain can also undergo posttranslational modifications (PTMs), such as phosphorylation *(a detailed overview of phosphorylation is provided in Section 1.6).*

S81 is located in the NTD and has been reported to undergo phosphorylation via members of the cyclin-dependent kinase (CDK) family: CDK1, CDK5 and CDK9 *(Koryakina et al., 2014).* Chemical inhibition of CDK1 blocks S81 phosphorylation, which results in decreased protein levels of AR, suggesting phosphorylation of this residue mediates receptor stability *(Chen et al., 2006).* Additionally *Chen et al., (2011)* demonstrated that CDK1/9 inhibition in LNCaP cells blocked expression of KLK3, implicating S81 in the regulation of downstream AR target genes.

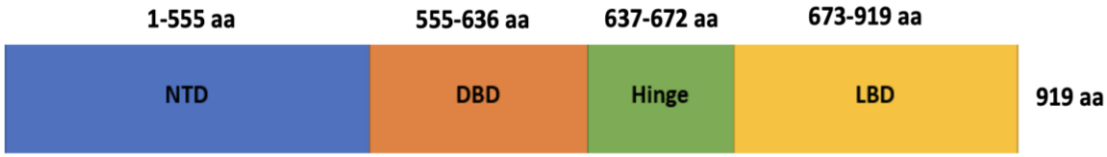

Figure 1.2. Domains of the Androgen Receptor (AR). The total length of the AR is 919 amino acids. The N terminal transactivation domain (NTD) contains the AF-1 region whereas the ligand binding domain (LBD) contains the AF-2 region *(Gioeli and Paschal, 2012).* The DNA binding domain (DBD) interacts with genes containing androgen response elements. The hinge region links together the DBD and LBD and has been implicated with regulating: DNA binding, nuclear translocation, receptor transactivation and receptor mobility *(Clinckemalie et al., 2012).* Figure adapted from *Gioeli and Paschal, (2012).*

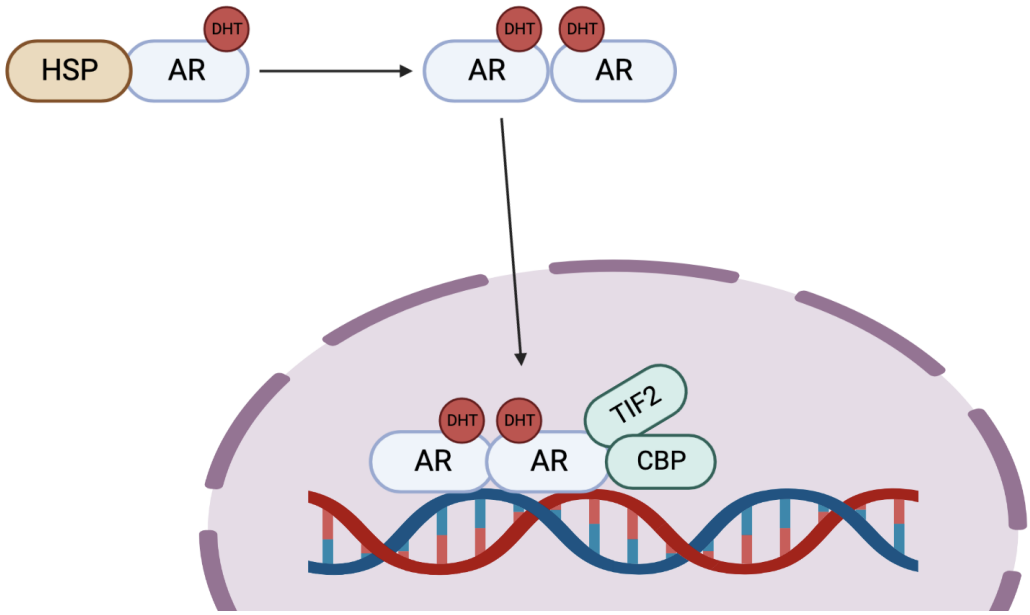

Figure 1.3. AR Signalling Schematic. Upon binding to DHT this initiates the release of AR from heat shock proteins (HSPs). This triggers receptor dimerization and translocation to the nucleus where AR can bind to genes harboring androgen response elements (ARE). Additional transcriptional co-factors such as CBP and TIF2 are recruited to AR to promote gene transcription. Figure created using BioRender.com.

1.4. The role of AR Signalling in Prostate Cancer

Stimulating AR activity in prostate cancer cells can trigger substantial transcriptome changes. For instance, *Massie et al., (2011)* showed *in vitro* that treating LNCaP cells with the synthetic androgen R1881 for 24h resulted in the differential expression of ~3300 gene transcripts. Many of the genes regulated by androgens have been implicated with cell proliferation, apoptosis, cell migration and angiogenesis *(Tang et al., 2021),* processes which if dysregulated can drive oncogenesis. In regards to the latter, stimulating the AR positive prostate cancer cell lines 22RV1 and LNCaP prostate cancer cell lines with the R1881 increases the mRNA expression of vascular endothelial growth factor (VEGF), a key regulator of tumour angiogenesis *(Eisermann et al., 2013).* Western blots also confirmed upregulation of VEGF protein expression in LNCaP cells after R1881 treatment *(Eisermann et al., 2013).*

In patients, PSA serum concentration below 4.0 ng/ml typically is not indicative of prostate cancer, whereas the concentrations of PSA can exceed 20ng/ml in prostate cancer and in other benign prostate diseases *(Arneth, 2009 ; Roussev et al., 2016).* PSA is encoded by the kallikrein related peptidase 3 (KLK3) gene and represents a classical AR target gene, with expression of this gene crucial for maintaining healthy prostate physiology. However, in malignancy elevated PSA expression can promote tumorigenesis. For example, when AR negative PC-3 cells overexpress PSA, this triggers the epithelial-mesenchymal transition (EMT), leading to reduced E-cadherin levels, increased vinculin expression and enhanced cell motility *(Veveris-Lowe et al., 2005).* Additionally reducing PSA expression via small molecule inhibition in LNCaP cells induces apoptosis, thus indicating PSA can influence cell survival *(Nicotera et al., 2009).* A potential explanation for how PSA regulates cell survival is through possible positive feedback with the AR. Knockdown of KLK3 expression in VCaP and LNCaP C4-2B prostate cancer cells was found to decrease AR mRNA and protein levels *(Saxena et al., 2011).*

There are various mechanisms which may account for why AR signalling is dysregulated in prostate cancer. Firstly, elevated AR expression can be seen throughout the progression of prostate cancer, with ~30-50% of advanced prostate cancers harbouring AR gene amplifications *(Fujita and Nonomura, 2019).* Additionally, *Mohler et al., (2011)* demonstrated in a spectrum of prostate cancer cell lines that the mRNA expression 17β-hydroxysteroid dehydrogenase 6 (17β-HSD6) is elevated, with this correlating with increased AR transactivation. 17β-HSD6 mediates the interconversion of androstanediol to DHT, thus indicating that prostate cancer cells can use additional pathways to generate DHT and activate AR signalling *(Mohler et al., 2011).*

As such deploying AR antagonists (such as flutamide and bicalutamide) or depleting circulating levels of androgens (via the administration ADT) reflects a gold standard for prostate cancer treatment *(Ferraldeschi et al., 2015).* Although ~80% of patients show an initial symptomatic or objective response to ADT after ~2-3 years the malignancy relapses, leading to the onset of castration- resistant prostate cancer (CRPC) (*Peehl., 2001 ; Karantanos et al., 2013).*

1.5. Mechanisms of Resistance in CRPC

One means of CRPC acquiring resistance to ADT can be due to the elevated expression of AR splice variants such as Androgen Receptor Splice Variant 7 (AR-V7). This variant contains a cryptic exon which is located in intron 3 of the AR gene, with the resulting encoded protein approximately 640 amino acids in size (*Zengerling et al., 2012 ; Luo 2016).* The defining feature of AR-V7 is that this splice variant lacks an LBD thus can aberrantly regulate gene expression in the absence of androgens *(Wang et al., 2018). Sharp et al., (2019)* determined using immunohistochemistry that the expression of AR-V7 is extremely rare in primary prostate cancers (under 1% of cases) relative to patients who previously received ADT (75% of cases).

AR-V7 has been reported to act as a transcriptional repressor, where shRNA knockdown of AR-V7 *in vitro* is associated with upregulation of 300 genes and downregulation of 129 genes *(Cato et al., 2019).* One notable gene which AR-V7 represses is Solute Carrier Family 30 Member 7 (SLC30A7), with deletion of this gene previously shown to accelerate prostate tumour formation *in vivo (Tepaamorndech,et al., 2011 ; Cato et al., 2019).* Additionally, several signalling networks can become aberrantly activated in CRPC that are mediated by kinases, such as the extracellular signal-regulated kinases-1/2 (ERK1/2), Proto-oncogene tyrosine-protein kinase Src (Src) and phosphoinositide 3-kinase (PI3K) *(Varkaris et al., 2014 ; Park et al., 2018 ; Nickols et al., 2019).*

1.6. The Function of Protein Kinases and Phosphatases

PTMs such as phosphorylation are crucial for regulation of the proteome, but in the context of cancer these processes can become dysregulated. Protein kinases are responsible for mediating the transfer of γ-phosphate from ATP onto amino acids harbouring hydroxyl groups which acts as phosphoacceptor residues. A kinase consensus sequence consists of amino acids that facilitate recognition of phosphoacceptor residues *(Kennelly and Krebs, 1991).* The most common phosphoacceptor is the amino acid serine where it's estimated that phosphorylated serine's account for 85-90% of phosphorylation sites in the proteome *(Hunter and Sefton, 1980 ; Olsen et al., 2006).* Whilst phosphorylated threonine's account for ~10% of phosphorylated species in the proteome, the abundances of phosphotyrosine is rare (0.5-2%) *(Hunter and Sefton, 1980 ; Olsen et al., 2006).*

The compounding reason for why serine and threonine phosphorylation predominates relative to tyrosine phosphorylation is that kinases which catalyse this PTM are the most common complement of the kinome *(Table 1.1).* First described by *Manning et al., (2002)* the human kinome classifies the 518 recorded protein kinases into 8 different groups *(Table 1.1).* These groups account for 478 members of the human kinome, with group members containing ~250 amino acid eukaryotic protein kinase catalytic domain *(Manning et al., 2002 ; Kostich et al., 2002).* The 8 different groups comprising the kinome are derived due to group members comprising sequence similarity in the catalytic domain.

However, the core features of the eukaryotic protein kinase domain are conserved across different group members. These features include conserved P-loop(comprising GxGxxG residues) which facilitates ATP binding and a HRD motif that is involved with transferring of γ-phosphate from ATP *(Kanevet al., 2019).* The remaining 40 proteins are referred to as atypical protein kinases which lack sequence similarity to the eukaryotic protein kinase domain.

Features of atypical protein kinases includes lacking glycine's in the P-loop and containing a DRH motif *(Kanev et al., 2019).* Despite lacking the core features which mediate ATP binding and of γ-phosphate transfer, kinase activity is still retained in atypical kinase members *(Su, and Jacinto., 2011; Widmann et al., 2012 ; Eisermann et al., 2013).*

The effect of protein phosphorylation is diverse and acts as a means to regulate substrate activity, stability, sub-cellular localisation and binding to other proteins *(Garcia-Garcia et al., 2016).* These effects are mediated through phosphorylation altering the surface properties and structural confirmation of proteins *(Johnson and Barford, 1993).* Due to the stark effect this PTM has upon the proteins of a protein, phosphorylation events are tightly regulated by phosphatases which remove the γ-phosphate group from phosphorylated species. It is estimated that the genome contains ~150 protein phosphatases which negatively regulate substrate phosphorylation *(Ardito et al., 2017).* Consequently a loss of protein phosphatases activity can lead to dysregulated substrate phosphorylation, aberrant signal transduction and oncogenesis *(Stebbing et al., 2014 ; Narla, et al., 2018).*

Table 1.1. Documentation of the 8 kinase groups that comprise the human kinome.

Kinase Group	**Residues Phosphorylated by Group Members**	**Number of Kinases in this group *(from Martin et al., 2009)***
Tyrosine Kinase (TK)	Tyrosine	91
Tyrosine Kinase-Like (TKL)	Serine and Threonine	48
STE20, STE11 and STE7 related (STE)	Serine and Threonine	61
Casein Kinase 1 (CK1)	Serine and Threonine	12
Protein kinase A, Protein Kinase G, and Protein Kinase C Related (AGC)	Serine and Threonine	82
Ca^{2+}/Calmodulin-Dependent Kinase (CAMK)	Serine and Threonine	95
Cdk, MAPK, GSK, Cdk-like related (CMGC)	Serine and Threonine	68
Receptor Guanylyl Cyclase (RGC)	Catalytically inactive	5
Other	Unknown	16

1.7. Lipid Kinases and Lipid Phosphatases– Their Role in the Phosphoinositide Pathway

In conjunction to the 518 protein kinases that influence protein function and dynamics, lipids harbouring hydroxyl groups can also undergo phosphorylation. There are 19 kinases which utilise different phosphatidylinositols for the generation of second messengers *(Brown and Auger, 2011).* Phosphatidylinositols are amphiphilic membrane spanning lipids. The general composition of a phosphatidylinositol is a diacylglycerol (DAG) backbone (comprised from polar fatty acids) which is integrated in the plasma membrane, and a polar myo-inositol head group facing towards the cytoplasm *(Figure 1.4).* Subsequently, the myo-inositol head group can be phosphorylated by kinases on positions 3, 4 and 5 on the inositol ring *(Table 1.2 and Figure 1.5).* This leads to the generation of monophosphorylated, biphosphorylated and triphosphorylated lipid species.

The most abundant phosphatidylinositol phosphate (PIP) is phosphatidylinositol 4,5-bisphosphate which accounts for 1% of the total lipid mass in cells *(Kielkowska et al., 2014).* The generation of PIPs are antagonised by lipid phosphatases which dephosphorylate positions 3, 4 and 5 on the myo-inositol head group *(Table 1.2 and Figure 1.5).* As with protein phosphorylation, PIPs can also trigger modifications to a proteins structure, localisation and activation state *(Martel et al., 2001 ; Stahelin, et al., 2014).* This is achieved through PIPs binding to specific binding domains present in protein substrates. *Table 1.3* summarises some of the common PIP binding domains found in the mammalian proteome, with the most common of these being the Pleckstrin Homology (PH) domain.

Table 1.2. Kinases and phosphatases which phosphorylate and dephosphorylate the inositol ring of phosphatidylinositols.

Inositol Ring Position	Kinases	Phosphatases
3	Class I , II , III PI3Ks	Myotubularins (MTMs) and Phosphatase and tensin homolog (PTEN)
4	Type II phosphatidylinositol-5-phosphate 4-kinases (PIP4Ks)	Inositol polyphosphate-4-phosphatases (INPP4s)
5	Type I phosphatidylinositol-4-phosphate 5-kinases (PIP5Ks) and Type III phosphatidylinositol-4-phosphate 5-kinase (PIKfyve)	Inositol polyphosphate-5-phosphatases (INPP5s)

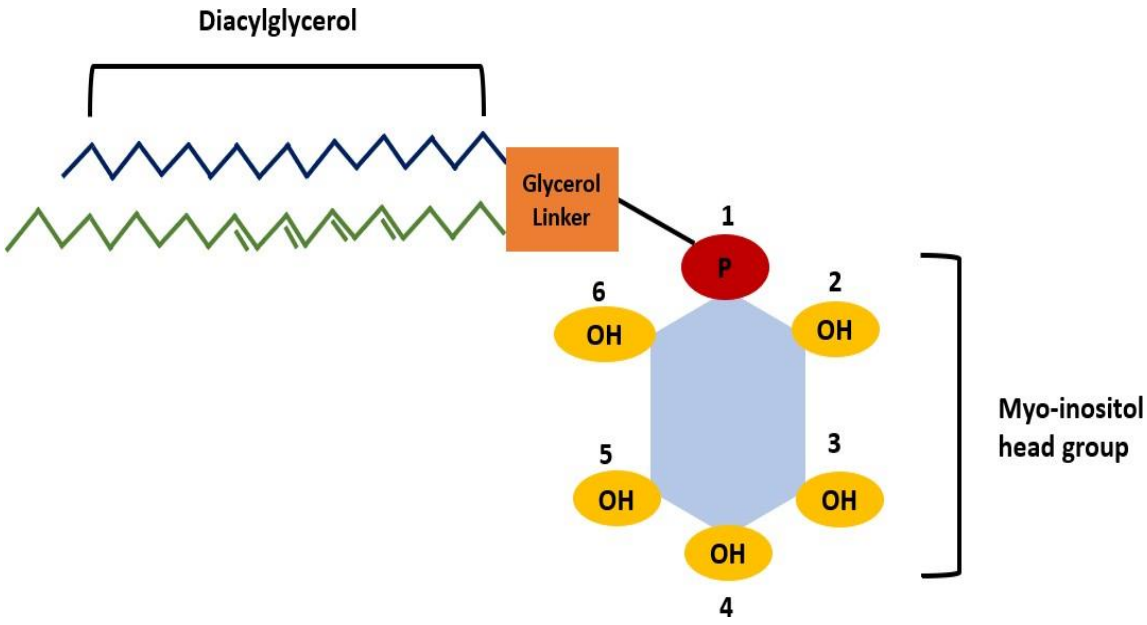

Figure 1.4. Schematic structure of a phosphatidylinositol molecule. The core elements of a phosphatidylinositol are a myo-inositol head group (inositol ring) tethered to a diacylglycerol backbone via a glycerol linker. The inositol ring hydroxyl groups can be phosphorylated by lipid kinases at positions 3, 4 and 5. At position 1 there is a phosphate group that is joined to the glycerol linker. The diacylglycerol backbone is composed of a saturated 18 carbon chain (typically stearic acid, shown in navy blue) and an unsaturated 20 carbon chain commonly arachidonic acid, shown in green. Schematic adapted from *Barneda et al., (2019).*

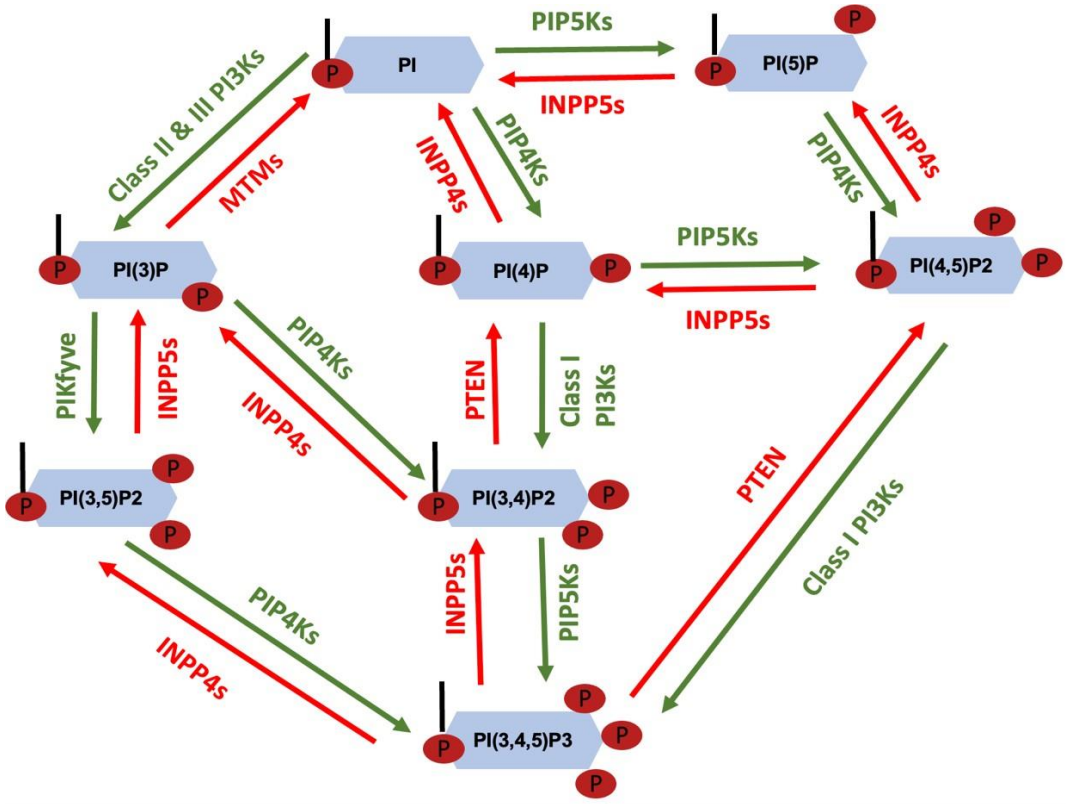

Figure 1.5. Schematic of the phosphoinositide cycle. Lipid kinases, which catalyse the addition of a phosphate group to the inositol ring structure, are shown in green. Lipid phosphatases that dephosphorylate the inositol ring are shown in red. Lipid species depicted are as followed: Phosphatidylinositol (PI) , Phosphatidylinositol 3-phosphate [PI(3)P] , Phosphatidylinositol 4-phosphate [PI(4)P] , Phosphatidylinositol 5-phosphate [PI(5)P] , Phosphatidylinositol (3,4)-bisphosphate [$PI(3,4)P_2$] , Phosphatidylinositol (3,5)-bisphosphate [$PI(3,5)P_2$] , Phosphatidylinositol (4,5)-bisphosphate [$PI(4,5)P_2$] and Phosphatidylinositol (3,4,5)-trisphosphate [$PI(3,4,5)P_3$].

Table 1.3. Common phosphatidylinositol binding domains found in proteins. Reported is the number of amino acids which comprises the domain, the lipid(s) which the domain binds to, and the number of reported proteins harbouring the domain.

Phosphatidylinositol Binding Domain	Number of Amino Acids	Lipid That Interacts With Domain	Number of Reported Proteins Containing Phosphatidylinositol Binding Domain	References
PH Domain	~100-120	$PI(4,5)P_2$ $PI(3,4)P_2$ $PI(3,4,5)P_3$	285	*Itoh and Takenawa., (2002) ; Lemmon, (2003) ; Lenoir et al., (2015)*
Phox Homology (PX) Domain	~110-120	PI(3)P	49	*Chandra et al., (2019)*
Fab-1, YGL023, Vps27, and EEA1 (FYVE) Domain	~60-70	PI(3)P	30	*Simonsen and Stenmark, (2001) ; Schoijet et al., (2010)*
Epsin N-terminal homology (ENTH) Domain	~150	$PI(4,5)P_2$	19	*De Camilli et al., (2002) ; Stahelin, (2008)*

1.8.Signalling Through Diacylglycerol and Inositol Trisphosphate

In the context of $PI(4,5)P_2$ this lipid can contribute to protein activation through its intermediates DAG and Inositol triphosphate (IP_3). These second messengers are released through $PI(4,5)P_2$ hydrolysis carried out by isozymes of the phospholipase C (PLC) family. It has been well documented the roles of DAG and IP_3 in signal transduction, most notably through their stimulatory effects upon members of the protein kinase c (PKC) family. This kinase family contains 10 isozymes which are grouped into three sub families, conventional, novel and atypical PKCs are activated by different stimuli *(Table 1.4).* However, a common feature is that all PKC family members can be stimulated by phosphatidylserine *(Antal and Newton, 2014).*

Table 1.4. Classification of PKC sub family members and their mode of activation.

Sub Family Name	Sub Family Members	Activated by
Conventional	PKC-α, PKC-βI, PKC-βII,PKC-γ	DAG , Phorbol Ester, Ca^{2+} , phosphatidylserine
Novel	PKC-δ PKC-ε , PKC-η , PKC-θ	DAG , Phorbol Ester , phosphatidylserine
Atypical	PKC-ι , PKC-ζ	Phosphatidic acid , arachidonic acid , ceramide, $PI(3,4,5)P_3$, phosphatidylserine

Both conventional and novel PKCs bind to DAG through two C1 domains (C1a and C1b) that are located in the regulatory region of these kinases *(Giorgione et al., 2006).* Maximal kinase activity for novel PKCs is achieved through DAG binding alone whereas conventional PKCs also require increases in intracellular calcium to facilitate their activation. This is because the C1b domain of novel PKCs contains tryptophan at position 22 relative to tyrosine found in conventional PKCs *(Dries et al., 2006).* C1b-Trp22 switches the affinity of DAG binding from low to high where it is thought that this residue makes more favourable hydrophobic interactions towards DAG when compared to tyrosine *(Wang et al., 2001; Dries et al., 2006).*

Conventional PKCs possess a C2 domain which contains a calcium binding motif. Increases in intracellular calcium concentrations is mediated by IP_3 binding to inositol trisphosphate receptors at the endoplasmic reticulum (ER) *(Hamada et al., 2017).* This causes calcium that is stored in the ER to be deposited in the cytosol. Calcium binding to conventional PKCs results triggers a conformational change in the C2 domain which facilitates PKC binding to phospholipids in the plasma membrane *(Bazzi and Nelsestuen, 1990 ; Lipp and Reither, 2011).* Whilst novel PKCs contain a C2 domain, the calcium binding motifin lost and instead acts as a sensor for tyrosine phosphorylated proteins*(Benes et al., 2005).* Atypical PKCs do not possess a C2 domain and contain a

single C1 domain and because of this, are not activated via $PI(4,5)P_2$ intermediates *(Diaz-Meco and Moscat, 2012).* Instead atypical PKCs can be activated by other molecules such as phosphatidic acid, arachidonic acid, ceramide and $PI(3,4,5)P_3$ *(Nakanishim et al., 1993 ; Limatola et al., 1994 ; Müller et al., 1995).*

In the context of prostate cancer, amplification of PKC family genes has been detected, with amplification of PRKCA (encoding PKC-α protein) and PRKCI (encoding PKC-ι protein) recorded at ~5% and ~10% respectively *(Figure 1.6).* It was recently reported by *Cook et al., (2022)* the role PKC-α exerts upon the transcriptome of prostate cancer cells. By using small interfering RNAs (siRNAs) to block the expression of PKC-α in PC-3 prostate cancer cells this resulted in the downregulation of 602 genes and upregulation of 848 genes *(Cooke et al., 2022).* Subsequent gene enrichment analysis revealed that knockdown of PKC-α contributed particularly to dysregulated expression of genes implicated with EMT and cell migration *(Cooke et al., 2022).*

In vitro cell migration assays confirmed impaired migration in PKC-α ablated PC-3 cells relative to control cells *(Cooke et al., 2022).* Novel PKCs have also been implicated with regulating the EMT and cell migration in prostate cancer cells. siRNA knockdown of PKC-ε in LNCaP cells has been show downregulate proteins which drive the EMT such the Twist Family bHLH Transcription Factor (TWIST1) *(Shiota et al., 2013).* Further work by *Shiota et al., (2017)* revealed that PKC-ε influences TWIST1 expression through positively regulating the NF-κB signalling pathway.

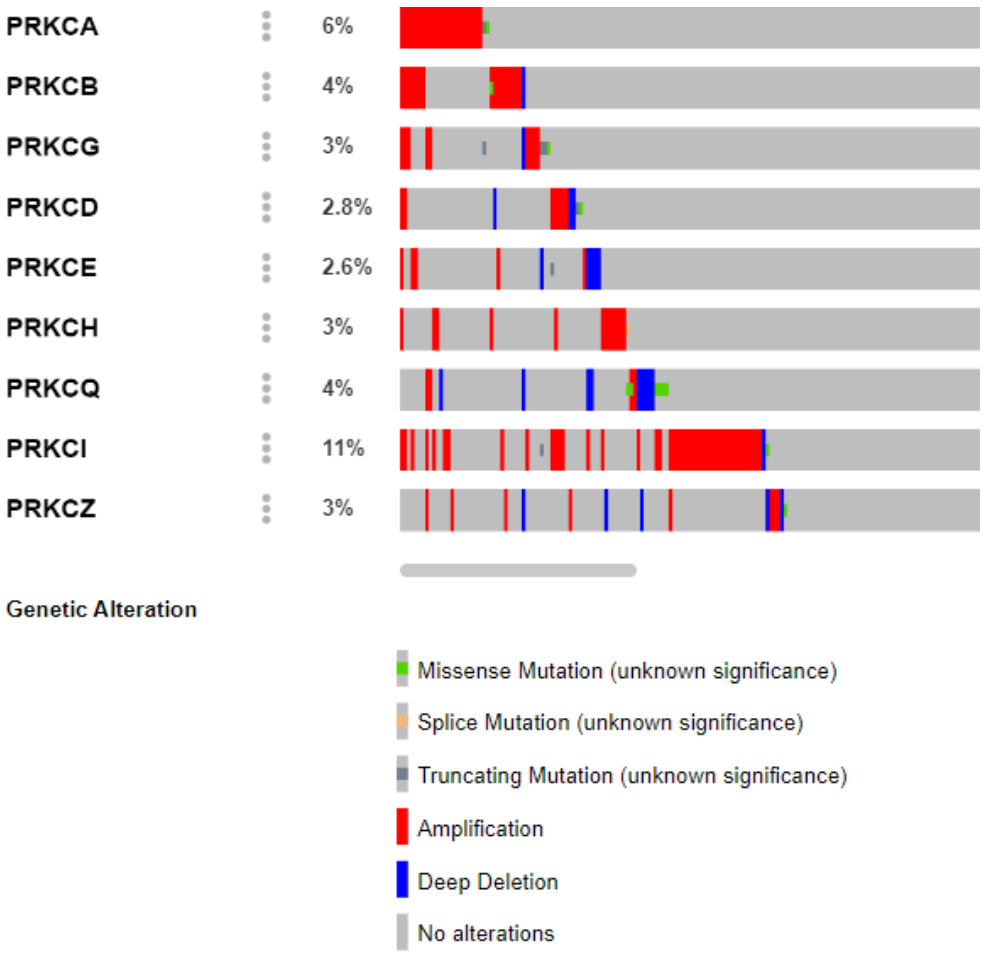

Figure 1.6. Gene amplification of PKC family genes in advanced prostate cancer. Data is from 444 advanced prostate cancer samples, as previously published by *Abida et al., (2019).* The percentages shown indicate the total number of genetic aberrations recorded for each gene throughout the 444 patient samples. Figure generated using cBioPortal *(Gao et al., 2013).*

1.9. PI3K Signalling in Prostate Cancer

Whilst PI(4,5)P_2 can exert second messenger functions (in part through the activation of certain PKC isozymes), this phosphoinositide is also a key substrate for PI3K family members. There are three classes of PI3Ks *(Table 1.5).* Emphasis shall be attained to Class IA PI3Ks due to their roles in malignancy, but Class IB, Class II and Class III PI3Ks will be discussed in brief. The prime difference of Class II PI3Ks relative to Class I and Class III PI3Ks is that they exist as a single catalytic subunit and are not tethered to a regulatory subunit *(Table 1.5).* Instead, catalytic activity of Class II PI3Ks is regulated through N terminal interactions with proteins such as clathrin and intersectin *(Jean and Kiger, 2014).* Furthermore, Class II PI3Ks do not use PI(4,5)P_2 as a substrate, and instead synthesise PI(3)P and PI(3,4)P_2, with these lipid pools largely concentrated in endosomes and lysosomes *(Koch et al., 2021).* As such, the function of Class II PI3Ks is largely attributed endocytosis; with the pools of synthesised PI(3,4)P_2 promoting recruitment of PI(3,4)P_2 dependent endocytic proteins, such as the sorting nexins (SXN) SXN9 and SXN18 *(Koch et al., 2021).*

Class III PI3K are heterodimers composed of a catalytic (VPS34) and a regulatory (VPS15) subunit *(Table 1.5).* VPS34 utilises just solely PI as a lipid substrate, which is used to synthesise PI(3)P *(Jaber and Zong, 2013).* The activity of Class III PI3Ks is particularly present in autophagy, with PI(3)P found at the membranes of phagosomes during the early stages of autophagy *(Iershov et al., 2019).* VPS15 undergoes autophosphorylation in yeast, however is considered to be a pseudokinase. This is due to lacking core key residues/motifs (such as the P-loop and HRD sequence) which is ubiquitous across the kinome, and no downstream substrate has ever been reported for VPS15 *(Ohashi et al., 2019).* The crystal structure of the VPS34-VPS15 heterodimer was determined by *Rostislavleva et al., (2015)* with this highlighting the functions VPS15 may exert upon VPS34 such as: contributing to membrane recruitment, stabilising the catalytic subunit and inhibiting catalytic activity by restricting VPS34s activation loop.

Class I PI3K kinases are split into two subfamily, Class IA and IB, both of which generate $PI(3,4,5)P_3$ from through phosphorylation of $PI(4,5)P_2$ on the 3rd position of the inositol ring structure *(Vogt et al., 2010).* Both Class IA and Class IB PI3Ks form heterodimers consisting of a regulatory and catalytic subunit. To facilitate this the expression of regulatory and catalytic subunits is largely equal as observed in immortalised cell lines and murine tissue *(Geering et al., 2007).* This is also evident in prostate cancer samples, where the mean fragments per kilobase of exon per million mapped fragments (FPKM) values are largely consistent between Class I catalytic and regulatory subunits *(Table 1.5).* FPKM values are a measure for gene expression, normalizing the number of mapped RNA reads to gene length.

The catalytic subunit of Class IA and Class IB PI3Ks contain a catalytic subunit which harbour a Rat sarcoma virus (RAS) binding domain (RBD) which mediates interactions with RAS GTPases and activates kinase activity *(Rodriguez-Viciana et al., 1994 ; Jimenez et al., 1998 ; Pacold et al., 2000 ; Suire, et al., 2002).* By RAS recruiting Class I PI3Ks to the plasma membrane, this localises the kinase to the plasma membrane, in close proximity to membrane associated effectors such as AKT and serum and glucocorticoid-inducible kinases (SGKs).

In terms of Class IB PI3Ks, they are comprised of a catalytic (P110γ) and regulatory subunit (p101/p84). Class IA PI3Ks are largely attributed to mediating downstream of activated receptor tyrosine kinases (RTKs) whilst Class IB PI3Ks are typically G protein coupled receptor (GPCR) effectors *(Stephens and Hawkins, 2013).* Class IB PI3Ks are associated with immune cell functions and has been attributed to mediating mast cell activation and lymphocyte chemotaxis *(Reif et al., 2004 ; Stephens and Hawkins, 2013).*

The regulatory subunits of Class IB PI3Ks couple to the Gβγ subunits of GPCRs with varying affinities. This was demonstrated by *Rathinaswamy et al., (2021)* through determining the Cryo-EM structure of p101-p110γ. This revealed that the primary interface of the p101-p110γ dimer consists of p101 interacting with the C2 domain of p110γ via its p110γ binding domain (PBD) *(Rathinaswamy et al., 2021).* The residues within p101 PBD show strong sequence homology to the PBD of p84. Further interactions to p110γ via p101 is mediated through its Gβγ binding domain, with these residues more poorly conserved between p84 and p101. This is believed to be reason why in lipid kinase assays conducted by *Rathinaswamy et al., (2021)* only a ~6 fold activation of p84-p110γ was observed relative to up to 200 fold activation for p101-p110γ, after Gβγ stimulation.

Class IA PI3Ks are also heterodimeric in nature. The catalytic subunits of Class IA PI3Ks *(Figure 1.7)* are p110α, p110β and P110δ. These are encoded by the phosphatidylinositol-4,5-bisphosphate 3-Kinase catalytic subunit (PIK3C) genes PIK3CA, PIK3CB, PIK3CD respectively. The regulatory subunits of Class IA PI3Ks *(Figure 1.8)* are p85α /p55α /p50α, p85β and p55γ. These are encoded by the phosphatidylinositol 3-kinase regulatory subunit (PIK3R) genes PIK3R1, PIK3R2 and PIK3R3 respectively. The p85α/p55α/p50α proteins arise through alternative splicing of PIK3R1, with both p55α and p50α lacking both the BH/RhoGAP and the SH3 domain. The BH/RhoGAP and SH3 domains which p85α possesses mediates interactions with small GTPases such as Cell division control protein 42 (Cdc42) and proline rich proteins like the E3 ubiquitin-protein ligase Cbl respectively (*Dombrosky-Ferlan and Corey, 1997 ; Tcherkezian and Lamarche-Vane, 2007).*

The core similarity between p85α/p55α/p50α proteins is that all contain three SH2 domains: N-terminal SH2 (n-SH2), inter-SH2 (i-SH2) and C-terminal SH2 (c-SH2). The i-SH2 domain is believed to act as a tether between p85/p110 subunits and mediates an additional interaction to the n-SH2 subunits that blocks p110 activity through conformational change *(Liu et al., 2014).* Upon growth factor stimulation this triggers the autophosphorylation of intracellular tyrosine residue on RTKs along with tyrosine phosphorylation on adaptor proteins.

Subsequently the n-SH2 and c-SH2 domains bind to phosophotyrosine (pY) containing consensus sequences, pYXXM *(Songyang et al., 1993 ; Piccione et al., 1993 ; Li et al., 2021).* PI3K activity is induced by RTKs as n-SH2 binding to intracellular phosophotyrosine residues relieves the negative inhibition this domain exerts upon p110's kinase activity *(Liu et al., 2014).* Another means of PI3K recruitment to growth factor receptors is used by Insulin and Insulin-like RTKs which possess IRS-1 and IRS-2 adaptor proteins. IRS-1 and IRS-2 use C their terminus to interact with the SH2 domains of p85 *(Metz et al., 2010).* Immunohistochemical analysis by *Szabolcs et al., (2009)* revealed that ~30% of prostate cancer specimens had elevated IRS-2 expression relative to healthy epithelium tissue.

Table 1.5. The catalytic and regulatory subunits of Class I, II , III PI3Ks. Documented are the gene and encoded protein for each Class of PI3Ks. Tabulated also are the mean fragments per kilobase of exon per million mapped fragments (FPKM) values for each gene. This data was taken from a prostate cancer cohort of 494 samples which is deposited on the Human Pathology Atlas *(Uhlen et al., 2017).*

Class of PI3Kand type of subunit	**Gene**	**Protein Subunit**	**Mean FPKM in Prostate Cancer Samples (n=494)**
Class I –Catalytic Subunits			
Class IA	PIK3CA	P110α	2.4
Class IA	PIK3CB	P110β	8.0
Class IA	PIK3CD	P110δ	1.5
Class IB	PIK3CG	P110γ	0.3
Total Class I Catalytic Subunit Expression	All of the above	All of the above	12.2
Class I – Regulatory Subunits			
Class IA	PIK3R1	P85α, P55α ,P50α	6.5
Class IA	PIK3R2	P85β	0.3
Class IA	PIK3R3	P55γ	5.7
Class IB	PIK3R5	P101	0.5
Class IB	PIK3R6	P84 (also referred to as $P87^{PIKAP}$)	0.3
Total Class I Regulatory Subunit Expression	All of the above	All of the above	13.3
Class II – CatalyticSubunits			
	PIK3C2A	PIK3C2α	8.0
	PIK3C2B	PIK3C2β	2.6
	PIK3C2G	PIK3C2γ	0.0
Total Class II Catalytic Subunit Expression	All of the above	All of the above	10.6
Class III-Catalytic Subunit			
	PIK3C3	Vps34	2.2
Class III – Regulatory Subunit			
	PIK3R4	Vps15	7.6

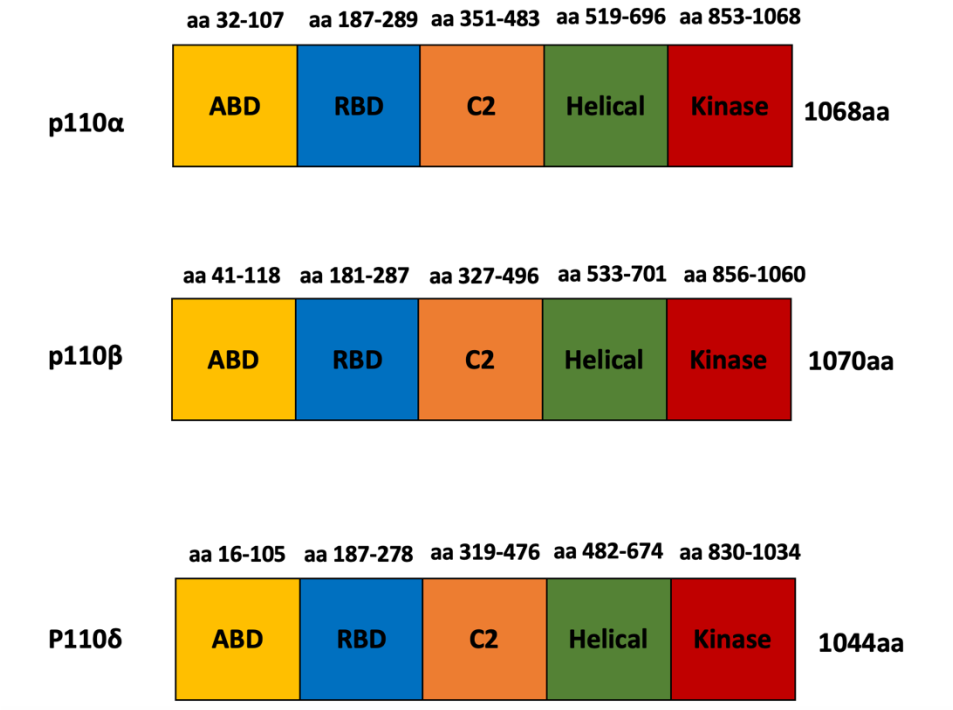

Figure 1.7. The structure of the catalytic subunits of Class IA PI3Ks. The catalytic subunits consist of adaptor binding domain (ABD), a RAS binding domain (RBD), a C2 domain, a helical and kinase domain. The kinase domain mediates PI(4,5)P_2 phosphorylation. The RBD mediates binding to RAS GTPases which positively stimulate PI3K activity and brings the kinase closer to the membrane *(Fruman et al., 1998).* The ABD and C2 domains are thought to interact with the central Src Homology 2 (SH2) domain of the regulatory subunit Inter-SH2 (i-SH2) *(Liu et al., 2014).* The helical domain interacts with N terminal SH2 domain of the regulatory subunit which attenuates basal catalytic activity *(Amzel et al., 2008 ; Burke, and Williams., 2013).*

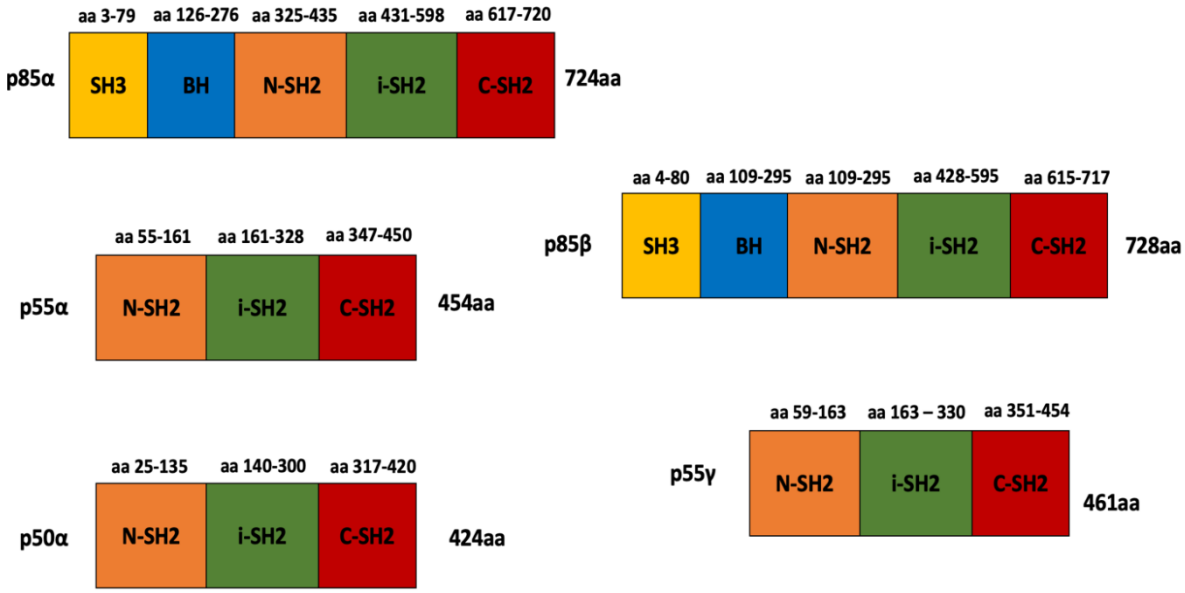

Figure 1.8. The structure of the regulatory subunits of Class IA PI3Ks. The regulatory subunit consists of three SH2 domains; SH2 domains either side of the iSH2 (N-SH2, C-SH2) couple to activated receptor tyrosine kinases via binding to phosphorylated YXXM motifs. Additionally, p85α/β possess Src homology 3 (SH3) and breakpoint cluster region-homology (BH) domains, also known as the RhoGAP domain. These domains allow p85α/β to interact with proline rich sequences and small GTPases respectively *(Dombrosky-Ferlan and Corey, 1997 ; Tcherkezian and Lamarche-Vane, 2007).* These interactions are not prominent between p55α, p50α and p55γ due to lacking both the SH3 and the BH/RhoGAP domains.

Gain of function mutations which induce aberrant PI3K activity are ubiquitously associated with oncogenesis. In the case of PIK3CA / p110α the 3 most common malignancies associated with these mutations are breast, endometrial and bladder cancer *(Madsen et al., 2018).* Over 80% of activating mutations map to three hotspot residues: E542K, E545K and H1047R, where E542K and E545K mutations reside in the helical domain of p110α *(Madsen et al., 2018).* These mutations are thought to impair binding to the N-SH2 domain of p85α , relieving the negative inhibition this subunit exerts upon kinase activity *(Hao et al., 2013).* Alternatively, the H1047R point mutation is located within the kinase domain of p110α and this triggers a conformational change resulting in augmented p110α binding to the plasma membrane, leading to greater access to PI(4,5,)P2 *(Mandelker et al., 2009).* However, activating mutations in PIK3CA in prostate cancer are rare, with a prevalence of ~2-3% *(Herberts et al., 2020).*

In the context of prostate cancer, signalling through p110β rather than p110α or p110δ is exhibited. For instance, *Hill et al., (2010)* showed in PC-3, LNCaP and DU145 prostate cancer cells that the protein expression of p110β dominates that of p110α. Subsequently siRNA knockdown of p110β in these cell lines lead to reduced AKT activation, whereas AKT phosphorylation was not altered after p110α knockdown *(Hill et al., 2010).* Signalling through p110β is dependent upon the CRK Like Proto-Oncogene, Adaptor Protein (CRKL) which via its N terminal SH3 domain binds proline rich regions of p85 *(Sattler et al., 1997 ; Zhang et al., 2017).* Subsequently shRNA mediated knockdown of CRKL in PC-3 prostate cancer cells blocked p110β signalling but had no effect upon insulin stimulated p110α activity *(Zhang et al., 2017).* Furthermore, knockdown of CRKL in PC-3 prostate cancer cells was shown to impair downstream AKT phosphorylation and attenuate cell growth. *(Zhang et al., 2017).*

Typically, increased p110β expression, rather than activating mutations are exhibited in prostate cancer. Microarray data analysis conducted by *Zhu et al., (2008)* reported that PIK3CB gene expression is significantly increased in prostate cancer specimens (52 samples with varying degree of aggressiveness) relative to 5 disease free prostate samples. Most notably, *Zhu et al., (2008)* found that PIK3CB gene expression correlates with the severity of prostate cancer, with elevated expression found in metastatic tumours (n=9) and tumours post ADT (n=17). The findings from the gene microarrays were then validated by reverse transcription quantitative polymerase chain reactions (RT-qPCR), which found increases of PIK3CB expression by over two fold in 14 out of 30 malignant tissues *(Zhu et al., 2008*). Whilst activating mutations in p110α are rare in prostate cancer patients, p110β activating mutations are even more novel. It was not until *Whale et al., (2017)* functionally characterised a point mutation in the kinase domain of p110β (E1051K) which was previously identified in 2 metastatic castration resistant prostate cancer patients (n=150) *(Robinson et al., 2015).*

1.10. Loss of Phosphatase Activity – Implications with Prostate Cancer

Another mechanism which drives prostate tumorigenesis is the loss of lipid phosphatase activity. The prime example of this involves the tumour suppressor PTEN. The classical function of PTEN is dephosphorylation of $PI(3,4,5)P_3$ at the 3rd position of the inositol ring, generating $PI(4,5)P_2$. Work by the Hawkins and Stephens laboratories subsequently revealed that PTEN can also dephosphorylate the 3rd position of $PI(3,4)P_2$ *(Malek et al., 2017).* This reflects another mechanism of which PTEN can regulate AKT activity, as $PI(3,4)P_2$ can also interact with the PH domain of AKT resulting in increased kinase activity *(Franke et al., 1997).* PTEN is inactivated in ~20-40% in primary prostate cancer cases, whereas PTEN inactivation reach up to ~60% in advanced, metastatic prostate cancers *(Phin et al., 2013).* PTEN inactivation can arise due to loss of heterozygosity (LOH) on chromosome 10q23.31, the region where the

PTEN gene resides *(Suzuki et al., 1999).* LOH of 10q23.31 is associated with more advanced and metastatic prostate cancer cases *(Kwabi-Addo et al., 2001).* For example, *Cairns et al., (2000)* identified LOH of 10q23 in 11/60 (18%) of primary malignancies relative to 12/20 (60%) of pelvic node metastases.

More recently, the lipid phosphatase INPP4B has been implicated with prostate oncogenesis. Analysis of 218 prostate tumours revealed loss of expression or mutations in INPP4B in 8% and 47% of primary and metastatic tumours respectively *(Agoulnik et al., 2011).* A potential mechanism to why a loss of INPP4B expression is associated with more aggressive cancer is that $PI(4,5)P_2$ levels are negatively regulated by this phosphatase. Thus, suppression of $PI(4,5)P_2$ dephosphorylation may lead to increases in $PI(4,5)P_2$ levels which are subsequently phosphorylated by Class I PI3Ks. Consequently, this may result in augmented $PI(3,4,5)P_3$ production and aberrant AKT phosphorylation. Indeed, *Hodgson et al., (2011)* demonstrated that siRNA knockdown of INPP4B in LNCaP cells results in increased activation of AKT and subsequent downstream phosphorylation of Forkhead Transcription Factors (FOXOs).

In addition, phosphatases which directly regulate AKT activity have also shown reduced activity in prostate cancer. For example, Protein Phosphatase 2A (PP2A) can dephosphorylate the T308 residue of AKT1 *(Kuo et al., 2007).* PP2A consists of three subunits: Scaffold (A), Regulatory (B) and catalytic (C) *(Xu et al., 2006). Pandey et al., (2013)* indicated that the expression of PP2A-A was lost in 128 out of 146 prostate cancer samples. Subsequently, *in vitro* knockdown of PP2A-A expression in PC-3 prostate cancer cells was found to elevated AKT phosphorylation and enhance cell migration *(Pandey et al., 2013).*

1.11. AKT – The Bona Fide Effector of PI3K Signalling

The Ser/Thr kinase AKT is a major downstream effector of the PI3K signalling cascade, for which there are three isoforms described: AKT1, AKT2, and AKT3. Whilst AKT1 and AKT2 expression is ubiquitous across human tissues, AKT3 expression is thought to be mainly expressed in the brain, kidneys and heart *(Okano et al., 2000).* At the amino acid level, the three AKT isoforms share approximately 80% sequence homology, and consist of the a core structure *(Figure 1.9)* encompassing a N terminal PH domain, a kinase domain and a C-terminal hydrophobic motif *(Bellacosa et al., 2004 ; Wang and Basson, 2008).* The PH domain allows AKT to primarily interact with $PI(3,4,5)P_3$, although the PH domain can also interact with $PI(3,4)P_2$ which leads to increases in kinase activity *(Frech et al., 1997 ; Miao et al., 2010).* The hydrophobic motif is truncated in the AKT3 splice variant (AKT3-y1) which can only achieve partial activation upon growth factor stimulation as S472 is lost in this splice variant *(Brodbeck,et al., 2001 ; Matheny and Adamo, 2009).*

Upon binding to membrane bound $PI(3,4)P_2$ / $PI(3,4,5)P_3$, AKT1 is subsequently phosphorylated in the activation loop (T-loop) of the kinase domain at T308 (T309 and T305 in AKT2 and AKT3 respectively) by phosphoinositide-dependent kinase-1 (PDK1), which also contains a PH domain *(Alessi et al., 1997 ; Bayascas et al., 2008).* A recent model for how $PI(3,4)P_2$ and $PI(3,4,5)P_3$ activates PDK1 has been suggested by *Levina et al., (2022).* In this, it is thought the activity of cytosolic PDK1 is inhibited by its own PH domain. Upon $PI(3,4)P_2$ / $PI(3,4,5)P_3$ genesis, this triggers PDK1 recruitment to the cell membrane, with PH domain binding to membrane bound phosphoinositides relieving the negative inhibition this domain exerts upon PDK1 activity *(Levina et al., 2022).*

Subsequently, this mediates the autophosphorylation of S241, located on the activation loop of PDK1 *(Levina et al., 2022).* This autophosphorylation event is necessary for PDK1 kinase activity *(Gao and Harris, 2006)* and allows the kinase to bind and phosphorylate downstream effectors *(Levina et al., 2022).*

Since the identification of AKT T308 phosphorylation via PDK1, additional kinases have been reported to phosphorylate T308 in malignancy, such a Calcium/calmodulin-dependent protein kinase kinase 2 (CaMKK2) *(Schmitt et al., 2011 ; Gocher et al., 2017).* This phosphorylation event has been observed through stimulating CAMKK2 activity through agonist (carbachol) treatment, and loss of AKT T308 phosphorylation has been recorded in ovarian and prostate cancer cell lines after knockdown of CAMKK2 expression *(Schmitt et al., 2011 ; Gocher et al., 2017).* Although phosphorylation of T308 initiates kinase activity, maximum activity of AKT1 is achieved when S473 (located in the C terminal hydrophobic tail) which also phosphorylated (S474 and S472in AKT2 and AKT3 respectively) *(Alessi et al., 1996 ; Bellacosa et al., 2004).* This phosphorylation event further stablises the N lobe of AKT, which partakes in ATP binding *(Hart, and Vogt., 2011 ; Cole et al., 2019).*

The kinase which is primarily responsible for phosphorylating this site is mammalian target of rapamycin (mTOR), as part of the mTORC2 signalling complex *(Sarbassov et al., 2005).* However under certain stresses such as DNA damage (arising from chemotherapy or ionizing radiation) S473 phosphorylation by DNA-dependent protein kinase (DNA-PK) has also been reported *(Toulany et al., 2011 ; Stronach et al.,2011 ; Sahlberg et al., 2013*). Activation of AKT results in the phosphorylation of an array of downstream proteins (~200) which have been associated with enhancing cell survival, migration, transcription and angiogenesis *(Toker, 2012).*

As the PH domain is crucial for AKT activation, mutations in this domain can trigger constitutive kinase activity. *Carpten et al., (2007)* demonstrated that the E17K mutation in AKT1s PH domain resulted in aberrant localisation to the cell membrane, leading to sustained T308 and S473 phosphorylation. Although this mutation is found at higher frequencies in breast and colorectal cancer cases the frequency of E17K in prostate cancer is rare, being detected in just 1% of patients *(Kim et al., 2008 ; Boormans et al., 2010).* Gene amplification of AKT1/2/3 are slightly more common in advanced prostate cancers, with a prevalence of ~5% in AKT1 and AKT3 respectively being previously recorded *(Figure 1.10).*

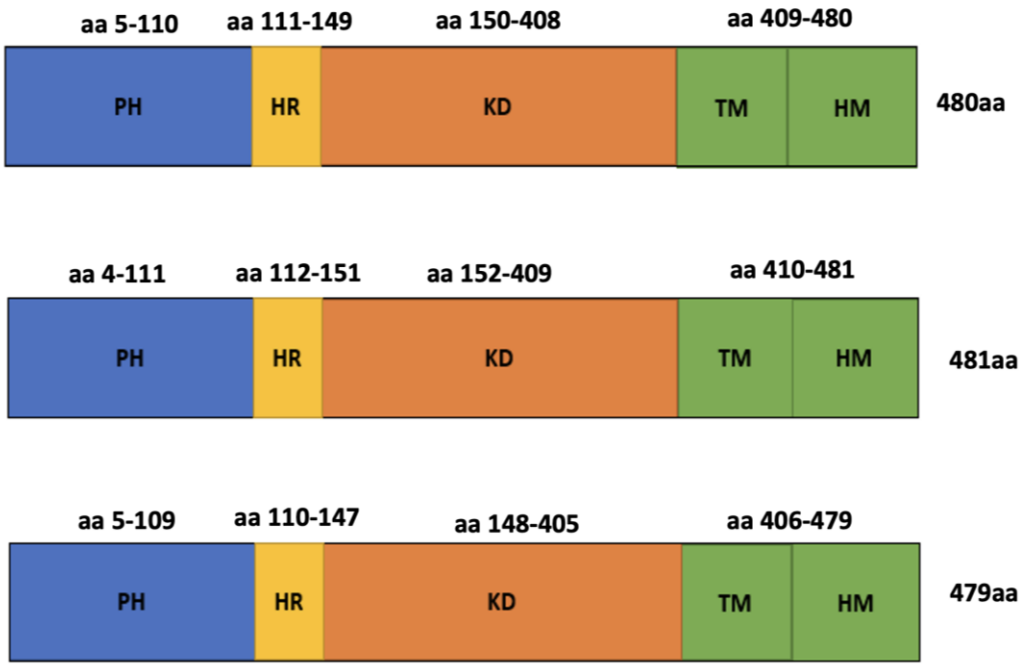

Figure 1.9. Core domain structure of AKT proteins. The PH domain mediates binding to membrane bound phosphatidylinositols required for kinase activity. The hinge region (HR) tethers the PH domain and kinase domain (KD) together. The regulatory domain (in green) consists of both the turn motif (TM) and hydrophobic motif (HM). Phosphorylation of the TM and HM via the mTORC2 signalling complex enhances downstream AKT activity *(Ikenoue et al., 2008).* Figure adapted from *Chautad et al., (2014).*

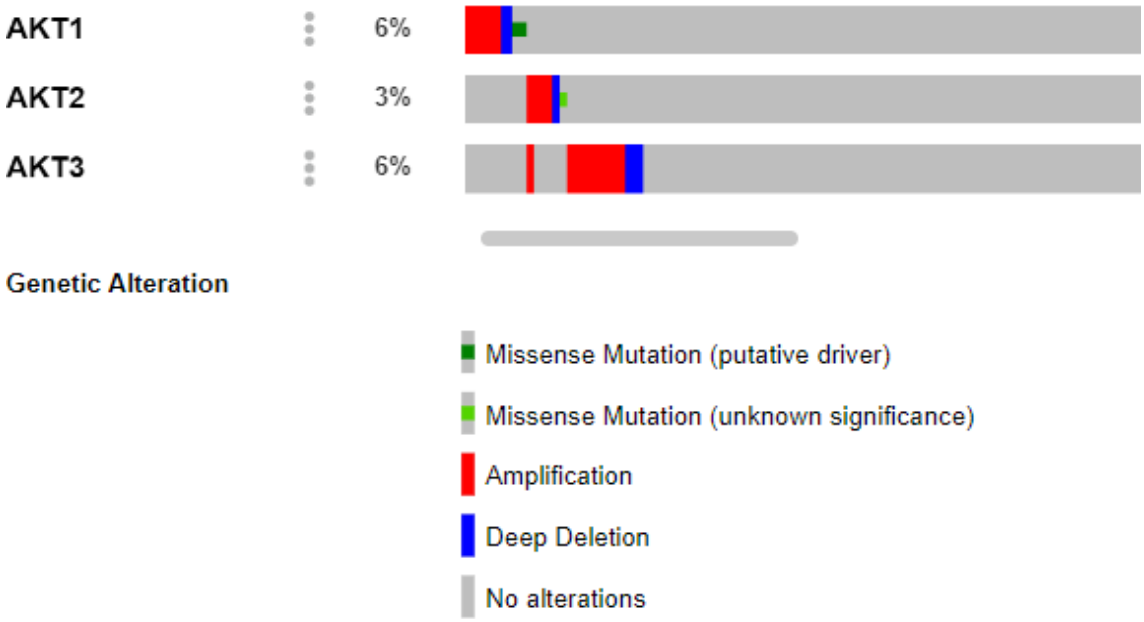

Figure 1.10. Gene amplification of AKT family genes in advanced prostate cancer. Data is from 444 advanced prostate cancer samples, as previously published by *Abida et al., (2019).* The percentages shown indicate the total number of genetic aberrations recorded for each gene throughout the 444 patient samples. Figure generated using cBioPortal *(Gao et al., 2013).*

1.12. MTOR Signalling Downstream of AKT Activation

Many of the oncogenic hallmarks downstream of AKT are mediated through mTOR. The mTOR kinase is central to mammalian target of rapamycin complexes 1 and 2 (mTORC1/2) which positively regulate cell size, growth and translation *(Fonseca et al., 2014 ; Saxton and Sabatini, 2017).* Although the core structure of mTORC1/2 is largely complementary, *(Table 1.6 and Figure 1.11)* the presence of complex specific subunits means that the PI3K/AKT signalling pathway can regulate complex activity differently. The central kinase in the signalling complexes (MTOR) has a mass of 289 kDa and is part of the PI3K-related kinase family *(Laplante and Sabatini, 2009).* This kinase family comprises several Ser/Thr kinases whose kinase domain shows sequence homology to that to the catalytic subunit of Class I PI3Ks *(Lempiäinen and Halazonetis, 2009).*

In mTORC1, the kinase activity of mTOR is in part regulated by two distinct protein subunits; Raptor and PRAS40. *Kim et al., (2002)* was able to demonstrate that N terminus of mTOR is responsible for Raptor binding, with this interaction impaired after treatment with the mTOR inhibitor rapamycin. Raptor acts as a scaffold protein which is responsible for recruiting mTORC1 substrates eukaryotic translation initiation factor 4E (eIF4E)-binding protein 1 (4E-BP1) and ribosomal protein S6 kinase β-1 (S6K1) *(Adami et al., 2007).* Deletion of Raptor attenuates the phosphorylation of both proteins *(Shaw, 2008).* Whilst Raptor is implicated with the positive regulation of mTORC1, kinase activity is also tightly controlled by PRAS40. When PRAS40 is overexpressed in cells this abrogates 4E-BP1 and S6K1 phosphorylation *(Sancak et al., 2007).* Furthermore, in growth factor deficient conditions this promotes PRAS40 binding towards mTOR, however after the addition of growth factors this interaction is abrogated *(Sancak et al., 2007).*

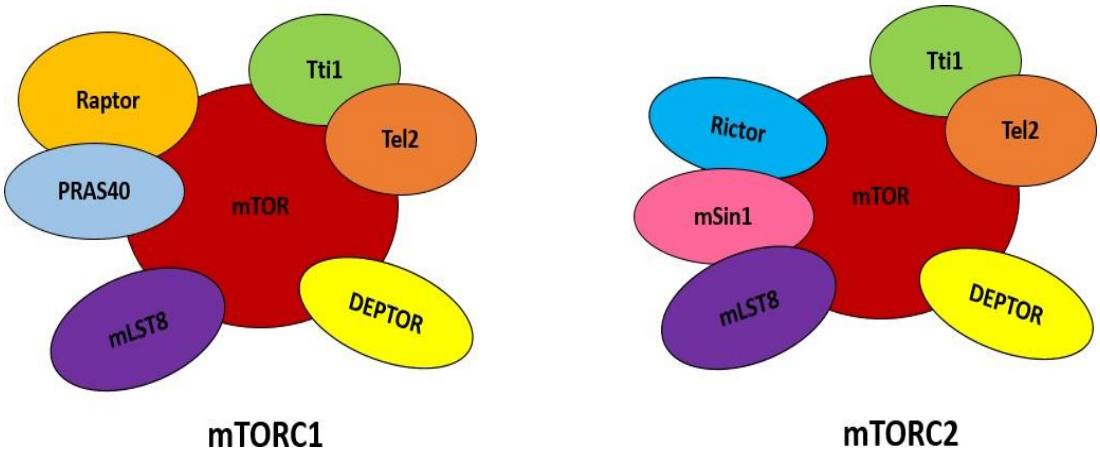

Figure 1.11. Schematic structure of mTORC1 and mTORC2 signalling complexes. Conserved proteins in both complexes are responsible for regulating complex formation and stability. Complex specific subunits influence substrate specificity and how kinase activity is regulated. Figure adapted from *Kim, Cook, and Chen, (2016).*

Full names of complex subunits are as followed mammalian target of rapamycin (mTOR), DEP domain-containing mTOR-interacting protein (DEPTOR) , Telomere length regulation protein TEL2 homolog (Tel2) , ELO2 Interacting Protein 1 (Tti1), mammalian target of rapamycin complex subunit LST8 (mLST8), mammalian stress-activated protein kinase-interacting protein (mSin1) , Rapamycin-insensitive companion of mammalian target of rapamycin (RICTOR) , Regulatory-associated protein of mTOR (Raptor) and proline-rich AKT substrate of 40 kDa (PRAS40).

Table 1.6. The complex subunits in mTORC1 and mTORC2. Documented are the genes encoding components of mTORC1 and mTORC2, their protein name, number of amino acids for each subunit, and whether the subunit is found in either/or mTORC1 and mTORC2. Tabulated also are the mean FPKM values for each gene. This data was taken from a prostate cancer cohort of 494 samples which is deposited on the Human Pathology Atlas *(Uhlen et al., 2017).*

MTOR Complex Encoding Gene	MTOR Protein Complex Subunit	Number of Amino Acids	Present in mTORC1	Present in mTORC2	Mean FPKM in Prostate Cancer Samples (n=494)
MTOR	MTOR	2549	✓	✓	8.1
DEPTOR	DEPTOR	409	✓	✓	9.9
MLST8	mLST8	326	✓	✓	14.6
TTI1	Tti1	1089	✓	✓	7.2
TELO2	Tel2	838	✓	✓	12.7
AKT1S1	PRAS40	256	✓	✗	12.8
RPTOR	Raptor	1335	✓	✗	4.8
RICTOR	Rictor	1708	✗	✓	2.3
MAPKAP1	mSin1	522	✗	✓	13.0

AKT activation triggers phosphorylation of PRAS40 on Thr246 resulting in binding to 14-3-3 chaperone proteins; in turn relieving the negative inhibition PRAS40 exerts upon mTORC1 substrate binding *(Kovacina et al., 2003 ; Wang et al., 2007 ; Nascimento et al., 2010).* Interestingly, the levels of phosphorylated PRAS40 (Thr246) are significantly increased in advanced prostate cancer *(Shipitsin et al., 2014*) suggesting that mTORC1 activity is dysregulated throughout disease progression. This highlights that AKT activity can positively regulate the cells translational machinery by stimulating mTORC1 activity, leading to 4E-BP1 and S6K1 phosphorylation *(Ma and Blenis, 2009).* Phosphorylation of 4E-BP1 relieves the negative inhibition this protein exerts upon the translation initiation factor eIF4E *(Qin et al., 2016).* This mediates the recruitment of 40s ribosomal subunits to mRNA transcripts allowing translation to pursue *(Qin et al., 2016).*

Activation of S6K1 is also attributed to downstream phosphorylation of additional proteins within the cells translational machinery such eukaryotic translation initiation factor 4B (eIF4B) and programmed cell death 4 (PDCD4) which increases the 5' helicase activity of eukaryotic initiation factor-4A (eIF4A) *(Magnuson et al., 2011).* Whilst the canonical function of S6K1 is to regulate translation and protein turnover, work by *Zhang et al., (2006)* was able to identify conditions in which S6K1 (rather than AKT) can phosphorylate the downstream substrate glycogen synthase kinase-3β (GSK3β). This phosphorylation event arises in tumour cells lacking a complex comprised of tuberous sclerosis proteins 1 and 2 (TSC1/2), a complex that antagonises mTORC1 activity *(Zhang et al., 2006).* Ser9 phosphorylation of GSK3β by S6K1 is attributed to enhancing cancer cell proliferation in the absence of growth factors *(Zhang et al., 2006).*

The two distinct protein subunits found in mTORC2 include Rictor and mSIN1. The former makes up ~60% of the total mass of the mTORC2 protein subunits *(Stuttfeld et al., 2018).* The function of Rictor within mTORC2 is to enhance the stability and substrate processing of this signalling complex *(Gkountakos et al., 2018). In vitro* RNA interference (RNAi) of Rictor in PC-3 prostate cancer cells has been shown attenuate AKT S473 phosphorylation, and inhibit tumour cell proliferation *(Hietakangas and Cohen, 2008).* Interestingly work by *Jebali and Dumaz, (2018)* suggested that the malignancy most commonly associated with upregulated RICTOR gene expression are neuroendocrine prostate tumours. What is currently unknown however is whether Rictor antagonists which have previously showed promise in glioblastoma therapy *(Benavides-Serrato et al., 2017)* could be utilised in treatment of neuroendocrine prostate tumours.

The prime kinase downstream of mTORC1, S6K1, can phosphorylate Rictor on T1135 *(Dibble et al., 2009).* Inactivating this phosphorylation site increases downstream AKT (S473) phosphorylation, thus suggesting that mTORC1 signalling can exert negative regulation on AKT activity *(Dibble et al., 2009).* Furthermore, inactivating T1135 does not affect the phosphorylation status of other mTORC2 substrates (SGK1 or PKCα) indicating this mode of regulation is AKT specific *(Dibble et al., 2009).* This is just one example of the feedback mechanisms which the MTOR signalling complexes exert upon each other.

The function of the mSIN1 subunit in mTORC2 is crucial for integrating upstream phosphoinositide signalling into pathway activation. In growth factor deficient conditions mSIN1 binds to mLST8, the C terminus of Rictor and the kinase domain of mTOR which limits substrate availability *(Yao et al., 2017).* When mSIN1 is overexpressed this abrogates downstream AKT (S473) phosphorylation, indicating that mSIN1 can negatively regulate mTORC2 activity *(Yao et al., 2017).* However, upon growth factor stimulation, mSin1 localises to cell membrane and binds to $PI(3,4,5)P_3$ via its C terminal PH domain *(Liu et al., 2015).* By binding to $PI(3,4,5)P_3$ this attenuates mSIN1s interaction with MTOR (via its PH domain) and instead exposes the active site of mTOR to AKT, resulting in S473 phosphorylation *(Liu et al., 2015).* This further highlights the complex crosstalk between PI3K, AKT and mTOR kinases.

1.13. Additional Effectors of PI3K Signalling

Whilst AKT and MTOR are classically associated with the PI3K signalling cascade, additional PI3K effectors must not go unnoticed, such as members of the SGK family. Like AKT, the SGKs are members of the AGC protein kinase group, and comprises three isozymes: SGK1, SGK2 and SGK3; SGK1 is the most studied member of this family *(Maestro et al., 2020).* Further similarities between SGKs and AKTs arise when their respective amino acid sequences; with SGK1 showing 54% amino acid identity to the kinase domain of AKT1 *(Brickley et al., 2002).* Subsequently, both SGK and AKT family members possess a near identical consensus sequence *(Table 1.7),* thus these kinases can activate similar signalling networks *(Pearce et al., 2010).*

For example, the same phosphorylation sites on FOXO3a that are phosphorylated by AKT1 (T32, S253 and S315) are also phosphorylated by SGK1 *(Brunet et al., 2001)*. On parallels with AKT1, SGK1 phosphorylation of FOXO3a also stimulates cell cycle re-entry and attenuates apoptosis *(Brunet et al., 2001)*. Cell cycle progression can also be enhanced through AKT1 and SGK1 phosphorylating p27 at T157 *(Hong et al., 2008).* This phosphorylation event causes p27 to accumulate in the cytoplasm which relieves the negative regulation this protein exerts upon nuclear cyclin E-CDK2 complexes *(Hong et al., 2008 ; Wander et al., 2010)*

Table 1.7. Consensus sequences of AKTs and SGKs. Residues phosphorylated by AKT and SGKs highlighted. Residues denoted as an X refer to any amino acid.

Kinase Family	Consensus Sequence
AKT	R–X–R–X–X–S/T
SGK	R/K–X–R–X–X–S/T

Activation of SGKs shows similarities to AKT isozymes, also requiring phosphorylation of amino acids (T256 and S422) which reside in the activation loop and the C terminal domain of SGK respectively *(Gleason et al., 2019).* PDK1 again is the kinase responsible for phosphorylation of T256 *(Kobayashi and Cohen, 1999).* However unlike AKT isozymes, both mTORC1 and mTORC2 phosphorylate S422, indicating functional crosstalk between these distinct signalling complexes in the regulation of SGKs *(Hong et al., 2008 ; Gleason et al., 2019).*

Another fundamental difference between SKG and AKT kinases is that the former lacks a PH domain, thus is not directly activated by $PI(3,4,5)P_3$ *(Sakoda et al., 2003).* Instead, SGK3 interacts with mono-phosphorylated inositol species, with this interaction mediated by the presence of a N terminal PX domain *(He et al., 2011).* The PX domain interacts with PI(3)P, which initiates maximal kinase activity and localises SGK3 to endosomal structures *(He et al., 2011).* Both SGK1 and SGK2 possess a shorter N terminus relative to SGK3 meaning these kinases lack a PX domain. Because of this, SGK1/2 localises to the plasma membrane or cytoplasm but upon growth factor stimulation this can induce nuclear translocation (*Leong et al., 1999 ; Brickley et al., 2002 ; He et al., 2011).*

Whilst it was previously observed in advanced prostate cancers amplifications of AKT1 and AKT3 were at a ~5% prevalence *(Figure 1.9),* in the same cohort, much greater SGK3 gene amplifications are observed *(Figure 1.12). In vitro studies* have also shown that R1881 or DHT treatment increases SGK3 expression, with a functional half ARE site conferring sensitivity towards androgens *(DePrimo et al., 2002 ; Wang et al., 2014a).* With dysregulated AR activity a driver in prostate cancer tumorigenesis, this could reflect a mechanism in which the AR contributes to the activation of mTORC1 signalling. Subsequent siRNA knockdown of SGK3 in LNCaP cells attenuated downstream S6K1 phosphorylation, in conjunction with reductions in cyclin D1 expression and impaired cell proliferation (*Wang et al., 2014a).*

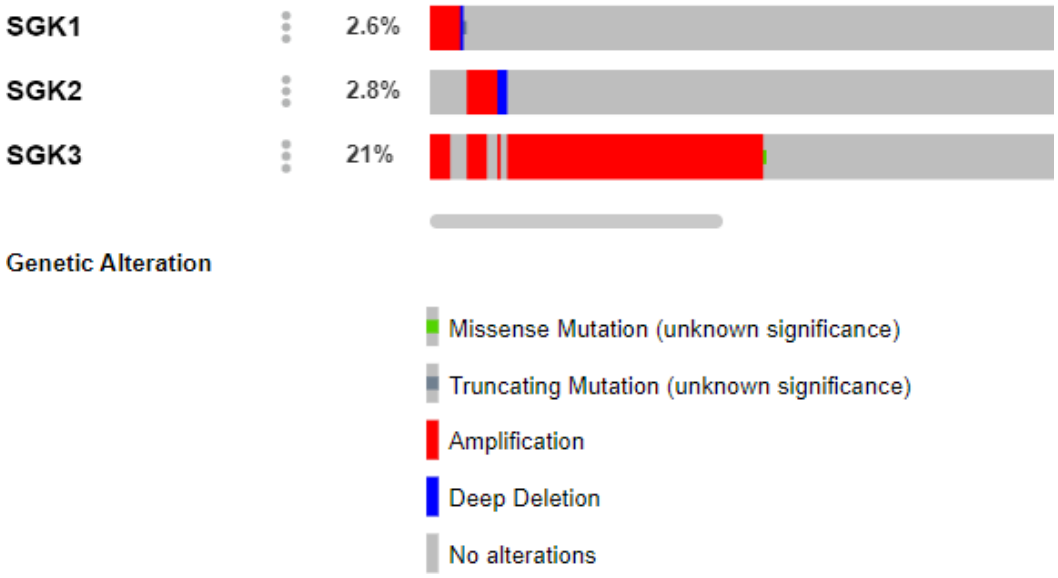

Figure 1.12. Gene amplification of SGK family genes in advanced prostate cancer. Data is from 444 advanced prostate cancer samples, as previously published by *Abida et al., (2019).* The percentages shown indicate the total number of genetic aberrations recorded for each gene throughout the 444 patient samples. Figure generated using cBioPortal *(Gao et al., 2013).*

Another PI3K effector is the RTK burtons tyrosine kinase (BTK) which transduces signals from Class IA PI3Ks through binding $PI(3,4,5)P_3$ via a PH domain *(Pal Singh et al., 2018).* This interaction initiates the recruitment of BTK to membrane, with $PI(3,4,5)P_3$ binding relieving the inhibitory effect the PH domain exerts on BTK *(Saito et al., 2001).* $PI(3,4,5)P_3$ allows membrane bound kinases such as Lyn to access and phosphorylate BTK's activation loop (Y551), which stimulates kinase activity *(Saito et al., 2001).*

Classically, the activities of BTK are associated with the immune response, with this kinase essential for B lymphocyte proliferation and maturation *(Rada et al., 2018).* More recently however, the function of BTK has been implicated in a range of solid tumours. Overexpression of BTK has been reported in brain, ovarian and prostate tumours *(Guo et al., 2014 ; Zucha et al., 2015 ; Wei et al., 2016).* Subsequent protein effectors activated downstream of BTK include PKCs, c-Jun N-terminal kinases (JNKs) and members of the signal transducer and activator of transcription (STAT) family; with these proteins implicated in increasing cell survival and modulating gene expression *(Qiu and Kung, 2000).*

1.14. The Structure and Function of PIP5Ks

A major influence on PI3K/AKT pathway activation is the availability of $PI(4,5)P_2$ substrate. Two kinase families are responsible for synthesising $PI(4,5)P_2$. The family of Type I PIP5Ks primarily synthesise $PI(4,5)P_2$ at the cell membrane and phosphorylate PI(4)P on the 5th position of the inositol ring *(Khadka and Gupta, 2019).* On the other hand Type II PIP4Ks generate $PI(4,5)P_2$ through 4th position phosphorylation of PI(5)P which occurs predominantly at the cytoplasm and endoplasmic reticulum *(Khadka and Gupta, 2019).* Focus will be paid to Type I PIP5Ks for which there are three described isozymes: PIP5K1α, PIP5K1β, and PIP5K1γ. The genes which encode these kinases (PIP5K1A, PIP5K1B and PIP5K1C) are located on chromosome 1, 9 and 19 respectively, each encoding several splice variants *(van den Bout, and Dievcha., 2009).* Whilst PIP5K1β, and PIP5K1γ will be discussed,the main emphasis of this work is attained to PIP5K1α due to the implication this kinase has with prostate cancer *(discussed in Section 1.18).*

The core structure of PIP5Ks is a central kinase domain flanked by disordered N and C termini *(Figure 1.13).* Between Class I PIP5Ks there is poor sequence conservation in both the N and C terminus *(Table 1.8).* This variance is thought to contribute to the differences in localisation of each isozyme *(Porciello et al., 2016).* Even though the kinase domain varies in length between the three isozymes (~330-380 amino acids) nevertheless, strong sequence homology of ~80% is retained *(Kwiatkowska, 2010 ; Table 1.8).* X-ray crystallography conducted by *Hu et al., (2015)* revealed key motifs within the kinase domain of zebrafish PIP5K1α that serve to regulate ATP binding and catalytic activity *(Figure 1.14).*

Using this available crystal structure (protein databank accession number 4TZ7) it is now possible to investigate *in silico* whether the 3D structure of the kinase domain of PIP5K1α is conserved across the kinome. Using the FolkSeek server (*van Kempen et al., 2023)* this measures *in silico* tertiary amino acid interactions. This facilitates comparisons of conservation of these interactions across available

proteins structures. The outputs of this are summarized *Table 1.9*. Interestingly whilst *Table 1.9* reveals conservation of PIP5K1α to members of Class II (PIP4K) and Class III phosphatidylinositol-5-phosphate 4-kinases (PIKfyv) conversation of tertiary interactions to members of the PI3K Classes was not identified. As such, whilst both PIP5Ks and PI3Ks synthesis phosphoinositide second messengers, the differences in 3D architecture between these two kinases facilities the production of different lipids.

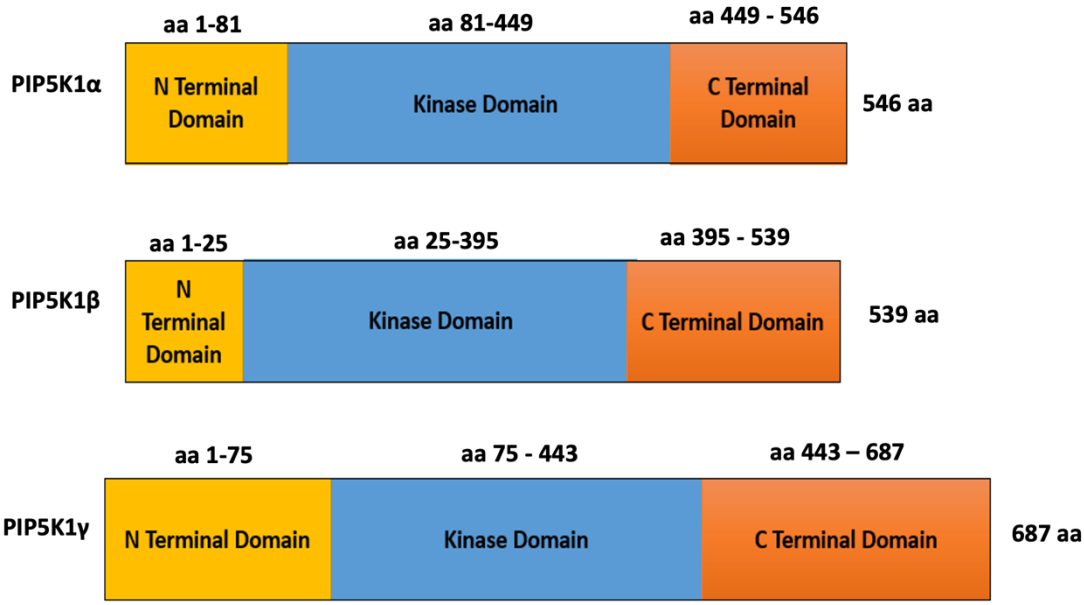

Figure 1.13. Schematic of the protein structure of PIP5K isozymes. Indicated are the poorly conserved N and C termini, where the sequence variation in these termini is thought to contribute to differences in localisation of PIP5Ks.The kinase domain is highly conserved between PIP5K1α, PIP5K1β, and PIP5K1γ. Figure adapted from *(Porciello et al., 2016)*

Table 1.8. Reported Sequence Identity of the N Terminus, C Terminus and Kinase Domain of PIP5K1α (isoform 1) relative to PIP5K1β (isoform 1) and PIP5K1γ (isoform 1). The Clustal Omega Multiple Sequence Alignment Tool *(Madeira et al., 2019)* was used to generate percentage identity scores.

Kinase Comparison	N Terminus Sequence Identity(%)	Kinase Domain Sequence Identity(%)	C Terminus Sequence Identity(%)
PIP5K1α -PIP5K1β	16.67	76.82	32.71
PIP5K1α–- PIP5K1γ	30.16	82.11	30.77

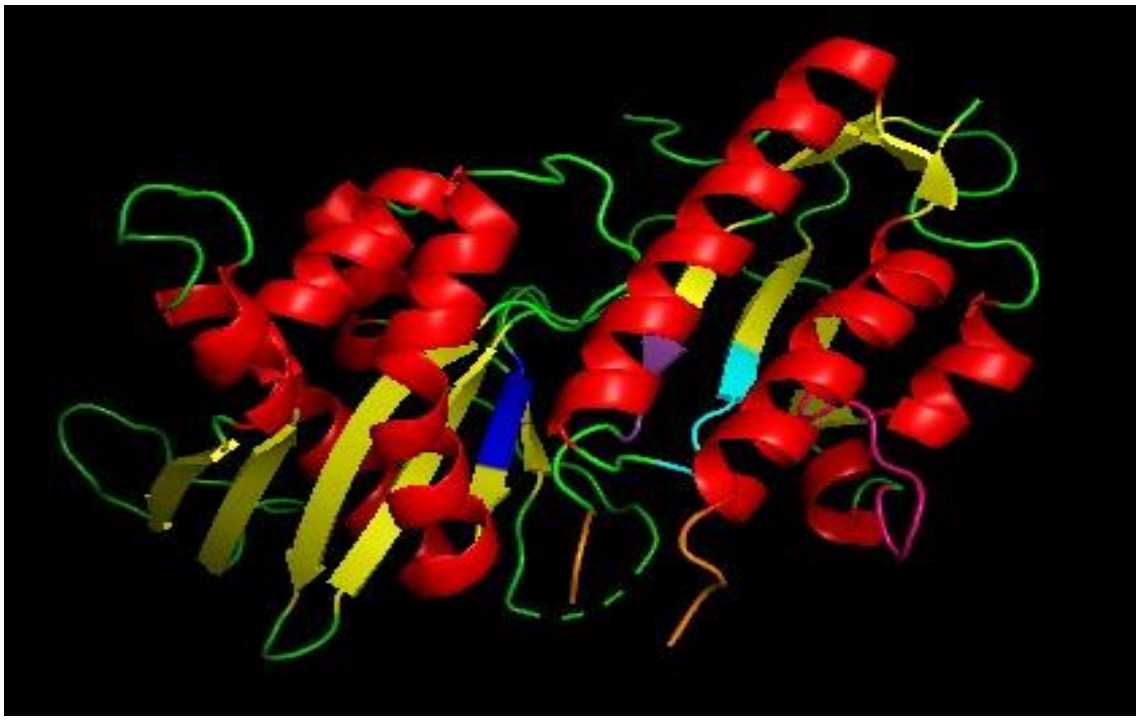

Figure 1.14. The crystal structure of zebrafish PIP5K1α kinase domain. This structure was deposited *by Hu et al., (2015)* into The Protein Data Bank *(Berman et al., 2000*) with the accession number, 4TZ7. In red are α-helices, in yellow are β-sheets and in green are disordered loop structures. Collectively these comprise the secondary structure of PIP5K1α.

The IIK motif consists of residues I169-K17 shown in blue. The MDYSL motif consists of residues M298-L302 depicted in cyan. In purple is the IDD motif comprising residues I376-D378. Amino acids K171, D299 and D378 (located in the IIK , MDYSL and IDD motifs respectively) serve a homologues function to K72, D166 and D184 found in PKA and participate in regulating catalytic activity. A partial sequence of the C terminal activation loop corresponding to 7 amino acids is shown in orange. Pymol 2.3.4 software was used to generate this ribbon diagram.

Table 1.9. FoldSeek outputs comparing the tertiary interactions of the PIP5K1α kinase domain (4tz7) to other available protein structures in the PDB100 database. E-scores generated by the FoldSeek server (*van Kempen et al., 2023)* highlight the conservation of tertiary structures between two different proteins. As a control, the crystal structure of PIP5K1α kinase domain (4tz7) was compared to itself, resulting in the most significant E-Score.

Crystal Structure (PDB ID)	Description	E-Score
4tz7	Crystal structure of zebrafish PIP5K1α kinase domain	3.85e-68
6ux9	Crystal structure of PIP4K2A	1.17e-28
1bo1	X-Ray diffraction of PIP4K2B	5.37e-27
2gk9	X-Ray diffraction of PIP4K2C	3.98e-20
7k2v	Electron microscopy of PIKfyve	1.43e-17

Whilst the kinase domain of PIP5K1α has been crystalized, additional structural biology approaches to characterise the N and C termini of PIP5K1α have been less successful. The compounding reason for this is that the poorly conserved N and C termini are highly disordered. However, one feature which has been successfully characterised and is conserved between Type I PIP5Ks and Type II PIP4Ks is the C terminal activation loop *(Kunz et al., 2000).* This structure (consisting of the residues QSYRFVKKLEHSWKALVH-----DGDTV) facilitates PI(4)P substrate processing and mediates recruitment to the plasma membrane *(Kunz et al., 2000).*

Using nuclear magnetic resonance, *Liu et al., (2016)* was able to show that in the absence of phospholipids the activation loop exhibits an unstructured conformation. Subsequently, in the presence of phospholipids this causes the activation loop to fold into a more structured amphipathic helix conformation *(Li et al., 2016).* By conducting proline scanning on the hydrophobic residues in the activation loop, mutagenesis of L389 and W393 suppressed PI(4)P processing and kinase activity *(Li et al., 2016).*

Interestingly *in silico* modelling from the Sansom group then suggested that PI(4,5)P_2 can also interact with the activation loop *(Amos et al., 2019).* This therefore could reflect a possible negative feedback mechanism where generated PI(4,5)P_2 could compete with PI(4)P substrates, in turn antagonising lipid kinase activity *(Amos et al., 2019).*

Further regulation of PIP5K kinase activity has recently been shown by the Lewis Cantley lab. This work initially found that triple knockout of PIP4K2A/B/C in HeLa cells induces paradoxical elevations of PI(4,5)P_2 levels, an ~2 fold increase (*Wang et al., 2019).* Upon insulin stimulation, levels of PI(3,4,5)P_3 were increased ~4 fold in triple knockout HeLa cells, with this inducing greater downstream AKT phosphorylation relative to control HeLa cells *(Wang et al., 2019).* Subsequently it was discovered that PIP4Ks contain a N terminal motif (VMLLPDD) which mediates direct interaction to PIP5Ks, which modulates kinase activity *(Wang et al., 2019).* Therefore, attenuating the expression of PIP4Ks would lose the negative regulation that this kinase family exerts upon PIP5Ks, resulting in aberrant kinase activity.

1.15. Regulation of PIP5Ks by Small GTPases

With PIP5K1a exerting a predominant membrane localisation, this is important in the regulation of membrane dependent signalling processes such as cell migration and proliferation *(Mao and Yin 2007).* A spectrum of small GTPases are crucial in regulating PIP5K1α activity in the context of plasma membrane signalling cascades, with a summary provided in *Table 1.10.* Some of the first small GTPases reported to interact with PIP5K1α (in conjunction with PIP5K1β and PIP5K1γ) include Cdc42, RAS homolog family member A (RhoA) and Rac Family Small GTPase1 (Rac1), in an GTP independent manner, with these interactions triggering PI(4,5)P_2 synthesis *(Weernink et al., 2003).*

In regards to Rac1, this GTPase regulates membrane ruffling *(Ridley et al., 1992 ; Allen et al., 1997)* the process of which actin rich protrusions form when the plasma membrane is reorganised rapidly *(Mahankali et al., 2011).* When MG-64 osteosarcoma cells are treated with platelet derived growth factor (PDGF) this induces membrane ruffling, which is then suppressed by overexpressing kinase dead PIP5K1α *(Doughman et al., 2003).* Similar phenomena were also observed in permeabilised platelets, where addition of kinase dead PIP5K1α attenuates actin assembly when platelets are treated with thrombin *(Tolias et al., 2000).*

It's thought that $PI(4,5)P_2$ produced from PIP5K1α binds to capping proteins (such as gelsolin), which reside on the barbed end of actin filaments *(Tolias et al., 2000).* $PI(4,5)P_2$ binding causes actin uncapping due to dissociation of capping proteins allowing actin monomers to join onto the barbed ends, leading to actin polymerisation *(Tolias et al., 2000).* Additionally, as PDGF stimulates $PI(3,4,5)P_3$ production this increases Rac1 activity as this GTPase possesses a PH domain adjacent to its Dbl homology (DH) domain, which drives GTPase activity *(Hoffman and Cerione, 2002 ; Doughman et al., 2003)*. In essence, upon agonist stimulation a feed forward loop arises in which elevated Rac1 activity will increase $PI(4,5)P_2$ levels leading to actin polymerisation. Subsequent synthesis of $PI(3,4,5)P_3$ would then further potentiate Rac1 activity.

More recently it has been identified that PIP5K1α can interact with constitutively active (G12V) Kirsten rat sarcoma viral oncogene homolog (KRAS) (*Adhikari and Counter, 2018).* The interaction between PIP5K1α and oncogenic KRAS is thought to stimulate $PI(4,5)P_2$ production where KRAS bound PI3K (in close proximity to PIP5K1α) can then phosphorylate $PI(4,5)P_2$ *(Adhikari and Counter, 2018).* KRAS (and Rac1) utilise residues located in their C-terminal hypervariable region to interact with PIP5K1α *(Weernink et al.,2003 ; Adhikari, and Counter., 2018).*

PIP5K1α binding to KRAS is thought to potentiate the oncogenic activity of the GTPase, with siRNA knockdown of PIP5K1α resulting in reduced cell proliferation, attenuated AKT phosphorylation and decreased ERK phosphorylation in pancreatic cancer cells *(Adhikari and Counter, 2018).*

Additionally, the role of the small GTPase ADP Ribosylation Factor 6 (ARF6) has been implicated in driving cell proliferation in a PIP5K1α dependent manner *(Tsai et al., 2017).* siRNA knockdown of ARF6 in HepG2 cells that have been treated with Hepatocyte Growth Factor (HGF) causes reductions in AKT phosphorylation *(Tsai et al., 2017).* Subsequently *Tsai et al., 2017* demonstrated through immunoprecipitation assays that cell treated with HGF or expressing constitutively active ARF6 enhances the interaction between PIP5K1α and the RTK c-Met. What is currently unknown is whether additional adaptor proteins are required to bring ARF6 and PIP5K1α to activated C-Met *(Tsai et al., 2017).*

Table 1.10. Summary of Small GTPases which have been reported to interact with PIP5K1α, and the effects of this interaction.

Small GTPase	Effect of PIP5K1A Interacting with Small GTPase	Reference
Cdc42	Initiates membrane ruffling which causes remodeling of the actin cytoskeleton.	*(Weernink et al., 2003).*
RhoA	Initiates membrane ruffling which causes remodeling of the actin cytoskeleton.	*(Weernink et al., 2003).*
Rac1	Initiates membrane ruffling which causes remodeling of the actin cytoskeleton.	*(Weernink et al., 2003).*
KRAS	Required for cell proliferation.	*(Adhikari and Counter, 2018).*
ARF6	Required for cell proliferation.	*(Tsai et al., 2017).*

1.16. Regulation of PIP5K Activity by Post Translational Modifications

An additional means of regulating the activity of PIP5Ks comes through PTMs. One of the earliest examples of this comes from the Wirtz and Anderson laboratories, both of which demonstrated that phosphatidic acid (PA) can increase the lipid kinase activity of PIP5Ks *in vitro (Moritz et al., 1992; Jenkins et al., 1994).* A possible mechanism accounting for increased lipid kinase activity after agonist treatment comes from Takenawa laboratory.

Park et al., (2001) demonstrated that mouse PIP5K1α can be dephosphorylated by the Ser/Thr phosphatase protein phosphatase 1 (PP1) which stimulated lipid kinase activity. The PKC pathway was thought to mediate this dephosphorylation event as the PKC agonists lysophosphatidic acid (LPA) and phorbol 12-myristate 13-acetate (PMA) also triggered increased lipid kinase activity *(Park et al., 2001).* On the other hand, PKAs exerted negative regulation on this signalling axis by phosphorylating S214, a central residue in the kinase domain of mouse PIP5K1α *(Park et al., 2001).* However, S214 is not conserved between mouse and human PIP5K1α. Interestingly, PKC was found to phosphorylate human PIP5K1β on S413 in light of PMA treatment and cell stress *(Van Den Bout et al., 2013). In vitro,* PIP5K1β harbouring a S413D mutation resulted in a 40% reduction in kinase activity relative to wildtype (WT) PIP5K1β *(Van Den Bout et al., 2013).* Interestingly the S413 residue is conserved in PIP5K1α (S460), with further possible PKC phosphorylation sites highlighted in *Table 1.11.*

In addition, work by *Itoh et al., (2000)* showed that *in vitro* all three PIP5K family members can undergo autophosphorylation in the presence of phosphatidylinositol. It was subsequently discovered that autophosphorylation of serine and threonine residues of PIP5Ks attenuates kinase activity *(Itoh et al., 2000).* This mode of regulation shares parallels with that of Class IA PI3Ks; where autophosphorylation of regulatory and catalytic subunits also reduces kinase activity (*Dhand et al., 1994 ; Vanhaesebroeck et al., 1999*).

The processss of SUMOylation involves formation of an isopeptide bond between the C terminus of small ubiquitin-related modifier (SUMO) and a lysine residue of a target protein *(Yang et al., 2017).* Four different SUMO isoforms have been reported in the literature *(Wilkinson and Henley, 2010).* However, in mammalian cells SUMO-1, SUMO-2 and SUMO-3 are the predominantly expressed, with as mass of ~11kDa *(Han et al., 2018).* Subsequent work by the Siddhanta group explored how SUMOylation could regulate PIP5K1α function. In the group's first PIP5K/SUMO publication, they identified that nuclear PIP5K1α is modified by SUMO-1; however in light of cell stress SUMO-2 modifications predominates *(Chakrabarti et al., 2013).* Then, using an *in silico* predictor tool (SUMOplot) revealed three lysines (K33, K244 and K490) as possible sites of SUMOylation *(Chakrabarti et al., 2015).* Subsequent mutagenesis of K244 and K490 (to alanine residues) blocked migration of PIP5K1α to the nucleus and nucleolus respectively *(Chakrabarti et al., 2015).* Interestingly when K490 is SUMOylated, this promoted the interaction between Histone H3 Lysine 9 Trimethylation (H3K9me3) and Heterochromatin Protein 1α (HP1-α) *(Chakrabarti et al., 2015).* This interaction resulted in downstream suppression of ribosomal RNA genes *(Chakrabarti et al., 2015).*

Table 1.11. Predicted PKC phosphorylation sites on PIP5K1α (isoform 1). Site predictions were made using Net Phos 3.1 *(Blom et al., 1999).* A cut of score of 0.5 used in these predictions.

Residue	Predicted Score
S6	0.672
S11	0.505
S27	0.661
S31	0.866
S68	0.595
T75	0.878
T76	0.873
T80	0.602
T81	0.662
S82	0.657
T96	0.664
S99	0.794
S101	0.642
T102	0.638
S175	0.603
S181	0.529

Residue	Predicted Score
T185	0.636
S251	0.521
S263	0.555
T264	0.860
S270	0.659
S317	0.588
T350	0.623
S408	0.901
T428	0.610
S430	0.833
T448	0.853
S460	0.804
S468	0.638
S470	0.695
S476	0.520
T486	0.819
T548	0.678

1.17. The PIP5K/PI(4,5)P_2 Signalling Axis in the Nucleus

It must not go unnoticed the role phosphoinositide signalling can exert on nuclear signal transduction, gene regulation and cell cycle progression. PIP5K1α kinase activity has been reported to be detected in the nucleus *(Loijens et al., 1996)* and synthesised PI(4,5)P_2 exhibits dynamic regulation. For instance, in HeLa cells, levels of PI(4,5)P_2 increase at the G1/S phase boundary and then decline more than 2 fold once cells enter S phase (*Stallings et al., 2005).* Prior this, *Clarke et al., (2001)* showed in murine erythroleukaemia cells that PI(4,5)P_2 concentrations can increase up to ~6 fold as cells progress from G1 to S phase.

The Anderson laboratory previously reported that PIP5K1α can localise to nuclear speckles, regions present in the nucleoplasm that contain mRNA-processing machinery *(Boronenkov et al., 1998).* Subsequently fibroblasts treated with transcription inhibitors have less nuclear speckles but increased the size of individual speckles *(Boronenkov et al., 1998).* This phenotype was characterised with alterations in PIP5K1α and PI(4,5)P_2 localisation, as shown through immunofluorescence using selective antibodies *(Fukami et al., 1988 ;*

Boronenkov et al., 1998). As the numbers of nuclear speckles decreases (and their individual sizes increases) this morphology is associated with reduced transcriptional output *(Misteli et al., 1997)* indicating a link between PI(4,5)P_2 and transcriptional control *(Boronenkov et al., 1998).* The localisation of PIP5K1α to the nucleus can be partly explained through nuclear localisation sequences being located within the C terminus, however these sequences are not found in all PIP5K1α isoforms *(Roberts et al., 2022).*

Nuclear PI(4,5)P_2 pools can be hydrolysed into IP_3 and DAG second messengers via the activities of nuclear phospholipases, this is predominately via PLC-β1 *(Martelli et al., 1992 ; Xu et al., 2001).* Seminal work by *Divecha et al., (1991)* showed in Swiss 3T3 cells that insulin-like growth factor 1 (IGF-1) treatment triggers nuclear DAG generation, with this leading to the recruitment of PKCα to the nucleus. Subsequently, the presence of additional PKC isoforms (βI, βII , δ, γ, ε, ζ) have shown nuclear localisation under differing stimuli where collectively they can phosphorylate histones, DNA topoisomerase and DNA polymerases which modulate gene expression *(Buchner, 2000 ; Martelli et al., 2006).*

PI(4,5)P_2 has been reported to interact with the C terminus of Histone H1, with this binding attributed to repressing the transcription inhibition Histone H1 exerts by RNA polymerase II *(Yu et al., 1998).* Interestingly a PKC phosphorylation site is located within the C terminus (S104) of Histone H1, which when phosphorylated is thought to reduce PI(4,5,)P2 binding to Histone H1 *(Yu et al., 1998).* Collectively this highlights the complex interplay of how PI(4,5)P_2 can modulate histones, either via direct interactions which can reverse transcription repression, or via generation of PI(4,5)P_2 which can ultimately activate PKC signalling.

Additionally, PIP5Ks have also been implicated with controlling gene expression networks through direct interactions with nuclear proteins. One of the first reports of this was by *Mellmen et al., (2008)* which found that PIP5K1α interacted with nuclear speckle targeted PIPKIα regulated-poly(A) polymerase (Star-PAP). This is a poly(A) polymerase which controls the expression of genes associated with oxidative stress

such as haem oxygenase-1 (HO-1) *(Mellman et al., 2008).* Co-immunoprecipitation assays confirmed that other PIP5K isoforms did not make this interaction with Star-PAP *(Mellman et al., 2008).* Subsequently RNAi of either PIP5K1α or Star-PAP attenuated the expression of HO-1 when HEK293 cells were subjected to oxidative stress *(Mellman et al., 2008).* Interestingly, $PI(4,5)P_2$ synthesised by PIP5K1α stimulates the kinase activity of PKCδ and CK1, both of which phosphorylate and activate Star-PAP's poly(A) polymerase activity *(Choi et al., 2016).*

Other nuclear proteins PIP5K1α has been reported to associate with includes c-FOS, a member of the activator protein 1 (AP-1) transcription factor family *(Ferrero et al., 2014).* As monomeric c-FOS can shuttle through cytoplasmic and nuclear compartments easier than its dimeric configuration, c-FOS can subsequently co-localise and physically associated with PIP5Ks *(Ferrero et al., 2014).* This was found to stimulate the production of nuclear $PI(4,5)P_2$ by ~2 fold *(Ferrero et al., 2014).* Similarly, the nuclear retinoblastoma protein (pRB), which regulates the transition of G1 to S phase was found to enhance PIP5K1α kinase activity ~4 fold *(Divecha et al., 2002).* Activation of PIP5K1α by pRB is mediated by the pocket domain of pRB interacting with the N terminus of PIP5K1α *(Divecha et al., 2002).*

Recently, the Anderson lab demonstrated that PIP5K1α can influence the stability of both wild type and mutant (R175H) p53 *(Choi et al., 2019).* The R175H p53 mutant is associated with oncogenic activities, such as attenuating the recruitment of MRE11-RAD50-NBS1 (MRN) complex which responds to double stranded DNA breaks *(Liu et al., 2009).* When cells expressing WT p53 are subjected to genotoxic or redox stress, this caused PIP5K1α to interact, whereas mutant p53 constitutively recruited PIP5K1α *(Choi et al., 2019).* $PI(4,5)P_2$ generated from PIP5K1α boundto the polybasic c-terminal regulatory domain (CTD) of p53, a region previously attributed p53 stability (*Ashcroft et al., 1999 ; Choi et al., 2019).* Synthesised $PI(4,5)P_2$ facilitated the recruitment of additional HSPs namely HSP27 and HSPB5 to further increase p53 stability *(Choi et al., 2019*

1.18. Chemical Inhibitors of PIP5K

With PIP5K1α activity implicated in a diverse range of signalling pathways, development of chemical probes reflects an important avenue of research in both academic and pharmaceutical settings. Classically, kinase inhibitors fall into three broad categories (*Table 1.12),* with most of the approved protein kinase inhibitors falling into Type I *(Roskoski, 2016).* The compounding issue with Type I kinase inhibitors however is poor selectivity towards the kinase of interest. This is due to the fact that the ATP binding pocket is conserved feature throughout the kinome (*Bhullar et al., 2018).* In the case of PIP5K1α, alternative approaches have utilised in order to antagonise this kinase.

Table 1.12. Mechanism of action of different types of kinase inhibitors.

Inhibitor Type	Mechanism of Action (as summarized by *Bhullar et al., 2018*)
Type I	Molecules which mimic the adenine moiety of ATP and compete for the phosphorylated active conformation of a kinases catalytic site
Type II	Molecules which target the unphosphorylated inactive conformation of a kinases catalytic site
Type III	Inhibitors which bind outside the ATP binding site / catalytic domain

Work by *Strätker et al., (2020)* previously explored whether chemical scaffolds in the form of pyranobenzoquinones could inhibit PIP5K1α activity. Screening of 29 different pyranobenzoquinones indicated that 11 compounds antagonise PIP5K1α at concentration of 50μM, with 4 from this pool then able to inhibit kinase activity at 10μM. Interesting, the most potent molecule from these inhibition studies (compound 13) did not act in an ATP dependent manner. This was revealed firstly through *in silico* docking where compound 13 was unable to dock to the kinase domain of human PIP5K1α. Secondly, in *vitro* assays with increasing concentrations of ATP then revealed that the IC50 for compound 13 was

not altered, highlighting that compound 13 antagonises PIP5K1α activity in an ATP independent manner.

Another example of ATP independent PIP5K inhibitors was recently described by *Sun et al., (2022).* In this approach, PI(4)P mimetics were synthesised which compete with the substrate binding site of PIP5Ks. Through *in vitro* kinase assays, the inhibition of the lead PI(4)P mimetic (compound 6) could be relieved by adding excess PI(4)P into the reaction mix, and not through excess ATP.

Whilst selective PIP5K1α (with an IC_{50} of ~15 μM) , compound 6 also antagonises PIP4Ks and most potently PIKfyve (an IC_{50} 6.2μM). Through kinase activity screening using the KinaseProfiler™ platform, this revealed that compound 6 had only modest effects towards Class I PI3Ks, with a reduction of activity of ~20% observed for just the p110β and p110γ isoforms.

The most widely used PIP5K1α inhibitor in the literature is ISA-2011B, developed by Persson laboratory *(Semenas et al., 2014).* This binding of this inhibitor was screened to 80% of the kinome using the KINOMEscan platform. ISA-2011B exhibited the highest binding affinity towards PIP5K1α, along with selectivity towards MAP/microtubule affinity-regulating kinases 1 and 4 (MARK1 and MARK4). Administration of ISA-2011B was shown to reduce the protein levels of PIP5K1α *in vitro (Semenas et al., 2014)* however, kinase assays by *Strätker et al., (2020)* then revealed that ISA-2011B was unable to block human PIP5K1α activity. As such, rather than directly reducing enzymatic activity, ISA-2011B may block $PI(4,5)P_2$ synthesis through acting as a destabilising agent which promotes PIP5K1α degradation. Whilst the mechanism of action of this compound is not fully clear, nevertheless ISA-2011B exerts potent anti-tumour activity.

1.19. The Role PIP5K1α in Prostate Tumorigenesis

Of interest to us and our collaborators *(Semenas et al., 2014 ; Sarwar et al., 2016 ; Mandel et al., 2018 ; Larsson et al., 2019 ; Wang et al., 2022)* is how the dysregulated PIP5K1α activity is implicated in prostate tumorigenesis. Whilst gene amplifications in PIP5K1A are not apparent in primary malignancies approximately 5-10% of advanced prostate cancer patients possess PIP5K1A gene amplifications *(Figure 1.15).* Overexpressing PIP5K1α in the immortalised prostatic cell line PNT1A resulted in increased $PI(4,5)P_2$ levels, elevated AKT phosphorylation and enhanced cell proliferation *(Semenas et al., 2014)*.

The therapeutic potential of targeting PIP5K1α has been shown *in vivo*. When chemical inhibition of this kinase through ISA-2011B administration was conducted on PC-3 tumour xenografts, this caused significant reductions in tumour volume and mass *(Semenas et al., 2014)*. Reductions in tumour volume and mass has also been observed after ISA-2011B treatment in mouse xenograft models for triple negative breast cancer *(Sarwar et al., 2018)*

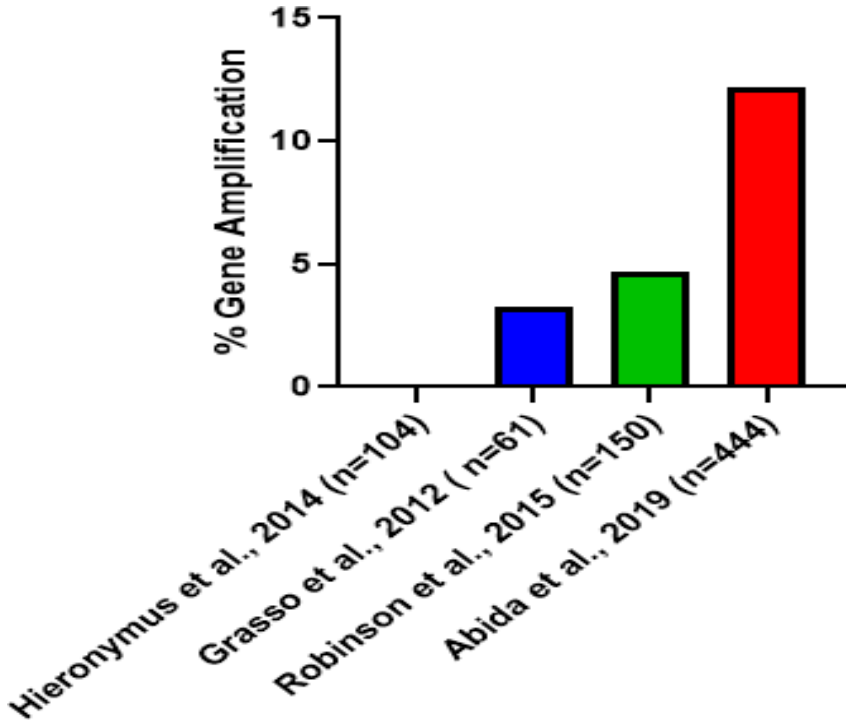

Figure 1.15. PIP5K1A gene amplifications in primary and advanced prostate cancers. In *Hieronymus et al., (2014),* 104 primary prostate cancers were sequenced. The three other studies listed *(Grasso et al., 2012 ; Robinson et al., 2015 ; Abida et al., 2019)* are from advanced prostate cancer patient cohorts. Data was obtained via the cBioPortal *(Gao et al., 2013).*

Aside from generating $PI(4,5)P_2$, PIP5K1α is also thought to influence prostate cancer tumorigenesis via interactions with AR and AR-V7. By immunoprecipitation assays PIP5K1α was shown to interact with AR / AR-V7 and CDK1 in cytoplasmic and nuclear fractions; where in complex these proteins are speculated to modulate target gene expression *(Sarwar et al., 2016*). Additionally, *Sarwar et al., (2016)* showed the administration of ISA-2011B not only reduces PIP5K1α protein levels but also AR, AR-V7 and CDK1 levels; suggesting that PIP5K1α binding to these proteins may increases their stability.

By inhibiting PIP5K1α by using ISA-2011B this has also shown to reduce the protein expression of the RTKs Epidermal Growth Factor Receptor (EGFR) and Vascular Endothelial Growth Factor Receptor (VEGFR) *(Mandel et al., 2018 ; Larsson et al., 2019).* In the context of prostate cancer, the expression of these RTKs are upregulated in advanced metastatic disease, therefore these proteins reflect valuable drug targets *(Kausbal et al., 2005 ; Tsourlakis et al., 2015). In vitro* blockade of EGFR and VEGFR1/2 expression via ISA-2011B was shown to reduce the invasive phenotype of VCaP prostate cancer cells *(Mandel et al., 2018, Larsson et al., 2019).* These findings suggest that PIP5K1α activity may also be needed for regulating the expression and activity of upstream RTKs, proteins which positively regulate phosphoinositide signalling pathways. However these results may be compounded by the non-selective mode of action of ISA-2011B, in which protein destabilisation is induced (*Strätker et al.,2020)*

1.20. Project Aims

The origins of this PhD project stem from collaboration with the Persson laboratory which developed the PIP5K1α inhibitor ISA-2011B. To supplement the small molecule work conducted by the Persson laboratory, the involvement of the Heery laboratory with this project was to take an genomics approach. This was to further explore the possible therapeutic of antagonising PIP5K1α function in the context of prostate cancer. Previous laboratory colleagues within the Heery lab used Clustered regularly interspaced short palindromic repeats (CRISPR)-Cas9 gene editing to generate cell lines with reduced or abrogated PIP5K1A expression.

The cell line which underwent CRISPR-Cas9 gene editing in this work was the LNCaP C4-2 prostate cancer cell line. This cell line was chosen as it mimics advanced prostate cancers, where C4-2 cells exhibit androgen independence *(Thalmann et al., 1994)* However, in the presence of elevated levels of androgens, growth of C4-2 cells can be induced *(Pfitzenmaier et al., 2003 ; Tararova et al., 2007).*

Chapter 3 of this thesis will provide an overview to the work conducted by previous laboratory co-workers, resulting in the generation of two CRISPR edited clones namely LNCaP C4-2 PIP5K1A-ΔN (ΔN) and LNCaP C4-2 PIP5K1A-KO (KO). The direction Chapter 3 then explores is clarifying what gene expression networks and signalling pathways are altered in ΔN and KO clones. RNA-Sequencing (RNA-Seq) highlights that both clones exhibited modulated expression of genes implicated with cell cycle progression and androgen signalling. To validate the results observed *in silico* a range of *in vitro* assays have been conducted, such as: proliferation assays, rescue experiments, and western blotting.

Whilst Chapter 3 will have an emphasis of how PIP5K1α modulates gene expression pathways and nuclear signalling events, Chapters 4 and 5 will have a more membrane orientated focus. Chapter 4 describes experimental approaches to determine how perturbation of PIP5K1α may affect intracellular levels of key phosphoinositides. To achieve this,

lipid biosensors were used to track the localisation and abundances of these phosphoinositides in WT and CRISPR edited clones. With the roles that PIP5K1α and $PI(4,5)P_2$ exerts upon PKC signalling and cell migration, Chapter 4 also presents preliminary data to assess if these processes are hampered in ΔN and KO C4-2 cells.

Finally, with the central role that phosphoinositides exert upon AKT activation, AKT pathway activation has been investigated in Chapter 5. Interestingly, the ΔN clone possesses increases in AKT phosphorylation, which seems paradoxical given that overall expression of PIP5K1α expression is reduced. Subsequently, Chapter 5 will detail *in silico* and *in vitro* assays which have explored how the loss of PIK3R1 expression in ΔN may contribute to AKT activation.

Chapter 2
Materials and Methods

2.1. General Procedures and Reagents

General laboratory reagents were purchased as molecular biology grade. Double distilled water or deionized water (diH_2O) was used for the preparation of buffers and solutions. diH_2O was prepared using the Millipore Synergy UV-R Ultrapure water purification system.

When making buffers, solutes were mixed thoroughly with solvents using a magnetic stirrer. The pH of buffers and solutions was checked using a Jenway 3510 pH meter which was calibrated against standards of known pH. Sterilisation of buffers and solutions was achieved through filtration of solutions through filters (typically with a 0.2µM pore size) or through autoclaving. Benchtop autoclaves sterilised reagents through autoclaving for 20 minutes at 121°C with pressure of 15 PSI. Antibodies and probes used in this work are summarised in *Table 2.1.* Constructs used or generated this work are summarised in *Table 2.2.*

2.2. Molecular Biology Reagents

- Luria-Bertani (LB) Medium = 1% (w/v) tryptone, 1% (w/v) sodium chloride (NaCl) and 0.5% (w/v) of yeast extract. The pH was adjusted to 7.0 using sodium hydroxide (NaOH) and then brought up to a final volume of 1L with diH_2O sterilised by autoclaving. For solid LB agar medium (for making bacterial selection plates) 2% (w/v) bacteriological agar was added.
- Super Optimal Broth (SOB) = 2% (w/v) tryptone, 10mM NaCl , 2.5mM potassium chloride, 0.5% (w/v) yeast extract and 10mM magnesium sulphate. Brought to a final volume (typically 1L) with ddH_2O. NaOH was used to adjust pH to 7.0. Before use 10mM of sterile filtered magnesium chloride was added. For solid medium 2% (w/v) bacteriological agar was added.
- Super Optimal Broth with Catabolite repression (SOC) = same constituents as SOB, supplemented with 20mM glucose.

- CCMB80 Buffer, pH 6.4 = 10mM potassium acetate, pH 7.0, 80mM calcium chloride dihydrate, 20mM manganese(II) chloride tetrahydrate, 10mM magnesium dichloride hexahydrate and 10% (v/v) glycerol. Brought to a final volume (typically 1L) with ddH_2O. 0.1M Hydrochloric Acid (HCl) was added to obtain the desired pH. If solution is below pH 6.4, do not adjust.
- Ampicillin Stock Solution (1000X) = 100mg/ml ampicillin in 50% ethanol and 50% diH_2O. Stored at -20°C.
- Kanamycin Stock Solution (1000X) = 50mg/ml kanamycin dissolve in diH_2O. Stored at -20°C.
- 5X Tris/Borate/EDTA (TBE) running buffer = 450mM Tris Base, 40mM Ethylenediaminetetraacetic acid (EDTA) (pH 8.0), 448.8mM Boric Acid. Prepared as a 1L solution with ddH_2O.

2.3. Cell Biology Reagents

- 3-(4,5-Dimethylthiazol-2-yl)-2,5-Diphenyltetrazolium Bromide) (MTT) Solution = 5mg/ml MTT powder in 1X phosphatase buffer saline (PBS). Solution was sterilized by passing through a 0.2µM filter and wrapped in foil. Short term MTT stock solutions were kept at 4°C for 2-3 weeks, whilst long term stocks were stored at -20°C.
- Immunofluorescence blocking solution = 1% bovine serum albumin (BSA) diluted in 1X PBS.
- Phosphate buffered saline with Tween (PBST) (v/v) = 1X PBS supplemented with 0.1% (v/v) Tween 20.
- PBST-BSA (w/v) = 1X PBS supplemented with 0.1% (v/v) Tween 20 and 0.1% (w/v) BSA.
- Propidium Iodide Staining Solution (v/v) = 0.1% triton x-100 (v/v), 10µg/mL propidium iodide and 100 µg/mL DNase-free RNAase A in 1X PBS.

- Clonogenic Assay Fixation Solution = prepared as a 3:1 ratio of 100% methanol (v/v) and 100% acetic acid (v/v).
- 0.5% (w/v) Crystal Violet Solution= 0.5% crystal violet (w/v) in a 1:1 solution of 100% menthol and ddH_2O-.

2.4. Biochemical Reagents

- 10% (w/v) Sodium Dodecyl Sulphate (SDS) solution = 10% (w/v) SDS in diH_2O.
- 10% (w/v) Ammonium Persulphate (APS) Solution = 10% (w/v) APS in diH_2O.
- 4X SDS Page Loading Dye = 0.2M Tris-HCl (pH 6.5), 277mM SDS, 6mM bromophenol blue and 4.3M glycerol, prepared in diH_2O. 0.4M Dithiothreitol added just prior to use.
- 5X Tris-Glycine-SDS (TGS) Buffer = 1.92M (w/v) glycine, 0.5M (w/v) Tris and 0.5% (v/v) SDS prepared in 1L of ddH_2O.
- 10x High Glycine Transfer Buffer = 1.91M (w/v) glycine and 553.08mM (w/v) Tris prepared in 800mL of ddH_2O. 100ml of 10X transfer buffer was diluted with 700ml ddH_2O and 200ml methanol to generate a 1X solution.
- 0.1% (w/v) Ponceau S Solution = 5% acetic acid (v/v) and 0.1% (w/v) Ponceau S. Made up to 500mls with ddH_2O.
- 10X (w/v) TBS Solution = 200mM (w/v) Tris and 1.5M (w/v) NaCl prepared in 900mL of ddH_2O. HCl was added to obtain a pH of 7.6M. The final volume of the solution was brought to 1L using ddH_2O.
- 1X TBST (w/v) Solution = 1X TBS solution supplemented with 0.1% (v/v) of Tween 20.
- Western Blot Blocking Solution – BSA = 3% (w/v) BSA in 1X TBS.
- Western Blot Blocking Solution – Milk = 5% (w/v) powdered milk in 1X TBS.

- Radioimmunoprecipitation assay (RIPA) Buffer = 150mM NaCl, 25mM Tris base (pH 7.4). 0.1% (v/v) SDS and 0.1% (v/v) Triton x-100 in an appropriate volume of ddH_2O. RIPA buffer was aliquoted into 1ml aliquots and stored at -20° C.
- 25X Protease Inhibitor Cocktail = One cOmplete Protease Inhibitor tablet (Roche) dissolved in 2ml of diH_2O.
- Cell Lysis Buffer = 1ml aliquots of RIPA buffer were supplemented with 25X Protease Inhibitor Cocktail (v/v) diluting this to 1X. Additionally RIPA aliquots were supplemented with 200mM (v/v) sodium orthovanadate and 500mM (v/v) sodium fluoride (diluting to a final concentration of 1mM and 50mM respectively).

Table 2.1 Antibodies and probes used in this work. Manufacturer details, product application and concentrations used are tabulated.

Name	**Supplier**	**Product Code**	**Concentration Used**	**Application**
Phospho-Histone H2A.X (Ser139) (20E3) Rabbit Monoclonal	Cell Signalling Technology	#9718	1 : 400	Immunofluorescence
PIP5K1A Rabbit Polyclonal Antibody	Cell Signalling Technology	#9693	1 : 1000	Western Blot
Anti-Rabbit Alexa-Fluor-488 Secondary Antibody	Upstate (Merck Millipore)	#AP132JA4	1:1000	Immunofluorescence and Flow Cytometry
PI3 Kinase p85α (6G10) Mouse Monoclonal	Cell Signalling Technology	#13666	1 : 1000	Western Blot
GAPDH (14C10) Rabbit Monoclonal	Cell Signalling Technology	#2118	1 : 1000	Western Blot

Total Akt Rabbit Polyclonal Antibody	Cell Signalling Technology	#9272	1 : 2000	Western Blot
Phospho-Akt (Thr308) (D25E6) XP® Rabbit Monoclonal	Cell Signalling Technology	#13038	1 : 1000	Western Blot
Phospho-Akt (Ser473) (D9E) XP® Rabbit Monoclonal	Cell Signalling Technology	#4060	1 : 1000 1 : 400	Western Blot (1:1000) Flow Cytometry (1:400)
Phospho-(Ser) PKC Substrate Rabbit Polyclonal Antibody	Cell Signalling Technology	#2261	1:1000	Western Blot
Total p53 (DO-1) Mouse Monoclonal Antibody	Santa Cruz Biotechnology	sc-126	1:500	Western Blot
Total p21 (F-5) Mouse Monoclonal Antibody	Santa Cruz Biotechnology	sc-6246	1:500	Western Blot
KLK3 (D6B1) XP® Rabbit Monoclonal Antibody	Cell Signalling Technology	#5365	1:1000	Western Blot
Androgen Receptor (D6F11) XP® Rabbit Monoclonal Antibody	Cell Signalling Technology	#5153	1:2000	Western Blot
Anti-Androgen Receptor, PG-21 Rabbit Polyclonal Antibody	Sigma-Aldrich	06-680	1:500	Western Blot

Anti-rabbit IgG, HRP-linked Secondary Antibody	Cell Signalling Technology	#7074	1 : 5000	Western Blot
Anti-mouse IgG, HRP-linked Secondary Antibody	Cell Signalling Technology	#7076	1 : 5000	Western Blot
Alexa Fluor™ 568 Phalloidin	ThermoFisher Scientific	A12380	Per sample – 0.5µL from 400X stock diluted in 200uL PBS	Immunofluorescence
DRAQ5™ Fluorescent Probe Solution	ThermoFisher Scientific	#62251	1:2000	Immunofluorescence
FITC conjugated mouse anti-Bromodeoxyuridine Antibody	BD Biosciences	#51-33284x	20µL used per sample from a 25 µg/mL stock	Flow Cytometry

Table 2.2. Documentation of constructs used or generated in this work. For constructs which were purchased from Addgene, their product codes are included.

Plasmid Name	**Source**	**Use**	**Cited in**	**Addgene Product Code (if applicable)**
mVenus-N1	Gift from Dr Chris Roberts	Cloning Vector	*Koushik et al., 2006* *Roberts, 2022*	N/A
mCherry-N1	Generated	Cloning Vector	N/A	N/A

PIP5K1α-mVenus-N1	Gift from Dr Chris Roberts	PIP5K1α Expression Vector	*Roberts, 2022*	N/A
PSG5-HA-p85α	Gift from Bart Vanhaesebroeck	p85α Expression Vector – used in subcloning	*Jimenez et al., 1998*	N/A
p85α-mVenusN1	Generated	p85α Expression Vector	N/A	N/A
p85α-mCherryN1	Generated	p85α Expression Vector	N/A	N/A
Tubby-cYFP-R332H	Gift from Andrew Tinker	$PI(4,5)P_2$ Biosensor	*Quinn et al., 2008*	N/A
NES-mCherry-P4Mx1	Addgene – deposited by Gerry Hammonds	PI(4)P Biosensor	*Zewe et al., 2018*	#108143
pcDNA3.1_AktPH-mCherry	Addgene – deposited by Moritoshi Sato	$PI(3,4,5)P_3$ Biosensor	*Kawano et al., 2015*	#67301
EGFP-Grp1-PH	Gifted by Gillian Griffiths	$PI(3,4,5)P_3$ Biosensor	*He et al., 2008 ; Yip et al., 2008 ; Gawden-Bone et al., 2018*	N/A
NES-EGFP-cPHx3	Addgene – deposited by Gerry Hammonds	$PI(3,4)P_2$ Biosensor	*Goulden et al., 2019*	#116855
EGFP-PKCγ-C1A	Gifted by Gillian Griffiths	DAG Biosensor	*Oancea et al., 1998 ; Gawden-Bone et al., 2018*	N/A

2.5. Making Bacterial Selection Plates

Solidified LB agar was heated in a microwave on a high setting until molten. In between heating, the LB agar was briefly mixed. Once fully melted, the LB agar was allowed to cool to a more appropriate temperature or stored in incubator (set to 50°C) until required.

Subsequently, antibiotics used for selection were added to the molten agar at a concentration of 1/1000. The working concentrations for ampicillin and kanamycin was 100µg/mL and 50µg/mL respectively. LB agar supplemented with the relevant antibiotic was then poured onto sterile petri dishes that had a diameter of ~10cm.

2.6. Preparing Chemically Competent Cells

Competent cell seed stocks were prepared by first streaking *Escherichia coli (E.coli)* DH5α cells onto a SOB agar plate lacking antibiotics and left to incubate overnight at 37°C. The DH5α *E.coli strain* F– endA1 glnV44 thi-1 recA1 relA1 gyrA96 deoR nupG purB20 φ80dlacZΔM15 Δ(lacZYA-argF)U169, hsdR17(rK–mK+), λ– *(Bethesda Research Laboratories, 1986)* was purchased from Stragene. The next day, single colonies were picked and grown overnight in 2ml SOB medium, at 30°C with shaking. Afterwards, 1ml volumes of the overnight cultures were aliquoted into cryovials, followed by the addition of 150µl of sterile filtered glycerol. The seed stocks were frozen at -80°C until required.

To prepare DH5α competent cells, one seed stock was added to 250ml of SOB medium and incubated at 30°C with shaking, until an OD600 of 0.3 was reached (taking approximately 3-4 hours). Once the desired OD was met, DH5α competent cells were placed on ice for 10 minutes, before being centrifuged at 3000rpm at 4°C in pre chilled 50ml falcon tubes. The supernatant was removed, and the bacterial pellets were

resuspended gently in 10mls of ice cold CCMB80 buffer. Pellets were left to incubate on ice for 20 minutes before being centrifuged at 3000rpm at 4°C. The supernatant was removed, and the bacterial pellets were resuspended gently in 10mls of ice cold CCMB80 buffer. A repeat pipette was used to aliquot 100µl volumes of the resuspended pellets into chilled 500µl tubes. After aliquoting the DH5α competent cells were flash frozen with liquid nitrogen and then stored at -80°C until required.

2.7. Bacterial Transformations

Competent cells and plasmids were first thawed on ice for 10 minutes before pipetting 50µl of competent cells into 1.5ml Eppendorf tubes. Next ~50ng of the relevant plasmid was added to the competent cells and mixed gently. As a negative control, a 50µl aliquot of competent cells without plasmid was used. Competent cells were then left to incubate on ice for 30 minutes before being heat shocked at 42°C for 2 minutes. Subsequently, cells were left on ice for 5 minutes and then 950µl of antibiotic free LB medium (or SOC medium) was added to each 1.5ml tube. Cells were then incubated for 1 hour at 37°C in a shaking incubator. After 1 hour cells were centrifuged for 2 minutes at 2500rpm. A total of 900µl of supernatant was removed from each tube, with the remaining 100µl used for resuspending the bacterial pellet. The bacterial suspension was then plated on plates containing the appropriate antibiotic and left to incubate overnight at 37°C.

For determining the transformation efficiency of newly generated competent cells, 1ng of pUC19 plasmid was used for transformations. The number of colonies seen after incubating streaked plates overnight at 37°C was counted and used to calculate transformation efficiency expressed as CFU/µg of DNA. Transformation efficiencies were calculated using the science gateway online calculator (https://www.sciencegateway.org/tools/transform.htm) where CFU/µg = (number of colonies on plate / ng of DNA plated) x 1000 ng/µg

2.8. Purification of Plasmids and Vectors From Bacteria by Miniprep

Plasmid minipreps were conducted for small scale purification of constructs from bacterial cultures. This involved inoculating a single colony from a previously transformed bacterial plate into 10 ml of LB medium containing the appropriate antibiotic and grown overnight at 37°C with agitation. A 9ml volume was then taken from the saturated overnight culture and centrifuged at 4000rpm for 10 minutes, at 4°C. Subsequently DNA was purified from pelleted bacteria by using the Macherey-Nagel™ NucleoSpin Plasmid QuickPure™ Kit as per the manufacturer's instructions.

2.9. Large Scale Purification of Plasmids From Bacteria by Maxiprep

For large scale plasmid purification, 250µl from a saturated starter culture was inoculated into 250 ml of LB medium containing the relevant antibiotic and grown at 37°C with shaking overnight. A saturated 250ml culture was then separated into five falcon tubes (50 mls per tube) and centrifuged at 4000rpm for 10 minutes, at 4°C. The QIAGEN Plasmid Maxi Kit was used to purify plasmid DNA, as per the manufacturers protocol with the following revisions:

- Buffer P1 was added to one bacterial pellet and resuspended with a subsequent bacterial pellet. This was repeated until all bacterial pellets were mixed in Buffer P1.
- Centrifugation steps using QIAGEN Plasmid Maxi Kit were conducted at a lower speed (4000rpm) but for a longer time frame, a minimum of 30 minutes.

Eluted DNA was dissolved in 100µl-200µl of diH_2O, with the concentration of DNA determined using a NanoDrop® 1000 Spectrophotometer (Thermofisher).

2.10. Determining DNA and RNA Concentrations

For determining the concentration of DNA or RNA samples a NanoDrop® 1000 Spectrophotometer (Thermofisher) was used in conjunction with its respective software package (NanoDrop 1000 v3.8). The absorbance of nucleic acids was recorded by the nanodrop, with readings taken at 230nm, 260nm and 280nm. Nucleic acids concentrations were expressed as ng/µl based upon sample absorbance at 260nm. A derivative of Beer-Lamberts law was used to calculate the concentration of nucleic acids: C = (A x e) / b

Where:

- C = Samples concentration
- A= Samples absorbance at 260nm.
- e = wavelength-dependent extinction coefficient. This is recorded as ng-cm/µl and has a value of 40 and 50 for RNA and double stranded DNA respectively.
- b = Path length (cm). For nucleic acids path length is given as a value of 1cm.

A 260/280 ratio is also determined by the NanoDrop® 1000 Spectrophotometer. This ratio indicates the purity of a given sample; with a ratio of ~1.8 and ~2.0 indicating a pure DNA and RNA sample respectively.

2.11. Ethanol Precipitation of Nucleic Acids

To further purify nucleic acids ethanol precipitations were conducted. All reagents were placed in a freezer beforehand. Once reagents were cold to the touch two volumes of 100% ethanol were added to the nucleic acid samples, followed by 0.1 volumes of 3M sodium acetate. Nucleic acids were then stored at -80°C for at least 1 hour. Subsequently the samples were centrifuged at 14,000rpm, for 30 minutes at 4°C, with the

pellets then resuspended in 100µl of 70% ethanol. The suspension was then centrifuged at 14,000rpm for 30 minutes at 4°C and the supernatant carefully removed to minimise disruption to the nucleic acid pellet. Remaining ethanol was removed by incubating on a heat block set to 37°C for ~10 minutes before then resuspending the pellet in an appropriate volume of deionized water.

2.12. DNA Sequencing

DNA Sequencing was conducted by Source Bioscience (Cambridge). Concentrations of 100ng/µl plasmid DNA were sent for sequencing, in conjunction with a complementary primer with a concentration of 3.2pmol/µl or using a stock primer supplied by Source Bioscience (Cambridge). Total sequencing reactions were 5µl in volume. Sanger DNA sequencing was carried out by using an Applied Biosystems 3730 DNA Analyzer with PeakTrace™ software. Sequencing data provided by Source Bioscience was analysed using Snapgene Viewer software (https://www.snapgene.com/).

2.13. Polymerase Chain Reaction (PCR)

To synthesis DNA fragments used in the construction of recombinant plasmids PCR reactions were carried out using New England Biolabs (NEB) Phusion® High Fidelity DNA polymerase. This DNA polymerase possesses fidelity ~50 fold higher than Taq Polymerase and 5'-3' exonuclease activity, ensuring accurate DNA synthesis. A typical reaction mixture is described in *Table 2.3.* Once reaction mixtures were made, a thermal cycler was used to run the reactions using settings described in *Table 2.4.* Once reactions were completed 10% of the reaction mixture was run on an agarose gel to check that the size of synthesized DNA fragments was correct.

Table 2.3. Typical composition of PCR reaction components using Phusion® High Fidelity DNA polymerase.

Reagent	Volume (µl)
50ng Template DNA	1.0
10µM Forward Primer	2.5
10µM Reverse Primer	2.5
10mM dNTP Mix	1.0
1X Dimethyl Sulfoxide (DMSO)	1.5
5X Phusion HF Buffer	5
Phusion® High Fidelity DNA polymerase	0.5
Sterile H_2O	36.0

Table 2.4. Typical cycling conditions for PCR reactions usingPhusion® High Fidelity DNA polymerase.

PCR Step	PCR Parameter	Cycle Length
Initial Denaturation	98°C for 5 minutes	1
Denaturation	95°C for 30 seconds	25- 35
Primer Annealing	Typically, 50-60 °C for 15-30 Seconds	
Extension	72°C for 30 seconds per kilobase of DNA	
Final Extension	72 °C for 5-10 minutes	1

2.14. Colony PCR

For screening transformants, colony PCR was conducted using Taq Polymerase (NEB). The constituents of these PCR reactions are detailed in *Table 2.5.* Colonies which grew on antibiotic selection plates were picked with a sterile pipette tip and were inserted into 0.5ml tubes containing 20µl of nuclease free water. The pipette tip was then

removed, and the samples were placed in a heat box set to 95°C for 5 minutes. Afterwards, the samples were centrifuged at 11,000rpm for 2 minutes, with 2µl of supernatant used in PCR reactions. Cycling conditions for PCR reactions using NEBs Taq Polymerase are detailed in *Table 2.6.*

Table 2.5. Typical composition of components for colony PCR reactions using Taq DNA Polymerase.

Reagent	**Volume (µl)**
10X Standard Taq Reaction Buffer	2.0
10mM dNTPs	0.4
10µM Forward Primer	0.4
10µM Reverse Primer	0.4
Taq DNA Polymerase	0.1
Colony Supernatant	2
Nuclease free water	14.7

Table 2.6. Typical cycling conditions for colony PCR reactions using Taq DNA Polymerase.

PCR Step	**PCR Parameter**	**Cycle Length**
Initial Denaturation	95°C for 5 minutes	1
Denaturation	95°C for 30 seconds	25- 35
Primer Annealing	Typically, 50-60 °C for 30-60 Seconds	
Extension	68°C for 60 seconds per kilobase of DNA	
Final Extension	68 °C for 5-10 minutes	1

2.15. Agarose Gel Electrophoresis

Agarose gel electrophoresis facilitated the separation and visualisation of DNA molecules. Agarose gels (typically 0.8% w/v) were prepared by weighing out an appropriate mass of agarose into an Erlenmeyer flask followed by the desired volume of 1X TBE running buffer. The agarose/TBE mixture was boiled in a microwave until the agarose completely dissolved. Every 30 seconds the agarose/gel mixture was mixed in between boiling. Once the agarose was completely dissolved the flask was cooled until warm to the touch. Then, 2µl of ethidium bromide (from a 10mg/ml stock solution) was added to the cooled agarose/TBE mixture, swirled briefly and poured onto a gel mould that had a gel comb in place. Once the agarose gel had set, the comb was removed and the gel mould was placed in a BIO-RAD horizontal electrophoresis chamber. 1X TBE running buffer was added to cover the gel completely. Once samples and a DNA ladder were loaded onto the gel, a BIO-RAD PowerPac™ was used to conduct electrophoresis at 100V which facilitated the separation of DNA molecules. Agarose gel electrophoresis was conducted for 45-60 minutes before using a BIO-RAD Universal Hood II UV transilluminator to visualize imagemigrated DNA molecules. Gel images were analyzed using Quantity One 1-D Analysis Software (BIO-RAD).

2.16. Restriction Digests

When molecular cloning this typically involved using restriction enzymes to digest 1-2µg of vector and DNA insert. Typically, double digests were conducted using NEBs high fidelity enzymes, which are compatible with NEB*s* 10X CutSmart® Buffer. Total reaction volumes for cloning restriction digests were 50µl which required: 5µl of 10X CutSmart® Buffer, 1µl of each restriction enzyme, and a volume of insert or vector comprising of a total DNA mass of 1-2µg. diH_2O was used to fill the reaction volume to 50µl. Double digests were left to incubate for a

minimum of 2h at the correct temperature (typically 37 °C) before DNA purification. If two restriction enzymes were not compatible with each other, for instance requiring different reaction buffers, a single restriction digest was first conducted. Then, the digested DNA was ethanol precipitated and resuspended in an appropriate volume of diH_2O, before being digested by a second restriction enzyme.

Diagnostic digests were conducted as a means of further validating the size of DNA constructs and vectors. For diagnostic digests, 500ng of template DNA was digested for 1h at the correct temperature in a total reaction volume of 25µl. Afterwards, samples were then run on an agarose gel to check the size of digested DNA. All restriction enzymes used for restriction digests (either cloning or diagnostic) were purchased from either NEB or Roche.

2.17. Purification of DNA from Agarose Gels

DNA bands of interest which were identified by agarose gel electrophoresis were excised using a sterile scalpel under a UV transilluminator or a safeVIEW-MINI2 Blue Light Transilluminator (Cleaver Scientific). Subsequently, the excised bands were purifiedusing the NEB Biolabs Monarch® DNA Gel Extraction Kit as per the manufactures instructions. The concentration of purified DNA was determined the NanoDrop® 1000 Spectrophotometer and then stored at -20˚C until further use.

2.18. Ligation of complementary DNA molecules

Ligation reactions were conducted to anneal digested inserts to digested vectors, creating circularized plasmid. Typically, ligation reactions were carried out using a molar ratio of 3:1, insert to vector. This ratio was calculated by using the NEB ligation calculator (http://nebiocalculator.neb.com/#!/ligation) which uses the following

formula: Required mass insert (ng) = desired insert / vector molar ratio x mass of vector (ng) x ratio of insert to vector lengths

10µl ligation reactions were conducted, using the volumes of insert and vector to achieve desired molar ratios, along with 1µl 10X T4 Ligase Buffer (NEB), 0.5µl T4 Ligase (NEB) and nuclease free water up to 10µl. Reaction mixtures were incubated overnight in a thermal cycler using temperatures which cycled between 10°C and 30 °C, for 7.5 hours. After cycling, the reaction mixtures were then incubated at a fixed temperature of 16°C until bacterial transformations were conducted. The premise for cycling between 10°C and 30°C was due to the fact this has been previously reported that efficiencies of ligation reactions increase several fold through temperature cycle ligation *(Lund et al., 1996).*

2.19. CRISPR-Cas9 Gene Editing

CRISPR-Cas9 gene editing was conducted by previous laboratory colleagues and was carried out as followed. Pairs of RNA guides for Cas9 nickase (Cas9n) were designed using the Massachusetts Institute of Technology's (MITs) CRISPR Design search engine *(Hsu et al., 2013).* Pairs of guide RNAs which target Exon 1 or Exon 6 that had no off-target cleavage sites (detailed in *Table 2.7)* were synthesised and then cloned into the pX461 vector via BbsI restriction digest. Ligated products were transformed into *E.coli* DH5α cells and selected for ampicillin resistance. 1µg of purified CRISPR-Cas9n plasmids were transfected into LNCaP C4-2 cells through the Neon Transfection system (Invitrogen), following the manufacturers recommendation at a pulse voltage of 1200V. Control cells were transfected with 2µg of single guide expression vector for the targeted exon. After 48 hours post transfections, cells were sorted for GFP expression by flow cytometry and single cells plated onto 96 well plates. This process resulted in the generation of two CRISPR clones, ΔN LNCaP C4-2 cells (targeted to Exon 1) and KO C4-2 cells (targeted to Exons 1 and 6).

Genomic DNA was harvested from CRISPR edited cells using the GenElute Mammalian Genomic DNA Miniprep Kit (Sigma Aldrich). Genotyping through PCR was conducted using primers targeting the Cas9n targeted regions: PIP5K1A Exon 1 Forward (CCTTGAGCTGGTCCAGGAG), PIP5K1A Intron 1/2 Reverse (TCTTCCTCCCATCGCATATT), PIP5K1A Exon 6 Forward (GGGAGCAACCTGACCCCTGC) and PIP5K1A Intron 5/6 (CACAAAAATCAACTACAGATGC). PIP5K1α protein expression in CRISPR clones was determined through western blotting. Both genotyping and western blotting of ΔN and KO LNCaP C4-2 cells was replicated during the course of this work to validate the cell lines. Further details regarding ΔN and KO LNCaP C4-2 cells is discussed Chapter 3.

Table 2.7. Guide RNAs used in CRISPR-Cas9 gene editing. CRISPR guides used by previous laboratory colleagues (Dr Miguel Hernandez-Quiles and Dr Jonathan Whitchurch) for generation of ΔN and KO LNCaP C4-2 cells. Guide RNAs were designed by using the MITs CRISPR guide design tool *(Hsu et al., 2013).*

Guide	Guide RNA Top	Guide RNA Bottom	Target Exon
1	CACCGGCCTGGCT CTCTTTCAATC	CCCGGACCCGAG AGAAAGTTAGCAA	1
2	CACCCGGGGGAGG GGGCTGCTAAGA	CCCCCCTCCCCC CGACGATTCTCAA	1
3	CACCGATGCTTACC AATAATCAT	CTACGAATGGTTC ATTAGTACAAA	6
4	CACCGCACTGTGA CTCCAGTATCAG	CGTGACACTGAG GTCATAGTCCAAA	6

2.20. RNA Extraction from Mammalian Cell Lines and cDNA synthesis

5×10^5 WT, ΔN and KO LNCaP C4-2 were centrifuged at 1500rpm for 5 minutes and the supernatant removed. RNA from cell pellets was harvested using the Qiagen RNeasy Mini Kit as per the manufacture's instructions. The concentration of eluted RNA was determined using a NanoDrop® 1000 Spectrophotometer (ThermoFisher). Eluted RNA was stored at -80°C. A minimum of 50ng of extracted RNA was used as a template for reverse transcription reactions using the QIAGEN QuantiTect Reverse Transcription kit as per the manufacturer's instructions.

2.21. Assessing Gene Expression by RT-qPCR

Master mixes containing the relevant volumes of RT-qPCR reagents were set up as described in *Table 2.8.* Reactions were set up in 96 well qPCR plates or qPCR strips *(*Agilent). For each reaction 1µl of WT, ΔN and KO LNCaP C4-2 cDNA was added to each well followed by 9µl of relevant master mix. Pulse centrifugation was conducted to ensure that cDNA mixed thoroughly. Samples were then placed into a Stratagene Mx3005P qPCR and SYBR dissociation curves were generated using machine programme described in *Table 2.9.* An example of dissociation curve analysis (using MXPRO software) can be found in *Figure 2*.1. A single curve can be viewed in *Figure 2.1* when ΔN C4-2 cDNA is used as input for RT-qPCR reactions using the GUSB housekeeping gene. A housekeeping gene is defined as a gene which is consistently expressed across different cell types and encodes proteins which are essential to cellular maintenance *(Joshi et al., 2022).* The function of GUSB is to encode a lysosomal enzyme which degrades large polysaccharides known as glycosaminoglycan *(Kong et al., 2022).* GUSB was selected as a housekeeper in RT-qPCR assays due to this gene showing minimal changes in RNA read counts and overall expression between WT, ΔN and KO LNCaP C4-2 cells.

The $2^{-\Delta\Delta Ct}$ method *(Livak, andSchmittgen, 2001)* was used to calculate relative gene expression from raw cycle threshold (Ct) values normalised to the expression of GUSB. Primers used in RT-qPCR reactions are detailed in Table 2.10.

Table 2.8. Per well reaction volumes for RT-qPCR reagents.

Reagent	**Volume per well (µl)**
Sterile H_2O	3.95
Forward primer (100 µM)	0.025
Reverse primer (100 µM)	0.025
Agilent Technologies Brilliant II SYBR Green qPCR master mix	5.0
cDNA	1
Total per well/PCR tube	10

Table 2.9. Cycling conditions for Stratagene Mx3005P qPCRmachine.

Number of Cycles	**Time**	**Temperature**
1	10 mins (Denaturation)	95°C
40	30 secs (Denaturation)	95°C
	1 min (Primer annealing)	60°C
	1 min (Extension)	72°C
1	1 min (melt curve analysis)	95°C
	30 secs	60°C
	30 secs	95°C

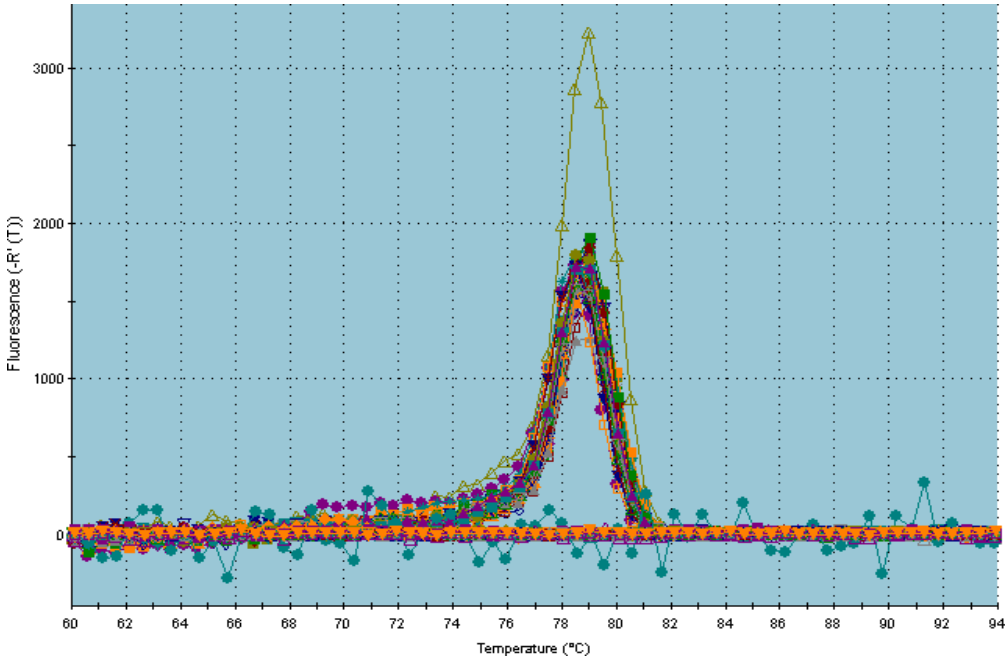

Figure 2.1. Dissociation curve analysis for GUSB housekeeping gene. ΔN LNCaP C4-2 cDNA as input for RT-qPCR reactions. MXPRO software was used to generated dissociation curve which indicates the presence of a single fluorescence peak.

Table 2.10. List of primers used in RT-qPCR assays.

Gene Name	Direction (5'-3')	Sequence	Source
GUSB	Forward	CTCATTTGGAATTTTGCCGATT	Described in *Abernathy et al., (2015)*
GUSB	Reverse	CCGAGTGAAGATCCCCTTTTTA	Described in *Abernathy et al., (2015)*
PIP5K1A	Forward	GCAGCGTGACTGTTTGGTG	Gift from Chris Roberts
PIP5K1A	Reverse	CACTGCTTAAGGGCTCTCGTT	Gift from Chris Roberts
KLK3	Forward	AGTGCGAGAAGCATTCCCAA	This work
KLK3	Reverse	GCAAGATCACGCTTTTGTTCCT	This work
PIK3R1	Forward	TGGAGCGGAGTTGGAGGAA	This work
PIK3R1	Reverse	CACACGAGCTTCACCCCG	This work

2.22. RT-qPCR primer design

In this work RT-qPCR primers were designed against transcript(s) of interest using NCBI Primer-BLAST *(Ye et al., 2012)*. The NCBI gene accession number was as an input for primer design. For detecting several mRNA splice variants the "*Allow primer to amplify mRNA splice variants"* function was enabled. This feature was disabled when designing isoform specific primers. Additional parameters used for primer design are detailed in *Table 2.11.*

Table 2.11. Parameters used for designing RT-qPCR primers in NCBI Primer-BLAST.

Parameter	Value
PCR Product Size	Between 70 – 200 bps
Number of primers to return	20 different primer sets
Primer melting temperatures	Minimum – 59– COptimal - 60–C Maximum - 61°C
Exon Junction Span	Primer must span an exon-exon junction
Primer specificity stringency	Ignore targets that have 1 or more mismatches to the primer.

Cell Biology Methods

2.23. Maintenance of Mammalian Cell Lines

The metastatic human prostate cancer cell line LNCaP C4-2 *(Thalmann et al., 1994)* was a gift from Dr Nigel Mongan. WT and CRISPR edited LNCaP C4-2 cells were cultured in Roswell Park Memorial Institute (RPMI)-1640 medium supplemented with 10% (v/v) foetal bovine serum (FBS), 1% (v/v) sodium pyruvate, 1% (v/v) penicillin/streptomycin and 1% (v/v) L-glutamine (complete medium). Cells were kept in a humidified incubator at 5% CO_2 and passaged when confluence reached ~80%.

2.24. Cryoprotection and Revival of Mammalian Cell Lines

WT, ΔN and KO LNCaP C4-2 cells were centrifuged at 1500rpm for 5 minutes and the supernatant removed and suspended in 3mls of complete medium before cell counts using a haemocytometer were conducted. Cells were then diluted to a density of $1x10^6$ cells/ml and then centrifuged again at 1500rpm for 5 minutes. The supernatant was then removed, and cell pellets were resuspended in 1ml of freezing medium, containing 90% (v/v) FBS and 10% (v/v) DMSO. Cryovials were then placed in an isopropyl alcohol freezing chamber and frozen at -80 °C overnight. The next day the cryovials were removed from the freezing chamber and transferred to a separate container in a -80 °C freezer (for short term storage) or transferred to a liquid nitrogen dewar for long term storage.

To revive frozen cell lines, cells were placed in 5mls of pre-warmed complete medium and centrifuged at 1500rpm for 5 minutes to remove the DMSO. The supernatant was removed and cell pellets were resuspended in 5mls of complete medium before being transferred to a sterile culture vessel.

2.25. Crystal Violet Staining Assay

Crystal violet staining assays were conducted to measure cell proliferation and growth. For this 2.5×10^3 WT, ΔN and KO LNCaP C4-2 cells were seeded in 6 well plates in technical triplicates and grown for 7 days in complete medium. The culture medium was changed after 3 days. After 7 days the culture medium was removed and wells were treated with 1ml of clonogenic assay fixation solution and incubated at room temperature for 15 minutes. Then the fixation solution was removed and each well was treated with 1ml of 0.5% (w/v) crystal violet solution for 15 minutes. Afterwards, the 0.5% (w/v) crystal violet solution was removed and each well was washed gently with 1ml of ddH_2O in

order to remove any excess crystal violet. Plates were inverted and left to dry overnight with photos of each plate taken the next day. Photos of individual wells were taken using an Apple iPhone 12, and the images were exported into ImageJ software *(Schneider et al., 2012)*. Area readings (reflecting the confluency of each well) were recorded inImageJ software. Individual area readings were processed using GraphPad Prism 9.2 software, where average area readings, and significance differences between the cell lines were calculated and plotted as a bar chart.

2.26. MTT Assays

MTT assays were conducted to assess CRISPR cell line viability relative to WT LNCaP C4-2 cells. For this, WT, ΔN and KO C4-2 cells were seeded in quintuplicates at a density of 5.0×10^3 cells per well (in a 96 well plate) and allowed to adhere overnight in a humidified incubator at 37 °C, 5% CO_2. Five separate wells were also filled with 100µl of complete medium. The next day 20µL of MTT solution was added to the cells and incubated at 37 °C, 5% CO_2 for 2 hours. Afterwards the media and MTT was aspirated from the cells, and 150µl 100% DMSO was added to each well to solubilize the formazan crystals formed after incubation. The 96 well plate was wrapped in foil and placed on an orbital shaker for 10 minutes, before the absorbance of each well read at 570nm using a Synergy HT microplate reader. This procedure was conducted at three time points: 24h , 48h and 72h. Average absorbance readings were taken with the absorbance readings for each cell line tested corrected by subtracting the background absorbance from complete medium wells. The readings were processed using GraphPad Prism 9.2 software, where significance differences between the cell lines after 24h, 48h and 72h was calculated.

2.27. Cell Cycle Analysis by Bromodeoxyuridine (BrdU) Incorporation

2×10^5 LNCaP C4-2 cells (WT, ΔN and KO) were seeded in triplicate into 12 well dishes and allowed to adhere overnight in complete medium. The next day the culture medium was removed and each well was supplemented with complete media containing 20µM BrdU. Cells were then incubated with BrdU for 2 hours at 37 °C , 5% CO_2. Afterwards, cells were resuspended in their media and then centrifuged for 5 minutes at 1500rpm with the supernatant then removed. Cells were fixed by resuspending in 0.5ml of ice-cold PBS, followed by the addition of 4.5ml of ice-cold 70% ethanol and left overnight at 4°C. The next day, fixed cell suspensions were centrifuged at 1500rpm for 5 minutes before being permeabilised by resuspending in 0.5ml of PBST-BSA. Cells were left to permeabilised at room temperature for 30 minutes before being centrifuged for 5 minutes at 1500rpm. The supernatant was removed and then each pellet was resuspended in 1M HCl and left to incubate for 1 hour at room temperature.

Cells were then centrifuged for 5 minutes at 1500rpm and resuspended in 1X PBS twice over. After PBS washes and respective centrifugation steps each cell pellet was resuspended in 100µl PBST-BSA followed by the addition of 20µl FITC conjugated mouse anti-BrdU antibody *(Table 2.1).* Cell suspensions were left to incubate with FITC conjugated anti-BrdU antibody for one hour in the dark at room temperature. Afterwards, cells were centrifuged at 1500rpm for 5 minutes, pellets washed in 1X PBS and pelleted again. Pellets were then resuspended in 500µl propidium iodide staining solution, with the contents transferred to 5ml Fluorescence-activated cell sorting (FACS) tubes. Samples were then wrapped in foil and transferred to School of Life Sciences Flow Cytometry Facility where sample fluorescence (at 488nm wavelength) was determined by using a Beckman Coulter FC500 Flow Cytometer.

2.28. Cell Migration Assays

Confluent cultures of WT, ΔN and KO LNCaP C4-2 cells were mechanically detached and centrifuged at 1500rpm for 5 minutes. The supernatant was removed and cells were resuspended in 4mls of fresh complete medium. Cell counts using a haemocytometer was conducted, in order to dilute cells to a final volume of 500,000 cells/ml. 70µl of diluted cells was applied into the wells of a Ibidi Culture-Insert 2 well dish and left to incubate overnight in a humidified incubator at 37 °C, 5% CO_2. The next day, the insert was gently removed using sterile tweezers and 1.8mls of complete medium was added dropwise to the adhered cells. Images of the cells (at time point 0h) were then taken using an Celestron Microscope Imager. Further images at 24h and 48h time points were also captured using an Celestron Microscope Imager. To track the changes in cell migration over the 48h time period, images were inputted into TScratch software *(Gebäck et al., 2009)* which captures the percentage of open area (gap) in a given image. These percentage values were inputted into GraphPad Prism 9.2 software to calculate the changes in cell migration at 24h and 48h time points.

2.29. Cell Adhesion Assays

WT, ΔN and KO LNCaP C4-2 cells were seeded in a 96 well plate at a density of 2×10^5 cells per well (5 wells per cell line) and allowed to adhere overnight in a humidified incubator at 37 °C, 5% CO_2. In these assays, 5 wells were also filled with 100µl of complete medium. The next day, the culture medium was aspirated, and cells were washed with 100µL of 1X PBS before being fixed with 3.8% (w/v) paraformaldehyde (PFA) solution. Cells were fixed for 20 minutes, before being stained with 50µL of 1% toluidine blue/3% PFA solution for 10 minutes. Next cells were washed twice with 100µL 1X PBS and then the 96 well plate was invented and blot dried. After the wells were dry, remaining adhered cells were lysed with 100µL of 2% (w/v) SDS and left on an orbital shaker for 5 minutes at room temperature before absorbance of each well read at 590nm using a Synergy HT microplate reader.

Differences in absorbance (reflecting changes in cell adhesion) were calculated and plotted using GraphPad Prism 9.2 software.

2.30. Immunofluorescence of Mammalian Cell Lines

2×10^4 WT, ΔN and KO LNCaP C4-2 cells were seeded onto sterile 8 well chambered coverslip (Ibidi) which were coated with 35µg/ml Poly-D-Lysine to improve cell attachment. Cells were left to in incubate overnight in a humidified incubator at 37 °C, 5% CO_2. The next day, the culture medium was removed and cells were washed twice with 150µl 1X PBS before each well was treated with 200µl 4% (w/v) PFA solution and left to incubate at room temperature for 10 minutes in a fume hood. Afterwards the wells were washed three times with 1X PBS in the fume hood before being treated with 150µl PBST permeabilisation solution for 5 minutes at room temperature. Subsequently the permeabilisation solution was removed and each well was treated with 200µl of immunofluorescence blocking solution.

Afterwards the blocking solution was removed and wells were washed twice with 1X PBS. Then, primary antibodies *(Table 2.1)* were diluted in immunofluorescence blocking solution, with 200µl added to each well and left to incubate for either 1 hour at room temperature or overnight at 4 °C. Afterwards, each well washed twice with 1X PBS before being treated with 200µL Alexa-Fluor-488 secondary antibody *(Table 2.1)* for 1h at room temperature in the dark. Afterwards the wells were washed twice with 1X PBS in the fume hood before being treated with 200µL of diluted DRAQ5 nuclear stain *(Table 2.1)* and left to incubate for 15 minutes at room temperature in the dark. Wells were then washed twice with 1X PBS to remove the DRAQ5 nuclear stain. Wells were coated with 200µL of 1X PBS, wrapped in foil and left 4°C until image acquisition. A Zeiss LSM510 Meta confocal microscope (in conjunction with its respective software package, LSM Image Browser) was used for taking and processing confocal images.

2.31. Phosphoinositide Detection Using Lipid Biosensors

2×10^4 WT, ΔN and KO LNCaP C4-2 cells were seeded onto sterile 8 well chambered coverslip (Ibidi) which were coated with 35µg/ml Poly-D-Lysine to improve cell attachment. Cells were left to incubate overnight before being transfected the next day with Lipofectamine 3000 Reagent (ThermoFisher). Prior transfection the complete medium removed and replaced with RPMI-1640 medium lacking FBS, sodium pyruvate, penicillin and streptomycin. Then 50ng of plasmids encoding phosphoinositide detecting biosensors *(Table 2.2)* were mixed with the desired volumes of Opti-MEM I medium and P3000 reagent. This mixture was then mixed 1:1 with Opti-MEM I medium supplemented with Lipofectamine 3000 and left to incubate for 15 minutes at room temperature. Then, this mixture was added to seeded cells in a drop wise manner, and cells were left to incubate for 24 hours in a humidified incubator at 37 °C, 5% CO_2.

The next morning the culture medium was removed from each well and replaced with complete medium and the cells were returned back to the humidified incubator. Cells were either left to incubate for a further 24 hours, or the complete medium removed after 8 hours. If the latter, complete medium with replaced with RPMI-1640 medium lacking FBS, sodium pyruvate, penicillin, and streptomycin. This was to serum starve the cells in preparation for agonist stimulation. The next morning these cell lines were treated with 20µM LPA, a phosphoinositide evoking agonist for 30 minutes at 37 °C, 5% CO_2.

After the 30 minute incubation the culture medium was removed and the cells were washed with 1X PBS before each well was treated with 200µL 4% (w/v) PFA solution and left to incubate at room temperature for 10

minutes in a fume hood. Afterwards the wells were washed three times with 1X PBS in the fume hood before being treated with 200µL of diluted DRAQ5 nuclear stain *(Table 2.1)* and left to incubate for 15 minutes at room temperature in the dark. Wells were then washed twice with 1X PBS to remove the DRAQ5 nuclear. Wells were coated with 200µL of 1X PBS, wrapped in foil and left 4°C until image acquisition.

A Zeiss LSM510 Meta confocal microscope (in conjunction with its respective software package, LSM Image Browser) was used for taking and processing confocal images. Confocal microscopy images were exported into ImageJ software *(Schneider, et al., 2012)* and converted to grey scale. Then intensities of the lipid biosensors were quantified by using a protocol previously described in *Várnai et al., (2017).* This involves drawing a line from cell membrane through the cytoplasm of a given cell, generating a line intensity histogram. This was typically conducted for 5 different transfected cells. An additional step was conducted in this work, where the average line intensity was recorded for each cell, with individual averages graphed using Graphpad Prism 9.2 software.

2.32. FACS Analysis

Cells which were transiently transfected with expression constructs underwent FACs to isolate desired populations. Fluorescent constructs used in FACs were as such: mVenus-N1, PIP5K1α-mVenus-N1, mCherry-N1 and p85α-mCherryN1. For preparing cells for FACS, ~8×10^5 were seeded onto 60mm sterile plastic culture dishes and allowed to adhere overnight. Prior transfection, complete medium was removed and replaced with RPMI-1640 media lacking FBS, sodium pyruvate, penicillin and streptomycin. Then 11µg of fluorescent constructs was mixed with the desired volumes of Opti-MEM I medium and P3000 reagent. This mixture was mixed 1:1 with Opti-MEM Imedium supplemented with Lipofectamine 3000 (Thermofisher) and left

to incubate for 15 minutes at room temperature. Then, this mixture was added to seeded cells in a drop wise manner, and cells were left to incubate for 24 hours in a humidified incubator at 37 °C, 5% CO_2.

The next day, the culture medium was removed from each well and replaced with complete medium and the cells were returned back to the humidified incubator and left to incubate for 24 hours. The next day, the culture medium was removed and cells were washed with 1X PBS, before being mechanically detached and centrifuged at 1500rpm for 5 minutes. After pelleting the cells, the supernatant was removed, and cells were resuspended in 0.5ml of 1X PBS. Samples were transferred to School of Life Sciences Flow Cytometry Facility where sorting of fluorescent cells (at 488nm and/or 610nm wavelength) was conducted using a Beckman Coulter MoFlo Astrios EQ, Cell Sorter.

2.33. Detecting AKT Phosphorylation Through Flow Cytometry

Cells were transfected with empty vector or cloned constructs as previously described in Section 2.32. After 48h cells were mechanically detached and pelleted at 1500rpm for 5 minutes. The cellpellet was then resuspended in 100µl 4% PFA and allowed to incubate for 15 minutes. Afterwards, 1ml of 1X PBS was added to the cells and centrifuged for 1500rpm for 5 minutes and the supernatant removed. Cells were then resuspended with 0.5ml of 1X PBS before the addition of 100% of ice cold methanol (diluting this to 90%). The ice cold methanol was added gradually to the cells with gentle vortexing. The cells were then left to permeabilise in methanol for 1h before 1ml of 1X PBS was added to the cells.

Afterwards the cells were centrifuged at 1500rpm for 5 minutes and the supernatant removed. The cells were resuspended in 100µl 1X PBS supplemented with 0.5% BSA with the addition of phospho-AKT S473 antibody*(Table 2.1),* diluting this to 1:400. Cells were incubated with the

phospho-AKT antibody for 1h at room temperature. The cells were placed on a rotation mixer to ensure adequate mixing of samples with the diluted primary antibody. After 1h, 1ml of 1X PBS was added to each sample and the cells were centrifuged at 1500rpm for 5 minutes. The supernatant was removed, and cells were resuspended in 100µl of 1X PBS supplemented with 0.5% BSA with the addition of Alexa-Fluor-488 Secondary Antibody *(Table 2.1),* diluting this to 1:1000. Cells were incubated with Alexa-Fluor-488 Secondary Antibody for 30 minutes at room temperature. The cells were placed on a rotation mixer to ensure adequate mixing of samples with the diluted secondary antibody. After 30 minutes, 1ml of 1X PBS was added to each sample and the cells were centrifuged at 1500rpm for 5 minutes. The supernatant was then removed, and the pellets were resuspended in 500µl of 1X PBS. Samples were transferred to School of Life Sciences Flow Cytometry Facility where sample fluorescent intensities (at 488nm and/or 610nm wavelength) were determined using a Beckman Coulter MoFlo Astrios EQ, Cell Sorter. Fluorescent intensity data from these assays was analysed using Kaluza Analysis Software developed by Beckman Coulter.

Biochemistry Methods

2.34. Protein Extraction from Mammalian Cells

Cultures of WT, ΔN and KO LNCaP C4-2 cells were detached mechanically and centrifuged at 1500rpm for 5 minutes. The culture medium was aspirated, and cells were resuspended in 4mls of fresh complete medium. Cell counts using a haemocytometer were conducted, where a minimum of $1x10^6$ cells were then centrifuged at 1500rpm for 5 minutes. The resulting cell pellets were then resuspended in 100µl of cell lysis buffer and frozen at -80°C for at least one hour.

After freezing, the cells were gradually thawed on ice. Once fully thawed, the cells were sonicated using a Diagenode Bioruptor waterbath sonicator. Sonication was performed for 5 minutes using cycles of 30 seconds on, 30 seconds off on the high power setting. The resulting cell lysate was then centrifuged at 14,000rpm for 15 minutes at 4°C. The supernatant containing extracted proteins was transferred to a fresh 1.5ml tube. The concentration of the extracted proteins was determined by the Bradford assay. Extracted proteins were stored at -80°C until further use.

2.35. Bradford Assay

2µl of extracted protein was mixed with 800µl of ddH_2O and 200µl of Bradford Reagent (BIO-RAD). Samples were mixed thoroughly and incubated at room temperature for 15 minutes in the dark. The samples absorbance was then read at 595nm using an Eppendorf BioPhotometer. The concentration of protein samples was calculated relative to values obtained from a BSA standard curve of known concentrations.

2.36. Protein Separation by SDS Polyacrylamide (SDS-PAGE) Gel Electrophoresis

SDS page gels consisted of a stacking and a resolving section *(Table 2.12)* and were composed depending on the mass of the protein that was being resolved *(Table 2.13).* 50µg of protein was mixed with 4X SDS page loading dye (diluting to 1X) and loaded onto the SDS page gel. One lane in the SDS page gel was filled with 5µl of Colour Prestained Protein Standard, Broad Range (NEB). Before loading gels with protein extracts, each sample was denatured by boiling for 5 minutes at 95°C. SDS page gels underwent electrophoresis in a Mini-PROTEAN® Tetra Vertical Electrophoresis Cell (BIO-RAD) at 150V for ~60 minutes in 1X TGS buffer.

Table 2.12. Volumes of reagents needed to make different percentage SDS-PAGE gels (stacking and resolving gels).

Reagent	8% Resolving	10% Resolving	12% Resolving	15% Resolving	5% Stacking
ddH_2O (ml)	4.6	4.0	3.3	2.3	3.4
30% w/v Acrylamide (ml)	2.7	3.3	4.0	5.0	0.83
1.5 M Tris pH 8.8 (ml)	2.5	2.5	2.5	2.5	X
1.0 M Tris pH 6.8 (ml)	X	X	X	X	0.63
10% SDS (ml)	0.1	0.1	0.1	0.1	0.05
10% APS (ml)	0.1	0.1	0.1	0.1	0.05
Tetramethylethylenediamine (TEMED) (ml)	0.006	0.004	0.004	0.004	0.005

Table 2.13. SDS-PAGE Gel percentages which correspond to proteins molecular mass.

Protein Mass (kDa)	SDS Page Gel Percentage (%)
25 – 200	8
15 – 100	10
10 – 70	12
12 – 45	15

2.37. Western Blotting

Once proteins were resolved, the SDS page gel was placed onto a nitrocellulose membrane and transferred at 50V for 2 hours at room temperature using 1X High Glycine Transfer Buffer. To check for successful transfer, the nitrocellulose membrane was immersed in a 1% Ponceau S solution and washed with TBS before then being placed in a blocking solution consisting of either 3% (w/v) BSA or 5% (w/v) milk in TBS. The nitrocellulose membrane was incubated in blocking solution for 1 hour, with agitation. Next the nitrocellulose membrane was placed

in a blocking solution containing an appropriate concentration of primary antibody *(Table 2.1)* and incubated with shaking at 4°C overnight.

The next day the nitrocellulose membrane was washed with TBST three times for 5 minutes with shaking to remove excess antibody. Then, the nitrocellulose membrane was incubated for 1 hour with agitation in a blocking solution supplemented with the appropriate concentration of secondary antibody *(Table 2.1).* Afterwards the membrane was washed three times in TBST before then subjected to 150-300µl of Pierce™ ECL Western Blotting Substrate developing solution (ThermoFisher*).* The membrane was incubated with developing solution for 1-2 minutes before being stored in a clean polythene bag. The membranes chemiluminescent signal was detected using a Fujifilm LAS-4000 system.

Bioinformatics and Statistics

2.38. Processing of RNA Sequencing Data

Cell lines were grown to 80% confluency before RNA extractions pursued. RNA from triplicate WT, ΔN and KO C4-2 cells was extracted using a Qiagen RNeasy Mini Kit as per the manufacturer's instructions. The quality of the extracted RNA was quantified by using a nanodrop, a qubit and an Agilent Bioanalyzer. All samples which were run through the Agilent Bioanalyzer had an RNA Integrity Number exceeding 9.7. RNA extraction and RNA quality checks was performed by Dr. Cíntia Monteiro. Extracted RNA (depleted for ribosomal RNA) was used to prepare RNA-Seq libraries using the Illumina TruSeq RNA Sample Prep kit following the manufacture's protocol. The construction of RNA-Seq libraries, and sequencing was performed by Novagene UK.

RNA reads from FASTq files were mapped to the human genome build hg38.83 using STAR *(Dobin et al., 2013)* and adaptor sequences removed by TrimGalore *(Krueger, n.d).* FeatureCounts *(Liao, et al.,*

2013) was used to generate RNA read counts. RNA read mapping, removal of adapter sequences and read alignment for WT, ΔN and KO C4-2 cells was previously conducted by Dr Nigel Mongan.

This work used the integrated web application for differential expression and pathway analysis (IDEP) 0.93 web application (*Ge et al., 2018*) for the analysis of RNA read data. Pre-processing was conducted on read counts by deploying a minimum counts per million (CPM) filter of 0.5. For subsequent transformations of gene expression data, EdgeR processing was conducted (*Robinson et al., 2009*). In this work a pseudo count of 4 was used for EdgeR processing: log2 (CPM + 4).

2.39. Identifying DEGs from RNA-Seq datasets

Once pre-processing of RNA-Seq data was carried out, genes which are differentially expressed (DEGs) between cell lines were identified using differential gene expression analysis based on the negative binomial distribution (DESeq2) *(Love et al., 2014).* DESeq2 was run through the IDEP 0.93 web application *(Ge et al., 2018).* For a given gene to be identified as being differentially expressed a minimum log2 fold change (Log2FC) was of 1 was required. A false discovery rate (FDR) of 0.01 was deployed to ensure that identified genes had a less than 1% probability of being deemed differentially expressed by chance. Venn diagrams comparing similarities of DEGs from this work relative to other studies were generated using Venny 2.1 *(Oliveros, 2007-2015*). Volcano plots of DEGs were generated by using VolcaNoseR *(Goedhart and Luijsterburg, 2020).* The Molecular Signatures Database (MSigDB) was used to perform gene set enrichment analysis *(Subramanian et al., 2005 ; Liberzon et al., 2015)*

2.40. *In Silico* quantification of RNA Splice Variants from RNA-Seq datasets

Kallisto *(Bray et al., 2016)* was used to estimate the expression of gene splice variants from RNA-Seq data. Kallisto was run through the publicly available Galaxy server *(Afgan et al., 2018).* Fastq files of WT, ΔN and KO LNCaP C4-2 cells were previously generated by Dr Nigel Mongan. All other triplicate Fastq files of cancer cell lines and patient cohorts were extracted from NCBI Short Read Archive (SRA). For Kallisto quantification, a reference cDNA transcriptome is required. For this, either NCBIs GRCh38 RefSeq Transcripts was used, or the complementary cDNA transcriptome for hg38.83 (Ensembl). Prior running Kallisto, quality control checks of data obtained from SRA was conducted through using FastQC *(Andrews., n.d).*

2.41. Statistical Analysis

Graphpad Prism 9.2 software was used for generating bar charts, variance calculations and determining statistical significance. Error bars on bar charts report variance as standard deviation from the mean. Statistical tests conducted in this work to determine significance between sample groups include: two sided t-tests, One-Way ANOVA and Two-Way ANOVA. Typically the Tukey Post-hoc test was used to explore difference between sample means in ANOVA calculations.

Chapter 3

The Effects of PIP5K1A Ablation on the Transcriptome of LNCaP C4-2 Prostate Cancer Cells

3.1. Introduction

PIP5K1α has been implicated in a wide range of important functions in different cell types including actin remodelling, cell adhesion, cell migration, formation of lamellipodia, phagocytosis, calcium signalling and GTPase activation *(van den Bout and Divecha, 2009 ; Kwiatkowska, 2010 ; Porciello et al., 2016).* Whilst these processes are typically membrane associated, PIP5K1α is also thought to regulate nuclear signalling events. This is thought to be through the synthesis of nuclear phosphoinositides and through direct protein-protein interactions of PIP5K1α with nuclear effectors *(Fiume et al., 2019).*

In the context of breast and prostate cancers chemical inhibition of PIP5K1α has been shown to modulate both oestrogen and androgen signalling pathways *(Sarwar et al., 2016 ; Larsson et al., 2019 ; Semenas et al., 2020),* However as PIP5K1α predominantly localises to the cell membrane (*Liu et al., 2016* ; *de la Cruz et al., 2019),* it is unclear what would trigger nuclear localisation of this kinase and how this influences steroid signalling pathways.

There is also limited evidence regarding the role PIP5K1α exerts upon global transcriptomic networks in different cellular models. Currently in the literature there is only one study which has explored this question, published by *Mellman et al., (2008).* In this study, knockdown of PIP5K1A expression by RNAi in HEK293 cells altered the polyadenylation state of approximately ~4500 transcripts, detected through using microarrays. Further work conducted by *Mellman et al., (2008)* reported that exogenous PIP5K1α can localise to regions known as nuclear speckles and interact with poly(A) polymerase Star-PAP/TUT1. This interaction was proposed to enhance the activity of Star-PAP dependent upon $PI(4,5)P_2$ synthesis by PIP5K1α *(Mellmann 2008).* The reported function of Star-PAP is to add a poly-A-tail to the 3' end of mRNA, which enhances transcript stability *(Colgan and Manley,*

1997 ; Mohan et al., 2015) although more recently it has been reported that Star-PAP in association with RNA Binding Motif Protein 10 (RBM10) regulates the turnover of select mRNAs *(Koshre et al., 2021).*

This chapter will describe previous CRISPR-Cas9 gene editing work from previous laboratory colleagues which was used to ablate or modify PIP5K1A expression in LNCaP C4-2 prostate cancer cells. This work generated two CRISPR clones (ΔN and KO LNCaP C4-2 cells) through using CRISPR-Cas9 nickase (D10A). The benefit of using the nickase strategy is that this enzyme makes a staggered single strand breaks (nicks) on opposing strands using 2 guides. These are recognised as double stranded breaks. In contrast WT Cas9 would use a single guide to induce a blunt ended double stranded break that can result in a high frequency of off-target indels which may perturb the expression of non-target genes *(Guo et al., 2018).* In comparison to using WT Cas9 for gene editing, Cas9 nickase is thought to reduce off-target mutagenesis by up to 1000-fold *in vitro (Ran et al., 2013).*

Previous work which led to the generation of ΔN and KO will be documented in this chapter. However, this chapter will also detail results from RNA-Seq analysis. RNA-Seq was conducted in order to understand how perturbing PIP5K1A expression effects the transcriptome of prostate cancer cells. The benefit of this approach is several fold. Firstly, CRISPR-Cas9 editing allows for sustained knockdown of PIP5K1A expression, which cannot be achieved through RNAi, which provides only transient knockdown. Secondly, microarrays only profile the expression levels of predefined transcripts whereas RNA-Seq mediates detailed coverage of the cell's transcriptome. By conducting differential gene expression analysis and enrichment analysis, this has highlighted that genes implicated with steroid signalling and the cell cycle are dysregulated in ΔN and KO LNCaP C4-2 cells. Subsequently wet lab assays were conducted to validate alterations in cell cycle progression and steroid signalling *in vitro.*

RNA-Seq also provides additional information regarding the expression of gene splice variants *(Rao et al., 2019).* A spectrum of computational packages are available for estimating the abundance of splice variants from RNA-seq data, such as TIGAR2 *(Nariai et al., 2014)*, Kallisto *(Bray et al., 2016)* and Cufflinks *(Trapnell et al., 2010).* Cufflinks and TIGAR2 require a reference transcriptome for full alignment of RNA reads to transcripts which reflects a major bottleneck in RNA-Seq quantification. The way Kallisto avoids this bottleneck is through pseudoalignment which does not conduct full read alignment, but instead, determines the combability of RNA reads to a given transcript.

This more streamlined process has been shown facilitate rapid splice variant analysis. *Bray et al., (2016)* reported that splice variant quantification from 30 million unaligned paired end reads can be achieved in under 10 minutes using non-specialised computer processing, making Kallisto more accessible and user friendly. Due to speed of processing, Kallisto was selected as the package for splice variant analysis. In this chapter, Kallisto has been used to quantify *in silico* the expression of PIP5K1A transcripts in WT, ΔN and KO LNCaP C4-2 cells.

3.2. Overview of ΔN and KO LNCaP C4-2 CRISPR Clones

This section will provide background information to the two CRISPR clones which were used throughout this work, ΔN and KO. The CRISPR-Cas9 gene editing was designed and carried out by previous laboratory members (Dr Miguel Hernandez- Quiles, Dr Jonathan Whitchurch , Dr Chris Roberts , Dr Hilary Collins and Professor David Heery). After transfection of guide RNAs (summarised in *Table 2.7)* LNCaP C4-2 cells underwent FACs sorting. In this, approximately 190 GFP positive cells were transferred as single cells to 96 well plates for clonal expansion rather than pooled. This approach was taken as pooled CRISPR screens do not support the use of bulk RNA-Seq for transcriptome profiling *(Datlinger et al., 2017).*

Multiple clones (typically n=9) which had grown sufficiently after 1-2 weeks were then selected for genotyping, an example of which is shown in *Figure 3.1*. In this example, several cell lines (named after their location on a 96 well plate) were genotyped using PCR. This section summaries the genotyping of PIP5K1α depleted clones, the effects of CRISPR editing on the growth rates of the clones is discussed in *Section 3.6.*

Through Sanger Sequencing, the 1C cell line was further characterised (*Figure 3.3*) and was denoted as clone ΔN. Through sequencing this confirmed that ΔN LNCaP C4-2 cells contained deletions of 53 and 63bp in Exon 1 for alleles 1 and 2 respectively *(Figure 3.3).*

KO LNCaP C4-2 cells were targeted with RNA guides to Exons 1 and 6. Genotyping of KO LNCaP is shown in *Figure 3.2*. Through Sanger sequencing, this revealed a 32bp insertion within Exon 1 *(Figure 3.3).* Sequencing also revealed that KO LNCaP C4-2 cells contained a 321bp insertion in Exon 6.

Through western blotting, reductions in PIP5K1α protein expression was observed in ΔN, compared to WT LNCaP C4-2 cells (*Figure 3.4).* This is consistent with the observation that CRISPR editing has removed the canonical ATG start codon, which is used for translational initiation.

However downstream AUG codons in Exon 1 such as AUG36 and AUG46 could act as alternative sites of translational initiation and may be less efficient, accounting for the reduced expression. Protein levels in KO C4-2 cells were strongly impacted by CRISPR editing due to both Exons 1 and 6 being targeted in this clone *(Figure 3.3).* It must be added whilst similar reductions of PIP5K1α protein expression was observed in these western blots relative to blots conducted by previous laboratory colleagues *(Hernandez-Quiles 2016 , Roberts 2022)* one difference has been the presence of additional bands in *Figure 3.4.* The reason for this is that these western blots were conducted using a different lot of PIP5K1A antibody (Cell Signalling Technologies). These additional bands could be non specific or equally reflect different splice variants of PIP5K1α. NCBI documents that there 5 recorded PIP5K1A protein encoding transcripts, (analysed further in *Section 3.3*) and 38 predicted protein encoding PIP5K1A transcripts.

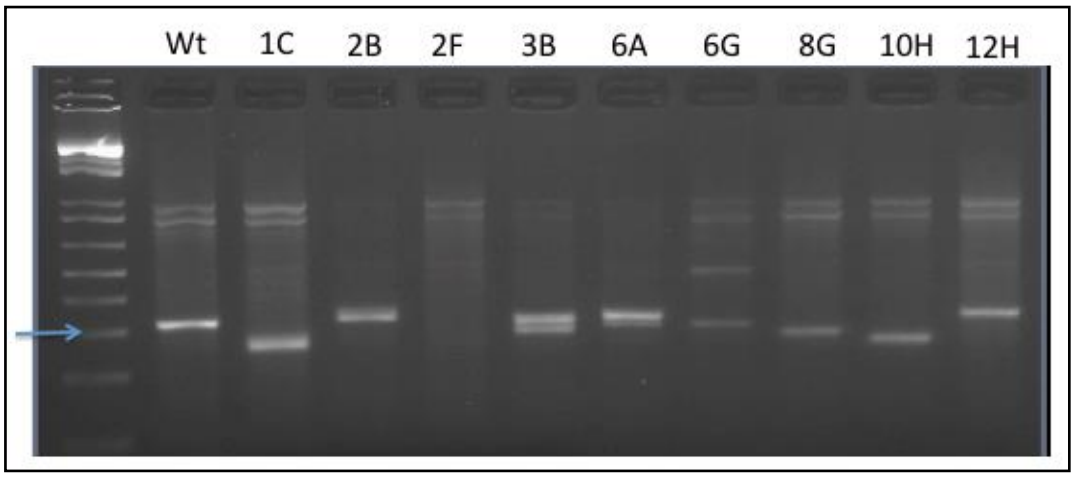

Figure 3.1. Genotyping of clone 1C (ΔN) through PCR. Genomic extractions from several clones were conducted, with PCR conducted with the following primers targeting Exon 1. Forward: CCTTGAGCTGGTCCAGGAG. Reverse: AATATGCGATGGGAGGAAGA Arrow denotes 300bp marker, with a WT amplicon of 325bp shown. Figure provided by Professor David Heery, from *Hernandez-Quiles 2016*

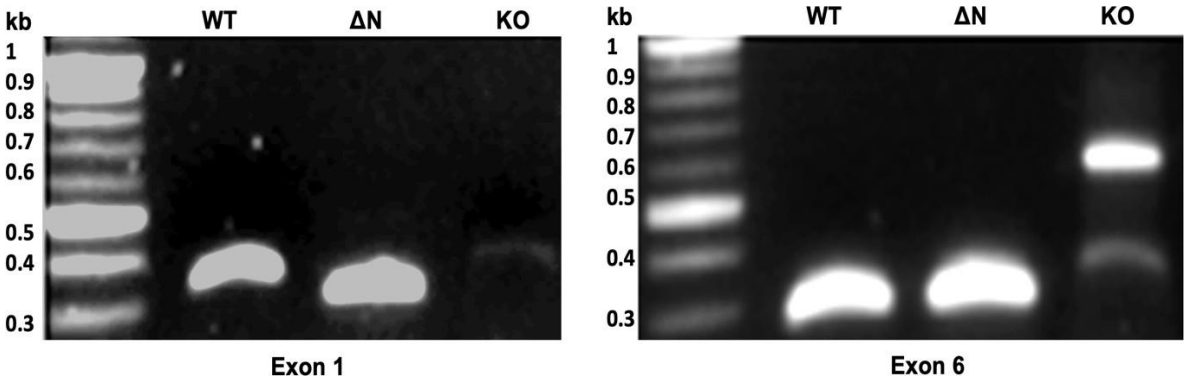

Figure 3.2. PCR amplification of Exon 1 and Exon 6 from WT, ΔN and KO LNCaP C4-2 cell genomic DNA. Primers used in PCR amplification of Exon 1 and Exon 6 are detailed in Chapter 2, CRISPR-Cas9 Gene Editing section.

Figure 3.3. Sequencing of CRISPR targeted Exons in ΔN and KO LNCaP C4-2 cells. Exon 1 and Exon 6 are indicated in **A and B** respectively. Highlighted on this schematic is the aberrations observed in CRISPR edited alleles in ΔN and KO LNCaP C4-2 cells. Sequence alignment schematic provided by Dr Chris Roberts and Professor David Heery.

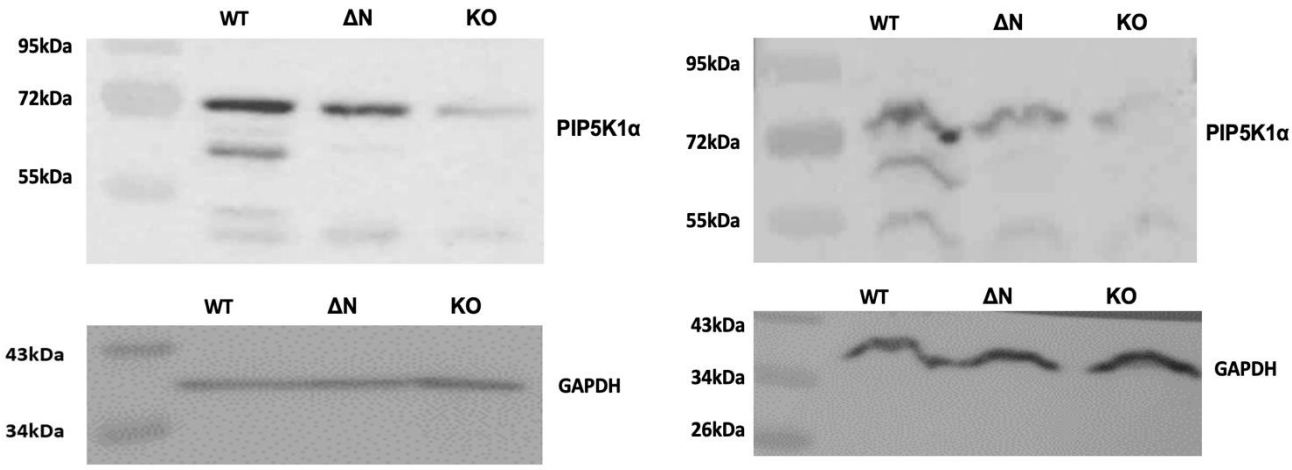

Figure 3.4. Western blot of PIP5K1α protein expression in WT , ΔN and KO C4-2 cells. Proteins were extracted using RIPA buffer and resolved on 10% SDS page gels before blotting for PIP5K1α or GAPDH (loading control)

3.3. PIP5K1A Splice Variant Analysis in WT and CRISPR Edited LNCaP C4-2

For RNA-Seq analysis *(described in detail in Sections 2.38, 2.39 and 2.40)* triplicate cultures of WT, ΔN, KO LNCaP C4-2 cells were all grown to 80% confluence and then underwent RNA extraction. Total RNA depleted for ribosomal RNA was used in the preparation of RNA-Seq libraries, with a read depth of ~20 million reads per sample *(Figure 3.5).* Shown in *Table 3.1* is the loss of PIP5K1A expression in ΔN and KO LNCaP C4-2 cells. In WT cells LNCaP C4-2 cells, PIP5K1A is the most abundantly expressed PIP5K gene, followed by PIP5K1C. The expression of PIP5K1C was unchanged between WT, ΔN and KO LNCaP C4-2 cells. Due to the extremely low read counts for PIP5K1B expression between WT, ΔN and KO C4-2 cells DeSeq2 analysis could not be conducted. Overall *Table 3.1* indicates that the expression of PIP5K1B and PIP5K1C is not altered after PIP5K1A CRISPR editing, ruling out any possible compensatory mechanisms by PIP5K1B and PIP5K1C.

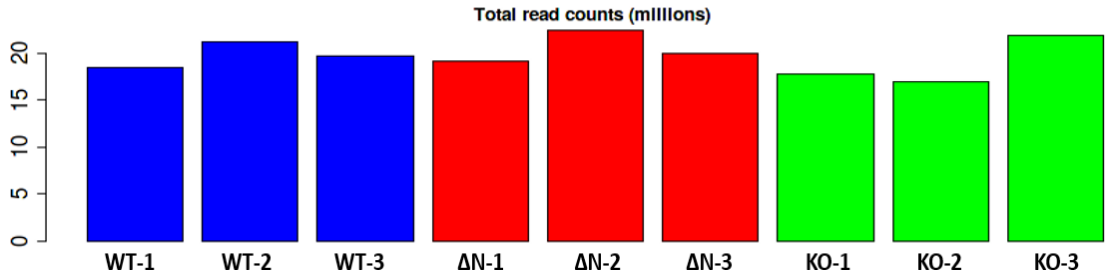

Figure 3.5. Total RNA-Read counts for triplicate WT , ΔN , KO LNCaP C4-2 cells. Graph of RNA read counts was generated through using the IDEP 0.93 web application *(Ge et al., 2018)*

Table 3.1. RNA expression of PIP5K1A, PIP5K1B and PIP5K1C in WT, ΔN and KO C4-2 cells. Reported is the Log2FC , FDR and the average (n=3) RNA reads for RNA expression of PIP5K1A, PIP5K1B and PIP5K1C. DeSeq2 was conducted to generate Log2FC and FDR values, whilst RNA Read counts were generated by FeatureCounts.

Gene Name	Protein Name	Log2FC ΔN – WT	FDR ΔN – WT	Log2FC KO- WT	FDR KO- WT	Average WT RNA Reads	Average ΔN RNA Reads	Average KO RNA Reads
PIP5K1A	PIP5K1α	-0.85	1.1E-14	-1.53	6.01E-44	1548	835	512
PIP5K1B	PIP5K1β	N/A	N/A	N/A	N/A	4	3	5
PIP5K1C	PIP5K1γ	-0.068	0.67	0.14	0.38	871	809	920

For subsequent analysis of PIP5K1A splice variants, triplicate Fastq files were analysed using Kallisto. This Kallisto analysis has focused on the 5 documented protein encoded transcripts (as recorded by NCBI, *Table 3.2).* It must be noted that two predicted PIP5K1A splice variants recorded by NCBI (encoding predicted isoforms 15 and 16) have since been validated by *Roberts, (2022).*

Figure 3.6 indicates that loss of PIP5K1A expression is observed in both ΔN and KO cells, and that PIP5K1A isoform 2 is the mostly abundantly expressed transcript across LNCaP C4-2 cells lines. To validate *in silico* observations RT-qPCR, was conducted using primers *(Table 2.10)* designed to amplify all PIP5K1A transcripts. The results from these assays confirm the loss of PIP5K1A expression in both CRISPR edited cell lines *(Figure 3.7).*

Table 3.2. Details of the PIP5K1A transcripts that have undergone Kallisto quantification in WT, ΔN and KO C4-2 cells.

Transcript Variant	Number of Exons	Size in Base pairs (bp)	Additional Information
PIP5K1A Isoform 1	16	3800	Encodes the longest PIP5K1α protein (562aa)
PIP5K1A Isoform 2	15	3761	Shorter PIP5K1α protein (549aa) but identical N and C termini to that Isoform 1
PIP5K1A Isoform 3	14	3680	Lacks two in frame exons in the coding sequence resulting in a shorter PIP5K1α protein (522aa). Identical N and C termini to that of Isoform 1
PIP5K1A Isoform 4	14	3614	Lacks two in frame exons in the coding sequence, resulting in a much shorter PIP5K1α protein (500aa). Nevertheless, identification N and C termini to that of Isoform 1
PIP5K1A Isoform 5	15	3764	Encodes a protein of 550aa, identical N and C termini to that of Isoform 1

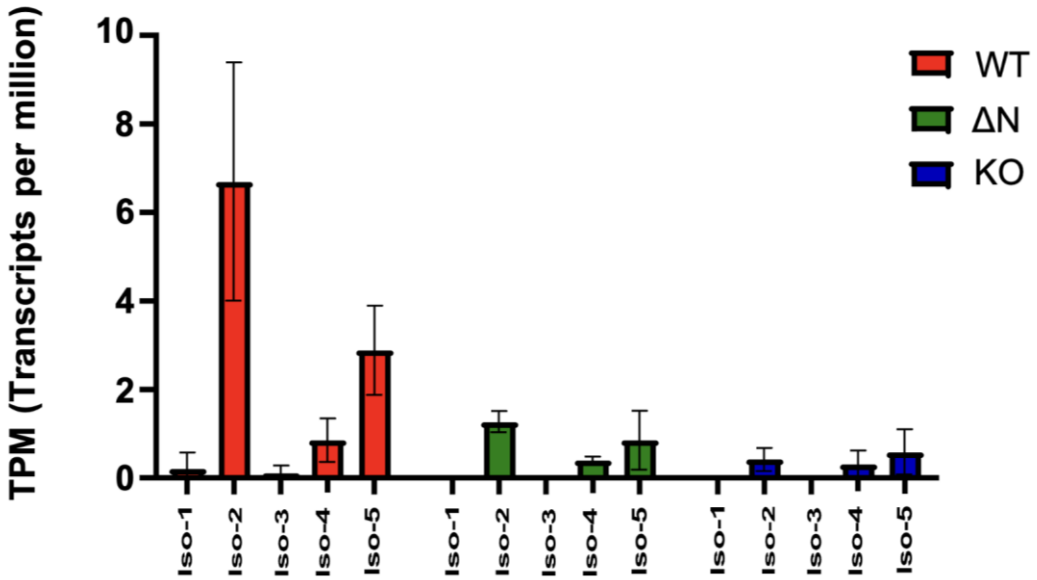

Figure 3.6. Kallisto quantification of expression of the 5 protein encoding transcripts of PIP5K1A in WT, ΔN and KO C4-2 cells. TPM scores are calculated from biological triplicate (n=3) Fastq files. The reference transcriptome used in the quantification of these transcripts was GRCh38 RefSeq Transcripts (NCBI).

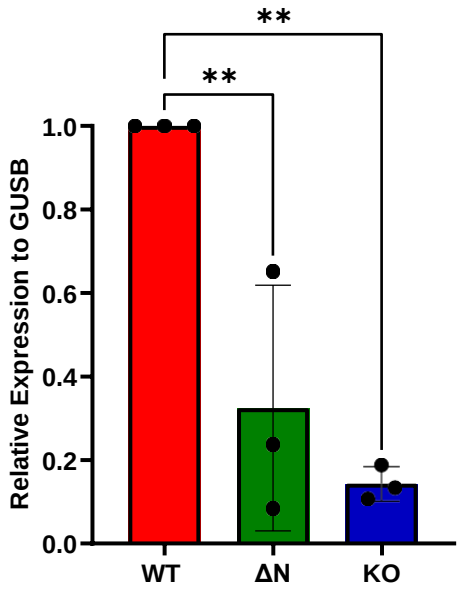

Figure 3.7. Relative expression of PIP5K1A in WT, ΔN and KO C4-2 cells. Data is of biological triplicates (n=3) with technical triplicates. Relative expression was calculated using the $2^{-\Delta\Delta Ct}$ method. Data was normalised to the expression of GUSB housekeeping gene per cell line. Statistical significance was determined by a one-way ANOVA with a Tukey's multiple comparisons test. ** P ≤ 0.01.

3.4. Identification of Differentially Expressed Genes in WT and CRISPR Edited C4-2 Cells

Pre-processing of RNA reads was conducted to facilitate the identification of differentially expressed genes. From the raw RNA-Seq data, 60675 genes were recorded across WT and CRISPR edited clones. This pool reflects genes which encode proteins, but also non protein encoding, for instance genes which encode for antisense RNAs. In order to remove genes which were detected to have minimal expression, a CPM of 0.5 was deployed as a filter. For subsequent transformations of gene expression data, EdgeR processing was conducted *(Robinson et al., 2009).* In this work a pseudocount of 4 was used for EdgeR processing: log2 (CPM + 4). This filtering strategy reduced the number of genes to 17390 across biological triplicates of WT, ΔN and KO C4-2 cells. Log transformed counts reveals strong similarity between technical replicates, with each cell line having distinct transcriptomes, as shown in *Figure 3.8* through principle component analysis (PCA).

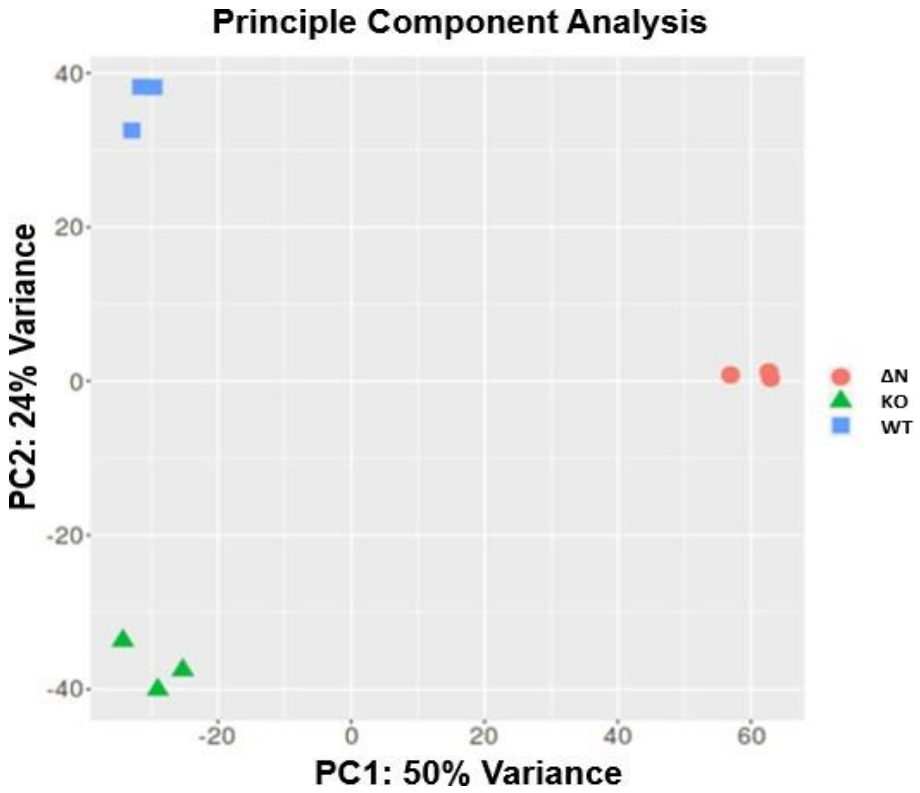

Figure 3.8. Plot of PCA showing the variance of triplicate RNA-Seq data between WT, ΔN and KO LNCaP C4-2 cells. PCA was conducted through the IDEP 0.93 web application *(Ge et al., 2018).*

Differently expressed genes between CRISPR clones relative to WT C4-2 cells were identified through DeSeq2 *(Love et al., 2014)* using stringent significance cut offs: Log2FC of 1 and an FDR of 0.01. *Table 3.3* indicates that approximately two-fold more upregulated and downregulated genes were identified between ΔN-WT cells, relative to KO-WT. Interestingly, between ΔN-WT and KO-WT gene lists there was 216 (20.2%) common upregulated DEGs and 151 (14.7%) common downregulated DEGs *(Figures 3.9).* Ultimately, this sizeable amount of shared DEGs would suggest that both CRISPR clones may share some common affected signalling pathways as will be discussed later. Further

visual representation of DEGs in CRISPR edited clones are shown in volcano plots *(Figures 3.11 and 3.12)* which also highlights the top 10 most significantly altered genes. From *Figure 3.10* it was apparent that Phospholipase A2 Group IIA (PLA2G2A) expression was elevated in clone ΔN. With this clone harbouring increased AKT activity *(Roberts, 2022 and detailed further in Chapter 5)* this could account for why PLA2G2A expression is dysregulated. It was previously shown by *Ganesan et al., (2008)* in gastric cancer cells that Wnt/β-catenin signalling positively regulates PLA2G2A expression, with elevated expression of this gene inhibiting cancer cell migration. As AKT can positively regulate Wnt/ β-catenin signalling by inhibiting the β-catenin degradation complex *(Fukumoto et al., 2001)* this could account for why PLA2G2A expression is elevated in clone ΔN.

It is interesting to highlight that UGT2B17 features in the top 10 as one of the most significantly downregulated genes both ΔN-WT and KO-WT C4-2 cells *(Figures 3.10 and 3.11).* This gene is part of the UDP-glucuronosyltransferase (UGT2B) family which mediates androgen conjugation through the addition of a glucuronyl moiety, which modulates the androgen signalling response in cells *(Bao et al., 2008).* Loss of UGT2B17, UGT2B15 and UGT2B11 expression in both CRISPR clones was previously validated by RT-qPCR by *Roberts, (2022).*

Additionally, in *Figure 3.11* cells loss of Calcium/Calmodulin Dependent Protein Kinase II Inhibitor (CAMK2N1) was observed in KO-WT comparisons. This is a gene has been shown to be negatively regulated by androgen signalling, where loss of CAMK2N1 expression has been observed after LNCaP cells are treated with the synthetic androgen R1881 *(Romanuik et al., 2009). In vitro,* loss of CAMK2N1 expression in DU145 prostate cancer cells has been shown to enhance cell migration *(Peng et al., 2023).*

Table 3.3. Total number of DEGs in ΔN-WT and KO-WT LNCaP C4-2 cells. Genes were defined as being differentially expressed if they met the following cut offs: Log2FC of 1 and an FDR of 0.01.

Comparisons	Upregulated DEGs	Downregulated DEGs	Total DEGS
ΔN-WT	852	823	1675
KO-WT	447	371	818

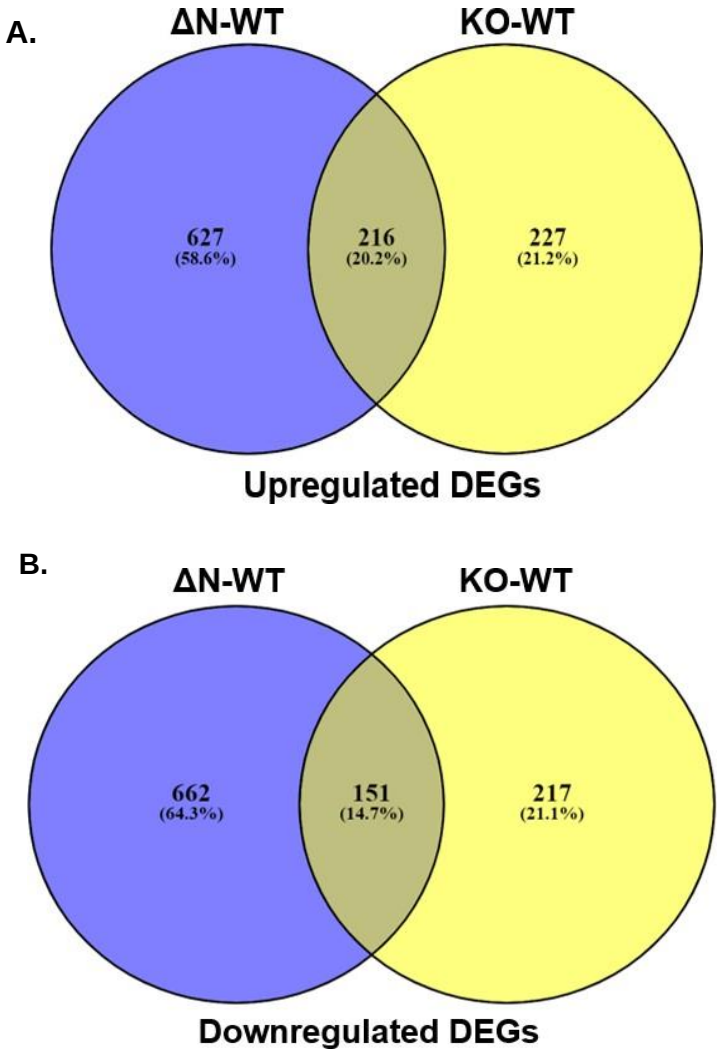

Figure 3.9. Venn diagrams of common DEGs between WT and CRISPR edited clones. A. The overlap of upregulated and downregulated DEGs between ΔN-WT C4-2 cells. **B.** The overlap of upregulated and downregulated DEGs between KO-WT C4-2 cells.

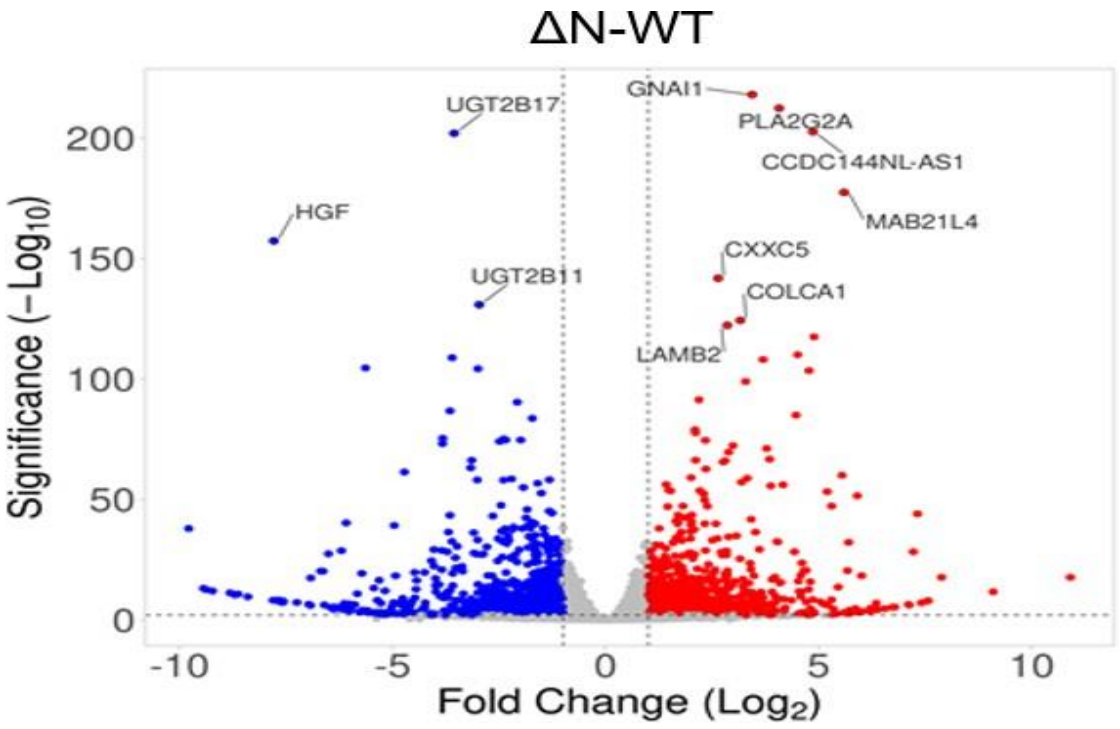

Figure 3.10. Volcano plots of upregulated (in red) and downregulated DEGs (in blue) in ΔN-WT C4-2 cells. The top 10 most significantly altered genes as according to their -Log10 significance score are highlighted. These scores were calculated through -Log10 transformation of a givengenes FDR.

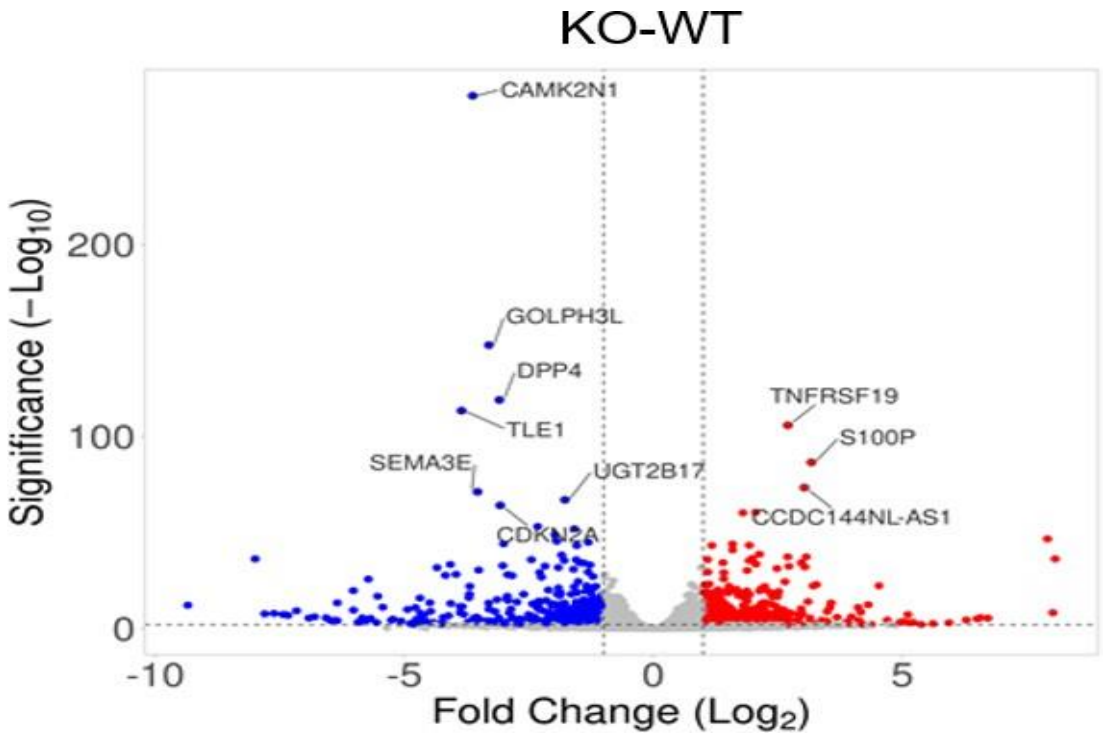

Figure 3.11. Volcano plots of upregulated (in red) and downregulated DEGs (in blue) in KO-WT C4-2 cells. The top 10 most significantly altered genes as according to their -Log10 significance score are highlighted. These scores were calculated through -Log10 transformation of a given genes FDR.

3.5. Analysis of Enriched Pathways in CRISPR Edited Clones

To gain further insights into the spectrum of pathways which are affected after PIP5K1A ablation, gene enrichment analysis of DEGs was conducted. For this, Gene Set Enrichment analysis was conducted using the MSigDB *(Subramanian et al., 2005 ; Liberzon et al., 2015)* with HALLMARK gene sets. From this analysis it was possible to distinguish the number of upregulated and downregulated genes which fall into the following categories: *tumour suppressors, oncogenes, translocated cancer genes, protein kinases, cell differentiation markers, homeodomain proteins, transcription factors, cytokines and growth factors.* In particular genes defined as a transcription factor or protein kinases showed the biggest changes in expression in both ΔN and KO C4-2 cells *(Table 3.4)*

The HALLMARK overlap enrichment analysis was able to reveal common processes and pathways which are enriched in both CRISPR lines Both CRISPR lines show enrichment for genes implicated in the response to steroid signalling *(Tables 3.5, 3.6 and 3.7)* consistent with publications linking PIP5K1α with the regulation of AR activity *(Sarwaret al., 2016 ; Wang et al., 2022).* Both CRISPR clones also share enrichment of genes implicated with KRAS signalling *(Tables 3.6, 3.7 and 3.8).* This is consistent with previous publications highlighting that PIP5K1α activity can be modulated through interactions with small GTPases such as Rac1, ARF6 and KRAS *(Weernink et al., 2003 ; Tsai et al., 2017 ; Adhikari and Counter, 2018).*

The starkest feature between both CRISPR clones is that they share significant upregulation of genes implicated with mitosis and cell cycle progression *(Tables 3.5 and 3.7).* Consistent with this observation, E2F transcription factor targets are highly enriched in both CRISPR clones also *Tables 3.5 and 3.7).* Interestingly, the N terminus of PIP5K1α has been shown to interact with pRB *(Divecha et al., 2002).* pRB binds to the

promoter region of E2F transcription factors which attenuates E2F transcriptional activity *(Hagemeier, et al., 1993).* As E2F transcription factors enhances the expression of cell cycle related genes, pRB reflects a major negative regulator in coordinating normal cell cycle progression *(Giacinti, and Giordano., 2006).* Whilst *Divecha et al., (2002)* showed pRB binding to PIP5K1α positively enhances PIP5K1α kinase activity, it was also demonstrated that transfection of PIP5K1A in cells expressing an E2F-sensitive promoter did not modulate promoter activity. However, *Divecha et al., (2002)* did not investigate whether PIP5K1A knockdown could modulate the activity of pRB-E2F signalling, which appears to be dysregulated in both our CRISPR clones.

Whilst there are several core pathways which are dysregulated in both CRISPR clones, there is also differences in some of the pathways enriched in ΔN and KO cells. For instance, there is loss of expression of a selection of genes implicated in EMT in KO cells *(Table 3.8).* This process is associated with several biochemical processes, such increased cell invasion, increased production of extracellular matrix components and actin remodelling *(Kalluri and Weinberg, 2009 ; Haynes et al., 2011).* $PI(4,5)P_2$ has been implicated in driving EMT, where *Huang et al., (2019)* showed in hepatocellular carcinoma cells that hypoxia induced $PI(4,5)P_2$ synthesis, driving F-actin polymerisation *(Huang et al., 2019).* However the results presented here suggests PIP5K1A could also influence actin remodelling at a transcriptional level.

Conversely, ΔN cells show have increased expression of a genes associated with mTORC1 signalling *(Table 3.5).* With this CRISPR clone possessing increased AKT phosphorylation *(Roberts, 2022 and further detailed in Chapter 5*) this kinase can positively regulate mTORC1 signalling. This can be through phosphorylation of PRAS40, a subunit of mTORC1 which negatively regulates mTOR kinase activity. Upon phosphorylation of PRAS40 (at Thr246) this relieves the negative

inhibition PRAS40 exerts upon mTORC1 substrate binding *(Kovacina et al., 2003 ; Wang et al., 2007 ; Nascimento et al., 2010).*

Additionally, AKT can enhance mTORC1 activity by suppressing the upstream negative regulation TSC1/TSC2 exerts on mTORC1. *Potter, et al., (2002)* showed in *Drosophila melanogaster* that AKT could phosphorylate S924 and T1518 residues (human equivalent resides: S924 and T1462). TSC2 phosphorylation impairs TSC1 binding which results in TSC1/TSC2 complex inactivation *(Potter et al., 2002).* Downstream activation of mTORC1 results enhanced translation, mediated by the two key effectors , S6K1 and 4E-BP1 *(Laplante and Sabatini, 2012)*

Table 3.4. Gene Families in upregulated and downregulated ΔN-WT and KO-WT DEg lists. The MSigDB was used to categorise DEGs into the appropriate gene families *(Subramanian et al., 2005 ; Liberzon et al., 2015).*

Gene Family	ΔN-WT Upregulated	ΔN-WT Downregulated	KO-WT Upregulated	KO-WT Downregulated
Tumour Suppressors	6	3	3	2
Oncogenes	12	12	9	3
Translocated Cancer Genes	12	10	9	2
Protein Kinases	35	27	19	9
Cell Differentiation Markers	16	10	17	9
Homeodomain proteins	9	14	9	3
Transcription Factors	45	57	27	26
Cytokines and Growth Factor	18	12	12	7

Table 3.5. Upregulated HALLMARKS in ΔN-WT LNCaP C4-2 cells. Tabulated is the number of genes from ΔN-WT DEGs lists that are common to the list of genes that comprise HALLMARK gene sets along with p-value and FDRq-value for each HALLMARK. The number of genes which comprise each HALLMARK is in square brackets. The MSigDB was used for HALLMARK enrichment analysis *(Subramanian et al., 2005 ; Liberzon et al., 2015)*

Hallmarks	**# Genes in Overlap**	**p-value**	**FDR q-value**
HALLMARK_G2M_CHECKPOINT [200]	55	8.66E-47	4.33E-45
HALLMARK_E2F_TARGETS [200]	53	3.46E-44	8.64E-43
HALLMARK_MITOTIC_SPINDLE [199]	32	5.12E-20	8.53E-19
HALLMARK_ESTROGEN_RESPONSE_LATE [200]	21	5.20E-10	6.50E-09
HALLMARK_HYPOXIA [200]	17	4.93E-07	4.93E-06
HALLMARK_SPERMATOGENESIS [135]	13	2.71E-06	2.26E-05
HALLMARK_ESTROGEN_RESPONSE_EARLY [200]	15	1.06E-05	7.56E-05
HALLMARK_GLYCOLYSIS [200]	14	4.43E-05	2.77E-04
HALLMARK_MTORC1_SIGNALLING [200]	13	1.72E-04	8.61E-04
HALLMARK_MYOGENESIS [200]	13	1.72E-04	8.61E-04

Table 3.6. Downregulated HALLMARKS in ΔN-WT LNCaP C4-2 cells. Tabulated is the number of genes from ΔN-WT DEGs lists that are common to the list of genes that comprise HALLMARK gene sets, along with p-value and FDR q-value for each HALLMARK. The number of genes which comprise each HALLMARK is in square brackets. The MSigDB was used for HALLMARK enrichment analysis *(Subramanian et al., 2005 ; Liberzon et al., 2015).*

Hallmarks	**# Genes in Overlap**	**p-value**	**FDR q-value**
HALLMARK_KRAS_SIGNALLING_UP [200]	18	3.16 E-8	8.63 E-7
HALLMARK_ANDROGEN_RESPONSE [100]	13	3.45 E-8	8.63 E-7
HALLMARK_UV_RESPONSE_DN [144]	14	4.14 E-7	6.9 E-6
HALLMARK_HYPOXIA [200]	16	8.98 E-7	1.12 E-5
HALLMARK_ESTROGEN_RESPONSE_LATE [200]	15	4.34 E-6	4.34 E-5
HALLMARK_ESTROGEN_RESPONSE_EARLY [200]	14	1.96 E-5	1.63 E-4
HALLMARK_COMPLEMENT [200]	13	8.23 E-5	4.57 E-4
HALLMARK_KRAS_SIGNALLING_DN [200]	13	8.23 E-5	4.57 E-4
HALLMARK_TNFA_SIGNALLING_VIA_NFKB [200]	13	8.23 E-5	4.57 E-4
HALLMARK_IL2_STAT5_SIGNALLING [199]	12	3.06 E-4	1.45 E-3

Table 3.7. Upregulated HALLMARKS in KO-WT LNCaP C4-2 cells. Tabulated is the number of genes from KO-WT DEGs lists that are common to the list of genes that comprise HALLMARK gene sets, along with p-value and FDR q-value for each HALLMARK. The number of genes which comprise each HALLMARK is in square brackets. The MSigDB was used for HALLMARK enrichment analysis *(Subramanian et al., 2005 ; Liberzon et al., 2015).*

Hallmark	**# Genes in Overlap**	**p-value**	**FDR q-value**
HALLMARK_G2M_CHECKPOINT [200]	24	1.76 E-18	8.81 E-17
HALLMARK_E2F_TARGETS [200]	20	4.4 E-14	1.1 E-12
HALLMARK_MITOTIC_SPINDLE [199]	18	4.59 E-12	7.65 E-11
HALLMARK_ESTROGEN_RESPONSE_LATE [200]	11	9.41 E-6	1.18 E-4
HALLMARK_ESTROGEN_RESPONSE_EARLY [200]	10	5.36 E-5	4.47 E-4
HALLMARK_P53_PATHWAY [200]	10	5.36 E-5	4.47 E-4
HALLMARK_GLYCOLYSIS [200]	9	2.77 E-4	1.73 E-3
HALLMARK_KRAS_SIGNALLING_UP [200]	9	2.77 E-4	1.73 E-3
HALLMARK_SPERMATOGENESIS [135]	7	5.68 E-4	3.15 E-3
HALLMARK_BILE_ACID_METABOLISM [112]	6	1.18 E-3	5.9 E-3

Table 3.8. Downregulated HALLMARKS in KO-WT LNCaP C4-2 cells. Tabulated is the number of genes from KO-WT DEGs lists that are common to the list of genes that comprise HALLMARK gene sets, along with p-value and FDR q-value for each HALLMARK. The number of genes which comprise each HALLMARK is in square brackets. The MSigDB was used for Hallmark analysis *(Subramanian et al., 2005 ; Liberzon et al., 2015).*

Hallmark	**# Genes in Overlap**	**p-value**	**FDR q-value**
HALLMARK_UV_RESPNSE_DN [144]	14	2.8 E-11	1.4 E-9
HALLMARK_GLYCOLYSIS [200]	9	5.84 E-5	7.3 E-4
HALLMARK_INFLAMMATORY_RESPONSE [200]	9	5.84 E-5	7.3 E-4
HALLMARK_KRAS_SIGNALLING_UP [200]	9	5.84 E-5	7.3 E-4
HALLMARK_EPITHELIAL_MESENCHYMAL_TRANSITION [200]	8	3.33 E-4	3.33 E-3

3.6. Alterations in Cell Proliferation in ΔN and KO LNCaP C4-2 cells.

With the observation that genes implicated with cell cycle progression are significantly enriched in both CRISPR edited clones *(Tables 3.5 and 3.7)* several assays were conducted to what effects this has *in vitro.* To explore how dysregulated cell cycle gene expression effects cell proliferation, crystal violet staining was first conducted. After 7 days of growth in complete medium, WT, ΔN and KO C4-2 cells were washed and stained with crystal violet. It was apparent that both CRISPR clones showed reduced cell density (indicative of halted proliferation) through crystal violet staining *(Figure 3.12).* Subsequently MTT assays were conducted to further measure cell proliferation and the viability of WT, ΔN and KO C4-2 cells. Impairment of KO C4-2 cell viability was detected after 24h of growth *(Figure 3.13).* By 72h both CRISPR lines showed significant reductions in cell viability relative to WT LNCaP C4-2 cells *(Figure 3.13).*

To gain a detailed understanding why proliferation is halted in CRISPR clones BrdU staining was conducted. BrdU is a thymidine analog which incorporates into newly synthesized DNA. By antibody staining for BrdU this facilitates the detection of active DNA synthesis, measured by flow cytometry. In conjunction with BrdU staining, the cells total DNA content can also be measured by flow cytometry through staining with propidium iodide. Brdu staining reveals that both CRISPR lines have stalled cell cycle progression due to a significant accumulation of cells in G1 phase of the cell cycle *(Figure 3.14).* Additionally, KO and ΔN cells show significantly reduced counts in S and G2 phase of the cell cycle respectively *(Figure 3.14).* Collectively, these results are consistent with a publication by *Wang et al., (2022)* highlighting the proliferation defects of clone ΔN *in vitro* and *in vivo.* This publication does not report the proliferation defects observed in clone KO, which is presented in these data.

A.

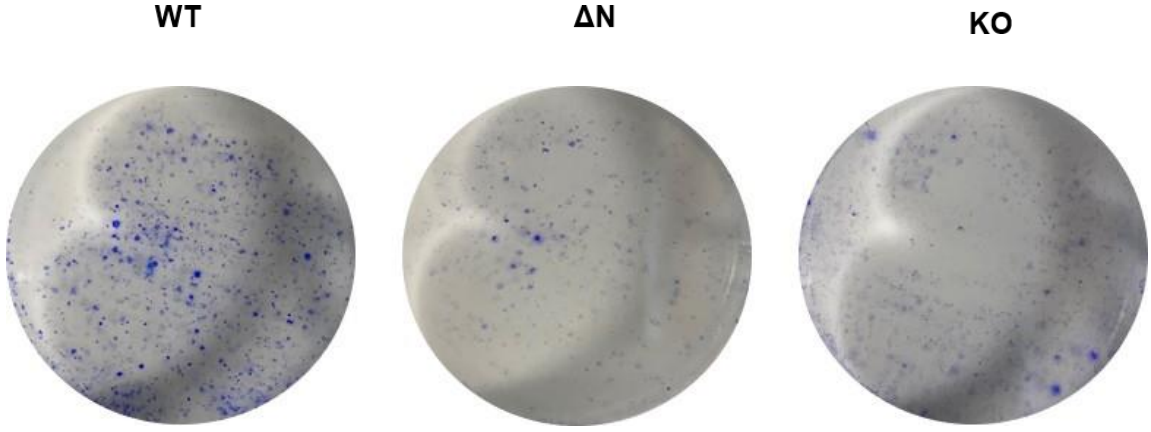

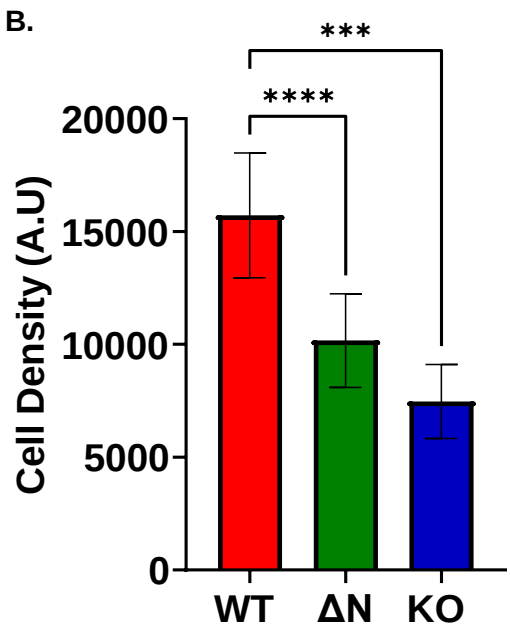

Figure 3.12. Crystal violet growth assays of WT , ΔN and KO C4-2 cells. **A.** Representative 6 well plate images of crystal violet staining of WT , ΔN and KO C4-2 cells. **B.** Quantification of cell proliferation assays (in arbitrary units). Data is of biological striplicates (n=3) with technical triplicates per cell type. Statistical significance was determined by a one-way ANOVA with a Tukey's multiple comparisons test. *** P ≤ 0.001 , **** P ≤ 0.0001.

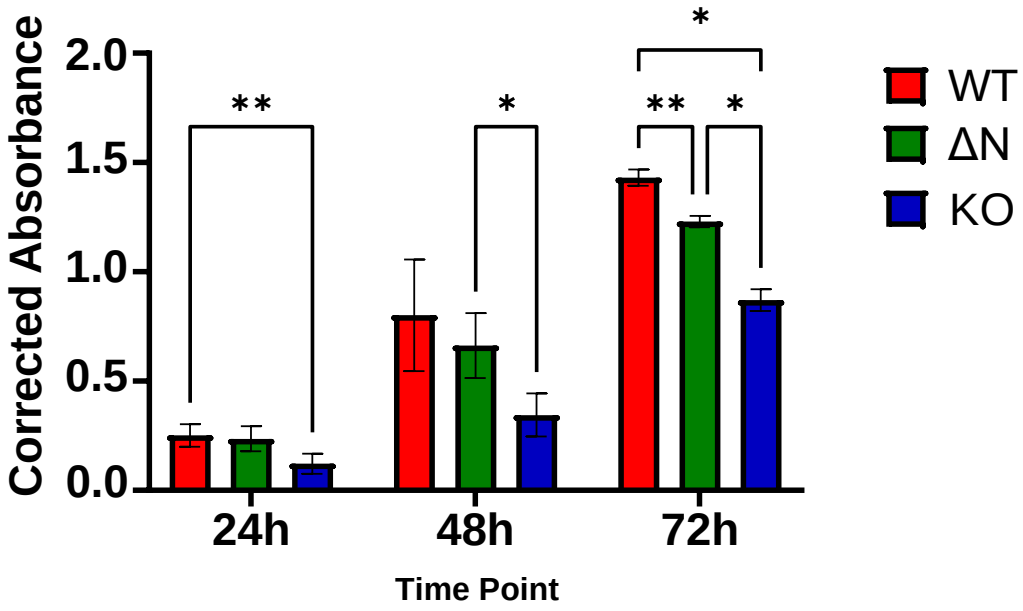

Figure 3.13. MTT viability assays of WT , ΔN and KO C4-2 cells. Data is of biological triplicates (n=3) with technical quintuplets per cell line. 24h , 48h and 72h time points were used in these assays. Statistical significance was determined by a two-way ANOVA with a Tukey's multiple comparisons test. P*≤ 0.05 , P** ≤ 0.01

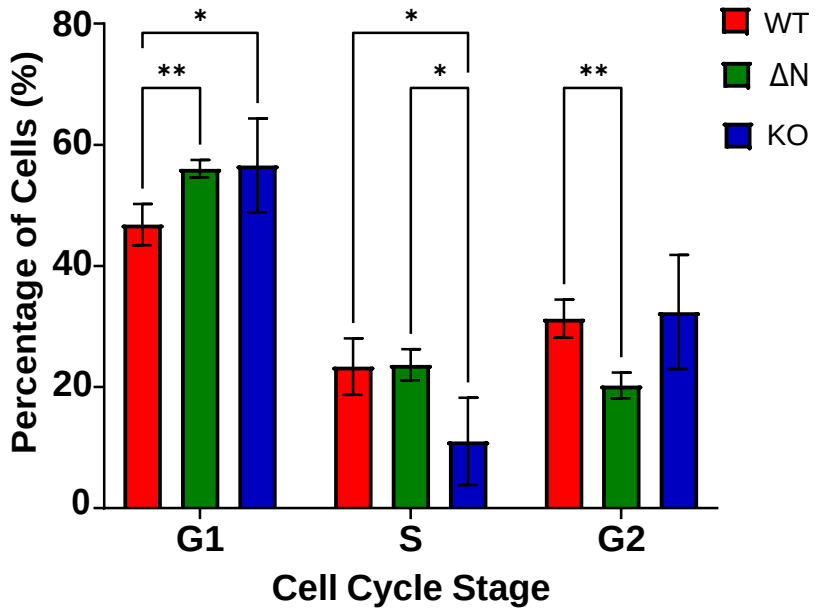

Figure 3.14. BrdU Cell Cycle Analysis in in WT, ΔN and KO C4-2 cells. Data is of biological duplicates (n=2) with technical triplicates per cell line. Statistical significance was determined by a two-way ANOVA with a Tukey's multiple comparisons test. *P ≤ 0.05, P** ≤ 0.01.

3.7. Increases in DNA Damage in ΔN and KO LNCaP C4-2 cells.

A possible explanation for the growth arrest which is exhibited by ΔN and KO C4-2 cells may be due DNA damage. In light of increased cell cycle gene expression in both CRISPR clones, this may contribute to a phenomenon known as oncogene induced replication stress. This theory has suggested that prolonged activation of cell cycle genes induces replication stress, leading to DNA damage and cell cycle arrest *(Sarni and Kerem, 2017).* The mechanisms of which cell cycle genes can induce replication stress includes inappropriate origin firing, the point of which DNA is unwounded, before the loading of DNA helicases *(Li and Araki, 2013).* Aberration in the Rb/E2F pathway has been attributed to dysregulation of origin firing *(Kotsantis et al., 2018).* This is consistent with previous HALLMARK analysis highlighting that this pathway is

upregulated in ΔN and KO cells *(Tables 3.5 and 3.7).* The consequences of dysregulated origin firing includes compromise of the replication fork; with cells entering mitosis with over replicate or under replicated DNA, inducing genomic instability *(Kotsantis et al., 2018).*

Replication stress induces double stranded DNA breaks, recognized by the kinases ataxia-telangiectasia mutated (ATM) and ataxia telangiectasia and Rad3-related (ATR) *(Fragkos et al., 2009).* In response to double stranded DNA breaks ATM and ATR phosphorylates H2AX at Ser139, generating γ-H2AX *(Fragkos et al., 2009).* γ-H2AX facilitates the recruitment of further repair proteins to the site of DNA damage, such as members of the MRN complex *(Podhorecka, et al. 2010).* Immunofluorescence with an γ-H2AX antibody was conducted to assess whether the CRISPR clones exhibit elevated levels of γ-H2AX, a feature of replication stress. This revealed that CRISPR clones (particularly ΔN C4-2 cells) exhibited elevated levels of γ-H2AX foci relative to WT C4-2 cells which is indicative of increased DNA damage *(Figure 3.15).*

A.

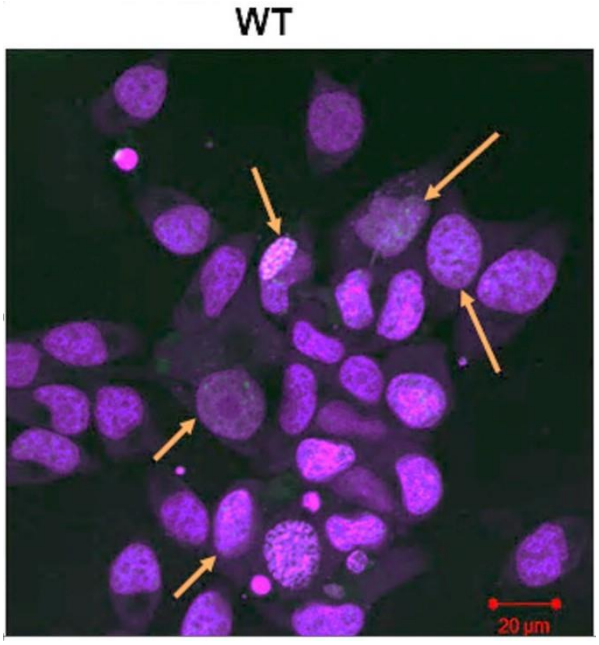

B.

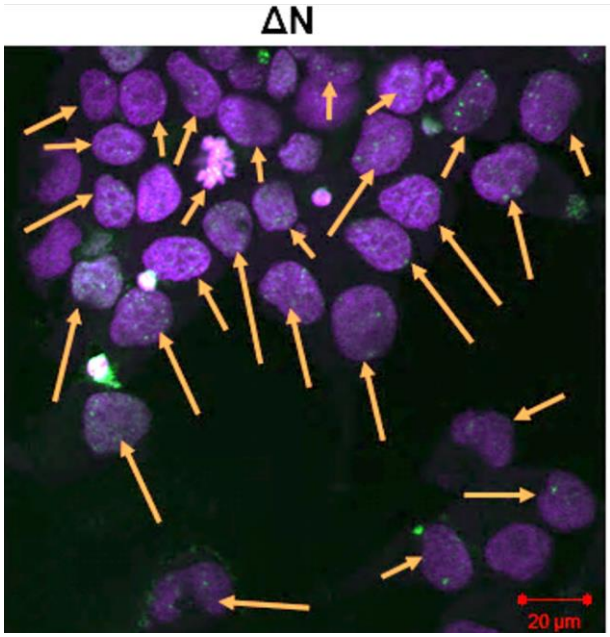

C.

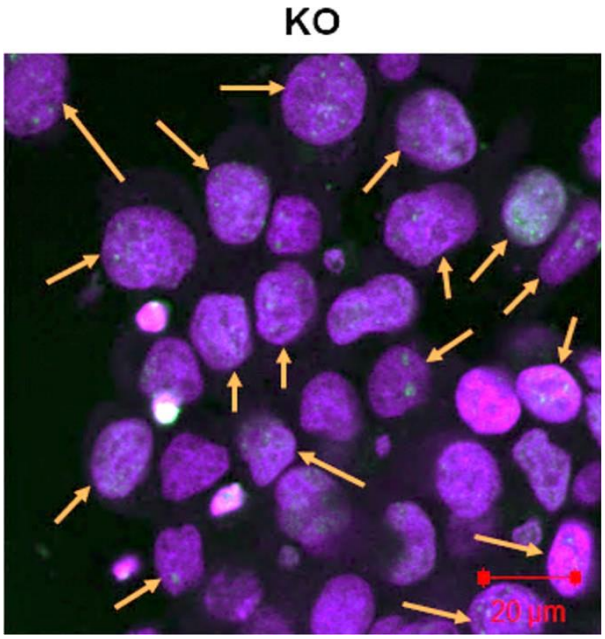

D.

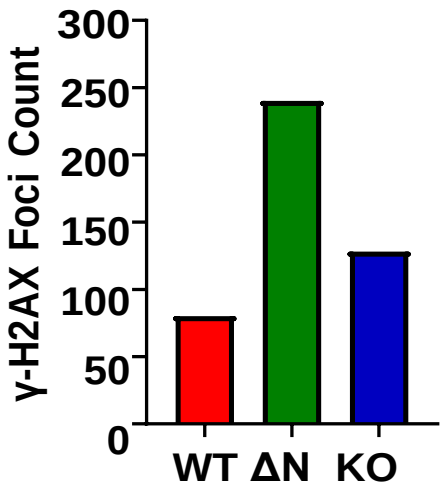

Figure 3.15. γ-H2AX detection in WT, ΔN and KO LNCaP C4-2 cells. A, B and C are representative immunofluorescence images of γ-H2AX foci (in green) and DRAQ5 nuclear stain (in purple) in WT, ΔN and KO LNCaP C4-2 cells respectively. Orange arrows indicate cells containing γ-H2AX foci. A Zeiss LSM510 Meta confocal microscope was used for image acquisition. **D.** Graphed is the number of γ-H2AX foci from WT, ΔN and KO LNCaP C4-2 cells. The number of γ-H2AX foci was counted manually from 75 cells.

Cell cycle progression is also influenced by the interplay between cyclins and CDKs, where sequential activation is required throughout the cell cycle to mediate the transition from each phase. Activation of CDKs is mediated through direct binding with a cognate cyclin. Activated CDKs can then phosphorylate pRB which relieves the negative inhibition pRB exerts upon E2F target genes *(Topacio et al., 2019).*

In the case of G1, key CDKs which drive progression through this phase include CDK2, CDK4 and CDK6 *(Jingwen et al., 2017).* Potent negative regulation of these three CDKs can be achieved through direct interactions with p21, which blocks kinase activity and progression through G1 *(Harper et al., 1995).* Subsequently, several accounts have indicated that elevated p21 levels induce G1 phase arrest, halting cell cycle progression (*Waldman et al., 1995 ; Niculescu et al., 1998 ; Barr et al., 2017).* Elevated p21 protein levels were found in ΔN and KO LNCaP C4-2 cells, relative to WT cells, as shown through western blotting *(Figure 3.15).* This consistent with the proliferation defects previously observed for both these clones *(Figures 3.12, 3.13 and 3.14).*

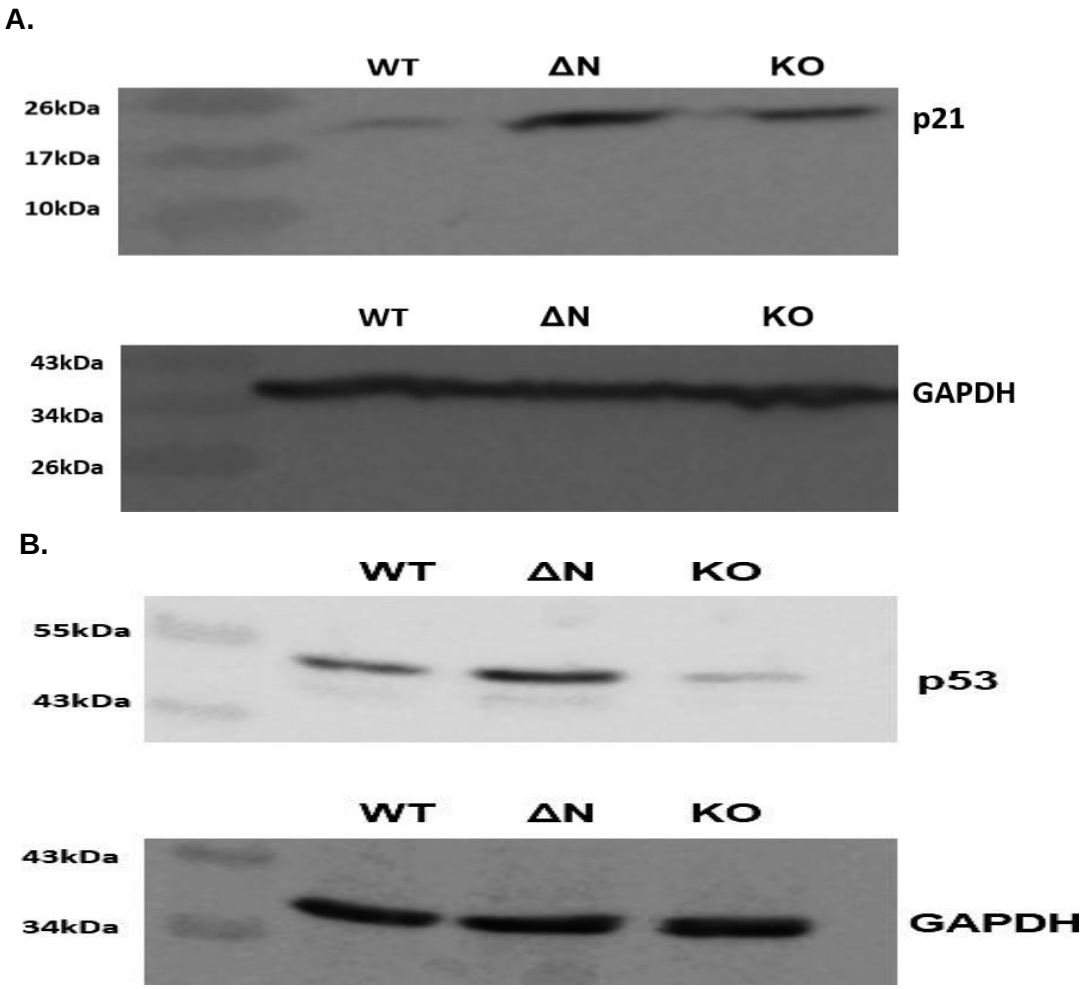

Figure 3.16. Western blot of p21 and p53 protein expression in WT, ΔN and KO C4-2 cells. A. Proteins were extracted using RIPA buffer and resolved on 15% SDS-PAGE gels before blotting for p21 expression. **B.** Proteins were extracted using RIPA buffer and resolved on 10% SDS-PAGE before blotting for p53 expression. Proteins used in GAPDH loading controls were resolved on either 10% or 15% SDS- PAGE gels before being blotted for GAPDH expression.

Additional western blotting was conducted to assess the levels of p53 in WT and CRISPR edited LNCaP C4-2 cells. The premise for this is that (in light of DNA damage) p53 positively regulates the transcription of p21. The p21 gene, Cyclin dependent kinase inhibitor 1A (CDKN1A), contains two p53 binding sites in its promoter *(el-Deiry et al., 1995).* Whilst ΔN cells show increased levels of p53 relative to WT C4-2 cells, decreases in p53 protein levels was observed in KO C4-2 cells *(Figure 3.16).* Nevertheless, p21 expression is elevated in both CRISPR clones *(Fig.16*

3.8. Alterations in Steroid Signalling in ΔN and KO LNCaP C4-2 cells.

With HALLMARK overlap analysis also revealing that steroid signalling pathways are altered in both CRISPR clones *(Tables 3.5, 3.6 and 3.7)* additional assays were conducted to investigate this further. In the context of prostate cancer, KLK3 reflects a classical AR target, with elevated expression associated with increased AR signalling (*Olsen et al., 2016).* This gene contains two ARE in its proximal promoter *(Lawrence et al., 2012).* The enhancer region contains a third ARE, and five non-consensuses accessory AREs, along with multiple binding sites for AR co-factors *(Lawrence et al., 2012).* Validation was conducted to highlight that in both our CRISPR lines possess elevated KLK3/PSA mRNA and protein expression *(Figures 3.17 and 3.18).*

However, increases in KLK3/PSA expression was not associated with increased AR protein expression, ruling out the possibly that elevated AR levels are driving increased KLK3/PSA expression *(Figure 3.19).* Interestingly modest reductions in AR expression was observed in ΔN LNCaP C4-2 cells *(Figure 3.19).* Subsequently, when both kinase depleted clones are rescued with a PIP5K1α construct (PIP5K1α-mVenus-N1) the expression of KLK3/PSA at the mRNA level is significantly reduce *(Figure 3.20).*

Confocal microscopy was conducted to assess the localisation of PIP5K1α-mVenus-N1 in WT and CRISPR edited clones. This revealed strong membrane of PIP5K1α-mVenus-N1 when expressed in WT and CRISPR edited clones *(Figure 3.21)* consistent with previous reports demonstrating membrane localisation of PIP5K constructs *(Tranet al., 2018 ; Gawden-Bone et al., 2018 ; Roberts, 2022*). This is in comparison to the predominant nuclear localisation when empty mVenus-N1 vector is transfected into WT, ΔN and KO LNCaP C4-2 cells *(Figure 3.21)*

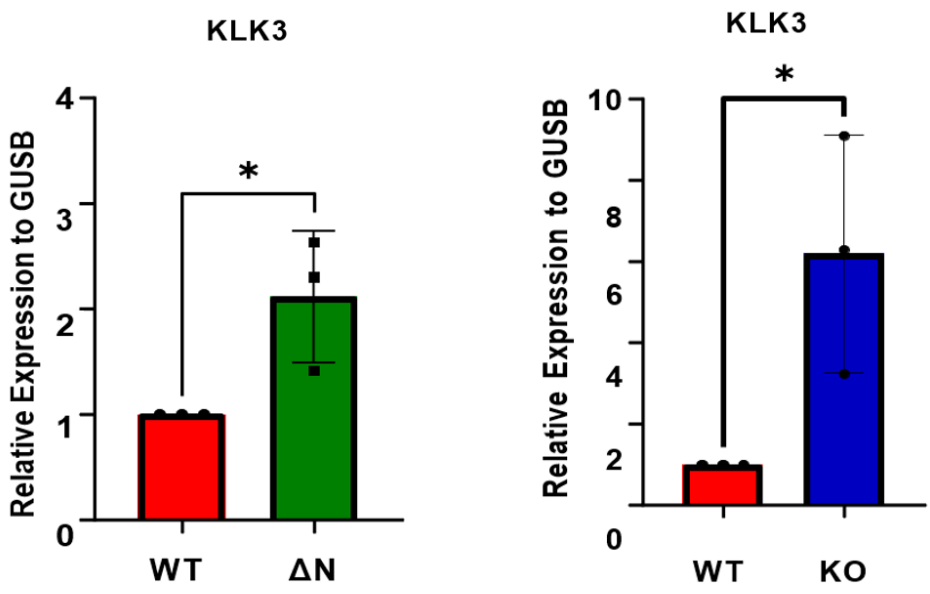

Figure 3.17. Relative expression of KLK3 in WT,ΔN and KO C4-2 cells. Data is of biological triplicates (n=3) with technical duplicates. Relative expression was calculated using the $2^{-\Delta\Delta Ct}$ method. Data was normalised to the expression of GUSB housekeeping gene per cell line. Statistical significance was determined by a one-way ANOVA with a Tukey's multiple comparisons test. * P ≤ 0.05.

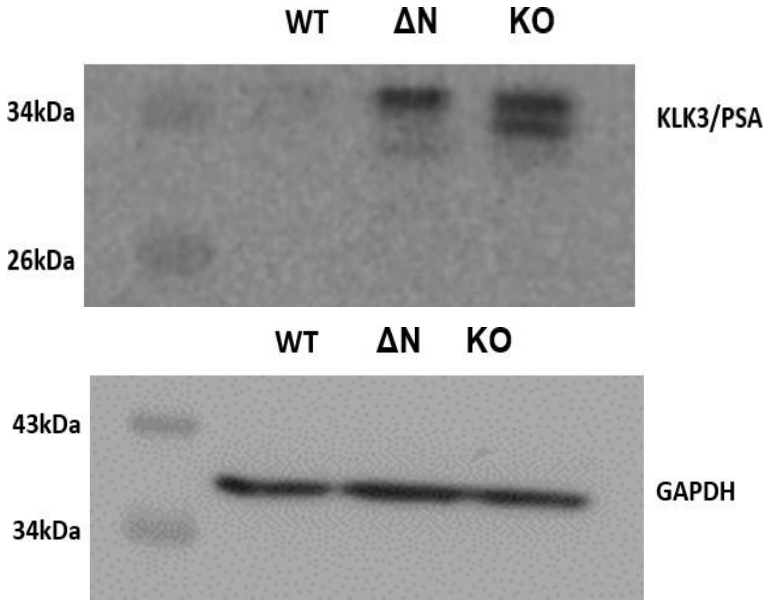

Figure 3.18. Western blot of KLK3/PSA protein expression in WT , ΔN and KO C4-2 cells. Proteins were extracted using RIPA buffer resolved on 10% SDS page gels before blotting KLK3/PSA and GAPDH (loading control) expression.

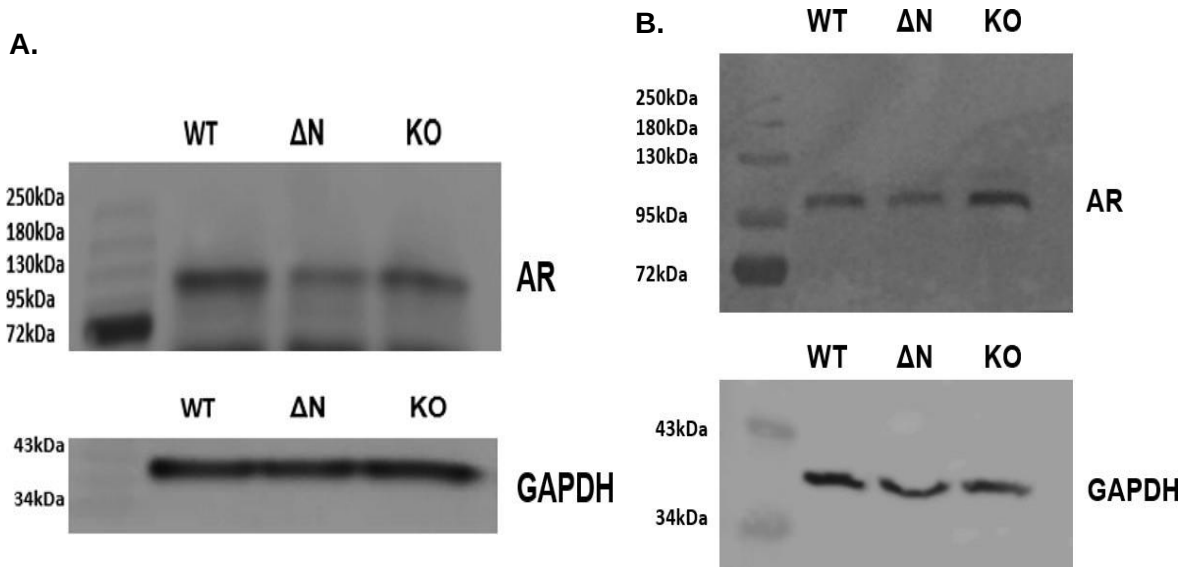

Figure. 3.19. Western blots of AR protein expression in WT , ΔN and KO C4-2 cells. Proteins were extracted using RIPA buffer resolved on 10% SDS page gels before blotting AR and GAPDH (loading control) expression. **A.** AR protein levels were detected using an anti-AR antibody (06-680) from Sigma Aldrich. **B.** AR protein levels were detected using an anti-AR antibody (#5153) from Cell Signalling Technology.

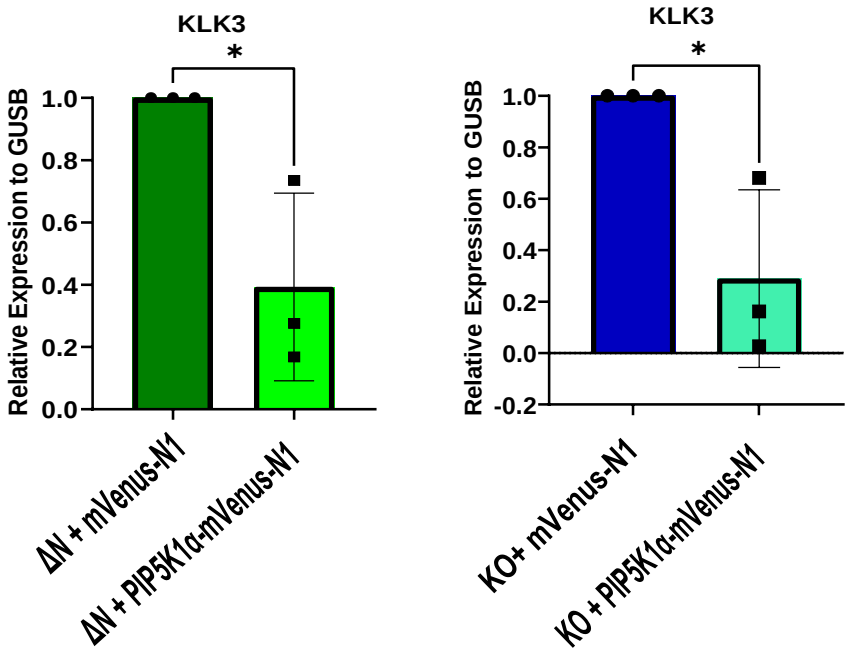

Figure 3.20. Relative expression of KLK3 in ΔN and KO C4-2 cells after rescue with PIP5K1α-mVenus-N1. Data is of biological triplicates (n=3) with technical duplicates. Relative expression was calculated using the $2^{-\Delta\Delta Ct}$ method. Data normalised to the expression of GUSB housekeeping gene per cell line. Two sided t-tests were used to show the significance between ΔN and KO cells transfected with mVenus-N1 and PIP5K1α-mVenus-N1. * $P \leq 0.05$

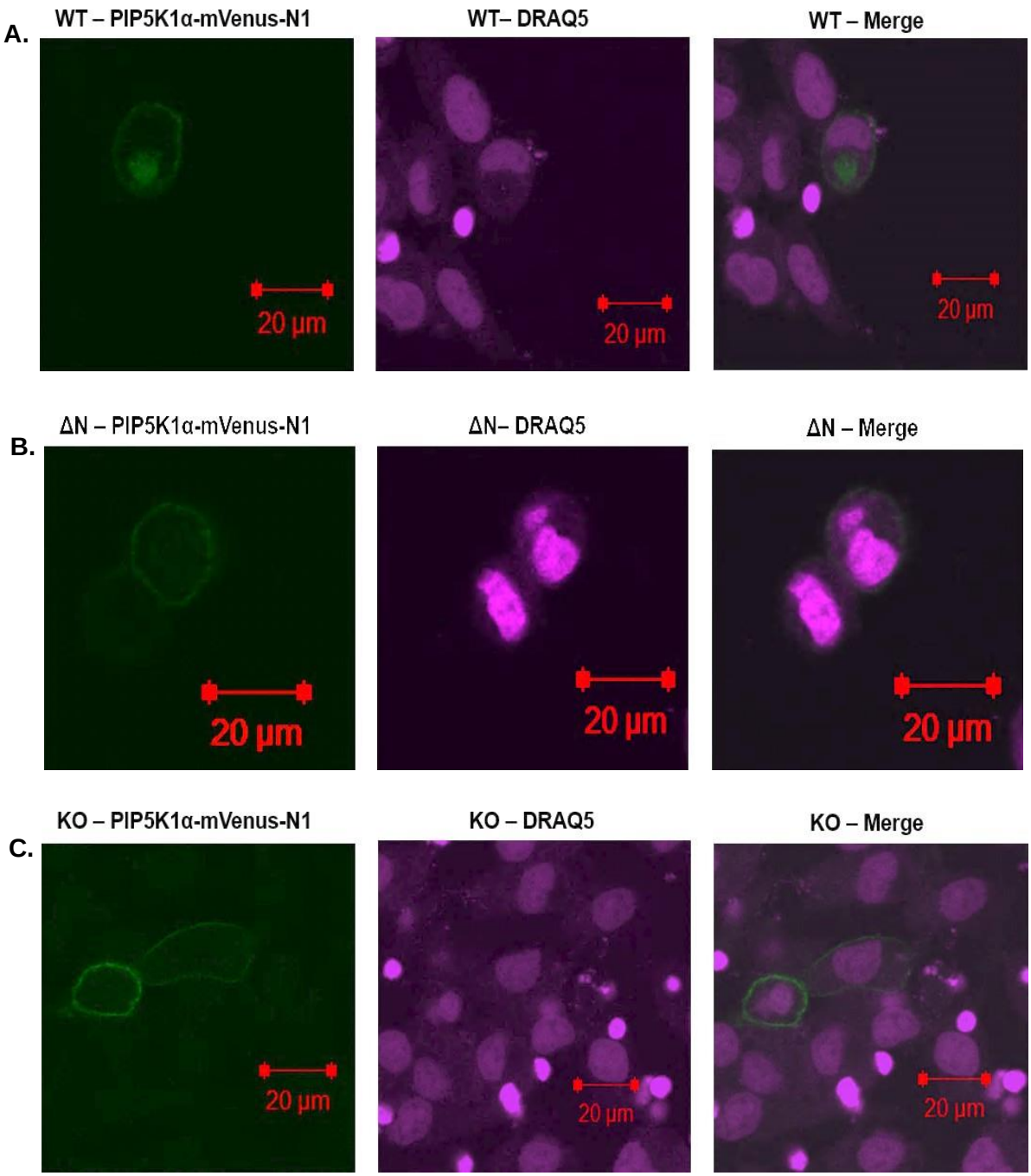
A.
WT – PIP5K1α-mVenus-N1
WT– DRAQ5
WT – Merge
20 µm
20 µm
20 µm
B.
ΔN – PIP5K1α-mVenus-N1
ΔN– DRAQ5
ΔN – Merge
20 µm
20 µm
20 µm
C.
KO – PIP5K1α-mVenus-N1
KO – DRAQ5
KO – Merge
20 µm
20 µm
20 µm

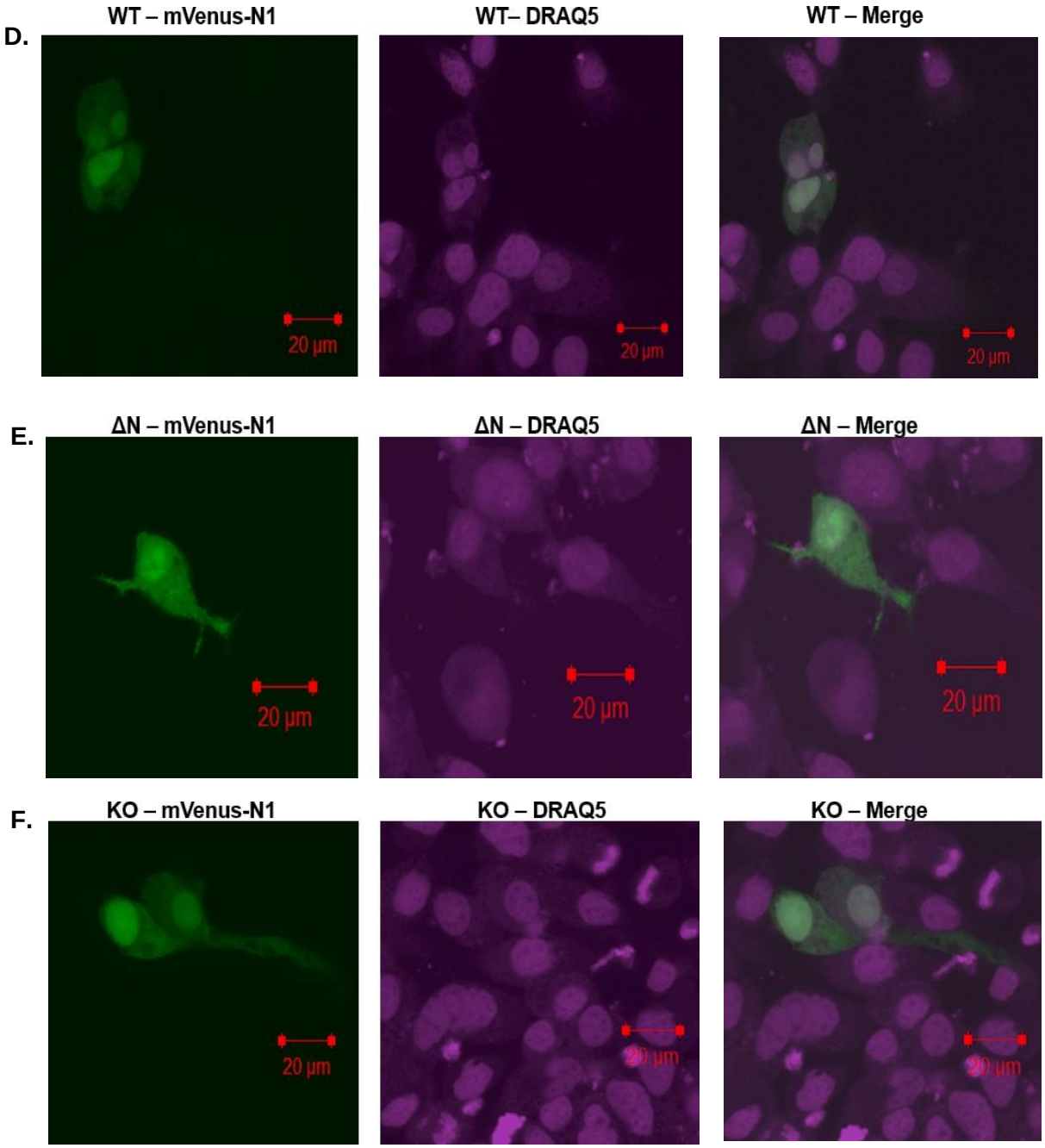

Figure 3.21. Localisation of PIP5K1α-mVenus-N1 and empty vector (mVenus-N1) in WT, ΔN and KO LNCaP C4-2 cells. Cells were transfected with either PIP5K1α-mVenus-N1 or empty vector (mVenus-N1), grown for 48h before being prepared for confocal microscopy. A Zeiss LSM510 Meta confocal microscope was used for image acquisition. **A, B and C.** The localisation of PIP5K1α-mVenus-N1 in WT, ΔN and KO LNCaP C4-2 cells respectively. **D, E and F.** The localisation of mVenus-N1 in WT, ΔN and KO LNCaP C4-2 cells respectively.

3.9. **Comparison of ΔN and KO transcriptomes with *Mellmen et al.. (2008)***

Finally, this section will explore possible overlaps of common DEGs observed in ΔN-WT and KO-WT comparisons to those reported in *Mellmen et al., (2008)*. Whilst it can be appreciated that these comparisons are of different types of data (bulk RNA-Seq from prostate cancer cells, and microarray data of polyadenylated transcripts in non-tumorigenic HEK293 cells) nevertheless genes highlighted in this comparison may suggest that PIP5K1α function is required for their regulation.

Before comparisons were made, additional processing of *Mellmen et al., (2008)* microarray data was conducted. Whilst DeSeq2 was conducted for RNA-Seq data, this package is only applicable with RNA count data. With microarray data being in the form of intensities arising from fluorophore staining of DNA hybridized to oligonucleotide probes *(Held, et al., 2006)* a different package was required for DEGs identification. Intensity data was analyzed through the Linear Models for Microarray Data (limma), a package which has been utilised over the last ~15 years *(Smyth, 2005 ; Ritchie et al., 2015).* A Log2FC of 1 and an FDR of 0.01 was required for a gene to be classed as differentially expressed in limma, the same significance cut-offs used in DeSeq2.

Using these parameters the number of upregulated and downregulated mRNAs between siRNA PIP5K1A knockdown and siRNA control data (n=3) was 674 and 845 respectively. Comparisons between upregulated and downregulated genes from ΔN-WT and KO-WT cells to DEGs from *Mellmen et al., (2008)* are documented in *Tables 3.9 and 3.10.* The biggest overlap was recorded when ΔN-WT downregulated DEGs were compared to siRNA PIP5K1A – siControl downregulated DEGs, with this revealing 61 common DEGs. Venn diagrams of common upregulated and downregulated genes between ΔN , KO and siRNA HEK293 cells

are shown in *Figures 3.22 and 3.23.* These comparisons revealed a small and diverse subset of common upregulated and downregulated genes, 4 and 12 respectively.

Table 3.9. Common upregulated gene– found in ΔN - WT and siRNA PIP5K1A – siControl DEG lists. siRNA PIP5K1A – siControl DEG lists were generated from the *Mellemen et al., 2008* gene microarray dataset, with limma used to identify differentially expressed genes.
Significance cut offs for limma was a Log2FC and an FDR of 0.01. The limma package was run through the IDEP 0.93 web application *(Ge, et al., 2018).*

	ΔN-WT Upregulated DEGs –852 DEGs)	**KO - WT Upregulated DEGs (447 DEGs)**
siRNA PIP5K1A – siControl : Upregulated DEGs (674 DEGs)	23 Common DEGs (1.5%)	6 Common DEGs (0.5%)

Table 3.10. Common downregulated gene– found in ΔN - WT and siRNAPIP5K1A – siControl DEG lists. siRNA PIP5K1A – siControl DEG lists were generated from the *Mellemen et al., (2008)* gene microarray dataset, with limma used to identify differentially expressed genes. Significance cut offs for limma was a Log2FC and an FDR of 0.01. The limma package was run through the IDEP 0.93 web application *(Ge, et al., 2018).*

	ΔN-WT Downregulated DEGs –823 DEGs)	**KO - WT Downregulated DEGs (371 DEGs)**
siRNA PIP5K1A – siControl : Downregulated DEGs (845 DEGs)	61 Common DEGs (3.8%)	17 Common DEGs (1.4%)

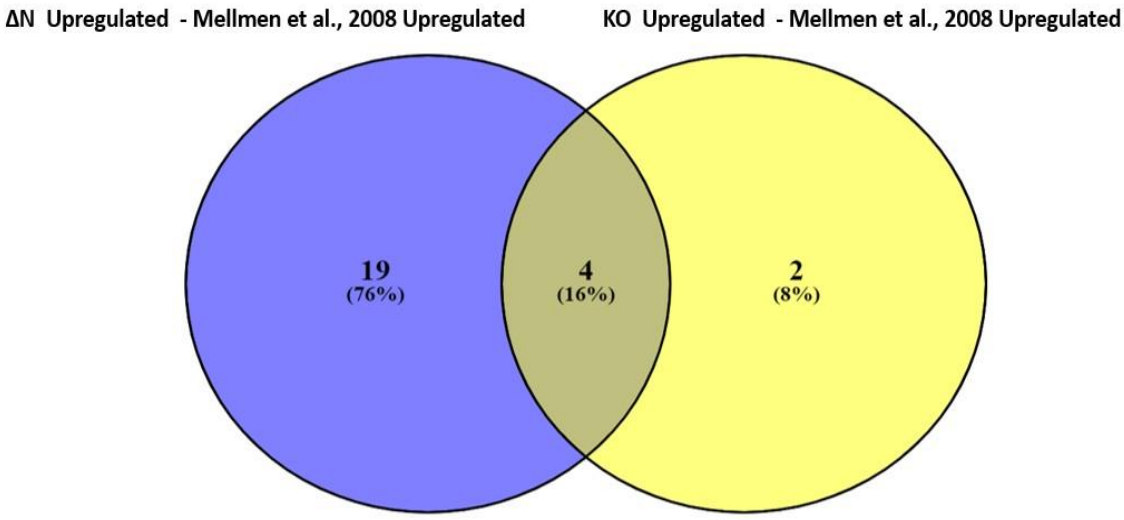

Figure 3.22. Venn diagrams highlighting the 4 common upregulated gen–s between ΔN - WT v siRNA PIP5K1A – siControl DEGs and KO – WT v siRNA PIP5K1A – siControl DEGs. The 4 common DEGs are: GPC4, QPRT, ZBTB47, GNAL.

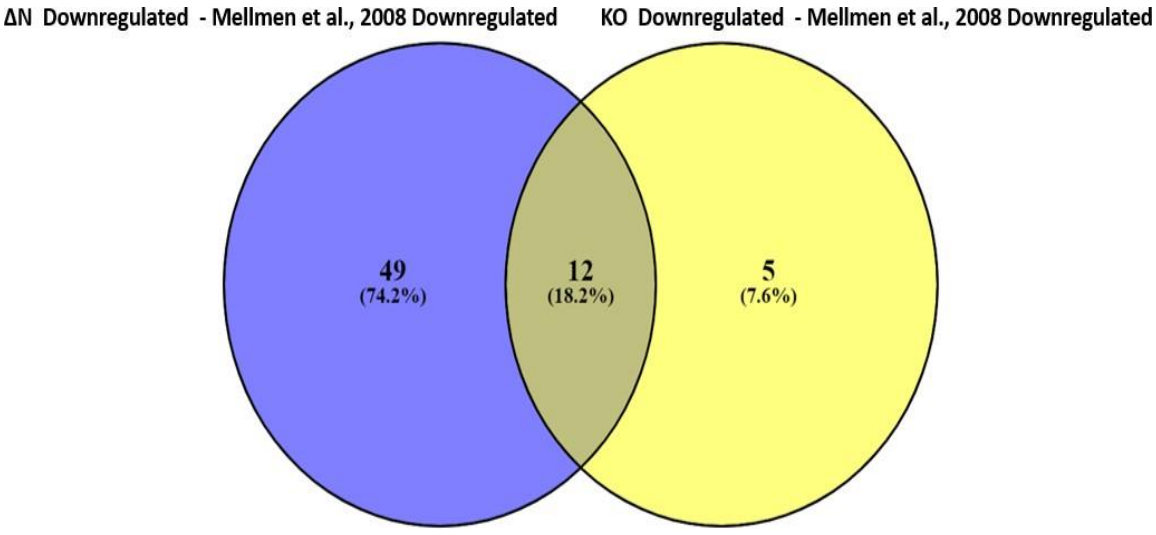

Figure 3.23. Venn diagrams highlighting the 12 common downregulated gen–s between ΔN - WT v siRNA PIP5K1A – siControl DEGs and KO – WT v siRNA PIP5K1A – siControl DEGs. The 12 common DEGs are: HS3ST1 , NEXMIF , CRYBG1 , SUSD4 , RAB39B , ZNF667-AS1 , BMERB1 , FRMD3 , TCIM , GPC6 , ZNF568 , H2BC7.

3.10. Discussion

The results from this chapter indicates that loss of PIP5K1α has a profound effect upon the transcriptome of LNCaP C4-2 prostate cancer cells. Observed was ~2 fold more DEGs in ΔN C4-2 cells relative to clone KO. Possible explanations for why ΔN C4-2 cells possessed greater numbers of DEGs include this CRISPR clone exhibiting elevated AKT activity *(Roberts, 2022 and detailed subsequently in Chapter 5).* AKT has been reported to phosphorylate ~200 different substrates *(Toker, 2012)* and through this, modulate pathways involved in gene transcription such as mTOR ,FOXO , and Wnt/ β-catenin signalling *(Creighton, 2007 ; Hoogeboom etal., 2008 ; Tenbaum et al., 2012).*

This chapter focused on pathways which are coordinated by AR and cell cycle genes, as from these data it appears PIP5K1α is implicated in their regulation. Both CRISPR clones show dysregulation of genes implicated in AR signalling, principally KLK3 where increased expression was observed at the mRNA and protein level *(Figures 3.16 and 3.17).* Subsequently, rescuing the kinase depleted clones with PIP5K1α-mVenus-N1 resulted in significant reductions in KLK3 expression *(Figure 3.19)* highlighting a possible function interplay between PIP5K1α and the regulation of KLK3/PSA expression. Elevated AR levels was ruled as a contributing factor to why KLK3/PSA expression is increased in ΔN and KO C4-2 LNCaP cells, with clone ΔN exhibiting reduced AR expression *(Figure 3.18).*

Whilst the levels of AR appear to be lower in ΔN , this wouldn't rule out the possibility of the AR in this CRISPR clone possessing elevated activity through aberrant AKT signalling. Several studies have reported that AKT can phosphorylate AR on S210/S213 and S790/791 which can enhance transcriptional activity *(Wen et al., 2000 ; Lin et al., 2001 , McCall et al., 2008).* For example, KLK3/PSA luciferase assays by *Wen et al., (2000)* demonstrated that expressing constitutively active AKT

enhanced luciferase activity ~5 fold relative to a dominant negative AKT control in LNCaP cells. The levels of phosphorylated AR in WT, ΔN and KO LNCaP C4-2 cells was not investigated in this work and reflects a possible avenue for further exploration.

Possible mechanism as why increased AR signalling was observed in both CRISPR clones includes the loss of expression of UGT2B genes *(Figures 3.10 and 3.11)* which conjugates androgens. The addition of glucuronyl moiety by UGT2B family members attenuates androgen signalling in two distinct mechanisms. Firstly, this moiety makes androgens more water soluble, which facilitates secretion *(Bao et al., 2008).* Secondly, the glucuronyl moiety is bulky, and when added to androgens, this impairs ligand binding to AR *(Bao et al., 2008).* Knockdown of either UGT2B15/17 in LNCaP cells further sensitises cells to DHT, and this triggers the upregulation of genes downstream of AR, such as KLK3 and VEGF *(Chouinard et al., 2007).* Possible regulation of UGT2B17 expression by PIP5K1α was highlighted by preliminary rescue experiments by *Roberts, (2022),* where transfection of KO LNCaP C4-2 cells with PIP5K1α-mVenus-N1 increased UGT2B17 mRNA expression. However further work is needed to fully validate whether rescuing the kinase depleted clones with PIP5K1α modulates the expression of UGT2B family members.

Alterations in cell cycle was also observed in ΔN and KO C4-2 cells, with the observations that both clones were experiencing growth arrest *(Figures 3.12, 3.13 and 3.14).* Contributing factors as to why both CRISPR clones were undergoing growth arrest includes the induction of DNA damage, as shown through elevated formation of γ-H2AX foci and increased p21 levels *(Figures 3.15 and 3.16).* Collectively whilst these assays show that the cell cycle is impaired in both CRISPR clones, further assays could be conducted to assess whether replication fork collapse was prominent in both CRISPR lines, a prominent feature of

oncogene induce replication stress *(Sarni and Kerem, 2017).* Such assays could include the DNA fibre assays which facilitates the monitoring of DNA replication fork dynamics at single molecule resolution *(Halliwell et al., 2020).* Possible caveats to these results however is that the growth rates of both clones were compared to WT LNCaP C4-2 cells. The WT LNCaP C4-2 cells used in this work did not undergo the stressful conditions induced by electrorotation and sorting. Additionally, to supplement the γ-H2AX immunofluorescence data *(Figure 3.15),* flow cytometry could have been utilised. This would have facilitated the detection of double stranded DNA breaks in larger, more random population of cells, rather than the 75 cells which were manually counted *(Figure 3.15).*

Whilst increases in p21 levels was observed in both CRISPR clones, upstream p53 protein levels were heavily reduced in KO C4-2 cells *(Figure 3.15).* A loss of p53 expression in KO C4-2 cells is consistent with a previous report suggesting that PIP5K1α is implicated in maintaining the stability of p53 *(Choi et al., 2019).* Knockdown of PIP5K1A through CRISPR-Cas9 reduces p53 levels in MDA-MB-231 breast cancer cells *(Choi et al., 2019).* It is postulated that PIP5K1α in conjunction with $PI(4,5)P_2$ directly interacts with p53, with $PI(4,5)P_2$ binding to the polybasic CTD of p53 *(Choi et al., 2019).* $PI(4,5)P_2$ binding to the CTD of p53 facilitates the recruitment HSPs which increases p53 stability *(Choi et al., 2019).* As KO cells underwent CRISPR editing of Exon 6, which encodes the PIP5K1α kinase domain, $PI(4,5)P_2$ dependent interactions with p53 may be impaired.

Although p53 levels were reduced in KO C4-2 cells, p21 expression can be induced in mechanisms which is not dependent on p53. For instance, AR signalling has been implicated with initiating p21 expression. CDKN1A harbours an ARE within its proximal promoter region and *in vitro* treating androgen responsive LNCaP cells with R1881 increases p21 expression *(Lu et al., 1999 ; Lu et al., 2000.)* With previous findings in this chapter highlighting alterations in androgen signalling in the CRISPR clones, this pathway maybe contributing to increases in p21

expression seen in both CRISPR clones, particularly in the case of KO. As such, an avenue for future work would be to explore whether the expression of CDKN1A/p21 is negatively regulated after rescue with PIP5K1α-mVenus-N1, which was shown to attenuate KLK3 expression *(Figure 3.19).*

Finally, the DEGs identified in this work were compared to the only previously published PIP5K1α transcriptomic dataset, generated by *Mellmen et al., (2008).* Between ΔN-WT , KO-WT and siRNA PIP5K1A–siControl data (*Mellmen et al., 2008)* only a small proportion of common DEGs were identified (4 upregulated genes and 12 downregulated genes). Limitations of these comparisons include differences in cell type (LNCaP C4-2 cells and HEK293 cells) and the type of data (bulk RNA-Seq and microarray of polyadenylated transcripts). If further transcriptome studies of cells with ablated PIP5K1A expression are published it would be important to compare DEGs from this work to these datasets. If DEGs identified in this work are replicated in future comparisons, this would add additional evidence that PIP5K1A is required for the regulation of these genes.

The next chapter explores the phosphoinositide pathway in WT and CRISPR edited clones in more detail. With KO LNCaP C4-2 cells undergoing CRISPR editing at Exon 6 (with this Exon encoding part of the PIP5K1α kinase domain), the effects this has on phosphoinositide production has assayed. For this, selective biosensors targeting certain phosphoinositides have been transfected into cells which have been used to track the localisation and abundance of the substrates and products of PIP5K1α phosphoinositides.

Chapter 4

Detection of Phosphoinositides in LNCaP C4-2 Prostate Cancer Cells Following PIP5K1A Abrogation

4.1. Introduction

PIP5Ks are cited as the primary kinase family implicated with the production $PI(4,5)P_2$ *(Bawazir et al., 2018).* This lipid is the most abundant phosphoinositide in the plasma membranes lipid bilayer, accounting for ~1% of cellular phospholipids mass *(Santos et al., 2013).* The glycerophospholipids comprise the vast majority of lipid bilayer, with sphingolipids and sterols constituting 30% and 20% respectively *(Dingjan and Futerman, 2021).* The prime function of sterols is to regulate the cell membrane fluidity, rigidity and permeability *(Kawakami et al., 2017).* Whilst sphingolipids have also been cited to contribute to the structure of cell membrane *(Breslow and Weissman, 2010)* these molecules, most notably ceramide, are thought to interact and regulate with a spectrum of signalling proteins such as Raf-1/c-Raf , ceramide-activated protein phosphatases and atypical PKCs *(Hla and Dannenberg, 2012).*

Whilst the amounts of $PI(4,5)P_2$ is marginal compared to that of sphingolipids and sterols, $PI(4,5)P_2$ is essential in the regulation of key cellular processes such as proliferation, cell migration and cell adhesion *(Mandal, 2020).* Cell migration arises through modulation of the actin cytoskeleton, which is in part mediated by small GTPases *(Zegers and Friedl, 2014).* A prime example of this is through Rac1, which via its hypervariable region can recruit PIP5Ks resulting in $PI(4,5)P_2$ production, actin uncapping and actin polymerisation *(Tolias et al., 2000 ; van Hennik et al., 2003).* Migration and cell adhesion can also be influenced by focal adhesion kinases (FAKs) which via its FERM domain binds to $PI(4,5)P_2$ *(Feng and Mertz, 2015).* Upon $PI(4,5)P_2$ binding this triggers FAK autophosphorylation that initiates the recruitment of Src which maximally activates FAKs through Y576 and Y577 phosphorylation *(Feng and Mertz, 2015). Goñi et al., (2014),* showed that knockdown of PIP5Kiγ expression in HeLa cells

attenuated Y576 and Y577 phosphorylation of FAK, and impaired cell adhesion to fibronectin. $PI(4,5)P_2$ has also been proposed to bind and modulate other adhesion proteins such as talin, ezrin, calpain and vinculin *(Sun et al., 2007).* With the critical roles that PIP5Ks and $PI(4,5)P_2$ exert in cell migration and adhesion, this chapter will detail how loss of PIP5K in LNCaP C4-2 affects these processes.

Much of the data presented in this chapter documents confocal microscopy experiments which have used selective biosensors to detect phosphoinositides in cells. These biosensors contain a specialised lipid binding domain fused to a fluorescent protein. When exogenously expressed in cells, the localisation of the biosensor indicates where lipid pools reside. Quantification of the fluorescent intensities of a given lipid biosensor can be captured by taking traces throughout a given cell. Typically these traces are across a whole cell, from the plasma membrane and then through cytoplasmic and nuclear compartments.

More than 20 phosphoinositide detecting biosensors have been recorded in the literature *(Hammond, etal., 2022).* Additionally, biosensors are also available to intermediates of phosphoinositides, for instance, the GFP-C1-PKCγ-C1A probe which detects DAG levels in cells *(Oancea et al., 1998).* PKCγ is a member of the classical PKC subfamily, characterised by harbouring a cystine rich C1 domain which has a high affinity for DAG *(Saito and Shirai, 2002).*

Along with the availability of different lipid biosensors, another benefit of deploying this approach to investigate lipid pools is the ease of use. Whilst mass spectrometry would give more quantitative view of phosphoinositide abundances in cells, it comes with several technical challenges. The first of which is due to low abundances of cellular phosphoinositides, detection these species can be difficult. If detected, then the low levels of ions generated through mass spectrometry (especially from highly phosphorylated phosphoinositides) impairs the resolution of the 3- , 4- , 5- phosphatase groups on inositol ring structures

(Kielkowska et al., 2014). Ultimately, this hinders the detection of regio-isomers of both PIP and PIP2 molecules from biological samples.

The low abundances of phosphoinositides means it is paramount that lipid extractions are conducted as efficiently as possible. Many of the methods used today are modifications from the protocol first developed by *Blight and Dyer, (1958)* in which lipids are dissolved in methanol and chloroform. Phase separation is then carried out to separate phospholipids from proteins and other hydrophobic molecules *(Zhao and Xu, 2010).* Whilst this approach can used successfully to detect membrane phospholipids such as phosphatidic acid, sphingolipids and phosphatidylinositol, it is not appropriate for the detection of PIP / PIP2 / PIP_3 species *(Zhao and Xu, 2010).* Modifications to the original *Blight and Dyer (1958)* protocol includes addition of certain acid and bases to further increase extraction efficiency *(Li et al., 2014)* and has been used successfully previously to assay sphingosine 1-phosphate and lysophosphatidic acid levels in platelets *(Yatomi et al., 2000).* However these approaches raise issues as too extreme acidic and basic conditions can induce the hydrolysis and degradation of other membrane phosphoinositides *(Pettitt et al., 2006 ; Li et al., 2014).*

The addition of trimethylsilyldiazomethane in methanol and chloroform reactions has since improved the analysis of phosphoinositides through mass spectrometry *(Clark et al., 2011 ; Kielkowska et al., 2014).* Trimethylsilyldiazomethane methylates the phosphate groups of phosphoinositides which neutralizes their positive charge and increases stability *(Mücksch et al., 2019).* Subsequently, this improves the number of ions released from phosphoinositide molecules when undergoing electrospray ionisation and facilitates greater detection *(Mücksch et al., 2019).*

The use of lipid biosensors has not come without its technical challenges too. Ultimately, these biosensors require transfection into cells which can make quantification difficult if low transfection efficiencies are observed. In the case of LNCaP cells, it has been cited this cell line is difficult to transfect *(Frønsdal et al., 2000 ; Stein et al., 2009 ; Thomas et al., 2021).* Similar challenges have been observed in the transient transfections of LNCaP C4-2 cells with different lipid biosensors (discussed subsequently). Consequently, this has impacted the number of cells which were used inthe quantification of biosensor fluorescent intensities.

Another bottleneck has been ensuring that the biosensors lipid binding domain is as selective as possible to the lipid of interest. This is so that the most accurate insight of relative abundances and localisation of lipids can be obtained. To negotiate this, there has been a continuous hunt within the field to identify the most selective lipid binding domains to use as biosensors. An example of this can be found by the attempts to develop a biosensor to PI(4)P, the substrate of PIP5Ks. Work by *Roy and Levine, (2004)* first highlighted the PH domain of the yeast homologs of oxysterol-binding protein (Osh1p and Osh2p) can bind and localise with cellular PI(4)P pools. However, using fluorescent constructs harbouring the PH domains oxysterol-binding proteins remained contentious, with these PH domains also exerting affinity towards PI(4,5)P_2 *(Roy, and Levine., 2004 ; Várnai et al., 2017)*.

A decade or so later saw the development of the highly selective PI(4)P biosensor, GFP-P4M-SidM *(Hammond et al., 2014).* For this approach, a novel lipid binding domain (P4M) from the SidM protein (secreted by *Legionella pneumophila*) was fused to fluorescent proteins. P4M was reported in earlier publications to be solely an PI(4)P effector protein *(Brombacher et al., 2009 ; Schoebel, et al., 2010)* whose function in the context of Legionnaires disease was to tether to host cell macrophages in a PI(4)P dependent manner *(Weber et al., 2006).* Ultimately, this small case study highlights how exploiting other biological systems be utilised to study mammalian phosphoinositides.

This chapter has utilised a spectrum of biosensors to investigate the abundance and localisation and of different phosphoinositides within WT, ΔN and KO C4-2 cells (highlighted in *Figure 4.0* and discussed in subsequent sections). Due to the number of different biosensors *(Figure 4.0)* and wanting to capture the spectrum of lipids which constitute the phosphoinositide cascade, only single experiments have been conducted.

The assay first described in this chapter will detail PI(4)P detection, the substrate utilised by PIP5Ks for the generation of $PI(4,5)P_2$. The levels of $PI(4,5)P_2$ were then assayed, in the presence and absence of the PIP5K agonist LPA, with this highlighting defects in $PI(4,5)P_2$ synthesis in clone KO. $PI(4,5)P_2$ can be hydrolysed by PLC family members, generating IP_3 and DAG. Through assaying DAG levels, no major alterations in this lipid were recorded in WT, ΔN and KOC4-2 cells. The final biosensor assays described in this work are attained to studying the localisation and abundance of Class I PI3K products, $PI(3,4)P_2$ and $PI(3,4,5)P_3$. Whilst the localisation and levels of $PI(3,4)P_2$ remain consistent between WT, ΔN and KO C4-2 cells, the localisation and abundance of $PI(3,4,5)P_3$ exhibited variability in the CRISPR edited clones, relative to WT C4-2 cells.

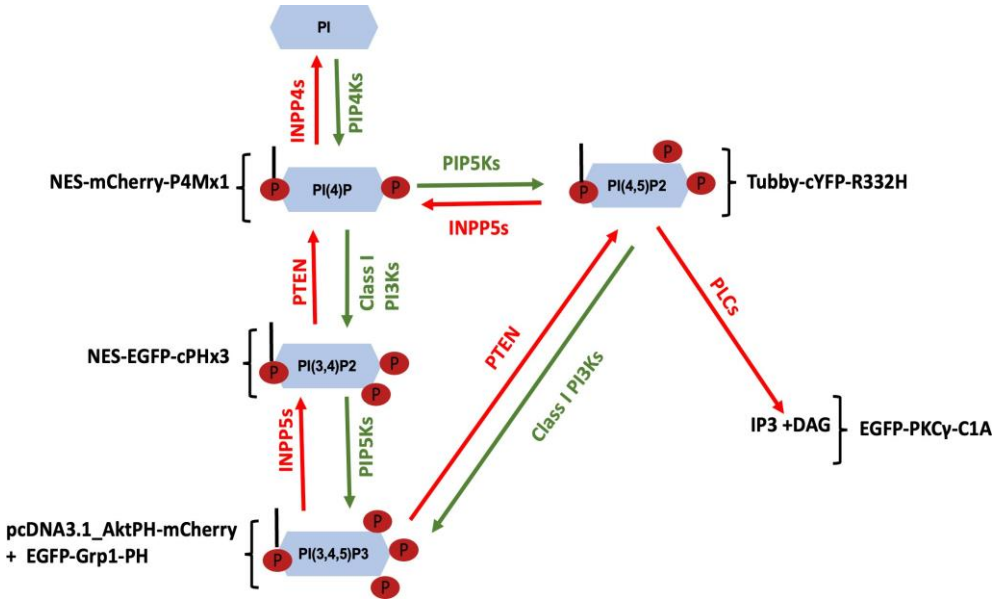

Figure 4.0. Biosensors used for the detection of phosphoinositides in WT and CRISPR edited LNCaP C4-2 cells. Schematic adapted from Figure 1.4 which depicts the phosphatidylinositol cycle. Biosensors are assigned next to the phosphoinositide they interact. PI(4,5)P2 is hydrolysed by PLC family members, leading to the formation of IP3 and DAG. The EGFP-PKCγ-C1A biosensor was used for the detection of DAG in WT and CRISPR edited LNCaP C4-2 cells.

4.2. Detection of PI(4)P in WT, ΔN and KO C4-2 Prostate Cancer Cells

One of the first phosphoinositide assayed in this work was PI(4)P. With PIP5Ks generating PI(4,5)P_2 from pools of PI(4)P it was important to investigate whether the levels of this lipid would be increased in cells lacking PIP5K1α expression. For assaying PI(4)P localisation and abundances in LNCaP C4-2 cells the mCherry-P4M-SidM biosensor was used. This plasmid encodes for the PI(4)P binding domain found in the SidM protein that's secreted by *Legionella pneumophila (Hammond et al., 2014).* Transient transfections of mCherry-P4M-SidM and other lipid biosensors (detailed in *Figure 4.0* and in subsequent sections) into WT, ΔN and KO C4-2 was at similar, albeit low transfection efficiencies.

After transfecting mCherry-P4M-SidM into WT, ΔN and KO C4-2 cells this revealed a predominant cytoplasmic localisation for this biosensor, *(Figure 4.1)* consistent with previous studies *(Hammond et al., 2014 ; Braun et al., 2021 ; Zhong et al., 2022).* One of the factors contributing to cytoplasmic accumulation of PI(4)P is due to the localisation of PIP4Ks to the Golgi apparatus *(Dickson et al., 2014).*

To quantify the relative levels of PI(4)P (and subsequent phosphoinositides) representative traces from the cell membrane through the cytoplasmic and nuclear compartments of (typically) 5 different WT, ΔN and KO C4-2 cells were taken. Only a small number of cells could be captured in this quantification due to the overall low transfection efficiencies. Intensity profiles for the cells were plotted which were able to capture the changes of biosensor intensity through the cell. Individual intensity values were then averaged, with these averages plotted and the median value scored. By using this method of quantification for assaying PI(4)P levels in WT, ΔN and KO C4-2 cells, this suggested that the levels of PI(4)P were not majorly altered by PIP5K1A CRISPR editing *(Figure 4.1).*

A.

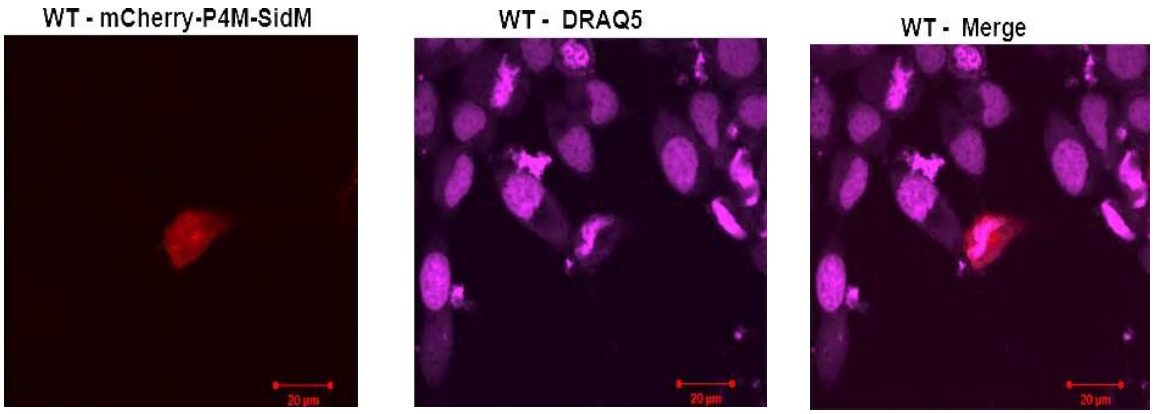
WT - mCherry-P4M-SidM
WT - DRAQ5
WT - Merge
20 µm

B.

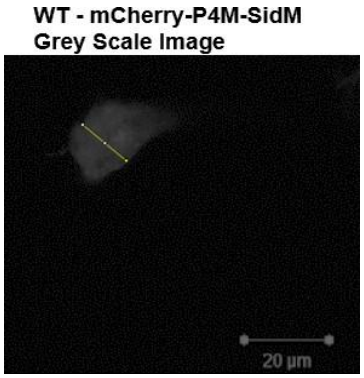
WT - mCherry-P4M-SidM
Grey Scale Image
20 µm

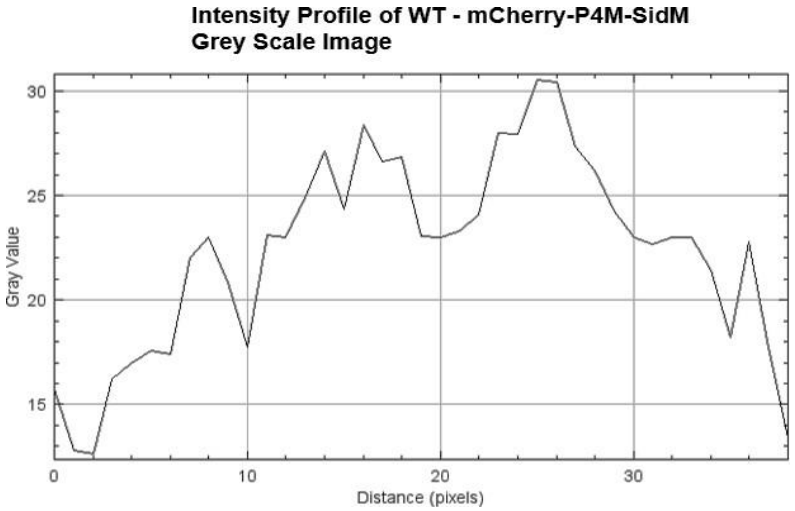
Intensity Profile of WT - mCherry-P4M-SidM
Grey Scale Image
Gray Value
Distance (pixels)
30
25
20
15
0
10
20
30

C.

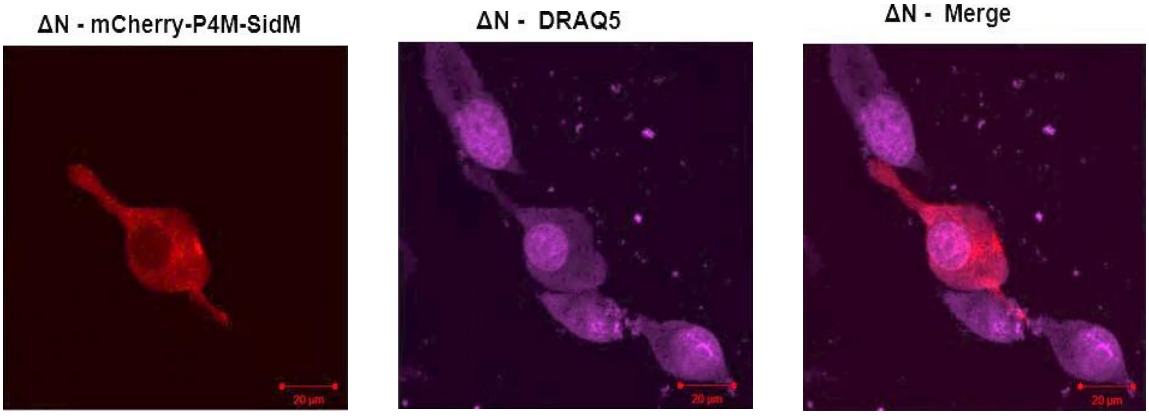
ΔN - mCherry-P4M-SidM
ΔN - DRAQ5
ΔN - Merge
20 µm

D.

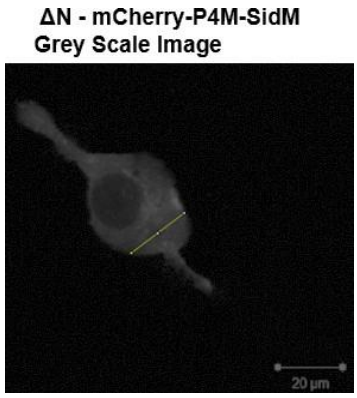
ΔN - mCherry-P4M-SidM
Grey Scale Image
20 µm

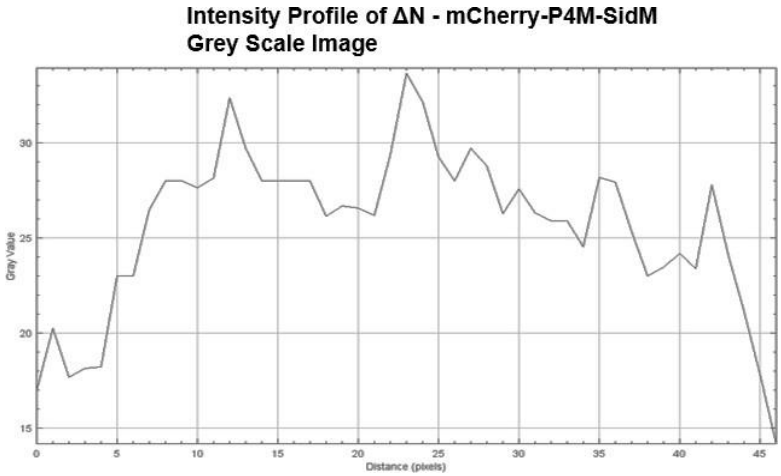
Intensity Profile of ΔN - mCherry-P4M-SidM
Grey Scale Image
Gray Value
Distance (pixels)
30
25
20
15
0
5
10
15
20
25
30
35
40
45

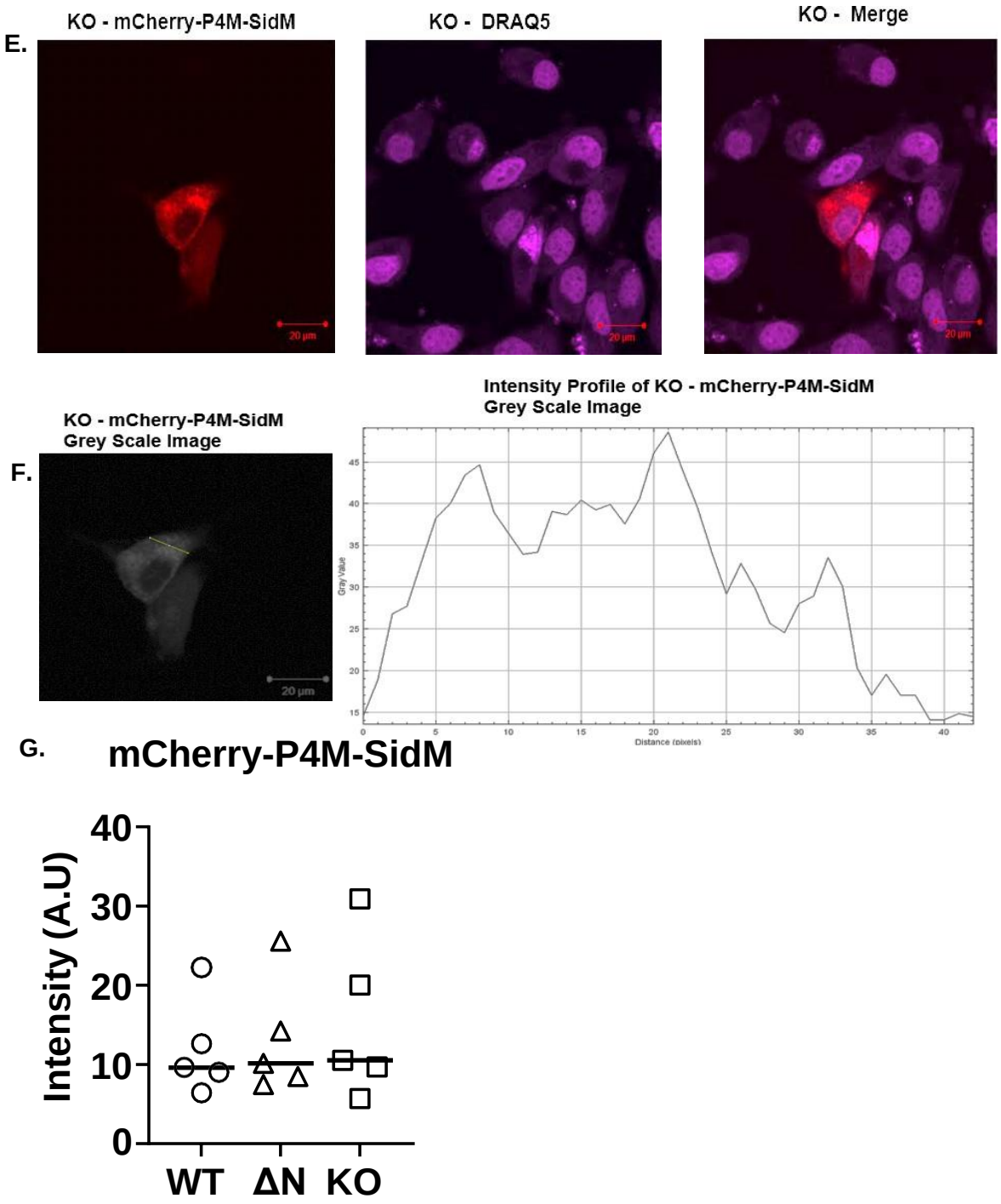

Figure 4.1. Detection of PI(4)P in WT, ΔN and KO C4-2 cells. Cell lines were transfected with the PI(4)P detecting construct mCherry-P4M-SidM, grown for 48h before being prepared for confocal microscopy. A Zeiss LSM510 Meta confocal microscope was used for image acquisition. **A.** Representative image of PI(4)P fluorescence in WT C4-2 cells. **B.** Grey scale image of **A** used in quantification of PI(4)P fluorescence in WT C4-2 cells, with fluorescence intensity plotted as a line graph. **C.** Representative image of PI(4)P fluorescence in ΔN C4-2 cells. **D.** Grey scale image of **C** used in quantification of PI(4)P fluorescence in ΔN C4-2 cells, with fluorescence intensity plotted as a line graph. **E.** Representative image of PI(4)P fluorescence in KO C4-2 cells. **F.** Grey scale image of **E** used in quantification of PI(4)P fluorescence in KO C4-2 cells, with fluorescence intensity plotted as a line graph. **G**. A chart of mCherry-P4M-SidM fluorescent intensities in 5 different WT, ΔN and KO LNCaP C4-2 cells.

4.3. Changes in PI(4,5)P_2 Levels in CRISPR Edited C4-2 Prostate Cancer Cells

With the main product of PIP5K1α activity being PI(4,5)P_2, it was important to assess whether CRISPR editing of PIP5K1A in LNCaP C4-2 cells effects the production of PI(4,5)P_2. With KO C4-2 cells undergoing CRISPR editing on Exon 1 and Exon 6 (with the latter Exon implicated in encoding part of the PIP5K1α kinase domain) the hypothesis would be this clone has impaired PI(4,5)P_2 production.

One way to assess the activity of PIP5Ks in both WT and CRISPR edited clones would be through treating cells with an agonist, to see whether the kinase can still generate PI(4,5)P_2 when stimulated. LPA is a PIP5K agonist and is thought to PIP5K activity partly through potentiating the activity of RhoA GTPases *(Yamazaki et al., 2002 ; van Horck et al., 2002).* For these experiments, LNCaP C4-2 cells were treated with 20μM of LPA for 30 minutes, a concentration previously shown to induce strong phosphorylation of AKT in cervical cancer cells *(Sui et al., 2015).*

The biosensor used in this experiment was the Tubby-cYFP-R332H, which harbours the C terminal PI(4,5)P_2 binding domain (the tubby domain) from the transcriptional regulator tubby *(Quinn et al., 2008).* The R332H mutation in this reporter increases the sensitivity of this reporter to membrane bound PI(4,5)P_2 *(Quinn et al., 2008 ; Tran et al., 2018).* As the R332H slightly weakens the interaction between the tubby domain and PI(4,5)P_2, particularly when cells are exposed to an agonist,changes in membrane PI(4,5)P_2 levels can be captured more sensitively*(Quinn et al., 2008).*

By transfecting WT , ΔN and KO C4-2 cells with the Tubby-cYFP-R332H plasmid, it was apparent that this reporter predominantly localises to the cell membrane, particularly after LPA treatment in WT and ΔN C4-2 cells *(Figure 4.2).* This is consistent with previous work which has shown agonist treatment of mammalian cell lines promotes membrane localisation of tubby-cYFP-R332H *(Quinn et al., 2008 ; Szentpetery et al., 2009 ; Liu et al., 2010).*

In KO C4-2 cells the localisation of Tubby-cYFP-R332H remained diffuse throughout the cytoplasm, even after LPA treatment *(Figure 4.2).* By quantifying the fluorescent intensity of the tubby-cYFP-R332H biosensor KO C4-2 cells showed no increases in $PI(4,5)P_2$ production after agonist stimulation *(Figure 4.2).* Clone ΔN showed a varied response to LPA stimulation, whilst WT LNCaP C4-2 cells saw ~2 fold increase in median intensity of the Tubby-cYFP-R332H biosensor *(Figure 4.2).*

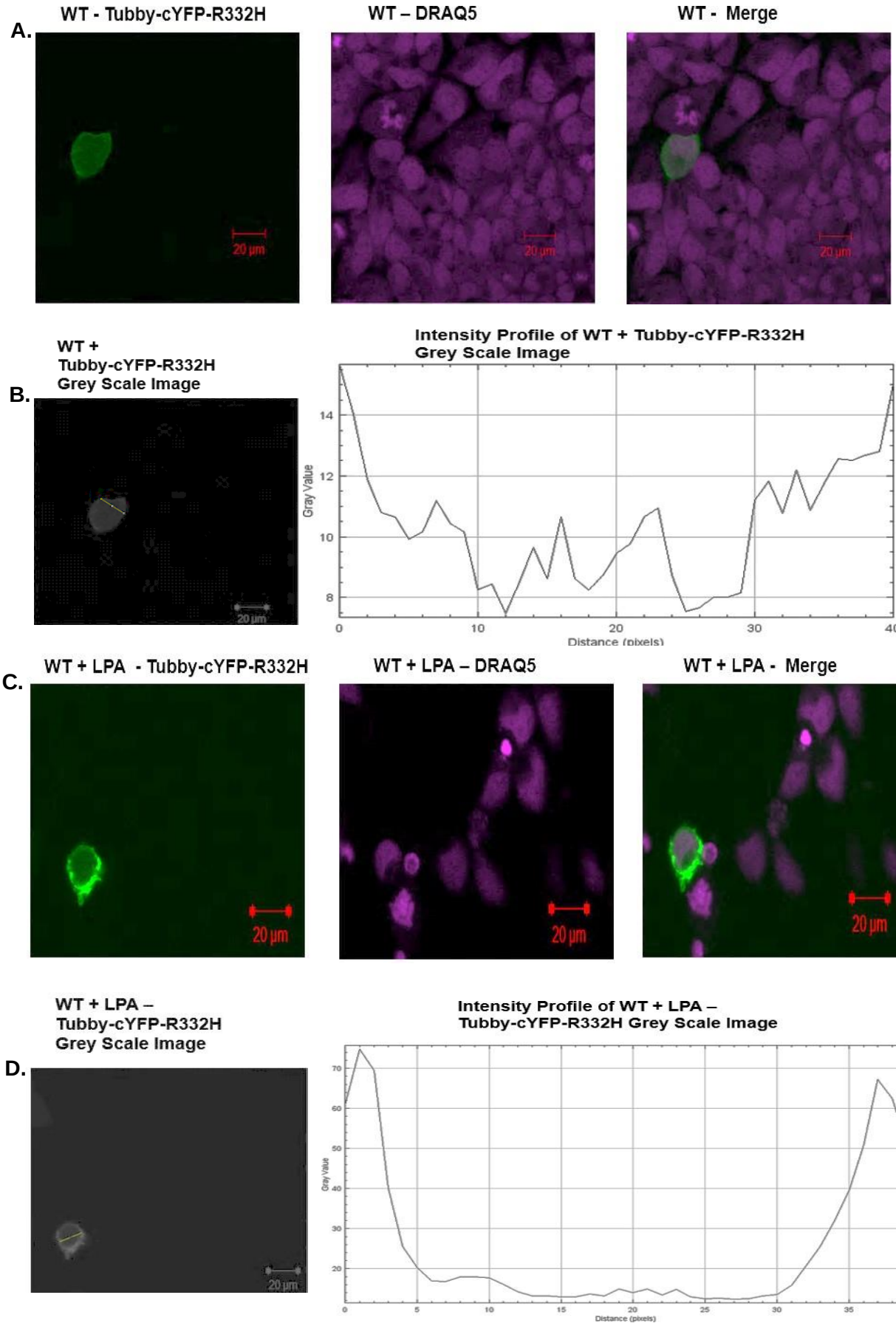
A.
WT - Tubby-cYFP-R332H
WT – DRAQ5
WT - Merge
20 µm
B.
WT +
Tubby-cYFP-R332H
Grey Scale Image
Intensity Profile of WT + Tubby-cYFP-R332H
Grey Scale Image
Gray Value
Distance (pixels)
C.
WT + LPA - Tubby-cYFP-R332H
WT + LPA – DRAQ5
WT + LPA - Merge
D.
WT + LPA –
Tubby-cYFP-R332H
Grey Scale Image
Intensity Profile of WT + LPA –
Tubby-cYFP-R332H Grey Scale Image

E.

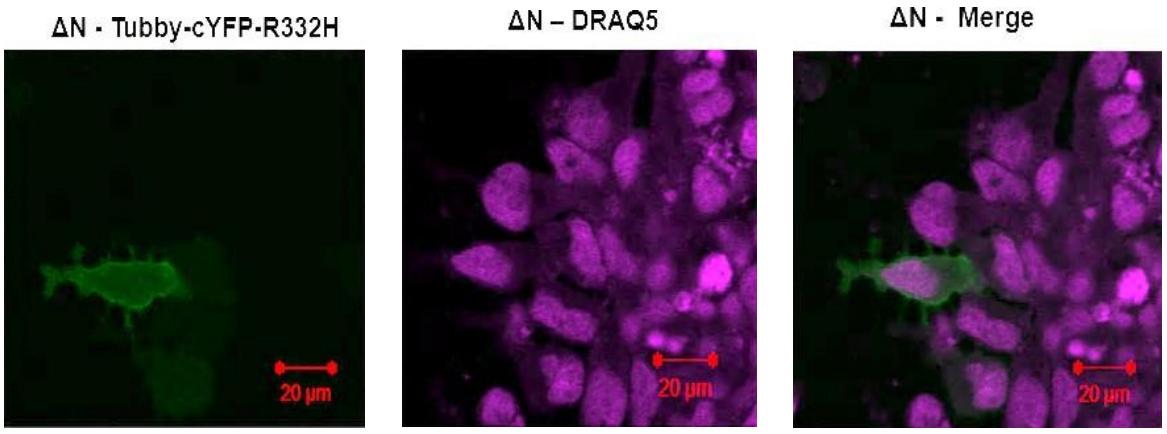
ΔN - Tubby-cYFP-R332H
ΔN – DRAQ5
ΔN - Merge
20 µm
20 µm
20 µm

F.

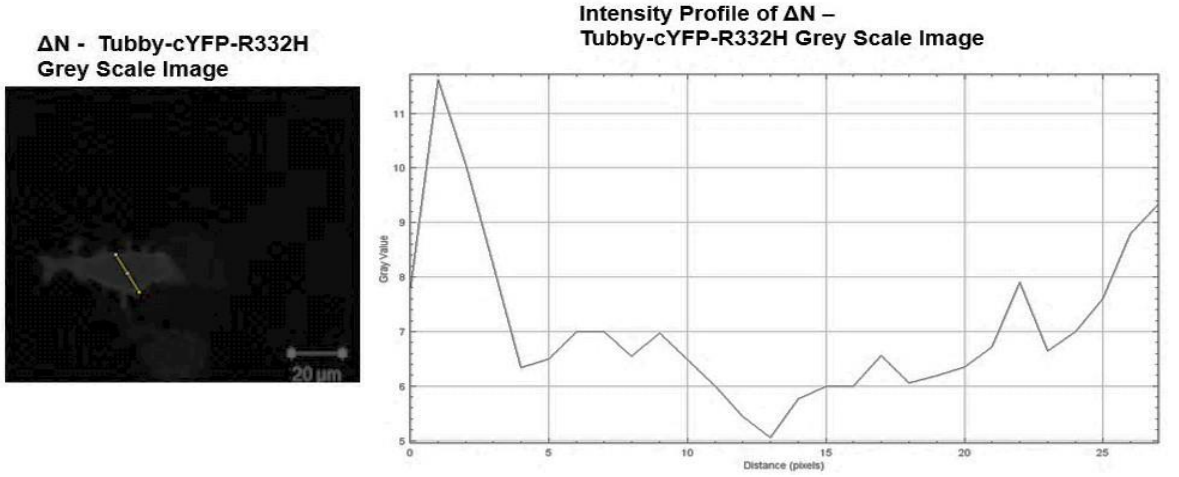
ΔN - Tubby-cYFP-R332H
Grey Scale Image
20 µm
Intensity Profile of ΔN –
Tubby-cYFP-R332H Grey Scale Image
Gray Value
Distance (pixels)

G.

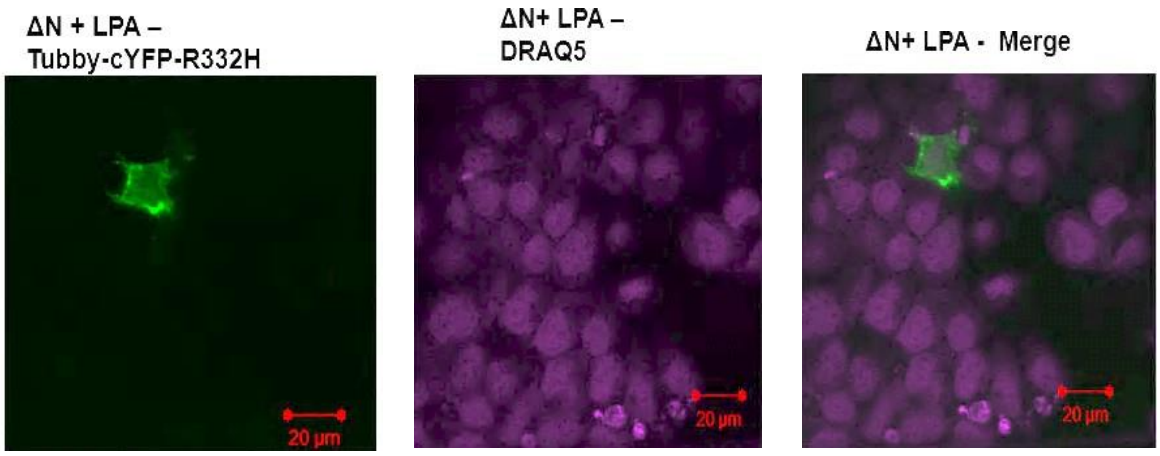
ΔN + LPA –
Tubby-cYFP-R332H
ΔN+ LPA –
DRAQ5
ΔN+ LPA - Merge
20 µm
20 µm
20 µm

H.

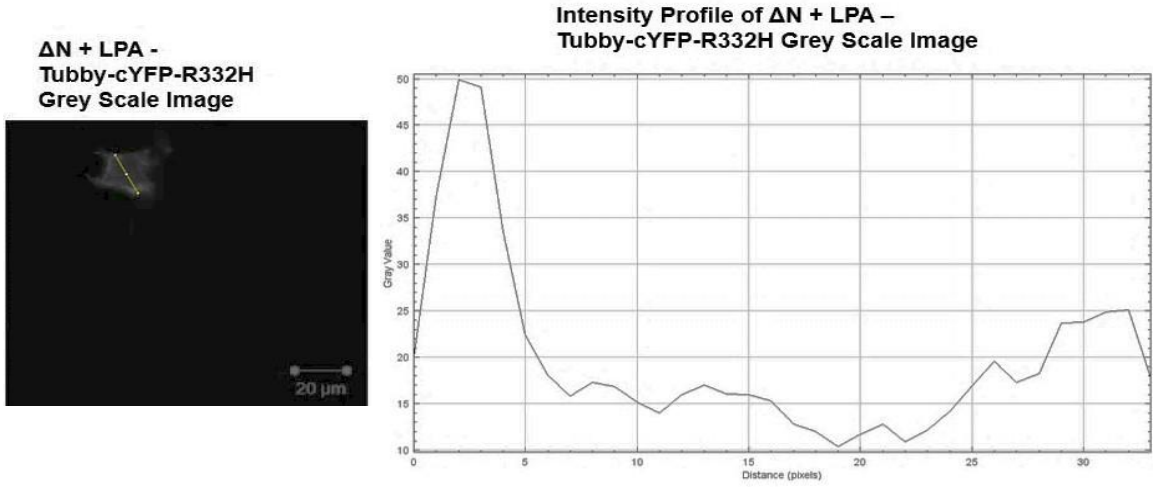
ΔN + LPA -
Tubby-cYFP-R332H
Grey Scale Image
20 µm
Intensity Profile of ΔN + LPA –
Tubby-cYFP-R332H Grey Scale Image
Gray Value
Distance (pixels)

I.

KO – Tubby-cYFP-R332H

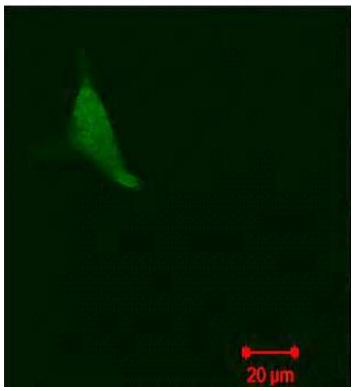

KO – DRAQ5

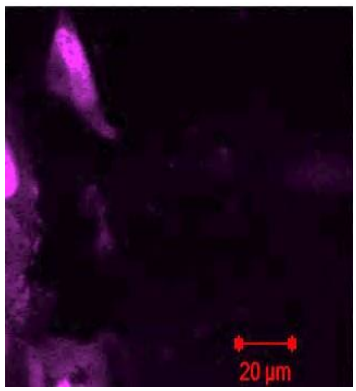

KO - Merge

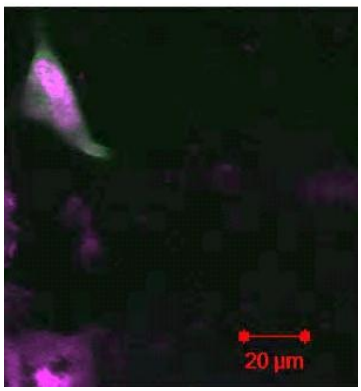

J.

KO -
Tubby-cYFP-R332H
Grey Scale Image

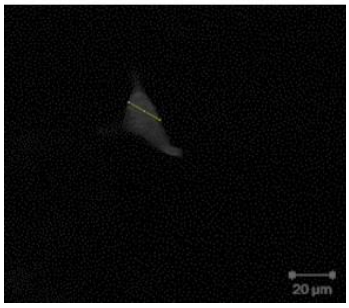

Intensity Profile of KO –
Tubby-cYFP-R332H Grey Scale Image

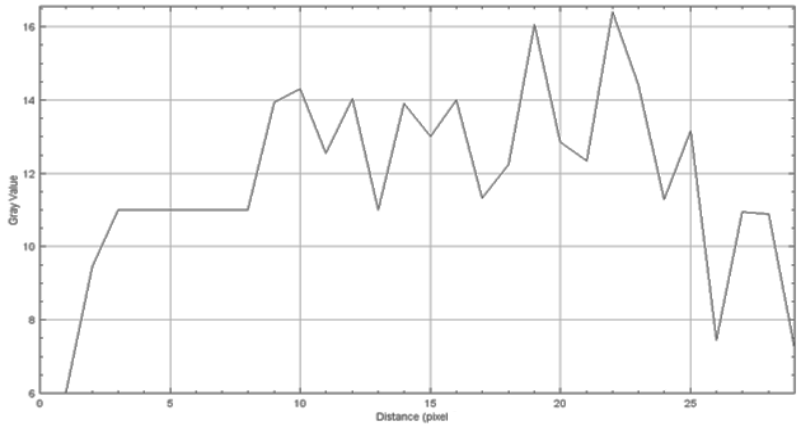

K.

KO + LPA –
Tubby-cYFP-R332H

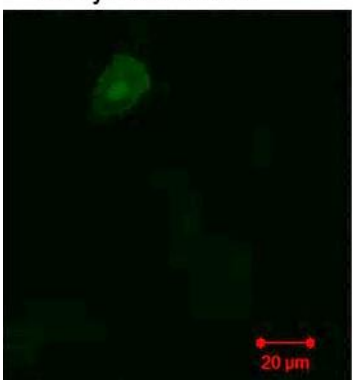

KO + LPA – DRAQ5

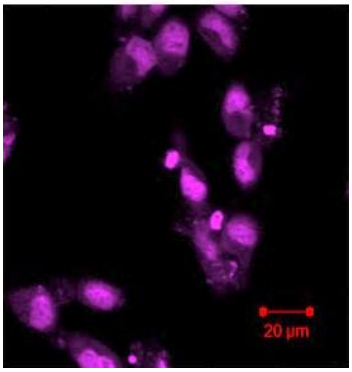

KO+ LPA - Merge

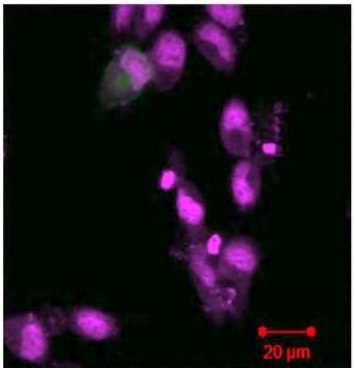

L.

KO + LPA -
Tubby-cYFP-R332H
Grey Scale Image

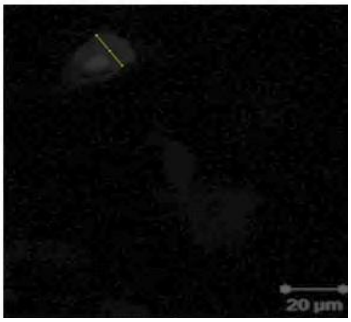

Intensity Profile of KO + LPA –
Tubby-cYFP-R332H Grey Scale Image

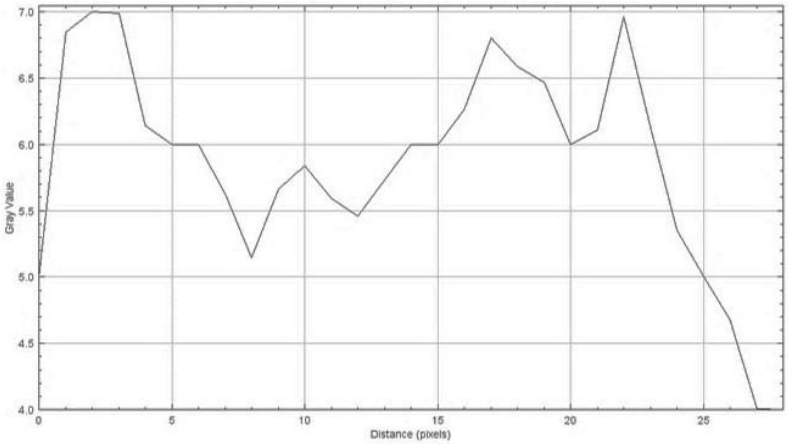

M.

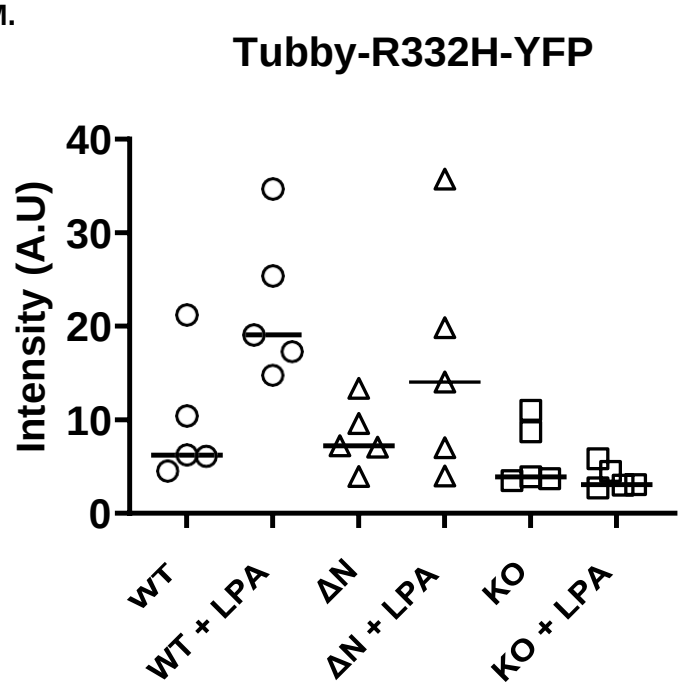

Figure 4.2. Detection of PI(4,5)P_2 in WT, ΔN and KO C4-2 cells. Cell lines were transfected with the PI(4,5)P_2 detecting construct Tubby-R332H-YFP, grown for 48h before being prepared for confocal microscopy. Just prior fixing cells for confocal microscopy, cells lines used for stimulation experiments were treated with 20μM LPA for 30 minutes at 37 °C, 5% CO_2. A Zeiss LSM510 Meta confocal microscope was used for image acquisition. **A.** Representative image of PI(4,5)P_2 fluorescence in untreated WT C4-2 cells. **B.** Grey scale image of **A** used in quantification of PI(4,5)P_2 fluorescence in WT C4-2 cells, with fluorescence intensity plotted as a line graph. **C**. Representative image of PI(4,5)P_2 fluorescence in LPA treated WT C4-2 cells**. D.** Grey scale image of **C** used in quantification of PI(4,5)P_2 fluorescence in LPA treated WT C4-2 cells, with fluorescence intensity plotted as a line graph. **E.** Representative image of PI(4,5)P_2 fluorescence in untreated ΔN C4-2 cells. **F.** Grey scale image of **E** used in quantification of PI(4,5)P_2 fluorescence in ΔN C4-2 cells, with fluorescence intensity plotted as a line graph. **G.** Representative image of PI(4,5)P_2 fluorescence in LPA treated ΔN C4-2. **H.** Grey scale image of **G** used in quantification of PI(4,5)P_2 fluorescence in LPA treated ΔN C4-2 cells, with fluorescence intensity plotted as a line graph. **I.** Representative image of PI(4,5)P_2 fluorescence in untreated KO C4-2 cells. **J.** Grey scale image of **I** used in quantification of PI(4,5)P_2 fluorescence in KO C4-2 cells, with fluorescence intensity plotted as a line graph. **K.** Representative image of PI(4,5)P_2 fluorescence in LPA treated KO C4-2 cells L. Grey scale image of **J** used in quantification of PI(4,5)P_2 fluorescence in LPA treated KO C4-2 cells. **M.** A chart of Tubby-R332H-YFP fluorescent intensities in 5 different WT, ΔN and KO LNCaP C4-2 cells, either untreated or treated with LPA.

4.4. Diacylglycerol Levels in WT and CRISPR Edited C4-2 Prostate Cancer cells.

$PI(4,5)P_2$ hydrolysis by phospholipase C family members generates IP_3 and DAG which promotes the activation of conventional and novel PKC family members; with novel PKCs being activated solely by DAG *(Liu et al., 2017).* Given the importance of DAG in signal transduction, the abundance and localisation of DAG in WT and CRISPR edited clones was investigated. To assay this, WT, ΔN and KO C4-2 cells were transfected with EGFP-PKCγ-C1A biosensor, which harbours the DAG binding domain (C1A) from PKCγ *(Oancea et al., 1998).*

By transfecting this biosensor into cells, the localisation of this reporter in WT and CRISPR edited C4-2 cells was found to be largely intracellular, with prominent detection at the nucleus *(Figure 4.3).* This observation is consistent with previous studies that have investigated DAG localisation and abundances *in vitro (Oancea et al., 1998 ; Oancea et al., 2003 ; Domart et al., 2012; Gawden-Bone et al., 2018).* Quantification of biosensor fluorescent intensities suggested that there were no major alterations in DAG levels between CRISPR edited clones relative to WT-C4-2 cells *(Figure 4.3).*

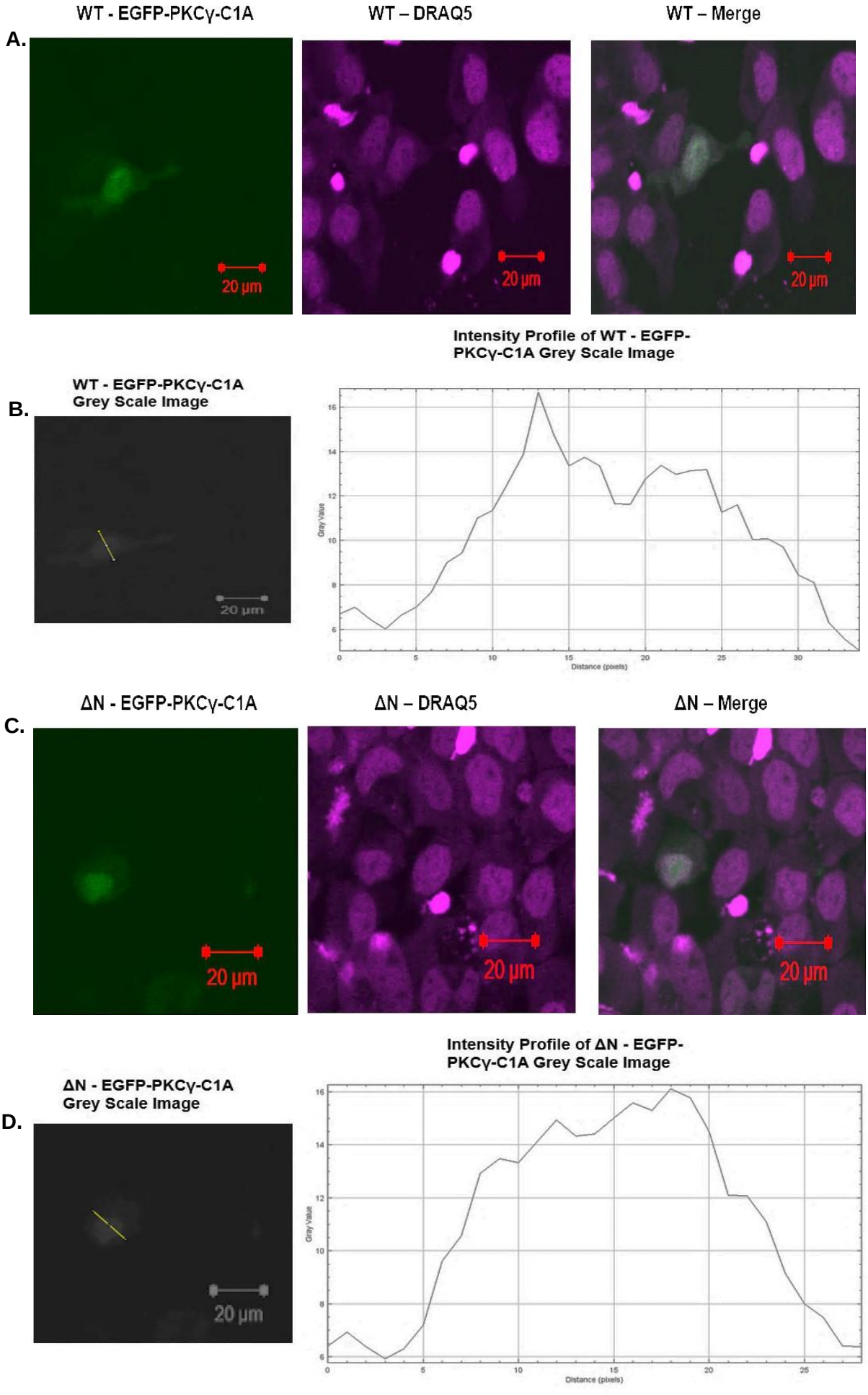
A.
WT - EGFP-PKCγ-C1A
WT – DRAQ5
WT – Merge
20 µm
20 µm
20 µm
B.
WT - EGFP-PKCγ-C1A
Grey Scale Image
20 µm
Intensity Profile of WT - EGFP-
PKCγ-C1A Grey Scale Image
Gray Value
Distance (pixels)
C.
ΔN - EGFP-PKCγ-C1A
ΔN – DRAQ5
ΔN – Merge
20 µm
20 µm
20 µm
D.
ΔN - EGFP-PKCγ-C1A
Grey Scale Image
20 µm
Intensity Profile of ΔN - EGFP-
PKCγ-C1A Grey Scale Image
Gray Value
Distance (pixels)

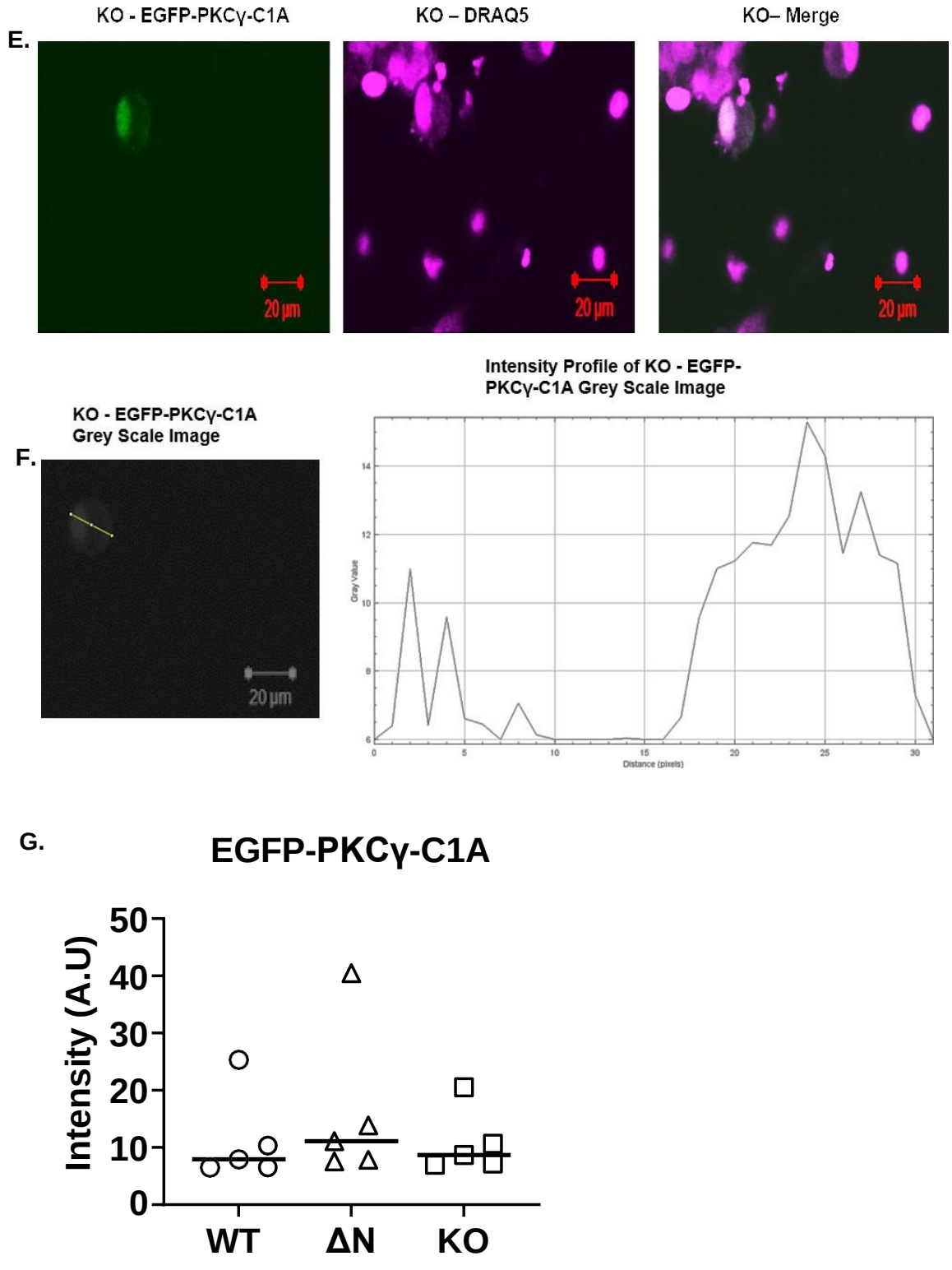

Figure 4.3. Detection of DAG in WT, ΔN and KO C4-2 cells. Cell lines were transfected with the DAG detecting construct EGFP-PKCγ-C1A, grown for 48h before being prepared for confocal microscopy. A Zeiss LSM510 Meta confocal microscope was used for image acquisition. **A.** Representative image of DAG fluorescence in WT C4-2 cells. **B.** Grey scale image of **A** used in quantification of DAG fluorescence in WT C4-2 cells, with fluorescence intensity plotted as a line graph. **C.** Representative image of DAG fluorescence in ΔN C4-2 cells. **D.** Grey scale image of **C** used in quantification of DAG fluorescence in ΔN C4-2 cells, with fluorescence intensity plotted as a line graph. **E.** Representative image of DAG fluorescence in KO C4-2 cells. **F.** Grey scale image of **E** used in quantification of DAG fluorescence in KO C4-2 cells, with fluorescence intensity plotted as a line graph. **G.** A chart of EGFP-PKCγ-C1A fluorescent intensities in 5 different WT, ΔN and KO LNCaP C4-2 cells.

4.5. PKC Signalling in WT , ΔN and KO C4-2 Prostate Cancer Cells

Previous confocal microscopy data suggested that there were no alterations in DAG levels in both WT and CRISPR edited C4-2 cells *(Figure 4.3).* Nevertheless, it was important to assess whether any global changes in PKC signalling could be captured through different means. For this, western blots were carried out using an phospho-antibody which recognizes substrates harbouring a phosphorylated PKC consensus sequence. These substrates have been phosphorylated at either serine or threonine residues surrounded by arginine or lysine at the -2 and +2 positions, and a hydrophobic amino acid at the +1 position *(Yang et al., 2009).* For these assays, cells were either untreated, or treated with the agonist, PMA. This agonist is a structural mimic of DAG and induces activation of PKC conventional and novel PKC isozymes *(Wada et al., 2002 ; Dobkin-Bekman et al., 2010 ; Liu et al., 2017).* By using this experimental approach this would identify any changes in PKC substrate phosphorylation between WT, ΔN and KO and whether phosphorylationis enhanced by presence of PMA. Treatment of WT and CRISPR edited clones with PMA was conducted for 1h at 100nM concentration, a concentration which previously was used to stimulate PKCε activity in LNCaP prostate cancer cells *(Meshki et al., 2010).*

Through western blotting this showed that in unstimulated conditions, the phosphorylation of PKC substrates in WT, ΔN and KO C4-2 cells remains largely consistent (*Figure 4.4).* With the addition of PMA, this evoked increases in PKC substrate phosphorylation, particularly in KO C4-2 cells where strong phosphorylation of proteins between ~90kDa – 120kDa was observed (*Figure 4.4).* PhosphoSitePlus *(Hornbeck et al., 2011)* was used to identify possible substrates in this molecular weight range which could be phosphorylated by PKC isozymes. This includes the ATPase Na+/K+ transporting subunit alpha 1 (ATP1A1), which has a molecular weight of 113kDA *(Feschenko and Sweadner, 1995 ;*

Hornbeck et al., 2011). The S16 site in ATP1A1 is phosphorylated by PKCs which increases the transporters affinity for sodium ions *(Feschenko and Sweadner, 1995 ; Hornbeck et al., 2011).* Another potential substrate is Protein Kinase D1 (PKD1), which has a molecular weight of 101kDa, and is phosphorylated by PKC on S412, S738 and S742 *(Hornbeck et al., 2011).* Both S738 and S742 residues are located in the activation loop of PKD1, with phosphorylation of these residues via PKCs responsible maximal activation of PKD1 *(Cowell et al., 2009).*

At both the RNA level, in WT, ΔN and KO C4-2 cells PKD1 and ATP1A1 are well expressed, and do not display significant differential expression *(Table 4.1).* Furthermore, DAG responsive PKCs (conventional, and novel) retain largely consistent expression in WT and CRISPR edited cells *(Table 4.1).* Only two PKC family genes made the significance cut offs for being differentially expressed, PRKCG and PRKCD *(Table 4.1).* Very modest reductions of PRKCG expression were observed between ΔN-WT LNCaP C4-2, whilst a more substantial loss of RNA reads was recorded for PRKCD *(Table 4.1).*

Collectively, this RNA-Seq analysis suggests that phosphorylation of PKC substrates in KO C4-2 cells was not due to an increased expression of certain PKC isozymes, or elevated substrate expression. Furthermore, these data highlight that in unstimulated conditions there are no major alterations of PKC substrate phosphorylation in in WT, ΔN and KO C4-2 cells. This aligns with previous confocal assays suggesting that DAG levels are not altered in CRISPR edited clones *(Figure 4.3).* When the three cell lines are treated with PMA, phosphorylation of PKC substrates occurs, with increased phosphorylation particularly noticed in KO C4-2 cells *(Figure 4.4).* This suggests that attenuating the expression of PIP5K1α in LNCaP C4-2 cells does not block sensitivity towards PMA.

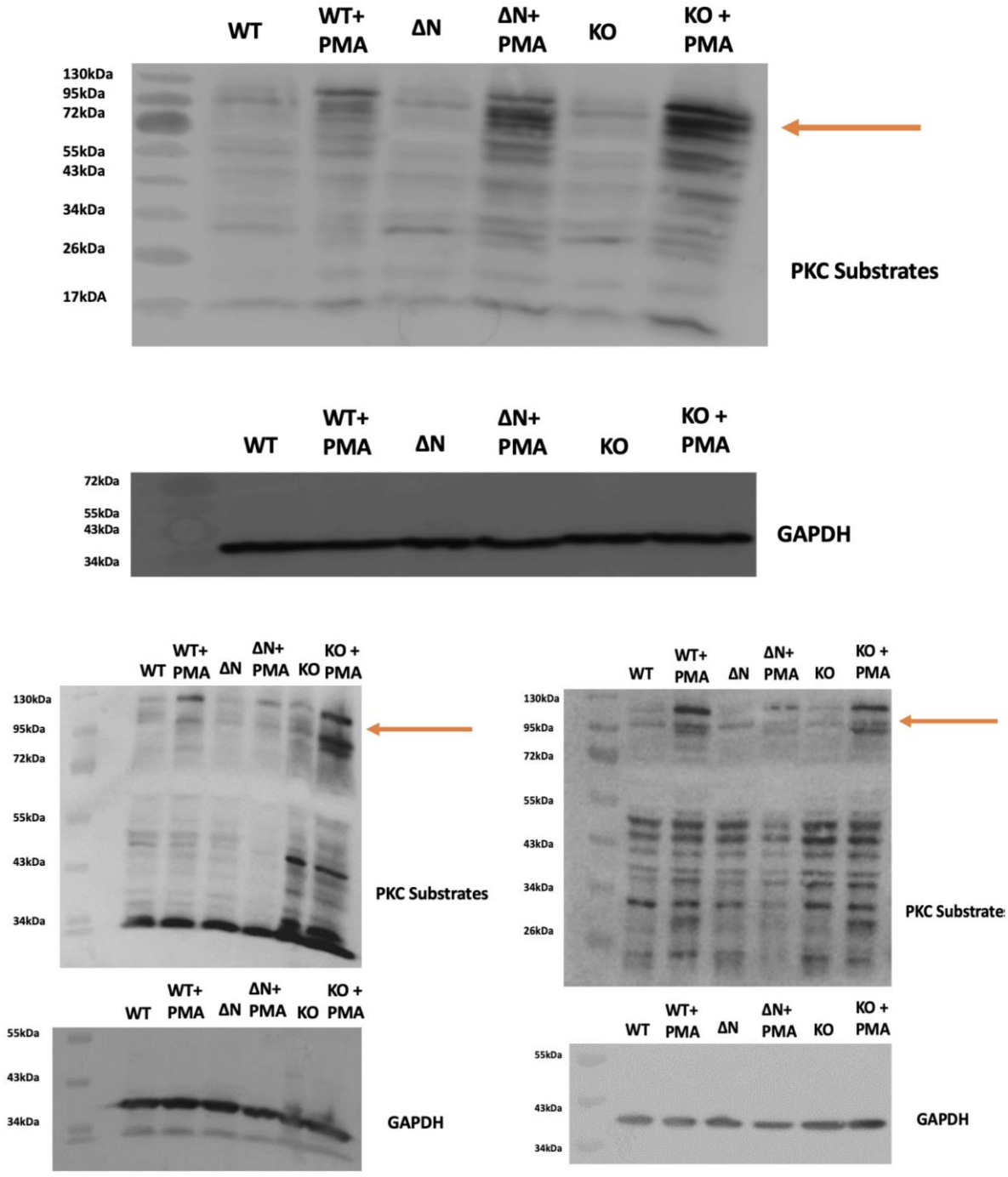

Figure 4.4. PKC substrate phosphorylation in WT, ΔN and KO LNCaP C4-2 cells in the presence or absence of PMA. Shown are three biological replicates of cell lysates blotted with an antibody which detects phosphorylated PKC substrates, with GAPDH used as a loading control.

Table 4.1 RNA expression of PRKCA, PRKCG, PRKCD, ATP1A1 and PRKD1in WT, ΔN and KO LNCaP C4-2 cells. Reported is the Log2FC , FDR and the average (n=3) RNA reads for RNA expression of PRKCA, PRKCG, PRKCD, ATP1A1 and PRKD1 in WT, ΔN and KO C4-2 cells. RNA reads for RNA expression of PRKCA, PRKCG, PRKCD, ATP1A1 and PRKD1. DeSeq2 was conducted to generate Log2FC and FDR values, whilst RNA Read counts were generated by FeatureCounts.

Gene Name	Protein Name	Log2FC- ΔN – WT	FDR- ΔN – WT	Log2FC- KO- WT	FDR- KO – WT	Average WT RNA Reads	Average ΔN RNA Reads	Average KO RNA Reads
PRKCA	PKC-α	-0.19	0.33	-1.13	0.00	250	212	110
PRKCG	PKC-γ	-5.78	6.69E-4	-3.95	0.02	10	0	1
PRKCD	PKC-δ	-1.05	2.19E-24	0.21	0.11	3160	1489	3506
ATP1A1	ATP1A1	-0.42	0.14	-0.28	0.44	7666	7710	8086
PRKD1	PDK1	0.00	0.99	0.20	0.12	1966	1915	2153

4.6. The Levels of Class I PI3K Products in WT , ΔN and KO C4-2 Prostate Cancer Cells

With $PI(4,5)P_2$ being the prime substrate for Class I PI3Ks it was important to investigate whether the levels of $PI(3,4,5)P_3$ are altered in CRISPR edited clones. Like conducted previously for $PI(4,5)P_2$ assays, WT, ΔN and KO C4-2 cells were treated with 20μM of LPA. Whilst considered a PIP5K1α agonist , treating cells with LPA can stimulate $PI(3,4,5)P_3$ production *(Laffargue et al., 1999 ; Milne et al., 2005).* Increased $PI(3,4,5)P_3$ levels would ultimately arise if there were greater pools of $PI(4,5)P_2$ present for Class I PI3Ks to phosphorylate.

An initial experiment to assess the localisation and abundance of $PI(3,4,5)P_3$ was conducted using the pcDNA3.1_AktPH-mCherry biosensor *(Kawano et al., 2015). Figure 4.5* indicates in both untreated and LPA treated cells, the localisation of pcDNA3.1_AktPH-mCherry is not only at the cell membrane, but in nuclear and cytoplasmic regions. This is consistent with other previous reports which show localisation of AktPH constructs is not cell membrane exclusive *(Mejillano et al., 2001 ; Kakumoto and Nakata, 2013).* The mean fluorescence intensity values of pcDNA3.1_AktPH-mCherry for WT cells was the greatest, albeit this data exhibited variability *(Figure 4.5).* Modest increases in pcDNA3.1_AktPH-mCherry intensity were recorded in both CRISPR clones after LPA treatment.

A.

WT - pcDNA3.1_AktPH-mCherry

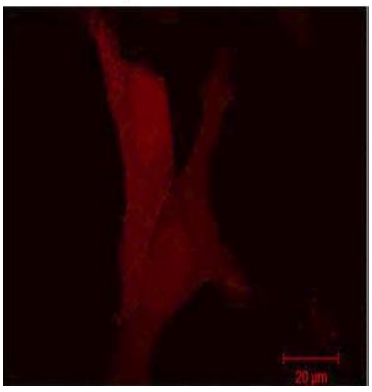

WT - DRAQ5

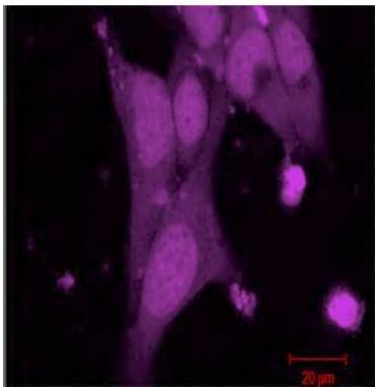

WT - Merge

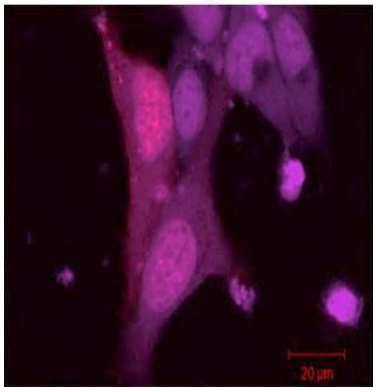

B.

WT - pcDNA3.1_AktPH-mCherry
Grey Scale Image

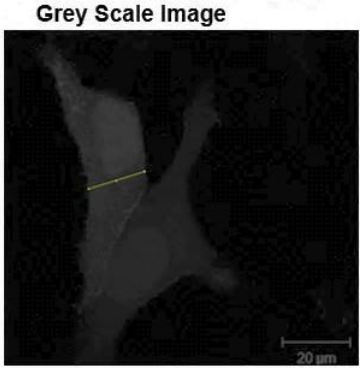

Intensity Profile of WT + LPA - pcDNA3.1_AktPH-mCherry
Grey Scale Image

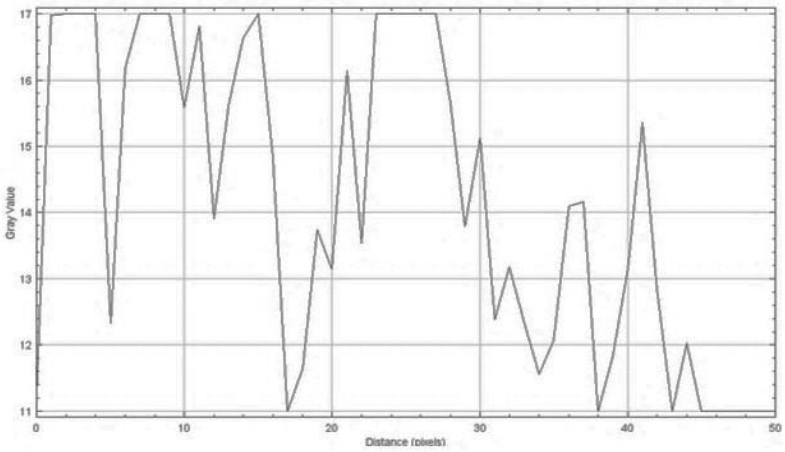

C.

WT + LPA - pcDNA3.1_AktPH-mCherry

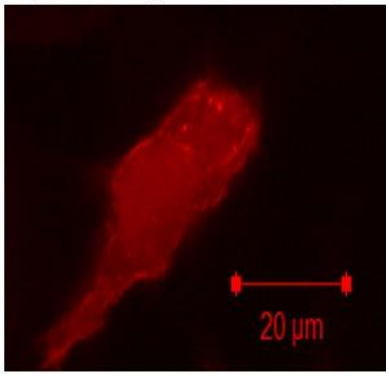

WT + LPA - DRAQ5

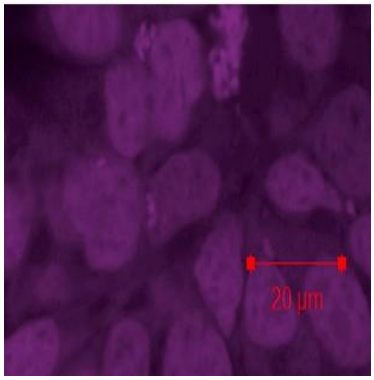

WT + LPA - Merge

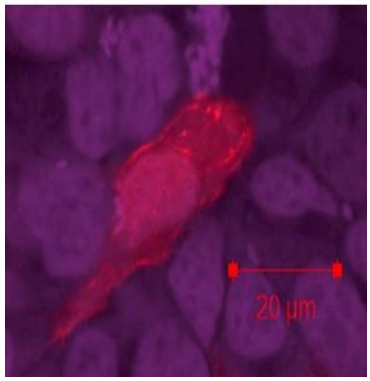

D.

WT + LPA - pcDNA3.1_AktPH-mCherry
Grey Scale Image

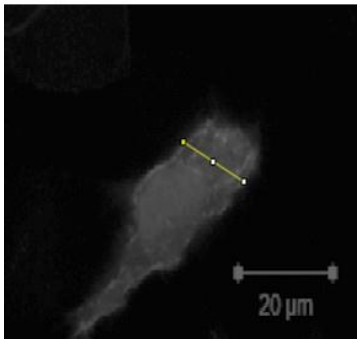

Intensity Profile of WT + LPA - pcDNA3.1_AktPH-mCherry
Grey Scale Image

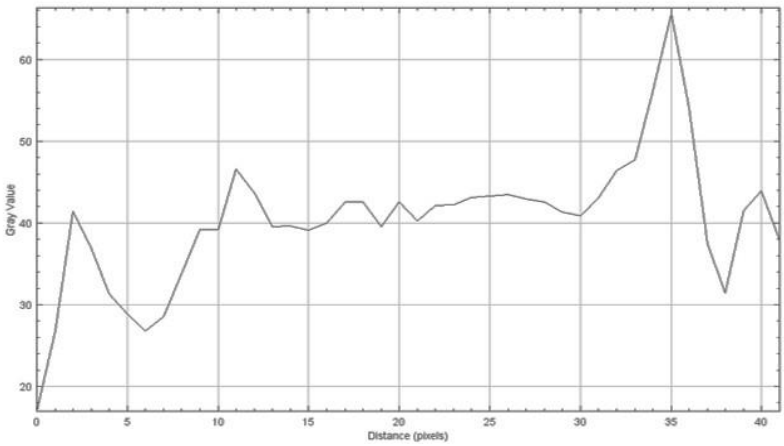

E.

ΔN - pcDNA3.1_AktPH-mCherry

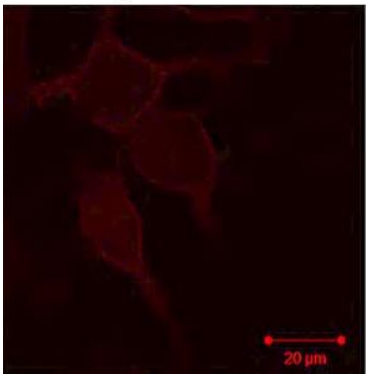

ΔN - DRAQ5

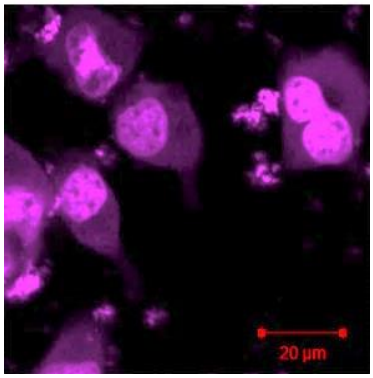

ΔN - Merge

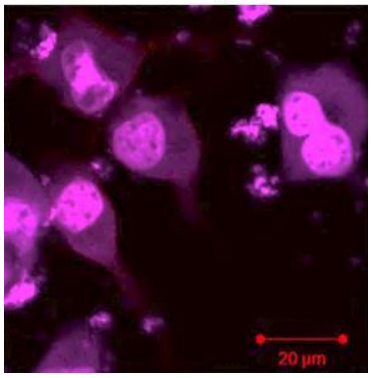

F.

ΔN - pcDNA3.1_AktPH-mCherry
Grey Scale Image

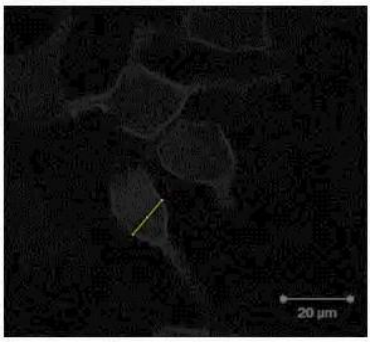

Intensity Profile of ΔN - pcDNA3.1_AktPH-mCherry
Grey Scale Image

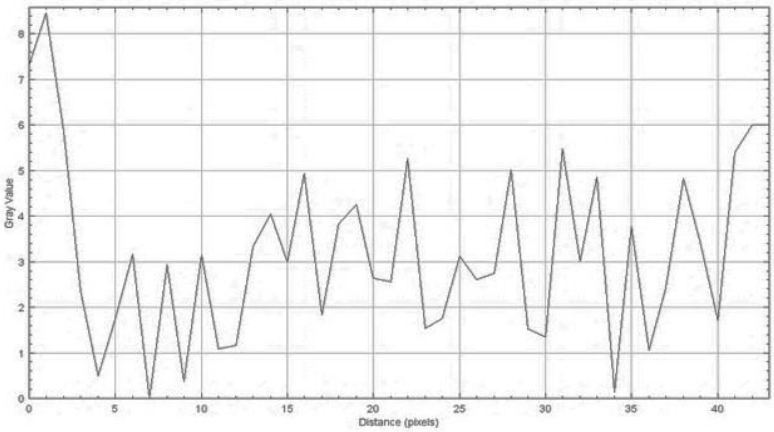

G.

ΔN +LPA - pcDNA3.1_AktPH-mCherry

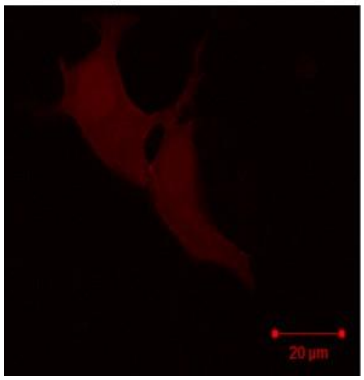

ΔN + LPA - DRAQ5

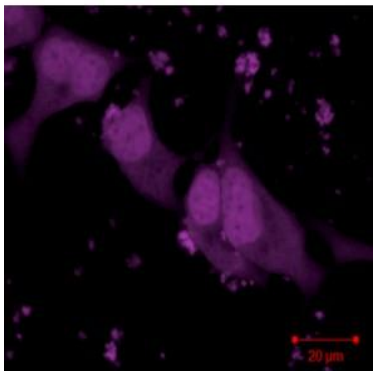

ΔN + LPA - Merge

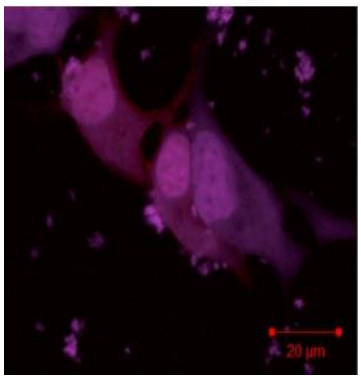

H.

ΔN + LPA - pcDNA3.1_AktPH-mCherry
Grey Scale Image

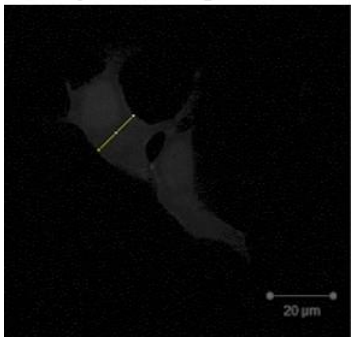

Intensity Profile of ΔN + LPA - pcDNA3.1_AktPH-mCherry
Grey Scale Image

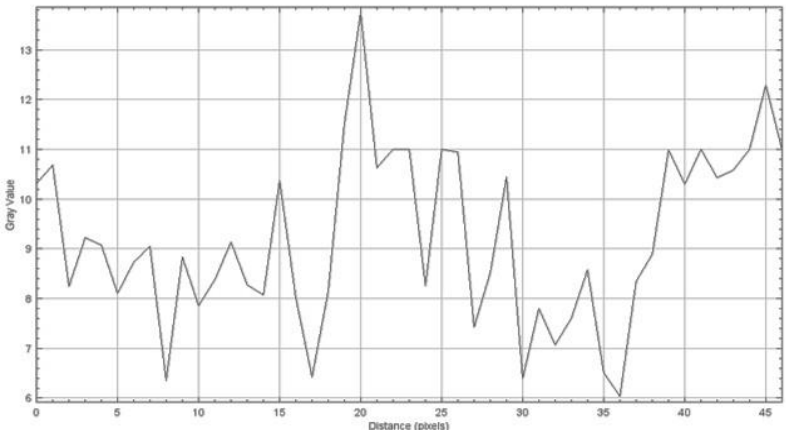

I.

KO - pcDNA3.1_AktPH-mCherry

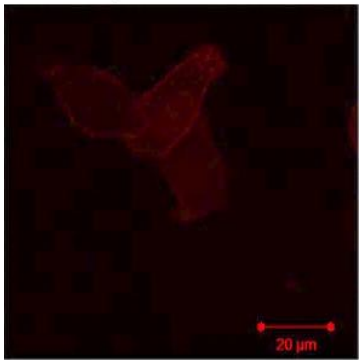

KO + LPA - DRAQ5

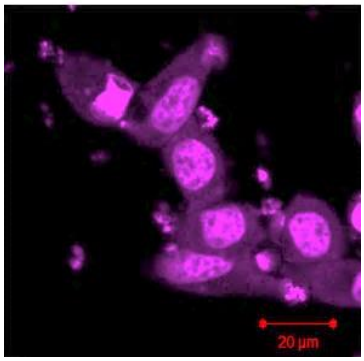

KO + LPA - Merge

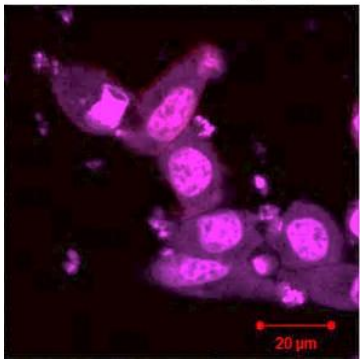

J.

KO- pcDNA3.1_AktPH-mCherry
Grey Scale Image

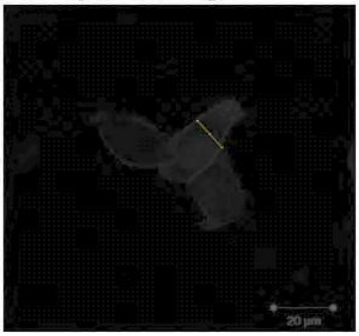

Intensity Profile of KO - pcDNA3.1_AktPH-mCherry
Grey Scale Image

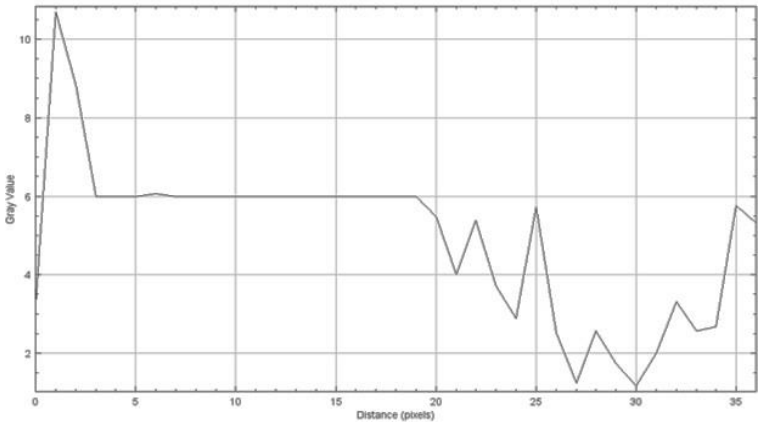

K.

KO + LPA - pcDNA3.1_AktPH-mCherry

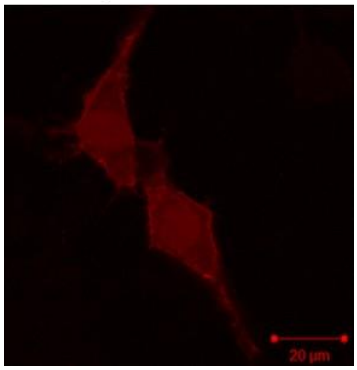

KO + LPA - DRAQ5

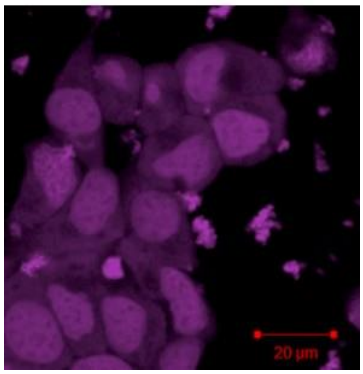

KO + LPA - Merge

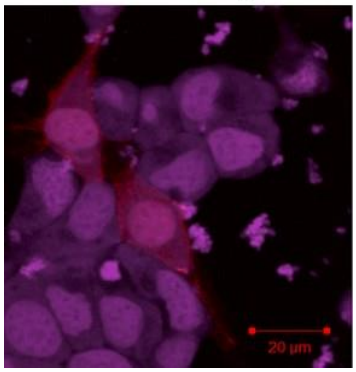

L.

KO + LPA - pcDNA3.1_AktPH-mCherry
Grey Scale Image

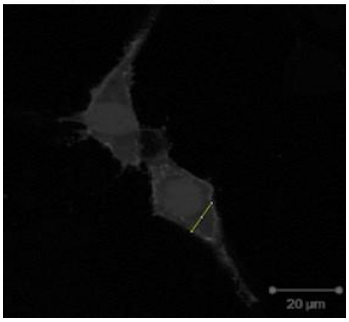

Intensity Profile of ΔN + LPA - pcDNA3.1_AktPH-mCherry
Grey Scale Image

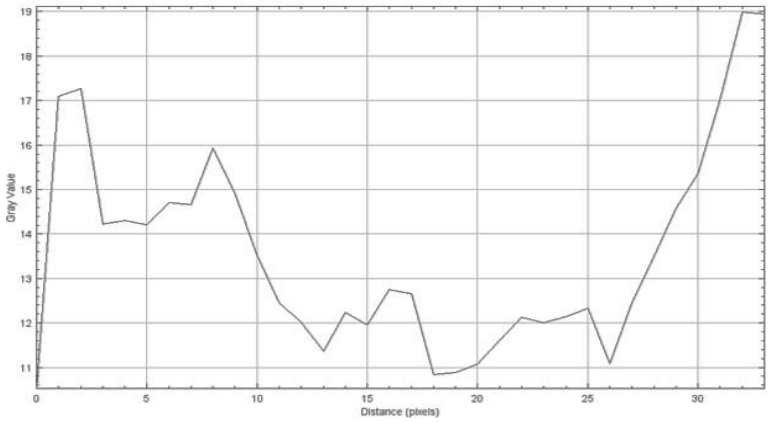

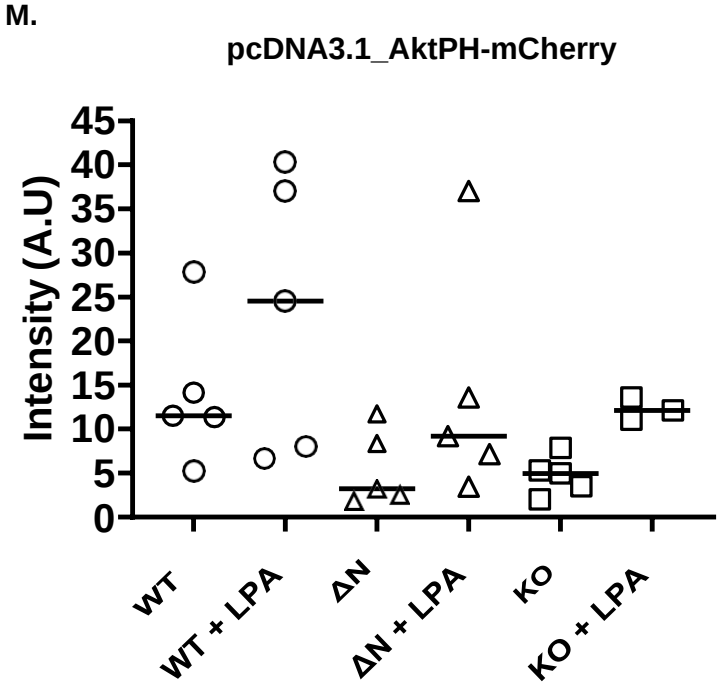

Figure 4.5. Detection of PI(3,4,5)P3 in WT, ΔN and KO C4-2 cells using pcDNA3.1_AktPH. Cell lines were transfected with the PI(3,4,5)P2 detecting construct pcDNA3.1_AktPH grown for 48h before being prepared for confocal microscopy. Just prior fixing cells for confocal microscopy, cells lines used for stimulation experiments were treated with 20μM LPA for 30 minutes at 37 °C, 5% CO2. A Zeiss LSM510 Meta confocal microscope was used for image acquisition. **A.** Representative image of PI(3,4,5)P3 fluorescence in untreated WT C4-2 cells. **B.** Grey scale image of **A** used in quantification of PI(3,4,5)P3 fluorescence in WT C4-2 cells, with fluorescence intensity plotted as a line graph. **C.** Representative image of PI(3,4,5)P3 fluorescence in LPA treated WT C4-2 cells. **D.** Grey scale image of **C** used in quantification of PI(3,4,5)P3 fluorescence in LPA treated WT C4-2 cells, with fluorescence intensity plotted as a line graph. **E.** Representative image of PI(3,4,5)P3 fluorescence in untreated ΔN C4-2 cells. **F**. Grey scale image of **E** used in quantification of PI(3,4,5)P3 fluorescence in ΔN C4-2 cells, with fluorescence intensity plotted as a line graph. **G.** Representative image of PI(3,4,5)P3 fluorescence in LPA treated ΔN C4-2. **H.** Grey scale image of **G** used in quantification of PI(3,4,5)P3 fluorescence in LPA treated ΔN C4-2 cells, with fluorescence intensity plotted as a line graph. **I.** Representative image of PI(3,4,5)P3 fluorescence in untreated KO C4-2 cells. **J.** Grey scale image of **I** used in quantification of PI(3,4,5)P3 fluorescence in KO C4-2 cells, with fluorescence intensity plotted as a line graph. **K.** Representative image of PI(3,4,5)P3 fluorescence in LPA treated KO C4-2 cells **L.** Grey scale image of **J** used in quantification of PI(3,4,5)P3 fluorescence in LPA treated KO C4-2 cells. **M.** A chart of pcDNA3.1_AktPH fluorescent intensities in 5 different WT and ΔN LNCaP C4-2 cells. For KO C4-2 cells, the fluorescent intensities of pcDNA3.1_AktPH is shown in 5 different KO C4-2 cells, and 3 different LPA treated KO C4-2 cells.

Whilst the PH domain of AKT has been used several studies to investigate $PI(3,4,5)P_3$ pools within cells, this PH domain can also interact with membrane bound $PI(3,4)P_2$ *(Virbasius et al., 2001 ; Ebner et al., 2018).* As such, it was important to assess whether there were any sustainable changes in $PI(3,4)P_2$ levels in WT, ΔN and KO C4-2 cells. For this, cells were transfected with NES-EGFP-cPHx3 biosensor which utilises the c terminal PH domains of Pleckstrin Homology Domain Containing A1 (TAPP1) that selectively bind to $PI(3,4)P_2$ *(Dowler et al., 2000 ; Goulden et al., 2018).* To improve the selectivity and avidity of this biosensor to $PI(3,4)P_2$, three isolated c terminal PH domains of TAPP1 have been fused together *(Goulden et al., 2018).*

Whilst PIP5K1α does not directly synthesis $PI(3,4)P_2$, an indirect method may arise from if less $PI(4,5)P_2$ is being generated from PI(4)P pools. A loss of PIP5K1α activity could mean more $PI(3,4)P_2$ could be generated through phosphorylation of PI(4)P by Class I PI3Ks. After transfecting NES-EGFP-cPHx3 into WT, ΔN and KO C4-2 cells, this biosensor exhibited strong membrane localisation *(Figure 4.6).* The mean fluorescence intensity values of NES-EGFP-cPHx3 for 5 differentcells *(Figure 4.6)* highlighted no major alterations in $PI(3,4)P_2$ levels in these cells, ruling out the possibility that elevated $PI(3,4)P_2$ could promote inappropriate recruitment of pcDNA3.1_AktPH-mCherry in C4-2 cell lines.

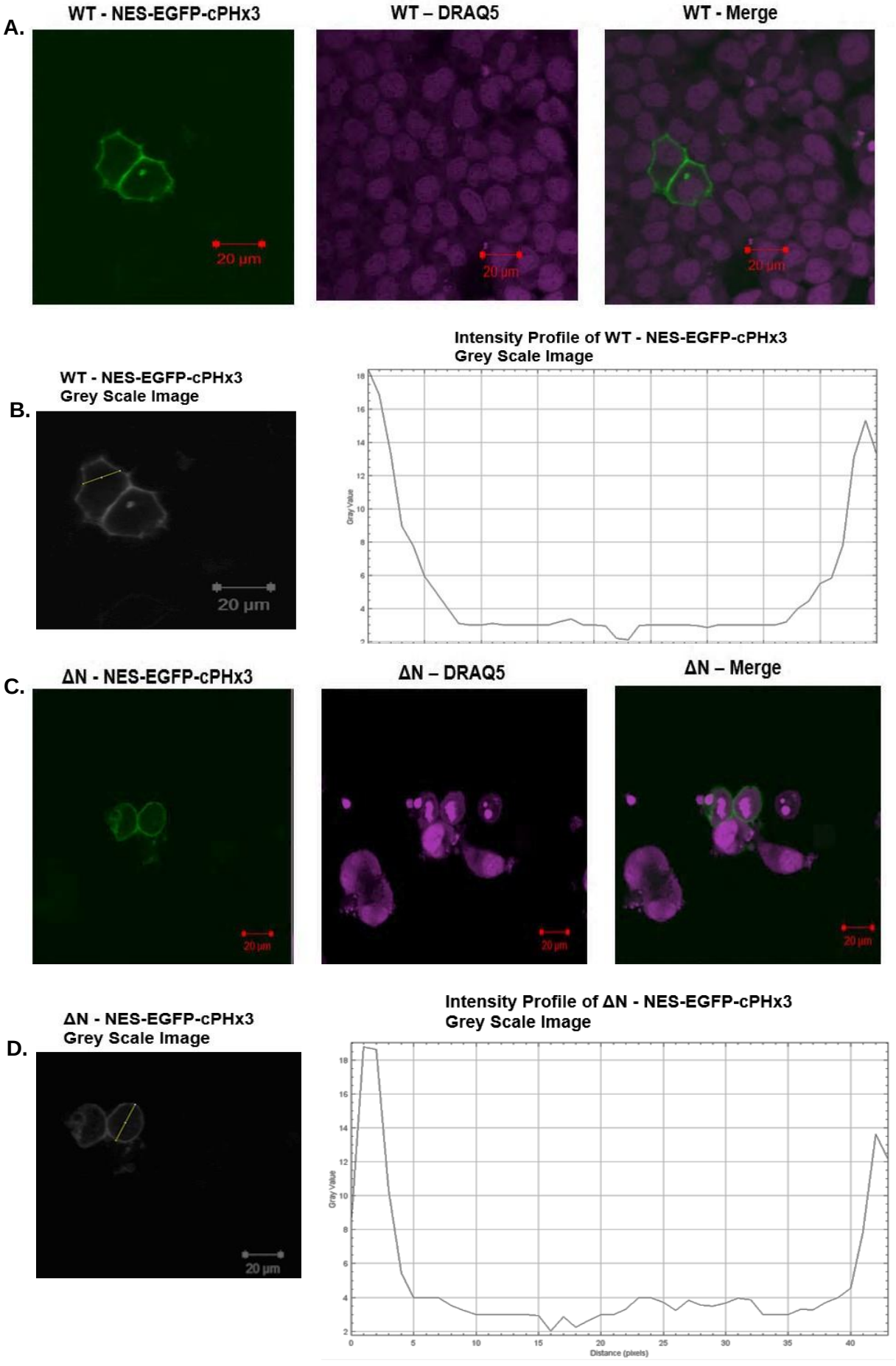
A.
WT - NES-EGFP-cPHx3
WT – DRAQ5
WT - Merge
20 µm
B.
WT - NES-EGFP-cPHx3
Grey Scale Image
Intensity Profile of WT - NES-EGFP-cPHx3
Grey Scale Image
Gray Value
C.
ΔN - NES-EGFP-cPHx3
ΔN – DRAQ5
ΔN – Merge
D.
ΔN - NES-EGFP-cPHx3
Grey Scale Image
Intensity Profile of ΔN - NES-EGFP-cPHx3
Grey Scale Image
Gray Value
Distance (pixels)

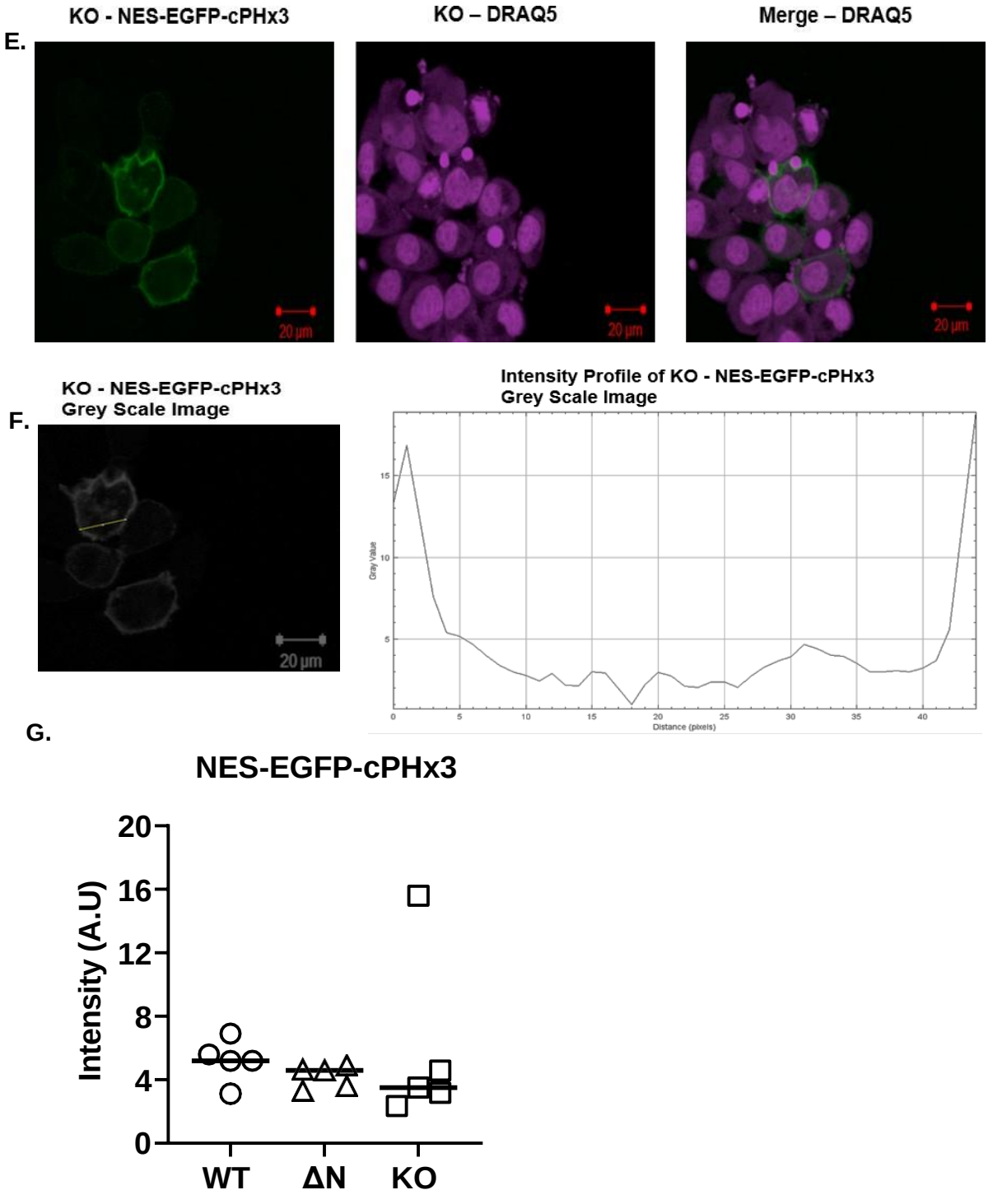

Figure 4.6. Detection of PI(3,4)P_2 in WT, ΔN and KO C4-2 cells. Cell lines were transfected with the PI(3,4)P_2 detecting construct NES-EGFP-cPHx3, grown for 48h before being prepared for confocal microscopy. A Zeiss LSM510 Meta confocal microscope was used for image acquisition. **A.** Representative image of PI(3,4)P_2 fluorescence in WT C4-2 cells. **B.** Grey scale image of **A** used in quantification of PI(3,4)P_2 fluorescence in WT C4-2 cells, with fluorescence intensity plotted as a line graph. **C.** Representative image of PI(3,4)P_2 fluorescence in ΔN C4-2 cells. **D.** Grey scale image of **C** used in quantification of PI(3,4)P_2 fluorescence in ΔN C4-2 cells, with fluorescence intensity plotted as a line graph. **E.** Representative image of PI(3,4)P_2 fluorescence in KO C4-2 cells. **F.** Grey scale image of **E** used in quantification of PI(3,4)P_2 fluorescence in KO C4-2 cells, with fluorescence intensity plotted as a line graph. **G.** A chart of NES-EGFP-cPHx3 fluorescent intensities in 5 different WT, ΔN and KO LNCaP C4-2 cells.

To assay PI(3,4,5)P_3 levels more robustly, a more selective biosensor was used in subsequent assays, EGFP-Grp1-PH *(He et al., 2008 ; Yip et al., 2008).* This construct utilises the PH domain from general receptor for phosphoinositides isoform 1 (GRP1), a member of the ADP-ribosylation factor of small GTPases which is recruited to plasma membrane through solely PI(3,4,5)P_3 binding *(Saxena et al., 2002 ; Garçon et al., 2008 ; Gawden-Bone et al., 2018).*

By transfecting WT, ΔN and KO C4-2 with EGFP-Grp1-PH, this revealed a more predominant membrane localisation in WT LNCaP C4-2, in the presence or absence of an agonist *(Figure 4.7).* However, LPA treatment appears to enhance membrane localisation of EGFP-Grp1-PH *(Figure 4.7).* In the ΔN clone , treatment with LPA triggered a greater membrane localisation of EGFP-Grp1-PH relative to untreated cells *(Figure 4.7).* However, the overall intensity values between untreated and LPA treated ΔN C4-2 remained largely consistent *(Figure 4.7).*

The same was also observed for KO C4-2 cells, where LPA treatment was unable to evoke increases in PI(3,4,5)P_3 levels *(Figure 4.7).* Whereas LPA treatment triggered membrane localisation of EGFP-Grp1-PH in the ΔN clone, diffuse biosensor localisation through the cytoplasm was observed in KO C4-2 cells, even after LPA treatment *(Figure 4.7).* Collectively the results from using the EGFP-Grp1-PH biosensor indicated that both CRISPR clones, but particularly clone KO exhibited impaired PI(3,4,5)P_3 dynamics.

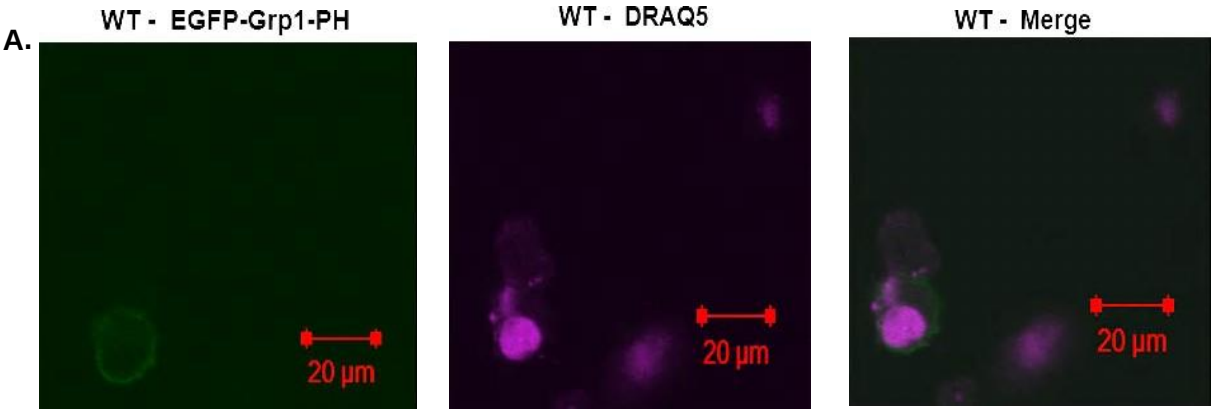
A.
WT - EGFP-Grp1-PH
WT - DRAQ5
WT - Merge
20 µm
20 µm
20 µm

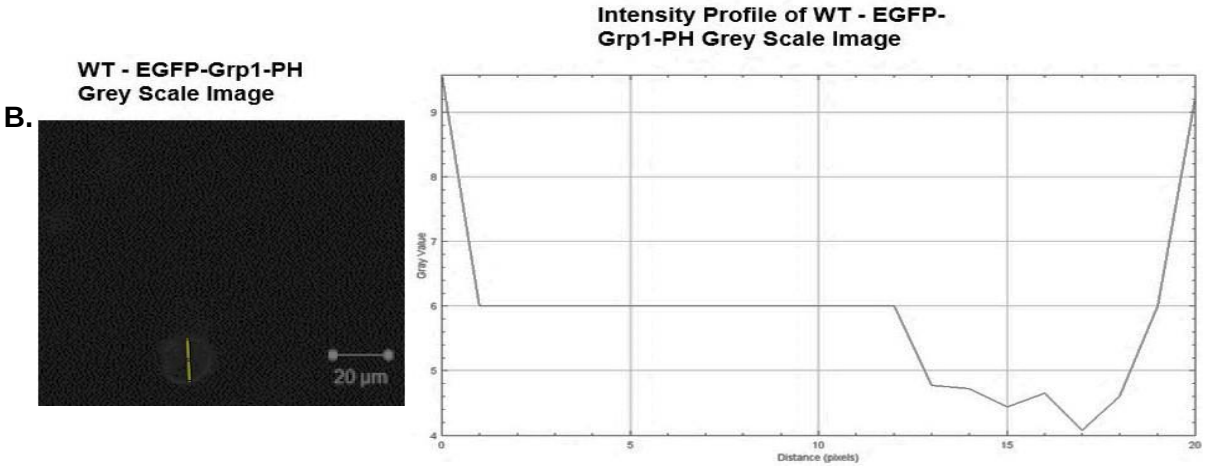
B.
WT - EGFP-Grp1-PH
Grey Scale Image
20 µm
Intensity Profile of WT - EGFP-
Grp1-PH Grey Scale Image
Gray Value
Distance (pixels)

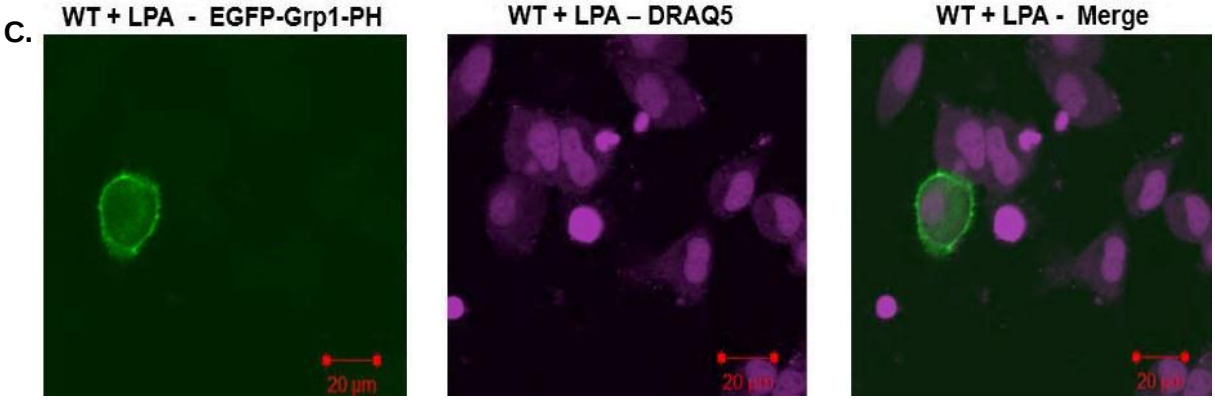
C.
WT + LPA - EGFP-Grp1-PH
WT + LPA – DRAQ5
WT + LPA - Merge
20 µm
20 µm
20 µm

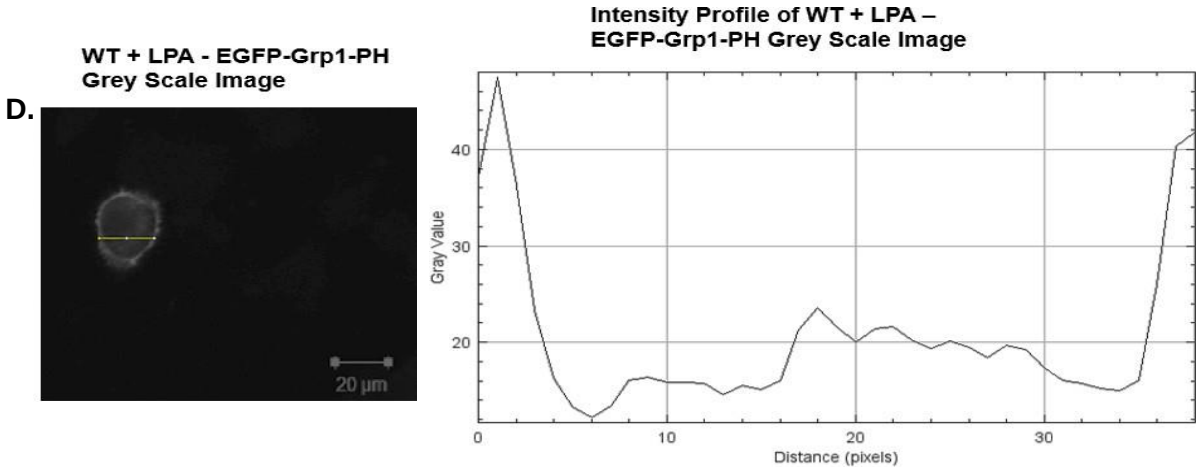
D.
WT + LPA - EGFP-Grp1-PH
Grey Scale Image
20 µm
Intensity Profile of WT + LPA –
EGFP-Grp1-PH Grey Scale Image
Gray Value
Distance (pixels)

E.

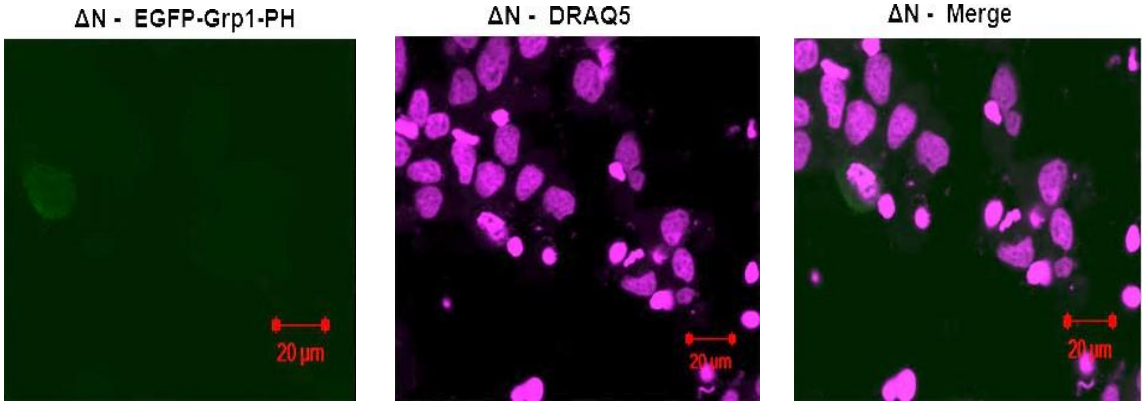
ΔN - EGFP-Grp1-PH
ΔN - DRAQ5
ΔN - Merge
20 µm
20 µm
20 µm

F.

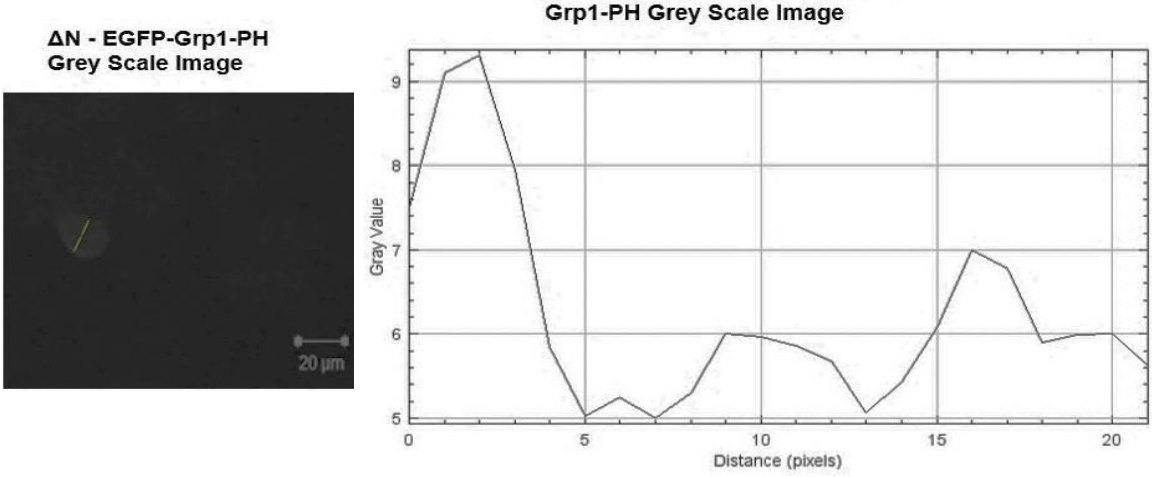
ΔN - EGFP-Grp1-PH
Grey Scale Image
20 µm
Intensity Profile of ΔN - EGFP-
Grp1-PH Grey Scale Image
Gray Value
Distance (pixels)
0
5
10
15
20
5
6
7
8
9

G.

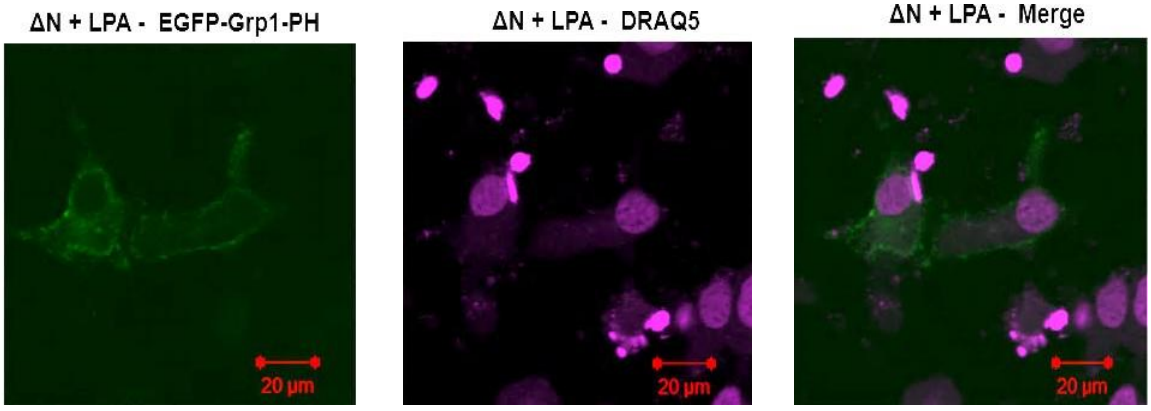
ΔN + LPA - EGFP-Grp1-PH
ΔN + LPA - DRAQ5
ΔN + LPA - Merge
20 µm
20 µm
20 µm

H.

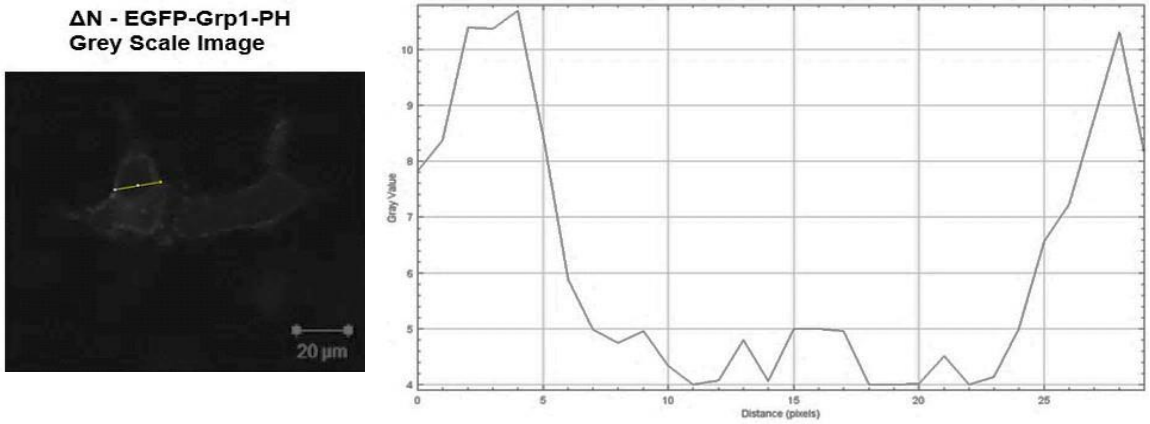
ΔN - EGFP-Grp1-PH
Grey Scale Image
20 µm
Intensity Profile of ΔN - EGFP-Grp1-PH
Grey Scale Image
Gray Value
Distance (pixels)
0
5
10
15
20
25
4
5
6
7
8
9
10

I.

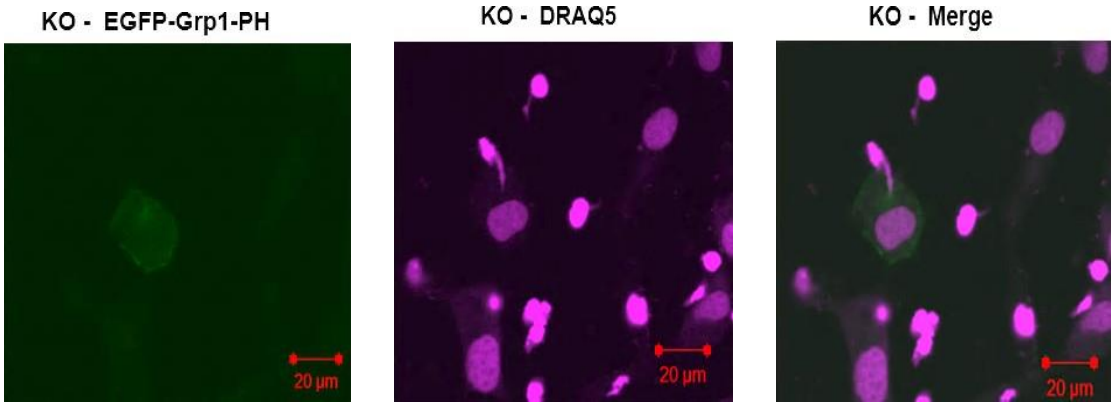
KO - EGFP-Grp1-PH
KO - DRAQ5
KO - Merge
20 µm
20 µm
20 µm

J.

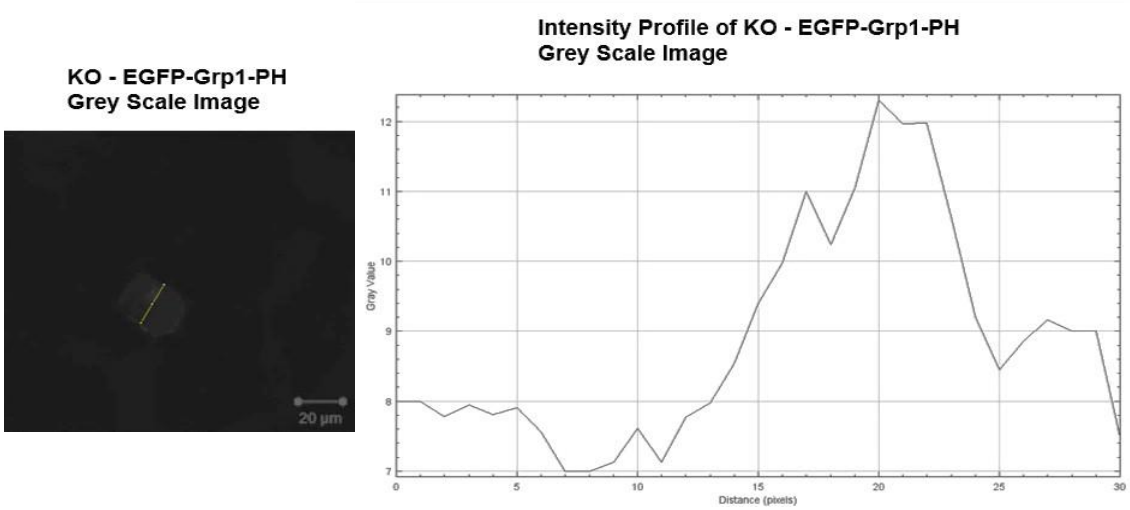
KO - EGFP-Grp1-PH
Grey Scale Image
20 µm
Intensity Profile of KO - EGFP-Grp1-PH
Grey Scale Image
Gray Value
Distance (pixels)

K.

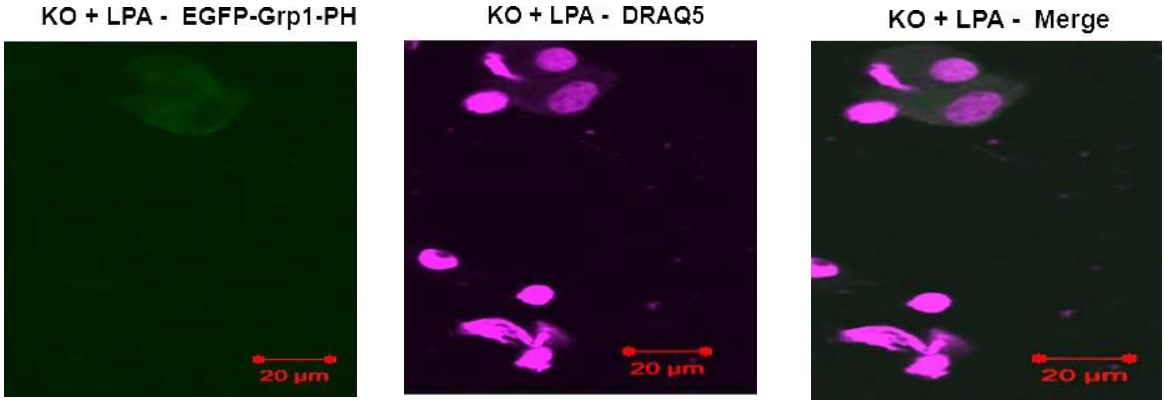
KO + LPA - EGFP-Grp1-PH
KO + LPA - DRAQ5
KO + LPA - Merge
20 µm
20 µm
20 µm

L.

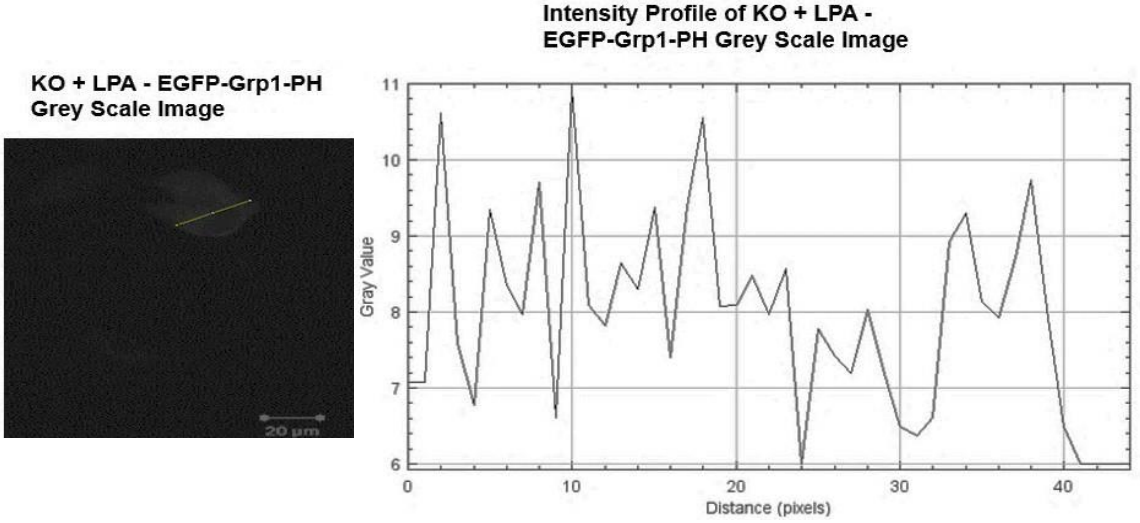
KO + LPA - EGFP-Grp1-PH
Grey Scale Image
20 µm
Intensity Profile of KO + LPA -
EGFP-Grp1-PH Grey Scale Image
Gray Value
Distance (pixels)

M.

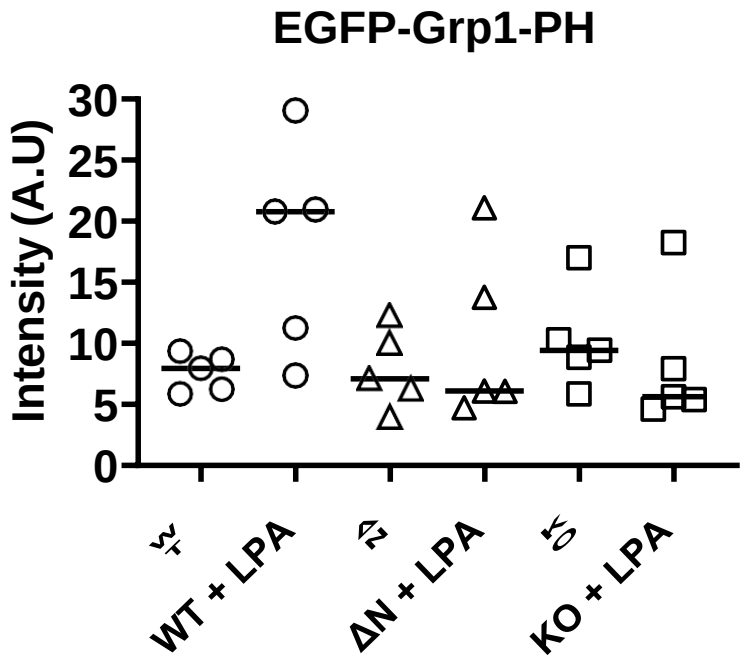

Figure 4.7. Detection of PI(3,4,5)P_3 in WT, ΔN and KO C4-2 cells using EGFP-Grp1-PH. Cell lines were transfected with the PI(3,4,5)P_3 detecting construct EGFP-Grp1-PH grown for 48h before being prepared for confocal microscopy. Just prior fixing cells for confocal microscopy, cells lines used for stimulation experiments were treated with 20μM LPA for 30 minutes at 37 °C, 5% CO_2. A Zeiss LSM510 Meta confocal microscope was used for image acquisition. **A.** Representative image of PI(3,4,5)P_3 fluorescence in untreated WT C4-2 cells. **B.** Grey scale image of **A** used in quantification of PI(3,4,5)P_3 fluorescence in WT C4-2 cells, with fluorescence intensity plotted as a line graph. **C**. Representative image of PI(3,4,5)P_3 fluorescence in LPA treated WT C4-2 cells**. D.** Grey scale image of **C** used in quantification of PI(3,4,5)P_3 fluorescence in LPA treated WT C4-2 cells, with fluorescence intensity plotted as a line graph. **E.** Representative image of PI(3,4,5)P_3 fluorescence in untreated ΔN C4-2 cells. **F.** Grey scale image of **E** used in quantification of PI(3,4,5)P_3 fluorescence in ΔN C4-2 cells, with fluorescence intensity plotted as a line graph. **G.** Representative image of PI(3,4,5)P_3 fluorescence in LPA treated ΔN C4-2. **H.** Grey scale image of **G** used in quantification of PI(3,4,5)P_3 fluorescence in LPA treated ΔN C4-2 cells, with fluorescence intensity plotted as a line graph. **I.** Representative image of PI(3,4,5)P_3 fluorescence in untreated KO C4-2 cells. **J.** Grey scale image of **I** used in quantification of PI(3,4,5)P_3 fluorescence in KO C4-2 cells, with fluorescence intensity plotted as a line graph. **K.** Representative image of PI(3,4,5)P_3 fluorescence in LPA treated KO C4-2 cells **L.** Grey scale image of **J** used in quantification of PI(3,4,5)P_3 fluorescence in LPA treated KO C4-2 cells. **M.** A chart of EGFP-Grp1-PH fluorescent intensities in 5 different WT, ΔN and KO LNCaP C4-2 cells.

4.7. Changes in Filamentous Actin Observed in ΔN and KO LNCaP C4-2 Prostate Cancer Cells

With the phosphoinositide pathway implicated with the regulation of actin filamentation *(Saarikangas et al., 2010),* immunofluorescence was conducted to assess how loss of PIP5K1α impacts this process. Produced the death cap mushroom *Amanita phalloides*, phalloidin is a bicyclic toxic peptide which binds to filamentous actin *(Yao et al., 2019)*. By isolating and making fluorescent conjugates of phalloidin, this allows actin filaments to be visualised. Using a red fluorescent conjugate of phalloidin in immunofluorescence assays, WT LNCaP cells exhibited the greatest actin staining *(Figure 4.8).* In both CRISPR clones, filamentous actin staining was impacted. This result is consistent with *Wang et al., 2022,* which also validated that actin filamentation was perturbed in clone ΔN through phalloidin staining. This ultimately suggests in LNCaP C4-2 cells, PIP5K1α has a role in regulating actin filamentation.

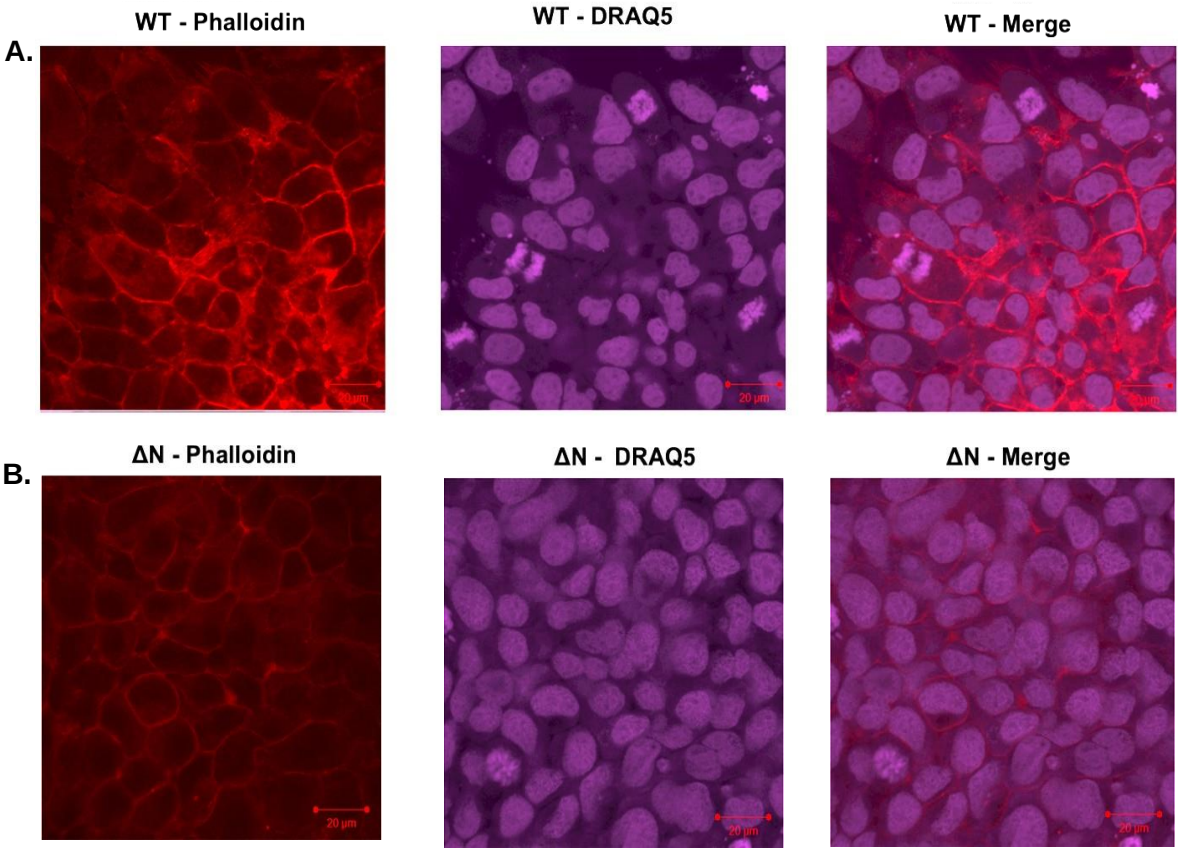

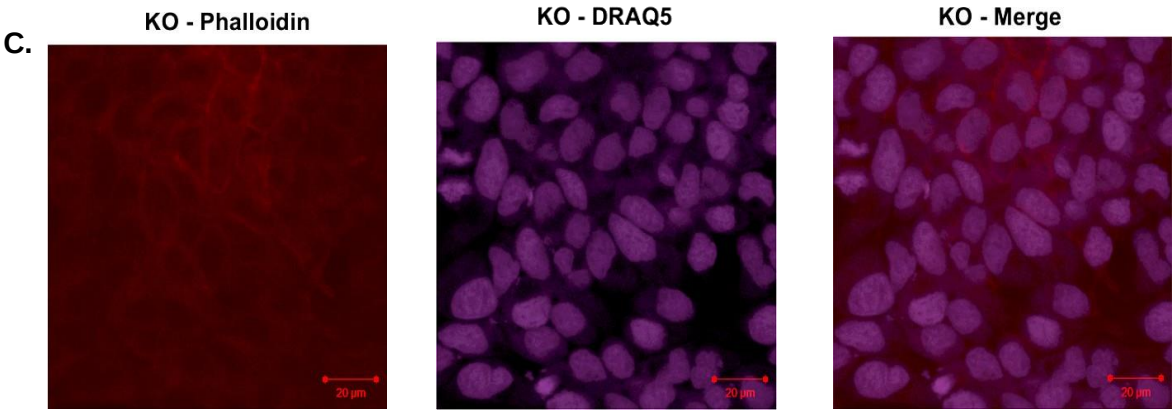

Figure 4.8. Staining of filamentous actin in WT , ΔN and KO LNCaP C4-2 cells. Representative confocal microscopy images of phalloidin stained actin filaments for WT , ΔN and KO LNCaP C4-2 cells are shown in **A, B** and **C** respectively.

4.8. Changes in Cell Adhesion in WT , ΔN and KO C4-2 Prostate Cancer Cells

With the PI(4,5)P_2 signalling also implicated in cell adhesion *(Mandal., 2020 ; Krajnik et al., 2020)* it was crucial to assay whether altering the expression of PIP5K1A in C4-2 cells affected this. Cells were allowed to adhere to 96 well plate overnight, before being subjected to a mixture of PFA and toluidine blue. After staining and several PBS washes, SDS lysis of remaining adhered cells was conducted, with the absorbances of the lysed cells measured. The results from these assays suggest that KO C4-2 undergo adhesion defects, with statistically significance differences recorded between KO and ΔN C4-2 cells. *(Figure 4.9).* Additionally these results suggest that cell adhesion is enhanced in clone ΔN *(Figure 4.9).*

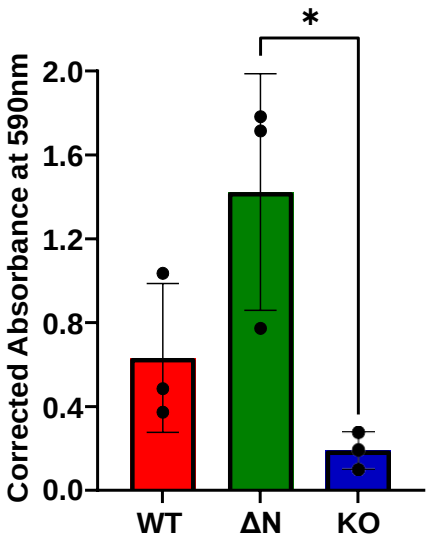

Figure 4.9. Changes in cell adhesion in CRISPR edited LNCaP C4-2 cells. Corrected absorbance readings from adhesion assays where WT, ΔN and KO LNCaP C4-2 cells were stained with a mixture of toluidine blue and PFA, before being lysed with SDS. Average absorbance readings were taken for each cell line, with the averages corrected by subtracting the average background absorbance from complete medium wells. Data is of biological triplicates (n=3), with technical quintuplets. A two-sided t-test indicates significance differences between ΔN and KO LNCaP C4-2 cells, * $P \leq 0.05$.

4.9. Alterations in Cell Migration in WT , ΔN and KO C4-2 Prostate Cancer Cells

In the context of cancer cell biology, a loss of cell adhesion increases cell motility which is necessary for metastasis *(Janiszewska et al., 2020).* With the alterations in cell adhesion shown in the CRISPR edited cell lines *(Figure 4.9),* cell migration assays were conducted to assess whether this is also affected by attenuating PIP5K1A expression. WT, ΔN and KO C4-2 were seeded either side of a plastic cell culture insert, which created a gap. After adhering to the culture insert overnight, this was gently removed, leaving a gap of ~500μm thick between two cell populations. Light microscope images were then taken right after the gap was generated, followed by images 24h and 48h later. The percentage of open area between the migrating cell populations was quantified at these time points using Tscratch software *(Gebäck et al., 2009).*

Whilst no significant differences were observed after 24h, there was statistically significant differences in the open area % between ΔN and WT cells after 48h *(Figure 4.10).* This suggests that ΔN cells are undergoing a migration defect. This outcome is consistent with previous publication, which instead used Transwell migration assays to show that clone ΔN has impaired migration *(Wang et al., 2022).* With the LNCaP cell line considered to be semi adherent *(Sanmukh and Felisbino. 2018)* this in part explains some of the variability in these data; as population of cells can be disrupted when removing the plastic insert. Furthermore, with *Figure 4.9* suggesting that the KO C4-2 line possesses an additional adhesion defect, this could the reason why variability is observed with this data. Whilst variable, results for KO C4-2 suggests that loss of PIP5K1A expression in this clone does not impede cell migration.

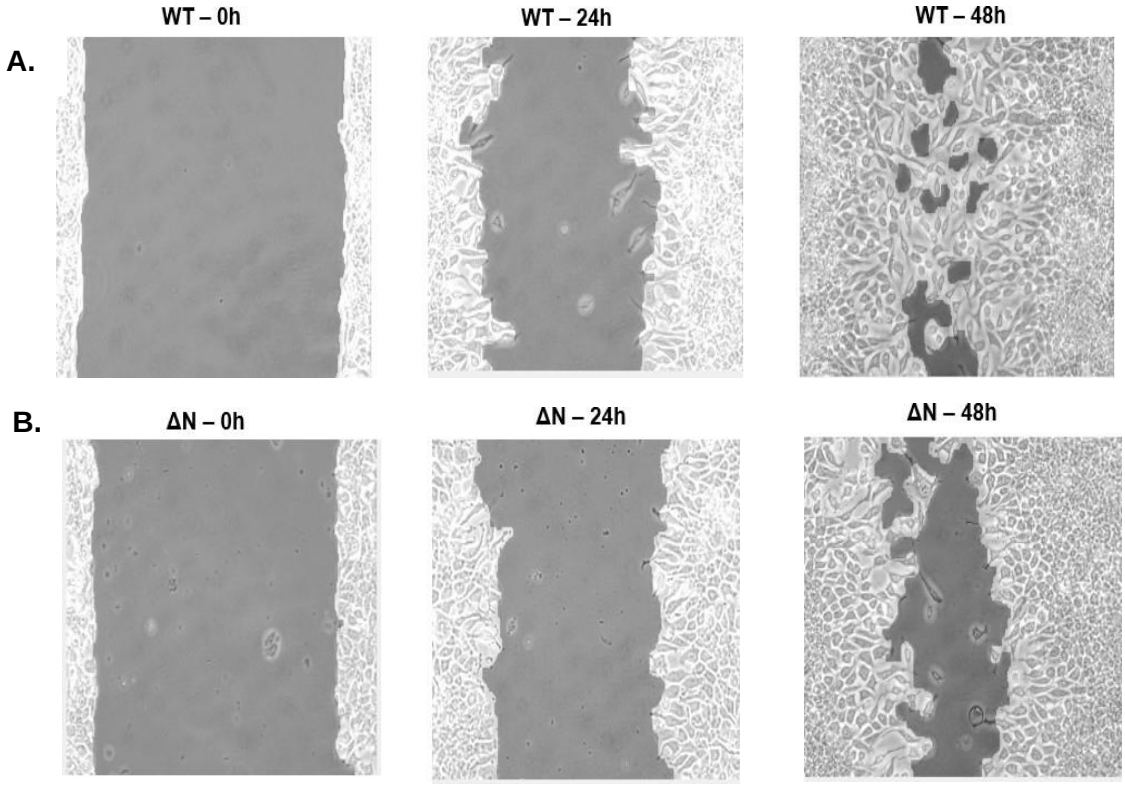

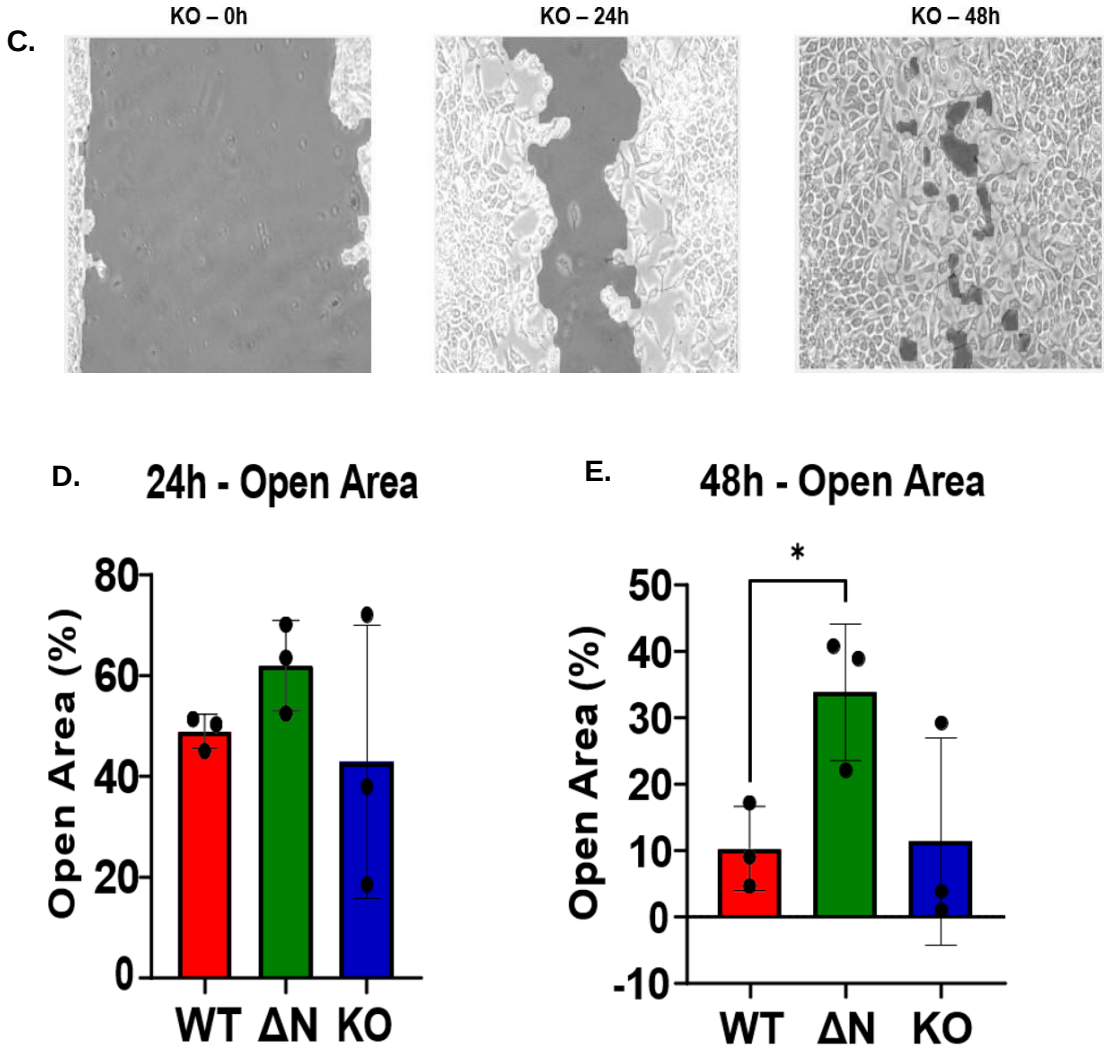

Figure 4.10. Cell migration of WT, ΔN and KO LNCaP C4-2 cells. Cell lines were seeded on a culture insert, forming a barrier, and left to incubate overnight at 37 °C, 5% CO_2. The culture insert was removed the next day, and images of cells were taken at 0h, 24h and 48h. **A, B and C** are representative images of cell migration assays for WT, ΔN and KO LNCaP C4-2. Using Tscratch software *(Gebäck et al., 2009),* the percentage of open area left after 24h and 48h was quantified, with this graphed in **D and E.** Experiments were conducted in biological triplicates (n=3) with technical triplicates. Significance between ΔN-WT C4-2 cells after 48h of cell migration was determined with a two sided t-test.

4.10. Discussion

This chapter has explored how CRISPR editing of PIP5K1A in LNCaP C4-2 cells alters phosphoinositide levels. Numerous experiments with selective lipid biosensors were conducted with the outcomes summarized in *Table 4.2*. One of the main findings from this work suggests that treatment with 20μM of LPA stimulates $PI(4,5)P_2$ and $PI(3,4,5)P_3$ generation in just WT C4-2 cells. On the other hand the CRISPR clones (particularly clone KO) appeared to exhibit a diminished response to PMA treatments. This suggests that PIP5K1α activity in both clones is impaired, and possibly a greater concentration of LPA would be needed to stimulate $PI(4,5)P_2$ and $PI(3,4,5)P_3$ synthesis in ΔN and KO C4-2. It must be stated, whilst PIP5K1α are classically implicated with $PI(3,4,5)P_3$ production by increasing the available pool of $PI(4,5)P_2$ available to Class I PI3Ks, PIP5Ks can also synthesise $PI(3,4,5)P_3$ directly. In this alternative pathway, $PI(3,4)P_2$ be utilised as substrate by PIP5K1α leading to the synthesis of $PI(3,4,5)P_3$ *(Zhang et al., 1997).* However, $PI(3,4,5)P_3$ production by PIP5K1α reflects a minor signalling axis, with PIP5K1α exhibiting a greater affinity towards the PI(4)P substrate instead *(Zhang et al., 1997).*

In the future, the levels of these phosphoinositides could be assayed in the presence of different agonists, which could help further confirm that phosphoinositide synthesis is impaired in both CRISPR clones. As PIP5Ks can be activated by EGFR *(Cochet et al., 1991*) stimulating WT, ΔN and KO C4-2 cells with EGF could be another treatment used in further studies. Previous work has shown that EGF treatment induces membrane ruffling in HeLa cells, with this process being dependent upon an Arf6/PIP5K1β signalling axis *(Funakoshi, et al., 2011).* In regards to PI(4)P and $PI(3,4)P_2$ the levels of these phosphoinositides did not majorly alter in the CRISPR edited lines *(Figure 4.1 and 4.6).* These assays were not conducted in the presence of PIP5K activating agonists and possible subsequent experiments could involve this.

Table 4.2. Summary of the results obtained from the series of lipid biosensor experiments described in this chapter.

Lipid	Biosensor	Result
PI(4)P	mCherry-P4M-SidM	Predominantly cytoplasmic localisation of biosensor. No alterations in PI(4)P levels between WT, ΔN and KO cells.
$PI(4,5)P_2$	Tubby-R332H-YFP	Diffuse localisation of biosensor in untreated conditions. LPA stimulation promotes plasma membrane localisation of Tubby-R332H-YFP, with this most prominent in WT cells. KO cells appear to exhibit a defect in $PI(4,5)P_2$ synthesis after LPA treatment.
DAG	EGFP-PKCγ-C1A	Nuclear localisation of biosensor with no obvious alterations in DAG levels between WT and CRISPR edited LNCaP C4-2 cells.
$PI(3,4)P_2$	NES-EGFP-cPHx3	Strong plasma membrane localisation of NES-EGFP-cPHx3. Levels of $PI(3,4)P_2$ remain consistent between WT, ΔN and KO cells.
$PI(3,4,5)P_3$	pcDNA3.1_AktPH-mCherry and EGFP-Grp1-PH	The pcDNA3.1_AktPH-mCherry biosensor exhibited a broad localisation (cytoplasm, nuclear, cell membrane) across WT, ΔN and KO cells. This biosensor suggested that $PI(3,4,5)P_3$ synthesis is increased in WT cells after LPA treatment, however there is variability between across the 5 datapoints. Modest increases in pcDNA3.1_AktPH-mCherry biosensor intensity in both CRISPR clones after LPA treatment. The EGFP-Grp1-PH biosensor exhibited localisation to the cell membrane, with a more pronounced localisation after LPA treatment in WT cells. The EGFP-Grp1-PH biosensor showed more cytoplasmic localisation in the CRISPR edited clones, particularly clone KO. No increases in EGFP-Grp1-PH intensity after LPA stimulation, suggesting impaired $PI(3,4,5)P_3$ synthesis.

The use of biosensors in this work has been able to capture the localisation of different phosphoinositides in LNCaP C4-2 cells. Variances in localisation was observed between two $PI(3,4,5)P_3$ detecting constructs, pcDNA3.1_AktPH-mCherry and EGFP-Grp1-PH. A more diffuse localisation of pcDNA3.1_AktPH-mCherry was observed in WT and CRISPR edited clones, with localisation to the cell membrane, cytoplasm and also the nucleus *(Figure 4.5).* However, a stronger membrane localisation was observed for EGFP-Grp1-PH particularly in WT and ΔN C4-2 cells after LPA treatment *(Figure 4.7).* The variances in localisation between the two biosensors ultimately highlights the importance of using constructs with the most selective lipid binding domains when probing phosphoinositide pools *in vitro.*

Whilst this work has been able to capture the localisation of different phosphoinositides in LNCaP C4-2 cell lines, quantification of the phosphoinositide levels in cells has been challenging. Firstly, drawing the most representative traces through the cells may be vulnerable to bias. With hindsight, a possible way this could be limited would be to ask co-workers to take the traces through the cells, in a manner which resembles a non-blind study.

Additionally only small number of cells (typically 5) were used in quantification due to limitations in transient transfection efficiencies. This also brought the additional challenge of how best to study the phosphoinositide signalling pathway in WT, ΔN and KO C4-2 cells. The decision was made to conduct single experiments, but with biosensors which capture multiple aspects of phosphoinositide signalling pathway. This route was decided as it was felt this could highlight how antagonising PIP5K1α expression could affect the levels of multiple phosphoinositides within cells.

An alternative approach which could have been adopted instead would have been to focus on phosphoinositides which PIP5K1α directly synthesises, principally PI(4,5)P_2. In this, multiple transient transfections with Tubby-R332H-YFP could have been conducted, with the results then pooled together, giving a greater sample size for quantification. Another way of generating a greater sample pool would be WT, ΔN and KO cells stably expressing Tubby-R332H-YFP. Collectively these are strategies which could be tested to optimise phosphoinositide detection by using lipid biosensors.

This however does not rule out that other approaches could deployed to further supplement lipid detection in WT, ΔN and KO cells. For analyzing whether the level of a certain phosphoinositide is modulated in the CRISPR edited clones [e.g PI(4,5)P_2], a competitive ELISA could be used. For a more global understanding of phosphoinositide dynamics in WT, ΔN and KO C4-2 cells, mass spectrometry (whilst more technically challenging) has the potential to identify a range of phosphoinositides from mammalian cell lipid extracts at great sensitivity.

This chapter also has sought to assess whether CRISPR editing of PIP5K1A contributes to alterations cell migration and cell adhesion, processes driven by the rapid assembly and disassembly of filamentous actin *(Garde et al., 2010).* With previous studies showing that blocking PIP5K1α disrupts F-actin structure and content *(Zhang et al., 2008 ; Muscolini et al., 2014),* this work highlights that ΔN and KO C4-2 also possess impaired F-actin dynamics *(Figure 4.8).* The staining of F-actin using phalloidin was carried out on PFA fixed cells. This only provides a snapshot into F-actin structure and content in WT and CRISPR edited LNCaP C4-2 cells. Future work could look to deploy live fluorescence imaging which would allow F-actin dynamics to visualised over a prolonged time frame. The development of cell permeable, fluorogenic probes now makes this possible, such as SiR-actin. This probe emits a far red fluorescence which is simply added to cell culture medium and

exhibits minimal cytotoxicity *(Lukinavičius et al., 2014).* SiR-actin is conjugated to a synthetic and less cytotoxic derivative of of jasplakinolide, a toxin synthesised by the marine sponge *Jaspis johnstoni*, whichpotently binds to F-actin *(Bubb et al., 1994 ; Schmitz-Elbers, et al., 2021).*

Whereas ΔN C4-2 cells appeared to show a stall in cell migration after 48h, the same was not observed for KO C4-2 cells. Whilst somewhat variable, the data suggested that there were no significant alterations in migration between KO and WT C4-2 cells *(Figure 4.10)* Whilst this was a surprising finding given as PIP5Ks localize and regulate key cytoskeletal proteins *(Ling et al., 2006),* there have been accounts where knockdown of PIP5Ks does not alter cell migration.

Through siRNA knockdown of the PIP5K1C splice variant PIPKIγ668 in HeLa , MtLn3 and A431 cell lines, this suppressed cell migration when EGF was used as a chemoattractant in Boyden chamber migration assays *(Sun et al., 2007).* However, when LPA or Stromal Cell-Derived Factor 1α (SDF1α) was used as a chemoattractant, knockdown of PIPKIγ668 did not impair migration *(Sun et al., 2007).* Finally, PIP5K1α siRNA knockdown in HeLa cells did not affect cell migration when EGF was used as a chemoattractant *(Sun et al., 2007).*

Collectively these results highlight that different PIP5K isozymes drive actin polymerisation, membrane ruffling and cell migration in different cell lines. Furthermore, the results by *Sun et al., (2007)* showed that migration defects observed in PIPKIγ668 knockdown cells could be overcome by treatment with LPA or SDF1α. The migration assays conducted in this work used cell culture medium supplemented with FBS, which contains a broad range of hormones, cytokines, growth factors, amino acids and proteins *(Pilgrim et al., 2022).* Future migration assays in reduced serum medium, supplemented with different agonists could be conducted to assess the effect this has on ΔN and KO C4-2 cell motility.

Additionally, KO LNCaP C4-2 cells possess attenuated expression of CAMK2N1 (Figure 3.10), with loss of this gene attributed to enhancing prostate cancer cell migration *(Peng et al., 2023).* This could reflect another mechanism as to why cell migration in KO LNCaP C4-2 cells was not heavily perturbed by loss of PIP5K1A expression. Future cell migration could be conducted in KO LNCaP C4-2 cells which have been rescued for CAMK2N1 expression, to assess whether loss of gene is contributing to cell migration in clone KO.

Cell adhesion to a substrate drives cytoskeletal remodelling, the formation of membrane protrusion and cell spreading *(De Pascalis and Etienne-Manneville, 2017).* With this reciprocal relationship considered, cell adhesion assays were conducted to assess whether alterations in cell migration observed in CRISR edited clones could be explained through changes in cell adhesion. Clone ΔN exhibited greater cell adhesion relative to KO LNCaP C4-2 cells and a possible mechanism for this could be through the increased AKT activity this clone possesses (*Roberts, 2022 and detailed further in Chapter 5).*

AKT can positively regulate FAK through phosphorylation of S517, S601 and S695 residues *(Wang and Basson, 2011).* The phosphorylation of these three serine residues promotes the autophosphorylation of FAK (at Y397) which is critical for FAK activity *(Wang and Basson, 2011).* FAK promotes cell adhesion, in part through the positively integrins to tether cells to a givensubstrate *(Michael et al., 2009).* To confirm whether enhanced FAK activity is contributing to enhanced adhesion in ΔN LNCaP C4-2 cells, replicate adhesion assays treating clone ΔN with a FAK inhibitor could be conducted.

The overall loss of cell adhesion exhibited in KO LNCaP C4-2 cells *(Figure 4.9)* could be explained through the lack of actin content this clone has, as shown by phalloidin staining *(Figure 4.8).* Actin filaments are necessary in linking focal adhesion to the cell-substrate contact site which is required for cell adhesion *(Ohashi, et al., 2017).* The adhesion assays conducted in this work used non coated plastic culture plates. In possible further work it would be relevant to coat the culture plates with physiological substrate, such as collagen or fibronectin, to assess whether adhesion is still impaired in KO LNCaP C4-2 cells.

Finally, this chapter investigated whether attenuating the expression of PIP5K1α would impede PKC signalling. In unstimulated conditions there was no obvious changes in the phosphorylation of PKC substrates between WT and CRISPR edited clones *(Figure 4.4).* Treatment of WT, ΔN and KO C4-2 cells with the PKC activating agonist PMA evoked phosphorylation of PKC substrates with both CRISPR clones, particularly KO C4-2 showing the greatest substrate phosphorylation *(Figure 4.4).* This highlights that knockdown of PIP5K1α expression does not impede LNCaP C4-2 responsiveness to PMA stimulation. Strong phosphorylation was observed particularly at ~90kDa – 120kDa with PhosphoSitePlus used to identify possible substrates (ATP1A1 and PKD1) which fall within this molecular weight range. To fully validate this however, tailored antibodies directed to known PKC sites on these substrates such as a phospho-PKD1 S738/S742 antibody, would be needed to confirm whether these sites undergo increased phosphorylation in PMA treated cells, particularly in clone KO.

The differences in substrate phosphorylation could not be accounted for by the CRISPR lines showing increased expression of conventional and novel PKC enzymes which are responsive to DAG/PMA. In fact significant downregulation of PKC expression was observed at the RNA level *(Table 4.1).* The expression of PRKCG and PRKCD was significant reduced in ΔN C4-2 cells, and the expression of PRKCA downregulated in KO C4-2 cells. RNA-Seq data also highlighted the expression of ATP1A1 and PKD1 was not altered between ΔN-WT and KO-WT LNCaP C4-2 cells.

Whilst PMA activates classical and novel PKCs, this agonist can also activate other signalling pathways mediated by Ras/MAPKs (*Masuda et al., 2003 ; Roux et al., 2004 ; Cervantes, et al., 2010*) stress kinases in the form of p38 and JNK *(Hii et al., 1998 ; Igarashi et al., 1999; Zhang et al., 1999)* and the IKK/ NF-κB network *(Peters et al., 2000 ; Baumann et al., 2000 ; Shambharkar et al., 2007).* Possible crosstalk between these diverse signalling pathways could contribute to the results observed in the PMA treatment work. *Figure 4.2* suggested that after LPA stimulation does not increase PI(4,5)P_2 levels in ΔN and KO C4-2 cells. Further work could explore whether the phosphorylation of PKC substrates is still elevated in both CRISPR clones when treated LPA.

Chapter 5

Alterations in AKT Signalling in ΔN LNCaP C4-2 Prostate Cancer Cells : Possible Roles for PIK3R1?

5.1. Introduction

With Chapter 4 detailing aberrations in the phosphoinositide network in clones ΔN and KO, this chapter will focus on downstream AKT signalling. Previous work by *Roberts, (2022)* observed that in in ΔN LNCaP C4-2 prostate cancer cells, sustained AKT activation is apparent. PIP5K1α is responsible for generating $PI(4,5)P_2$ which is subsequently phosphorylated by Class I PI3Ks which mediates AKT activation. Therefore, it seems paradoxical that attenuating the expression of PIP5K1α could positively stimulate AKT phosphorylation. However, knockdown of other phosphoinositide pathway components such as PIK3R1 has been shown to induce AKT phosphorylation in a variety of cancer models.

Whilst the SH2 domains of the regulatory subunit of PI3K are critical in mediating $PI(3,4,5)P_3$ production through coupling the catalytic subunit to RTKs, they can also negatively regulate phosphoinositide synthesis. Previous work by the groups of Lewis Cantley and Ronald Kahn suggested that ~30% p85 proteins are not tethered to p110 catalytic subunits, and instead exist in a monomeric form *(Ueki et al., 2002 ; Mauvais-Jarvis etal., 2002).* In turn, the p85 monomers can compete with p85-p110 dimers for activated RTKs which can attenuate $PI(3,4,5)P_3$ synthesis. Therefore, knockdown (but not complete loss) of PIK3R1 expression would limit the pool of monomeric p85 and promote p85-p110 dimers binding to activated RTKs, generating $PI(3,4,5)P_3$ and triggering AKT activation. In diabetes models, mice harbouring either a homozygous or heterozygous deletion for PIK3R1 possessed increased phospho-AKT levels in their livers, significantly improved glucose intolerance, lower blood glucose levels and increased insulin sensitivity *(Mauvais-Jarvis et al., 2002).*

Whilst modulating the expression of PIK3R1 saw intense speculation as to whether this could be a treatment strategy for diabetes *(Terauchi et al., 1999 ; Ueki et al., 2002 ; Mauvais-Jarvis et al., 2002)* in the context of cancer, loss of PIK3R1 expression has dramatic effects. In an *in vivo* model for EGFR2 driven breast cancer breast cancer, mice harbouring either a heterozygous or a homozygous mutations of PIK3R1 were characterised with significantly reduced tumour onset time than control mice *(Thorpe et al., 2017).* Additionally, mice lacking PIK3R1 in the liver formed hepatocellular carcinomas after 14-20 months, with mice older than 16 months forming lung metastases *(Taniguchi et al., 2010).* Both these *in vivo* studies indicate the tumour suppressive properties of PIK3R1.

The downstream signal transduction events arising from PIK3R1 loss is diverse and varies between tumour models. In renal cancer cell lines knockdown of PIK3R1 was shown to induce greater cell growth and promote a more migratory phenotype through the activation of Wnt/β-catenin signalling pathway, arising through increased AKT activity *(Lin et al., 2015).* Elevated downstream GSK3β Ser9 phosphorylation was observed in PIK3R1 ablated 786-O and A-704 renal cancer cell lines *(Lin et al., 2015).* With GSK3β being a component of the β-catenin degradation complex, AKT mediated Ser9 phosphorylation inhibits GSK3β activity *(Fukumoto et al., 2001).* This prevents β-catenin degradation, resulting in elevated nuclear translocation of the β-catenin and increased expression of the β-catenin responsive genes *(Fukumoto et al., 2001).*

In ovarian cancer cell lines with depleted PIK3R1 expression elevations of phospho-AKT levels, enhanced cell migration, and increase cell proliferation were observed *(Li et al., 2019).* However, unlike the PIK3R1 depleted 786-O and A-704 renal cancer cells, no alterations in β-catenin levels were reported in PIK3R1 depleted ovarian cancer cells *(Li et al.,*

2019). Instead, *Li et al., (2019)* found that PIK3R1 loss in three different ovarian cancer cell lines caused activation of JAK/STAT signalling pathway, and reductions in GRB2-associated-binding protein 2 (Gab2) S210 phosphorylation. Gab2 is an adaptor protein which can couple to activated growth factors via interactions with the SH2 domain containing protein, growth factor receptor-bound protein 2 (Grb2) *(Higo et al., 2013).* Additionally, after growth factor stimulation, Gab2 becomes heavily tyrosine phosphorylated, which mediates recruitment of SH2 domain containing proteins, such as p85 *(Brummer et al., 2008).*

In order to prevent sustained PI3K/AKT pathway activity phosphorylation of Gab2 on S210 and T391 recruits 14-3-3 proteins which dissociate Gab2 from Grb2 *(Brummer et al., 2008).* The reductions in Gab2 S210 phosphorylation observed by *Li et al., (2019)* could initiate AKT activity if 14-3-3 protein recruitment is inhibited. To mimic this, a phospho-null Gab2 S210A mutant was expressed in OVCAR5 cells (a cell line with low Gab2 protein levels) and this elevated phospho-AKT levels *(Li et al., 2019).* Collectively these studies show that PIK3R1 loss can induce activation of AKT in diverse mechanism, and the downstream pathways which are activated show cancer cell line variability.

Clone ΔN exhibits downregulation of PIK3R1 (detailed subsequently). With this considered, this work has sought to clarify whether loss of PIK3R1 expression in this clone is a factor as to why ΔN LNCaP C4-2 cells show elevated AKT phosphorylation. To investigate this, fluorescent PIK3R1 constructs were generated, and used in rescue experiments. These preliminary experiments suggested that PIK3R1 may exert a role in regulating AKT phosphorylation in clone ΔN, but additional regulators may also be involved in this process.

5.2. Enhanced AKT phosphorylation in ΔN C4-2 cells

To ensure consistency with previous work by *Roberts, (2022)* that upregulation of phospho-AKT levels were observed in ΔN C4-2 cells, western blotting was again conducted. From the western blots, both classical AKT activation sites (T308 and S473), underwent increased phosphorylation in ΔN C4-2 cells *(Figure 5.1).* In the T308 western blot an additional band was apparent, which has been observed using T308 phospho-AKT antibodies *(Wainstein et al., 2022).* This could be due to non-specific antibody binding, or detection of AKT2s T309 residue being phosphorylated.

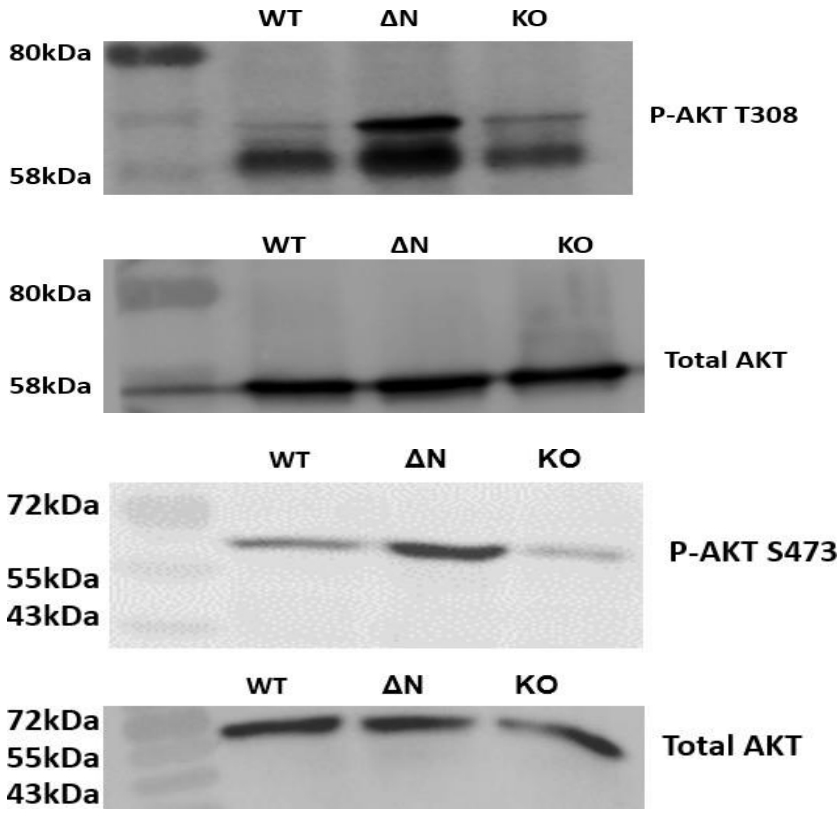

Figure 5.1. Phosphorylation of AKT in WT, ΔN and KO LNCaP C4-2 cells. Proteins were extracted using RIPA buffer and resolved on 10% SDS-PAGE gels before blotting for phospho-T308 and phospho-AKT S473. Shown are two separate western blots, for T308 and S473 phosphorylation, with each blot also containing a total AKT loading control.

A confocal microscopy assay was also conducted to assess the effects of elevated phospho-AKT in ΔN C4-2 cells. This involved transfecting an AKT activity reporter (pSBbi-FoxO1_1R_10A_3D) into the cell lines and observing the translocation of the reporter (*Gross et al., 2019).*

AKT is implicated with the regulation of FoxOs through phosphorylation. Upon phosphorylation of Thr24 , Ser256 and Ser319 on FoxO1 by AKT, this suppresses transcriptional activity and causes nuclear to cytoplasmictranslocation *(Brunet et al., 1999).* Note, other kinases can phosphorylate FoxO1 and trigger cytoplasmic translocation, such as dual specificity tyrosine phosphorylation regulated kinase 1A (DYRK1A) which phosphorylates the conserved Ser329 residue on FOXO-3A *(Wood et al., 2001).* To compensate for this, deletion of 234 C-terminal amino acids, in conjunction with site directed mutagenesis of a further 10 amino acids was conducted to limit the number of residues which could be phosphorylated by other kinases (*Gross et al., 2019).* A negative control construct (pSBbi-FoxO1_1R_13A_3D) was also developed by *Gross et al., (2019229)* in which the AKT phospho-sites (T24, S256 and S319) were mutated causing nuclear retention of this construct.

Transfection of pSBbi-FoxO1_1R_13A_3D revealed strong nuclear localisation in WT, ΔN and KO C4-2 cells, consistent with the T24 , S256 and S319 being mutated *(Figure 5.2).* However cytoplasmic localisation of pSBbi-FoxO1_1R_10A_3D was observed in all three cell lines *(Figure 5.2).* This suggests that the basal activity of AKT in WT and KO C4-2 cells is sufficient alone to trigger cytoplasmic localisation of pSBbi-FoxO1_1R_10A_3D.

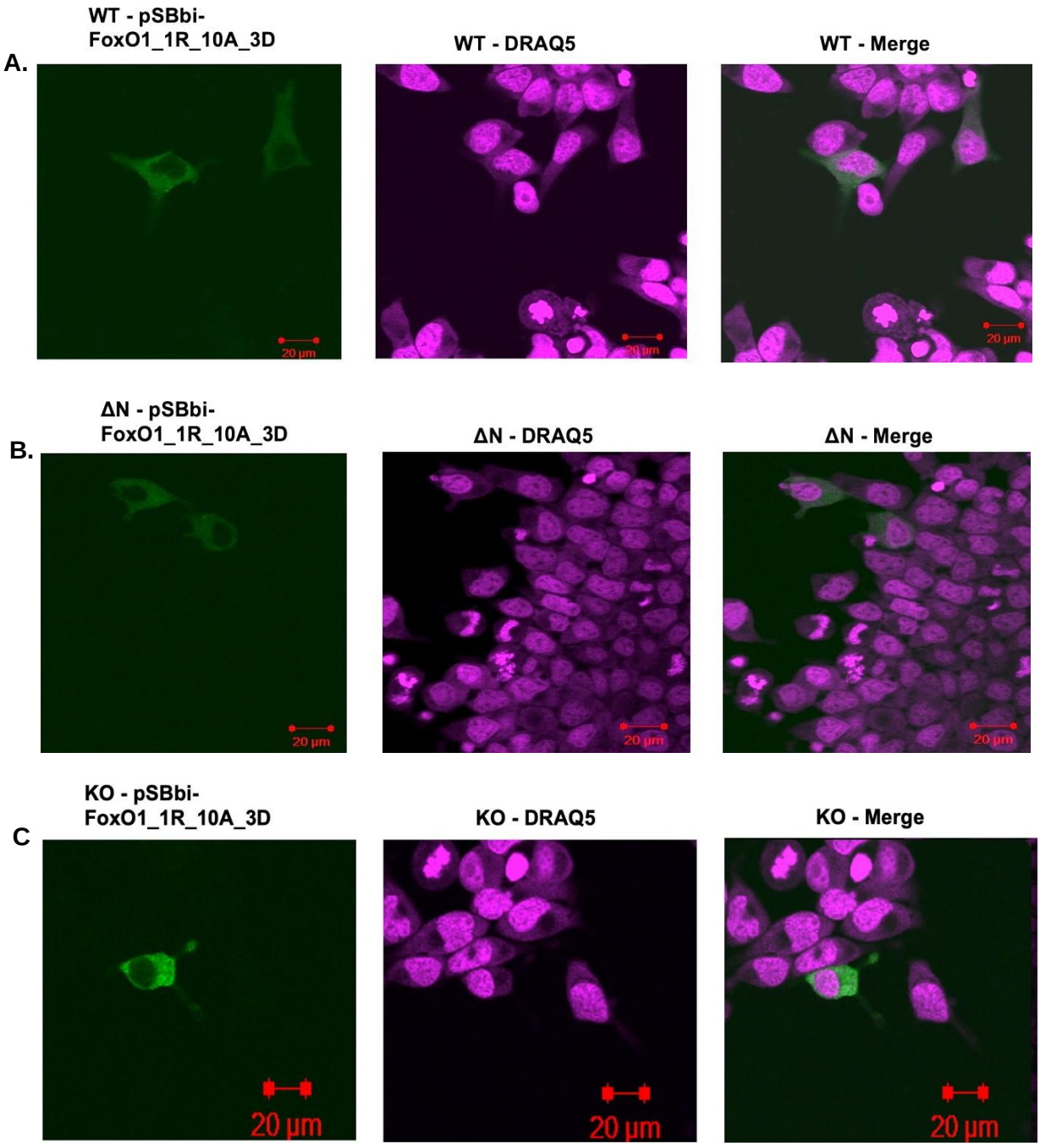
A.
WT - pSBbi-FoxO1_1R_10A_3D
WT - DRAQ5
WT - Merge
20 µm
B.
ΔN - pSBbi-FoxO1_1R_10A_3D
ΔN - DRAQ5
ΔN - Merge
20 µm
C
KO - pSBbi-FoxO1_1R_10A_3D
KO - DRAQ5
KO - Merge
20 µm

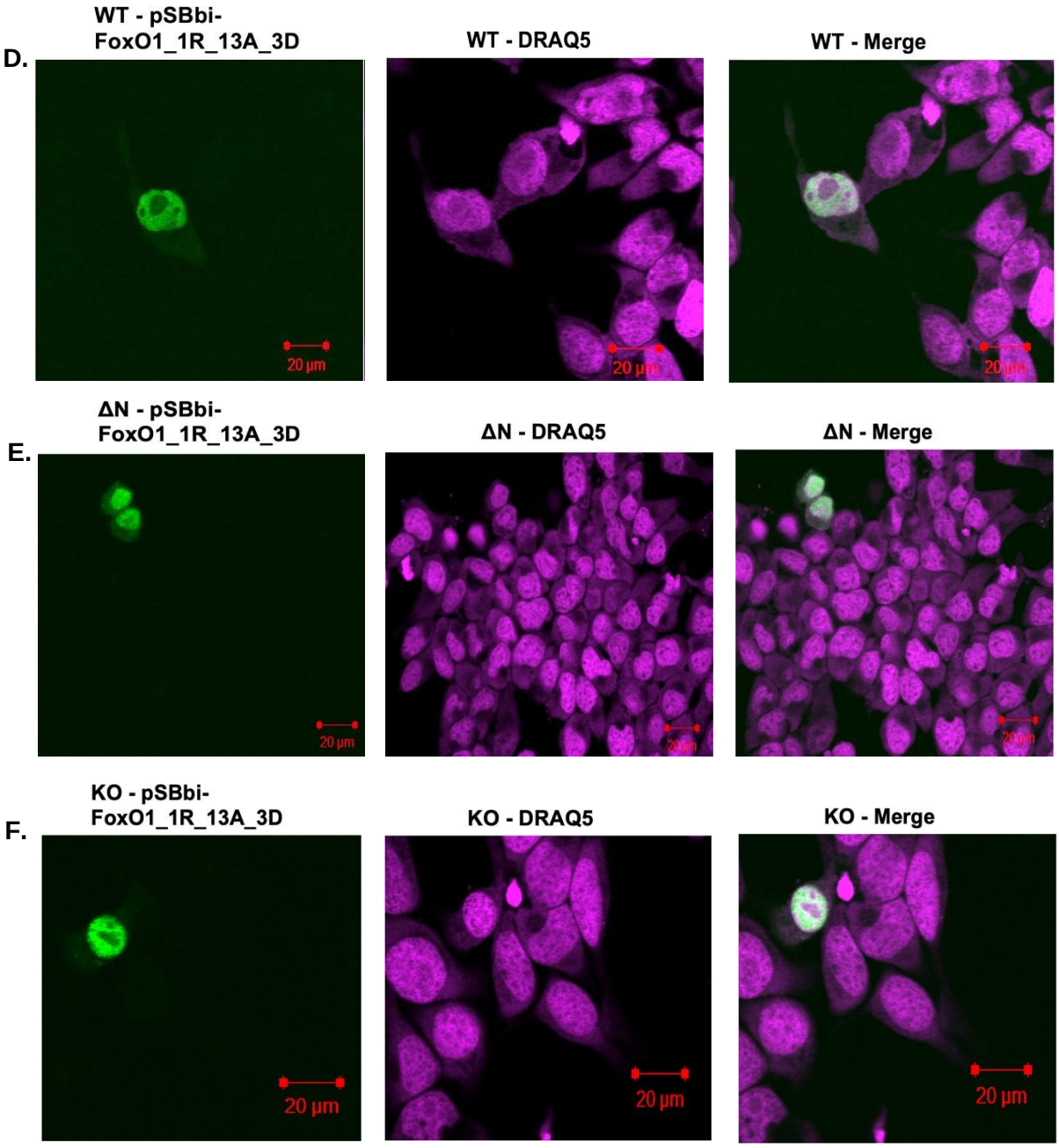

Figure 5.2. Localisation of pSBbi-FoxO1_1R_10A_3D and pSBbi-FoxO1_1R_13A_3D in WT, ΔN and KO LNCaP C4-2 cells. Cell lines were transfected with either pSBbi-FoxO1_1R_10A_3D or pSBbi-FoxO1_1R_13A_3D and grown for 48h before being prepared for confocal microscopy. **A, B, C** shows the localisation of pSBbi-FoxO1_1R_10A_3D in WT, ΔN and KO C4-2 cells respectively. **D, E, F** shows the localisation of pSBbi-FoxO1_1R_13A_3D in WT, ΔN and KO C4-2 cells respectively.

5.3. Comparing the ΔN Transcriptome to Other Models of AKT Activation

With the aberrant activation of AKT observed in ΔN C4-2 cells, DEGS from this clone were compared to other cancer cell lines also exhibiting enhanced AKT activity. This was to identify common genes whose expression may be modulated by AKT signalling, granted additional mechanisms may also contribute to these results. For these comparisons ΔN DEGs were compared to two different breast cell line datasets exhibiting enhanced AKT signalling. This was due to a lack of suitable prostate cancer cell line models available for these comparisons *(discussed further in Section 5.11).*

The first published datasets which ΔN-WT C4-2 cell DEGs were compared to was that of *Chan et al., (2021)* in which the triple negative breast cancer cell line MDA-MB-231 was transduced with myristylated AKT. The addition of Src myristylation signal sequence on AKT promotes sustained recruitment to the cell membrane, which triggers constitutive kinase activity *(Kohn, et al., 1996 ; Eyster et al., 2005).* EdgeR processing and DESeq2 analysis (using the same parameters as ΔN-WT and KO-WT DEG analysis, described in Section 2.39) was conducted on the *Chan et al., (2021)* RNA-Seq dataset. This identified 520 upregulated DEGs and 802 downregulated DEGs in MDA-MB-231 cell lines transduced with myrislated AKT relative to control MDA-MB-231 cells.

Comparing these DEGs to those of ΔN-WT C4-2 revealed 25 (1.9%) and 56 (3.6%) common upregulated and downregulated DEGS respectively *(Figures 5.3 and 5.4).* Particular genes of interest highlighted in these comparisons include serine protease inhibitor Kazal-type 1 (SPINK1) *(Figure 5.3)* which has implicated with stimulating the AKT pathway *(Tiwari etf al., 2021).* In LNCaP cells, knockdown of SPINK1 expression has been shown decrease phospho-AKT levels *(Tiwari et al., 2020).*

Another gene of interest highlighted in these comparisons was INPP4B, downregulated in both datasets *(Figure 5.4).* Loss of expression or mutations in INPP4B has been recorded in 8% and 47% primary and advanced prostate cancers respectively *(Agoulnik et al., 2011).* INPP4B dephosphorylates $PI(3,4)P_2$, $PI(4,5)P_2$ and $PI(3,4,5)P_3$, with loss of INPP4B expression enhancing AKT activity *(Hodgson et al., 2011).*

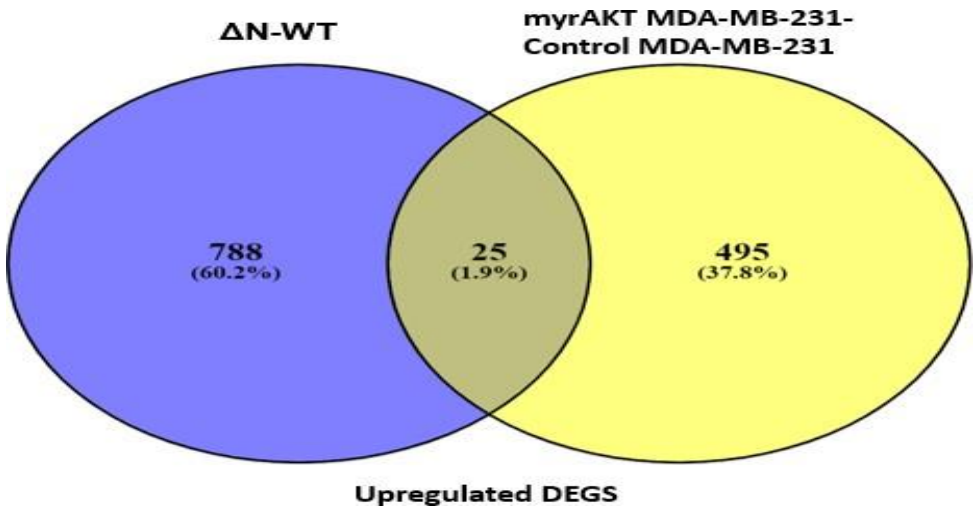

Figure 5.3. Venn Diagrams highlighting the shared upregulated DEGs between ΔN-WT and myr-MDA-MB-231 v Control MDA-MB-231 breast cancer cells. Common DEGs are as followed DPYSL3, PTGFR, PMEPA1, GNMT, ARHGEF6, RTN1, HUNK, AFF3, SLC16A2, FRMPD3, PTPRR, KCNMA1, SPINK1, STOX1, WDR72, CXXC4, OTUD7A, HCLS1, SLITRK6, FIRRE, ITPRID2-DT, LOC100129534, BCAN-AS1, CD24,LNC-NES-2 (Antisense to BCAN). MDA-MB-231 breast cancer cell data was obtained from *Chan et al., (2021)*

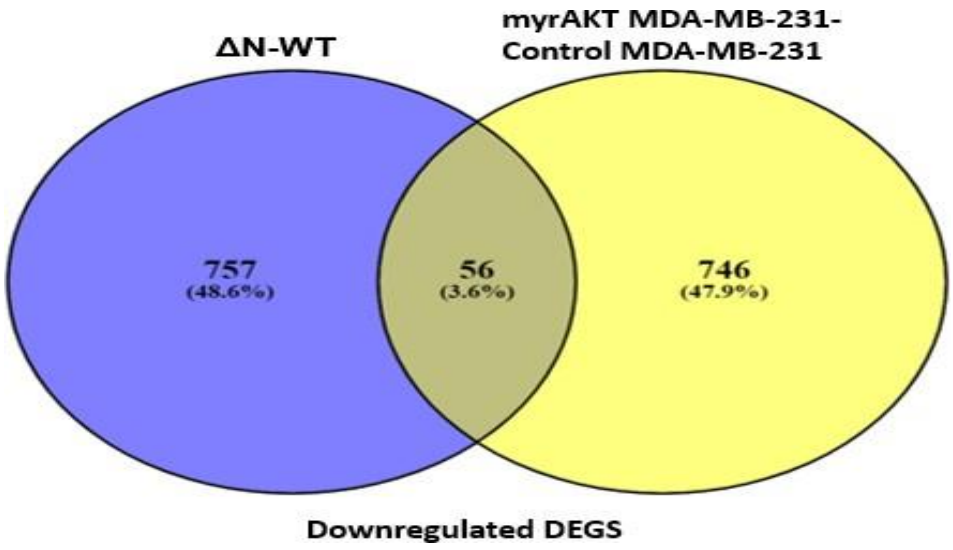

Figure 5.4. Venn Diagrams highlighting the shared downregulated DEGs between ΔN-WT and myr-MDA-MB-231 v Control MDA-MB-231 breast cancer cells. Common DEGs are as followed: NRXN3, GYG2, ARG2, OAS1, FCGRT, OLFM2, GIMAP2, INPP4B, MDK, COL12A1, GRB14, HS3ST3B1, OPRL1, MCF2L, PRKCG, CHN1, CFAP300, CYP11A1, SKAP1, GUCY1A2, BANK1, OBSCN, PIK3AP1, AUTS2,TFF2, DMKN, LRATD1,KLF15, F2RL1, SYK, ADAMTS15, CLMP, GPRC5B, RBFOX3, ZNF558, STXBP6, SYT9, HS6ST2, FRMD3, DMRT2, TP53I11, AC008969.6, FGD6, F2R, NOTUM, GREB1, CASP4, ZNF665, DPP4, DMD, MUC5AC, ZNF702P, SMIM31, Lnc-BRF2-15, ZNF253, Lnc-CXCR5-1. MDA-MB-231 breast cancer cell data was obtained from *Chan et al., (2021).*

Published data from Peter Vogt's group was next analysed, using the same parameters as previously described. In this work, rather than inducing aberrant AKT activity through myristylation, instead upstream PI3K activity was amplified. In this study, RNA-Seq was conducted (in biological triplicates) on the immortalised breast epithelial cell line MCF-10A along with the MCF-10A-H1047R cell line *(Hart et al., 2015).* The MCF-10A-H1047R line was previously developed by Ben Ho Park's group in which the H1047R hotspot mutation in PIK3CA was knocked in MCF-10A cells *(Gustin et al., 2009).* This substitution mutation is located in the kinase domain of p110α and triggers constitutive PI3K activity and enhanced downstream phosphorylation of AKT *(Gustin et al., 2009).*

MCF-10A and MCF-10A-H1047R cells were grown in serum free medium, containing 10mg/mL EGF, with cells harvested for RNA-Seq at varying time period *(Hart et al., 2015).* In this work, the RNA reads from time points 0h and 24h were pre-processed with differentially expressed genes identified by DeSeq2. At the 0h time point, 476 upregulated DEGs and 592 downregulated DEGs were identified between MCF-10A-H1047R and WT- MCF-10A. The number upregulated and downregulated DEGs that were common between ΔN-WT and 0h MCF-10A-H1047R-WT-MCF-10A cells was 29 (2.2%) and 38 (2.8%) respectively *(Figures 5.5 and 5.6).*

The number of DEGs for the 24h timepoint was greater than the 0h timepoint, with 571 and 1088 upregulated and downregulated DEGs respectively. This greater number of DEGs for 24h time point could be accounted for by MCF-10A-H1047R and WT-MCF-10A cells being exposed to EGF stimulation for a sustained period. The number of upregulated and downregulated DEGs that were common between ΔN-WT and 24h MCF-10A-H1047R–WT-MCF-10A cells is 28 (2.0%) and 56 (3.0%) respectively *(Figures 5.7 and 5.8).*

When comparing the number of common upregulated and downregulated genes for ΔN-WT and MCF-10A-H1047R – WT-MCF-10A cells at 0h and 24h time points, this revealed only a small number of common genes. The number of common upregulated and downregulated DEGs in these comparisons are 5 (9.6%) and 7 (8%) respectively *(Figures 5.9 and 5.10).* This ultimately highlights the differences in the expression of DEGs between 0h and 24h time points relative to ΔN-WT C4-2 cells.

Even though the proportion of common genes is low for these comparisons, they nevertheless may have some biological importance. For instance, the downregulation of Paternally Expressed 10 (PEG10) was observed in *Figure 5.10.* A previous report by *Yahiro et al., (2019)* found that siRNA knockdown of PEG10 in SW1353 chondrosarcoma cells induces AKT phosphorylation.

Additionally, increased FUT3 expression was observed in these comparisons *(Figure 5.9).* FUT3 is part of the fucosyltransferase (FUT) family which synthesis fucosylated oligosaccharides, of which there are 13 members *(Kim et al., 2020).* Family members have been implicated regulating AKT phosphorylation, with knockdown of either FUT4, FUT6 or FUT8 attenuating AKT phosphorylation in hepatocellular carcinoma cells *(Cheng et al., 2013).* However, the effects of FUT3 knockdown on AKT phosphorylation was not investigated by *Cheng et al., (2013).*

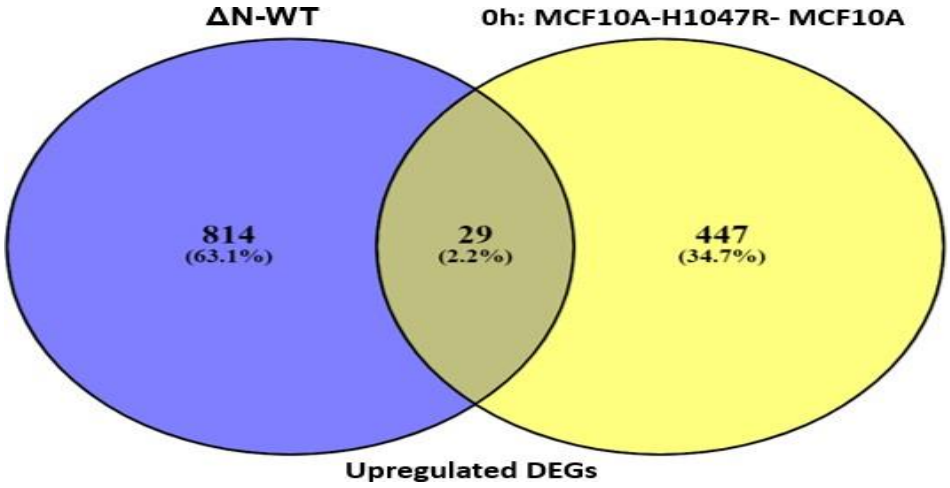

Figure 5.5. Venn diagrams highlighting the shared upregulated DEGs between ΔN-WT and MCF10A-H1047R v MCF10A cells untreated with EGF. Common DEGs are as followed: PRSS22, SAMD4A, MYO16, NAV3, SEMA3A, SULT2B1, PTK6, RGS2, KLF7, CSTA, SLPI, OASL, IL1RN, DUSP5, AOX1, PHLDA1, PHLDB2, LCN2, S100P, ELOVL7. E2F7, ENTPD3. PXDC1, TM4SF1, FUT3, HOPX, SFN, PNLIPRP3, SMIM22. MCF10A cell line data was obtained from *(Hart et al., 2015).*

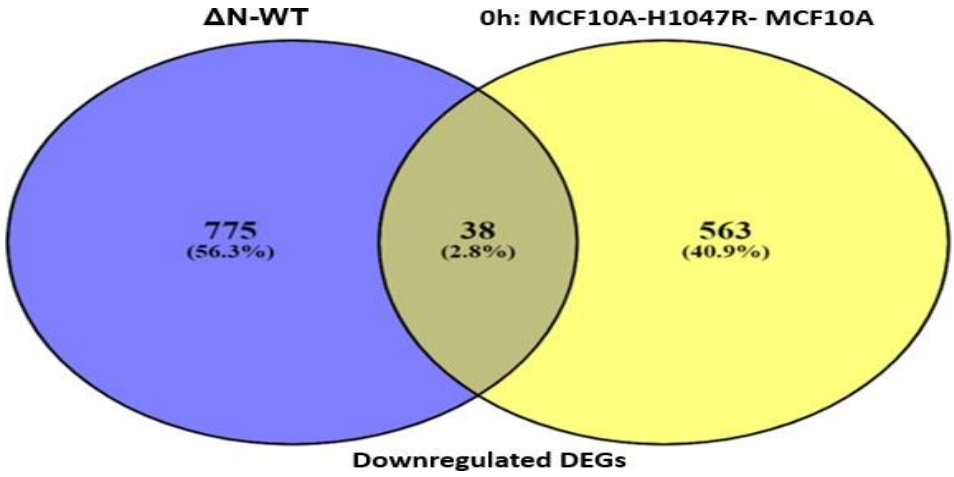

Figure 5.6. Venn diagrams highlighting the shared downregulated DEGs between ΔN-WT and MCF10A-H1047R v MCF10A cells untreated with EGF. Common DEGs are as followed: SLC7A2, EYA2, SNAP91, DOCK3, NRCAM, FN1, ONECUT2, CHN1, TMOD2, SHC2, GSTT2B, ANKRD6, SYTL2, SORD, SLC27A2, PLCL2, RAB39B, CARMIL2, GFI1, KCNK5, ZNF606, BMERB1, FRMD3 MANEAL, C5orf38, NUDT11, ZNF569, H2AC13, STMN3, ZNF433, ZNF568, SCAMP5. ARHGEF25, PEG10, ZNF253, SORD2P, H2BC7, ZNF229. MCF10A cell line data was obtained from *(Hart et al., 2015).*

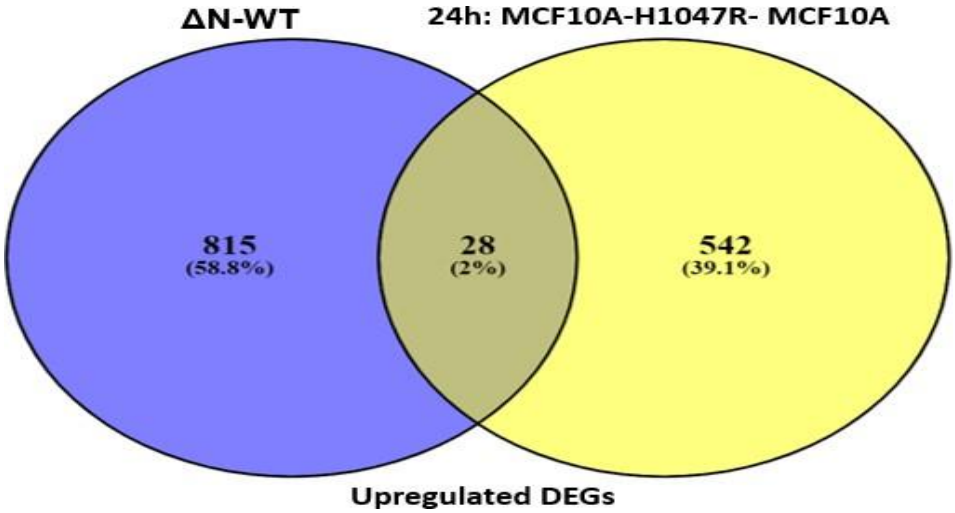

Figure 5.7. Venn diagrams highlighting the shared upregulated DEGs between ΔN-WT and MCF10A-H1047R v MCF10A cells after 24h treatment with 10mg/mL EGF. Common DEGs are as followed: FAS, CAMK2B, MOCOS, TGM1, PTGS1, PCK2, TRIB3, KIF21B, CSTA, CHAC1, IL1RN, TRIM29, RGS3, NUF2, TTC39B, CCNB2, SGO2, HMGB2, GASK1B, ENTPD3, DDIT4, TMEM154, FUT3, IL20RB, PTP4A3, PNLIPRP3, IKBKE, RAB7B. MCF10A cell line data was obtained from *(Hart et al., 2015).*

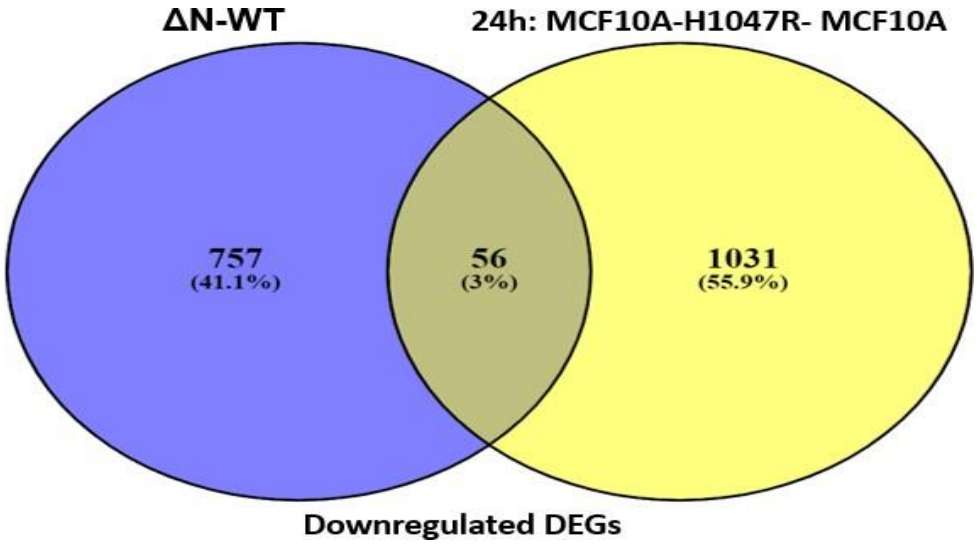

Figure 5.8. Venn diagrams highlighting the shared downregulated DEGs between ΔN-WT and MCF10A-H1047R v MCF10A cells after 24h treatment with 10mg/mL EGF. Common DEGs are as followed: AGPAT4, FAM214A, RORA, ZNF532, GPR137B, NAALAD2, DOCK3, HCN2 ,LIPG, PCSK1N, NFAT5, AP3B2, FN1, ONECUT2, CLU, ARHGAP9, PMEPA1, SHC2, ETS1, SERPINE2, TUBB2A, DISP2, DUSP10, DEGS1, GULP1, PLK2, SLC16A2, FARP1, nLRRK1, KLF15, CITED2, CREBRF, PCDH19. TCP11L2, ADAMTS15, NKX3-1, FAM110B, DSEL, FRMD3, VEGFB, TNFRSF10D, MSRB3, JUN, MAF, GGN, DNHD1, TCEAL9, IRS2, SPRED3, NUDT11, ZNF442, ZBTB10, S1PR3, PEG10, TMEM158, CD24. MCF10A cell line data was obtained from *(Hart et al., 2015)*

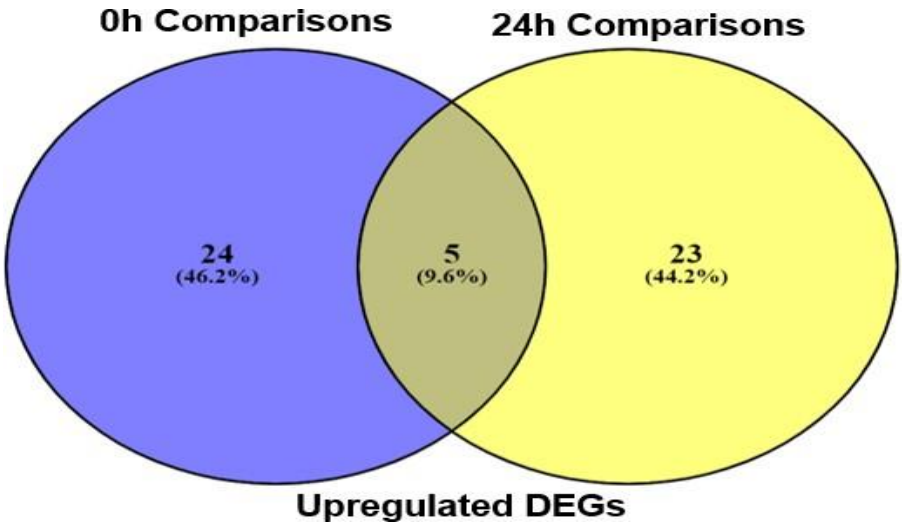

Figure 5.9. Venn diagrams highlighting the shared upregulated DEGs after ΔN-WT were compared to untreated MCF10A-H1047R v MCF10A cells and MCF10A-H1047R v MCF10A cells treated with 10mg/mL EGF for 24h. Common DEGs are as followed: CSTA, IL1RN, ENTPD3, FUT3, PNLIPRP3. MCF10A cell line data was obtained from *(Hart et al., 2015).*

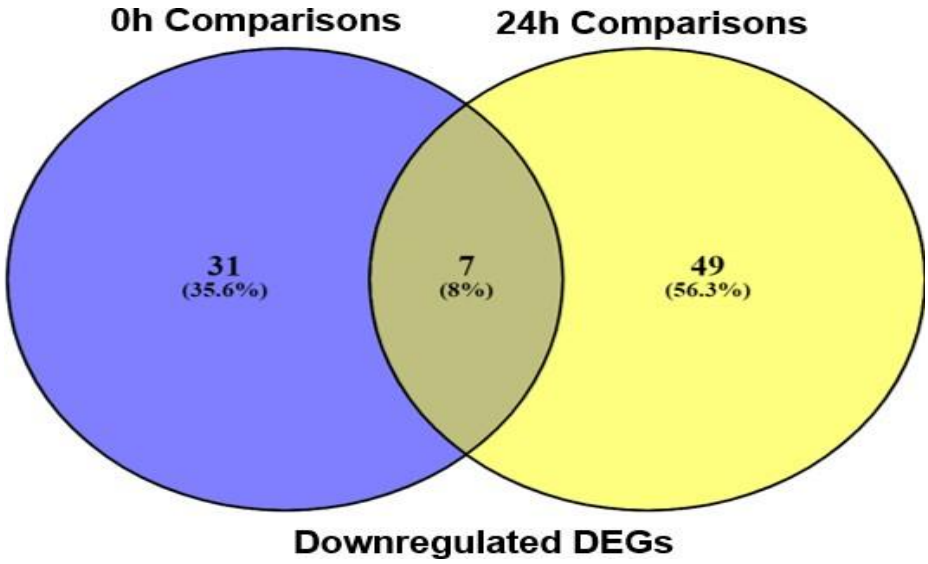

Figure 5.10. Venn Diagrams highlighting the shared upregulated DEGs after ΔN-WT were compared to untreated MCF10A-H1047R v MCF10A cells and MCF10A-H1047R v MCF10A cells treated with 10mg/mL EGF for 24h. Common DEGs are as followed: DOCK3, FN1, ONECUT2, SHC2, FRMD3, NUDT11, PEG10. MCF10A cell line data was obtained from *(Hart et al., 2015).*

5.4. Loss of PIK3R1 Expression in ΔN C4-2 Cells

Through scrutinising ΔN-WT DEGs, this revealed that the expression of PIK3R1 was downregulated in ΔN *(Table 5.1).* With the implications the loss of PIK3R1 has upon AKT activation this was investigated further. *In silico* quantification using Kallisto assessed the abundances four protein encoding PIK3R1 transcripts in WT, ΔN and KO. These transcripts are summarized in *Table 5.2*. For subsequent Kallisto analysis, the Ensembl ID for each PIK3R1 transcript has been used. Kallisto analysis has also extended to quantifying the RNA expression *(in silico)* of PIK3R2 and PIK3R3 transcripts (*Table 5.1, 5.2).* Whilst the PIK3R2 and PIK3R3 genes were not differently expressed in ΔN and KO, both genes encode regulatory subunits (p85β and p55γ) that couple to catalytic subunits of Class IA PI3Ks *(Fox, Mott and Owen, 2020).* Additionally, loss of PIK3R2 expression has been attributed to mediating resistance to p110β inhibitors through AKT activity *(Dunn et al., 2022).*

Table 5.1. PIK3R1/2/3 RNA expression. Reported is the Log2FC, FDR andthe average number (n=3) RNA reads for PIK3R1/2/3 in WT, ΔN and KO LNCaP C4-2 cells. DeSeq2 was conducted to generate Log2FC and FDR values, whilst RNA Read counts were generated by FeatureCounts.

Gene Name	Protein Name	Log2FC ΔN– WT	FDR ΔN– WT	Log2FC KO– WT	FDR KO – WT	Average WT RNA Reads	Average ΔN RNA Reads	Average KO RNA Reads
PIK3R1	P85α p55α p50α	-2.21	2.97E-59	N/A	N/A	1429	299	1393
PIK3R2	p85β	-0.35	0.81	0.61	0.73	6	5	4
PIK3R3	p55γ	-0.57	6.0E-4	0.46	0.011	845	553	1108

Table 5.2. Details of the PIK3R1/2/3 transcripts that have undergone Kallisto quantification in WT ΔN and KO C4-2 cells.

Transcript Variant	Ensembl ID	Number of Exons	Amino Acids	Additional Information
p85α	PIK3R1-211	16	724	Full length isoform with an extensive untranslated region
p85α	PIK3R1-213	16	724	Same number of amino acids as PIK3R1-211. Splice variant PIK3R1-213 has a much shorter untranslated region (lacking ~3000bp)
p55α	PIK3R1-202	10	454	Different N terminus to that of p85α transcripts. Lacks the 6 exons which encode SH3 and BH/RhoGAP domains
p50α	PIK3R1-201	10	424	Different N terminus to that of p85α and p55α transcripts. Also lacks the 6 exons which encode SH3 and BH/RhoGAP domains
p85β	PIK3R2-201	16	728	Encodes for full length p85β
p55γ	PIK3R3-201	10	461	Encodes for full length p55γ

Kallisto quantification revealed that PIK3R1-211 transcripts are the most abundant in LNCaP C4-2 cell lines, followed by PIK3R1-201 transcripts *(Figure 5.11).* Both these transcripts showed significantly reduced expression in ΔN C4-2 cells *(Figure 5.11).* PIK3R1-213 and PIK3R1-202 transcripts are barely expressed in all three cell lines, no significant alterations in their expression were observed between WT and CRISPR edited cell lines *(Figure 5.11).* Likewise PIK3R2-201 was minimally expressed across WT, ΔN and KO LNCaP C4-2 cells *(Figure 5.12).* On the other hand the expression of PIK3R3-201 was recorded at far more abundance across WT, ΔN and KO LNCaP C4-2 cells *(Figure 5.12).*

With the results from Kallisto analysis highlighting that PIK3R-211 (encoding p85α) is the most abundant transcript in C4-2 cells, and that this is significantly downregulated in ΔN C4-2 cells, validation at the protein level was conducted. An antibody which recognises N terminal residues of p85α was used in western blotting with this highlighting a loss of p85α expression at the protein level *(Figure 5.13).* Motivated by this, ΔN C4-2 cells were then transfected with PIP5K1α-mVenus-N1 to see whether the expression of PIK3R1-211 could be rescued. Using isoform specific primers *(Table 2.10)* the overall expression of PIK3R1-211 after transfection with PIP5K1α-mVenus-N1 was increased, albeit not statistically significant *(Figure 5.14).*

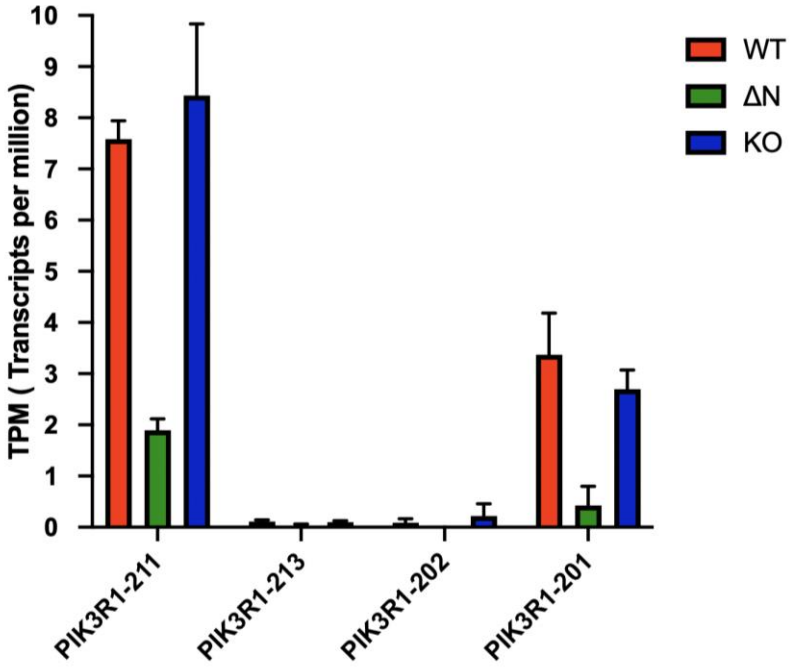

Figure 5.11. Kallisto quantification of expression of PIK3R1 transcripts in WT, ΔN and KO C4-2 cells. TPM scores are calculated from biological triplicate (n=3) Fastq files. The reference transcriptome used in the quantification ofthese transcripts was the hg38.83 cDNA transcriptome (Ensembl).

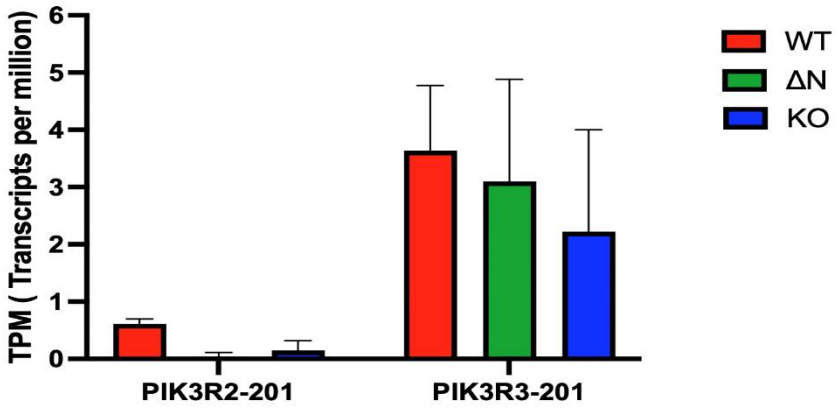

Figure 5.12. Kallisto quantification of expression of PIK3R2-201 and PIK3R3-203 in WT, ΔN and KO C4-2 cells. TPM scores are calculated from biological triplicate (n=3) Fastq files. The reference transcriptome used in the quantification ofthese transcripts was the hg38.83 cDNA transcriptome (Ensembl).

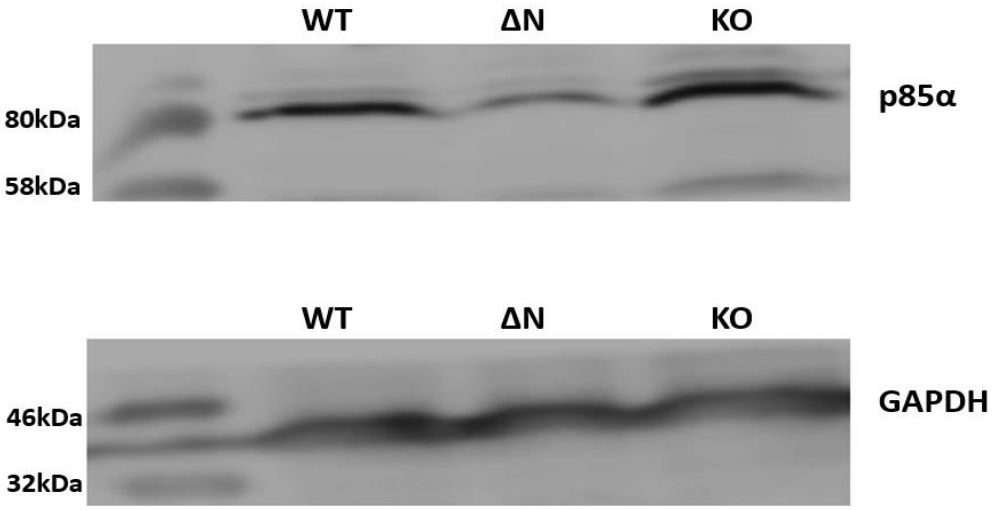

Figure 5.13. Western blot of p85α protein expression in WT , ΔN and KO C4-2 cells. Proteins were extracted using RIPA buffer and resolved on 10% SDS page gels before blotting for p85α or GAPDH (loading control)

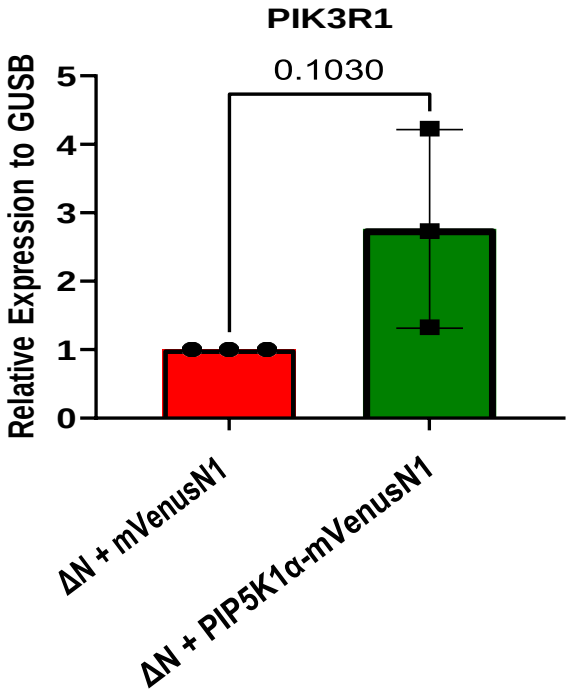

Figure 5.14. Relative RNA expression of PIK3R1 in ΔNC4-2 cells after rescue with PIP5K1α-mVenus-N1. Data is of biological triplicates (n=3) with technical duplicates. Relative expression was calculated using the $2^{-\Delta\Delta Ct}$ method. Data was normalised to the expression of GUSB housekeeping gene per cell line. A two sided t-test was calculated between ΔN cells transfected with mVenus-N1 and PIP5K1α-mVenus-N1, with the p-value shown.

5.5. PIK3R1/PIK3R2/PIK3R3 Expression in Different Prostate Cancer Cells Lines

Further Kallisto analysis was conducted to assess expression of PIK3R1, PIK3R2 and PIK3R3 transcripts in different prostate cancer cell lines *(Table 5.3).* The expression of PIK3R1 transcripts in different prostate cancer cell lines was also compared to that of RWPE-1, an immortalized, non- tumorigenic prostate epithelia cell line *(Merrick et al., 2019).* The expression of PIK3R1 transcripts in different prostate cancer cell lines were also compared to the WT LNCaP C4-2 dataset documented in this work. *Figure 5.15* indicates in both non-tumorigenic and tumorigenic prostate cell lines that the expression of PIK3R1-211 is the most predominant PIK3R1 transcript. The expression of PIK3R1-213 was found to be highest in non-tumorigenic RWPE-1 cells, whereas the abundance of this transcript is very low in the prostate cancer cell lines. A stark loss of PIK3R1-202 expression was observed between LNCaP C4-2 cells and the parental LNCaP line.

Table 5.3. Studies used for Kallisto analysis of PIK3R1 transcripts from different prostate cancer cell lines, and an immortalised prostate epithelial cell line (RWPE-1). For when data was obtained from SRA, respective project code are documented.

Authors	RNA-Sequencing Data	SRA Project Code
Koirala et al., (2020)	Wildtype RWPE-1 cells	SRP234462
Niermira et al., (2020)	Wildtype LNCaP cells	SRP263179
Fernandes et al., (2021)	Wildtype 22RV1cells	SRP221000
Huang et al., (2020)	Wildtype PC-3 cells	SRP221256
Niermira et al., (2020)	Wildtype DU145 cells	SRP263179
This work	Wildtype LNCaP C4-2 cells	N/A

A.

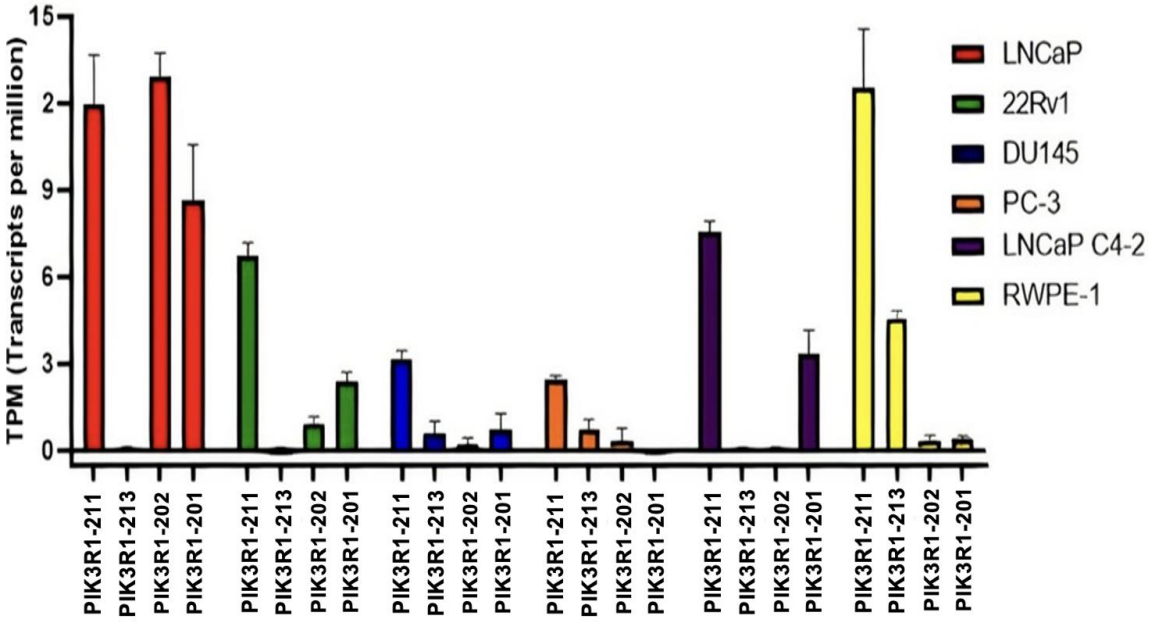

B.

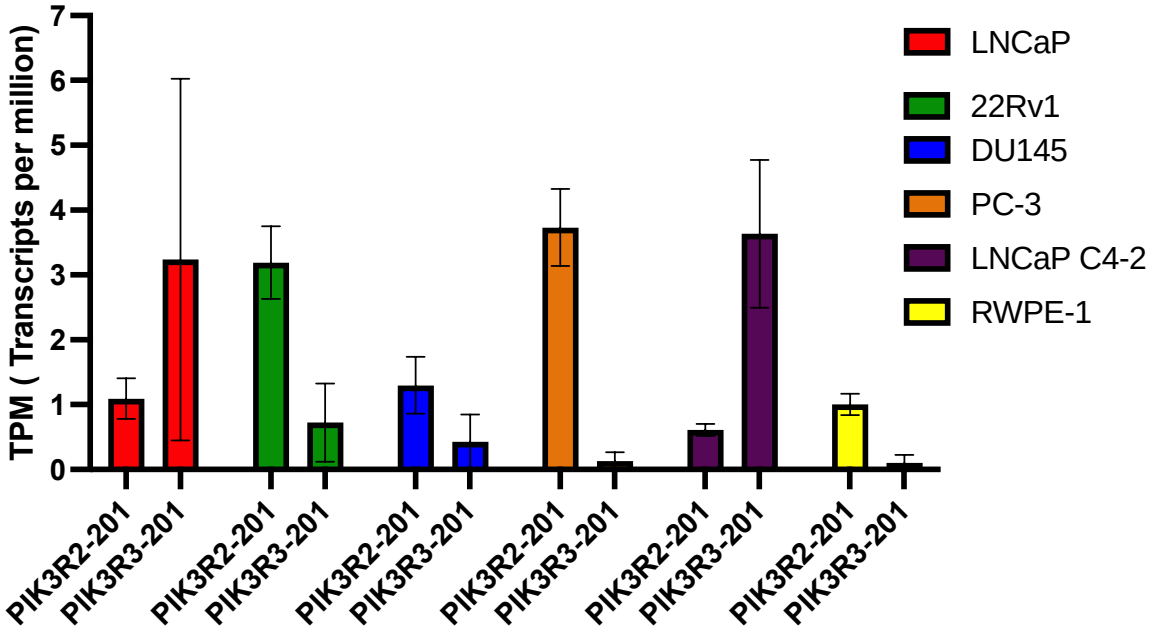

Figure 5.15. Kallisto quantification of the expression of PIK3R1, PIK3R2, PIK3R3 transcripts in different prostate cancer cell lines, and an immortalised prostate epithelial cell line (RWPE-1). TPM scores are calculated from biological triplicate (n=3) Fastq files. The reference transcriptome used in the quantification of these transcripts was the hg38.83 cDNA transcriptome (Ensembl). **A.** The expression of PIK3R1-211, PIK3R1-213, PIK3R1-202 and PIK3R1-201 transcripts. **B.** The expression of PIK3R2-201 and PIK3R3-201 transcripts.

5.6. The Regulation of PIK3R1/2/3 Expression by Androgens

Previously *Munkley et al., (2015)* revealed that treatment of LNCaP cells with the synthetic androgen R1881 decreases the mRNA and protein expression of PIK3R1/p85α and PIK3R3/p55γ. This was one of the first reports that androgen signalling could regulate the expression of the regulatory subunits of PI3Ks. Subsequently, *in silico* work was conducted to analyse whether the expression of PIK3R1/2/3 transcripts is modulated by androgen signalling.

Firstly, Kallisto analysis was conducted on RNA-Seq data generated by *Metzger et al., (2016)* (SRA project code SRP051583) in which triplicate RNA samples was extracted from cells either untreated or treated with 10^{-7}M DHT for 6 hours. Statistically significant decreases in the expression of all PIK3R1 transcripts, expect PIK3R1-213 and PIK3R2-201 was observed in DHT treated LNCaP cells relative to untreated controls *(Figure 5.16).*

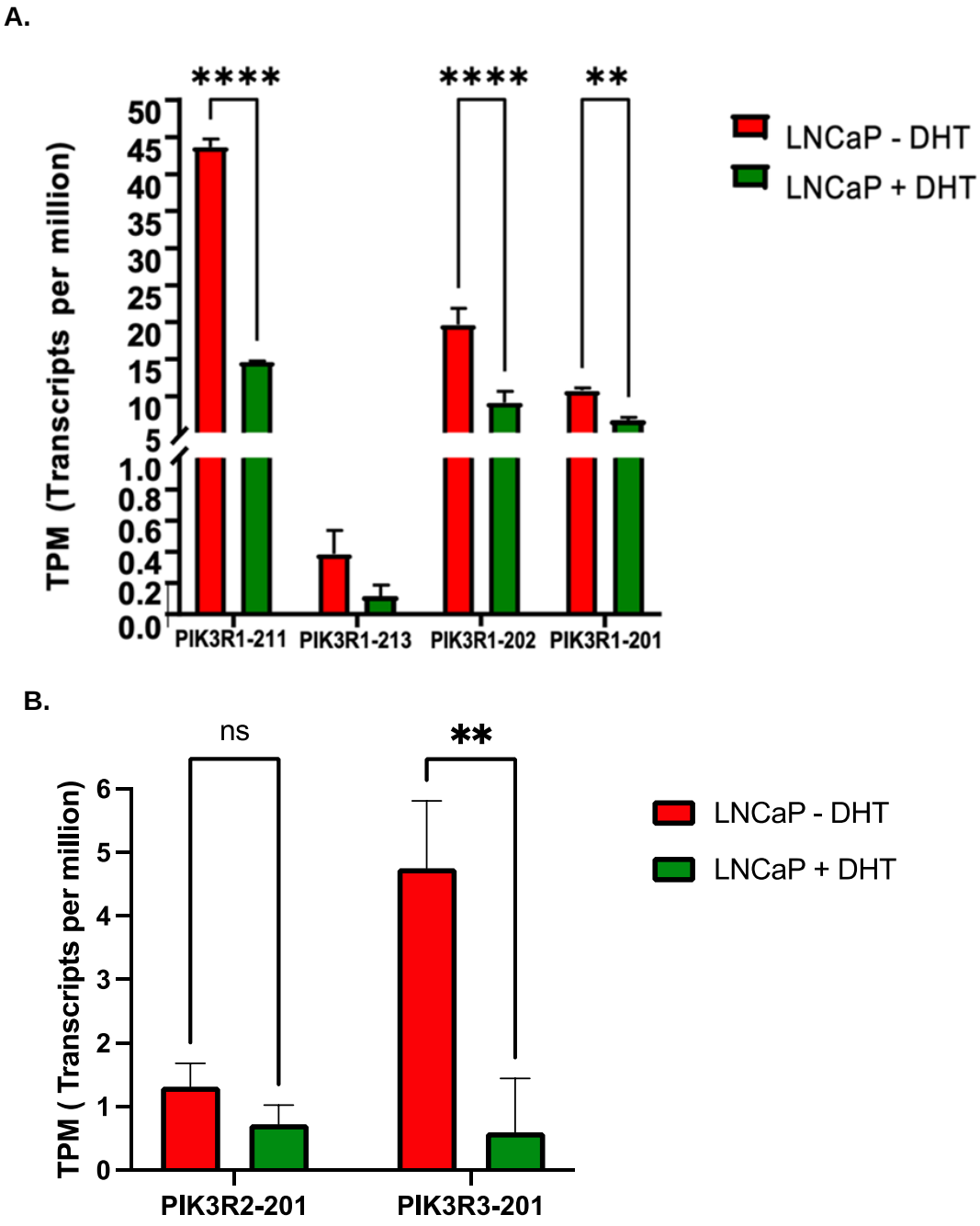

Figure 5.16. Kallisto quantification of expression of PIK3R1, PIK3R2 and PIK3R3 transcripts in DHT treated LNCaP cells. TPM scores are calculated from biological triplicate (n=3) Fastq files from *Metzger et al., (2016).* The reference transcriptome used in the quantification of these transcripts was the hg38.83 cDNA transcriptome (Ensembl). A 2way ANOVA with a Šídák's multiple comparisons test was used to highlight significant differences in expression between untreated and DHT treated LNCaP cells. ** $P \leq 0.01$. **** $P \leq 0.0001$. **A.** The expression of PIK3R1-211, PIK3R1-213 , PIK3R1-202 and PIK3R1-201 transcripts. **B.** The expression of PIK3R2-201 and PIK3R3-201 transcripts.

Analysed next was whether the negative inhibition AR signalling exerts upon PIK3R1 expression can be repressed through chemical inhibition. For this, data published by *Baumgart et al., (2020)* (SRA project code SRP255892) was analysed which conducted RNA-Seq on VCaP cells treated either a DMSO control, 1nM R1881, 1nM R1881 + 0.5μM Darolutamide or 1nM R1881 + 2μM Darolutamide. The VCaP prostate cancer cell line is androgen responsive and was previously derived from a patient harbouring a vertebral metastatic lesion *(Korenchuk et al., 2001).* Darolutamide is an AR antagonist which binds to the ligand binding domain of AR *(Baumgart et al., 2020).*

Darolutamide blocks receptor dimerization which impairs nuclear translocation and attenuates the expression of AR target genes *(Baumgart et al., 2020).* When VCaP cells are exposed to R1881 for 8 hours, this significantly reduces the expression of PIK3R1-211 and PIK3R1-202 transcripts *(Figure 5.17).* Treatment with either 0.5μM or 2μM Darolutamide (for 8 hours) was able to significantly rescue the expression of PIK3R1-211 transcripts *(Figure 5.17).*

However, Darolutamide treatment did not significantly increase PIK3R1-211 transcript expression further than the DMSO control *(Figure 5.17).* Whilst statistically significant reductions in p55α expression was observed after R1881 treatment, the expression of these transcripts was not rescued by Darolutamide treatment *(Figure 5.17).* Minimal expression of p50α transcripts was detected in VCaP cells, with the expression of these transcripts not influenced by AR agonist or antagonist treatment *(Figure 5.17).* The expression of PIK3R-213 transcripts was not observed in VCaP cells and is not documented in this analysis. Minimal expression of PIK3R2-201 was recorded in VCaP cells , whereas PIK3R3-201 was expressed more abundantly in VCaP cells *(Figure 5.17). Figure 5.16* indicated that in LNCaP C4-2 cells treated with DHT there was a statistically significant reduction in PIK3R3-201 expression. In *Figure 5.17* VCaP cells exhibit an overall reduction of PIK3R3-201 expression after R1881 treatment , but this reduction was not statistically significant.

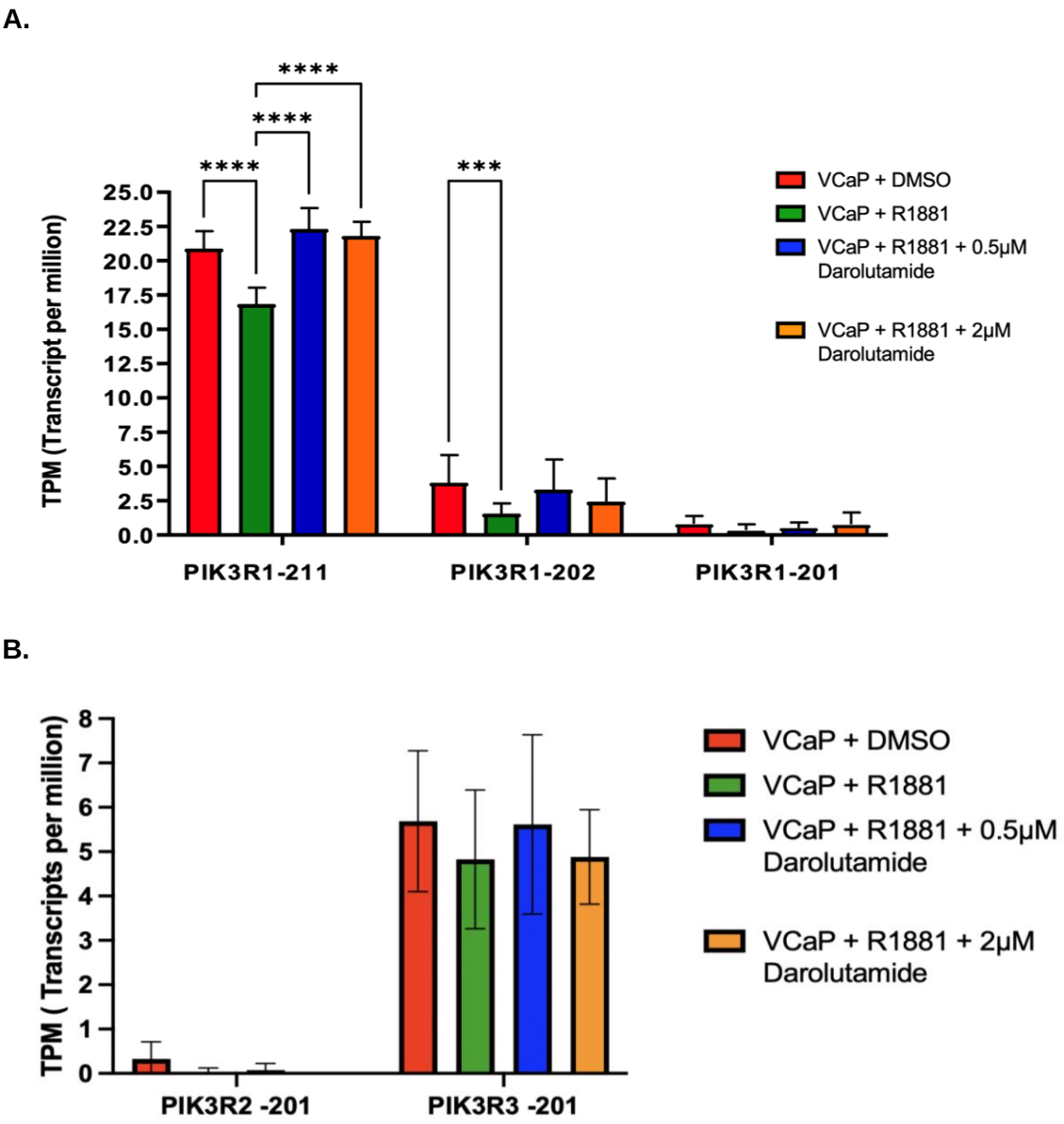

Figure 5.17. Kallisto quantification of expression of PIK3R1, PIK3R2 and PIK3R3 transcripts in VCaP cells treated with R1881 and Darolutamide. TPM scores were calculated from Fastq files of 10 biological replicates (n=10) for VCaP cells treated with either DMSO or R1881, 4 biological replicates (n=4) for VCaP cells treated with R1881 and 0.5 μM Darolutamide and 5 biological replicates (n=5) for VCaP cells treated with R1881 and 2μM Darolutamide. R1881 and Darolutamide treatment proceeded for 8 hours. Fastq files were taken from *Baumgart et al., 2020.* The reference transcriptome used in the quantification of these transcripts was the hg38.83 cDNA transcriptome (Ensembl). Statistical significance was determined by a one-way ANOVA with a Tukey's multiple comparisons test. *** $P \leq 0.005$, **** $P \leq 0.0001$.

5.7. Loss of PIK3R1 Expression in a Patient Cohort

With aberrant androgen signalling a driving factor in prostate tumorigenesis *(Zhou et al., 2014 ; Feng and He, 2019),* and with PIK3R1 expression influenced by androgens (*Munkley et al., 2015) ;* Kallisto analysis was conducted to assess whether the expression of PIK3R1 transcripts was reduced in a patient cohort. This cohort (SRA project code SRP212704) consisted of 15 prostate cancer patients with RNA-Seq conducted on disease free and tumour biopsies *(Kumar et al., 2021).* In the tumour samples relative to disease free controls statistically significant reductions in PIK3R1 expression were observed in all transcripts except PIK3R1-201 *(Figure 5.18).* This data is in agreement with the fact that PIK3R1 exerts tumour suppressive properties, and reduced expression of this gene can drive oncogenesis *(Dirican and Akkiprik, 2017).* No significant changes in expression was observed for PIK3R2-201 and PIK3R3-201 transcripts between healthy and malignant samples; both these transcripts were expressed in low abundance *(Figure 5.18)*

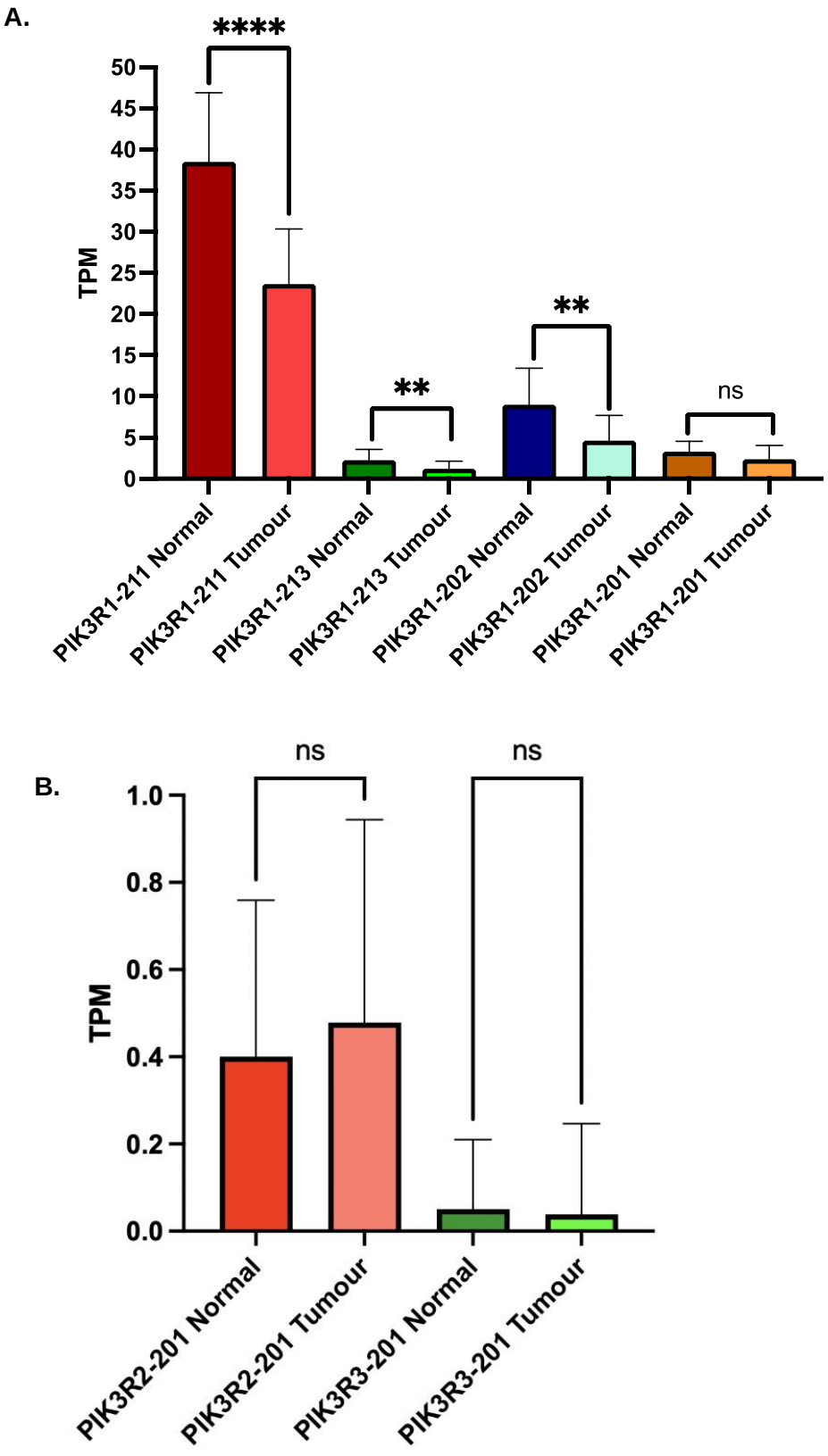

Figure 5.18. Kallisto quantification of PIK3R1, PIK3R2 and PIK3R3 transcript expression in a prostate cancer patient cohort. TPM scores were calculated from Fastq files of prostate cancer samples (n=15) with RNA-Seq conducted in technical duplicates (Kumar et al., 2021). The reference transcriptome used in the quantification of these transcripts was the hg38.83 (Ensembl) cDNA transcriptome. Statistical significance was determined by a one-way ANOVA with a Tukey's multiple comparisons test. ** P ≤ 0.01 , **** P ≤ 0.0001. **A**. Quantification of PIK3R1-211, PIK3R1-213, PIK3R1-202 and PIK3R1-201 transcript expression. **B.** Quantification of PIK3R2-201 and PIK3R3-201 transcript expression.

5.8. The Generation of Fluorescent PIK3R1 Constructs

After identifying the downregulation of PIK3R1 expression, next it was necessary to explore whether this gene regulate AKT signalling in ΔN LNCaP C4-2 cells. For this, fluorescent PIK3R1 constructs were generated and subsequently used in rescue experiments (detailed in *Section 5.10*). Prior making these constructs, the mVenus-N1 vector was adapted to generate a red fluorescent vector, mCherry-N1. This approach was designed and outlined by *Roberts, (2022)* with subsequent details also provided in this work.

Dr Chris Roberts identified restriction sites which could be used to remove the mVenus tag from mVenus-N1. These sites were a BamHI site, located at towards the end of the multiple cloning site (MCS) and a NotI site located immediately after the mVenus stop codon *(Figure 5.19).* Through digestion with BamHI and NotI, this released the mVenus tag from mVenus-N1 *(Figure 5.20),* with the resulting digested vector backbone gel extracted and purified. A mCherry insert was generated through using the previously detailed PI(3,4,5)P_3 probe, pcDNA3.1_AktPH-mCherry *(Table 2.2)* as input in PCR reactions. Primers designed to amplify the mCherry tag from pcDNA3.1_AktPH-mCherry *(Table 5.4)* worked successfully in PCR reactions, generating a single product of ~700bp *(Figure 5.21)* containing BamHI and NotI adaptors which were digested by complementary restriction enzymes.

Table 5.4. Primers used for amplifying mCherry fluorescent tag with BamHI, MluI and NotI restriction sites. pcDNA3.1_AktPH-mCherry was used as template in PCR reactions using these primers.

Name	Sequence	Additional Information
mCherry Forward	AAAAGGATCC**ACGCGT**CG CCACCATGGTGAGCAAGG GCGAG	BamHI restriction site- GGATCC MluI restriction site- **ACGCGT**
mCherry Reverse	AAAAGCGGCCGCTTACTT GTACAGCTCGTCCATGC	NotI restriction site- GCGGCCGC

After ligation reactions and subsequent transformations in DH5α competent cells, colony PCR was conducted on a selection of positive colonies *(Figure 5.22).* A band at the desired size (~700bp) was observed for colony 1 *(Figure 5.22)* with this colony subsequently miniprepped and plasmid DNA sent for sanger sequencing. By using a forward primer (CAACGGGACTTTCCAAAATG) which binds to cytomegalovirus (CMV) promoter region, it was possible to sequence past the multiple cloning site of mVenus-N1 and observe whether the mVenus tag had been substitute for mCherry. The sequencing results from colony 1 revealed successful substitution of the mCherry tag to mVenus-N1 *(Figure 5.23).* The new construct (mCherry-N1) possesses an almost identical MCS to that mVenus-N1. This cloning strategy substituted the last restriction site in the MCS of mVenus-N1 (an AgeI site) for a MluI site *(Figure 5.23).*

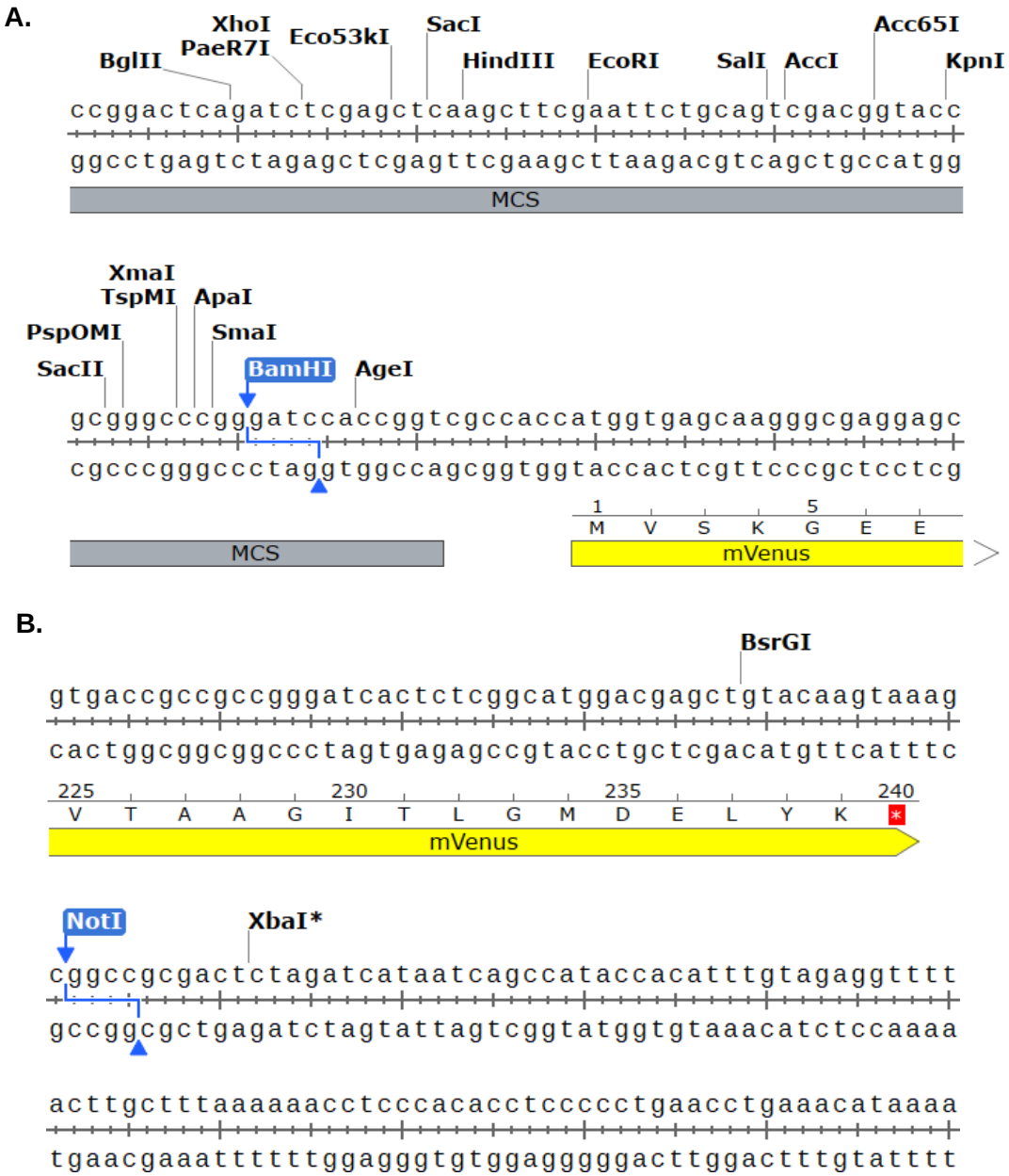

Figure 5.19. Restriction enzyme sites in mVenus-N1 used for removing the mVenus tag. A. Partial sequence of the MCS of mVenus-N1. The BamHI site located in the MCS underwent restriction digest *(as shown in Figure 5.20).* **B.** Partial sequence of the mVenus tag. The NotI site is located immediately after the mVenus stop codon (indicated by a white asterisk in a red box). The NotI site underwent restriction digest *(as shown in Figure 5.20).* Images are from Snapgene Viewer software.

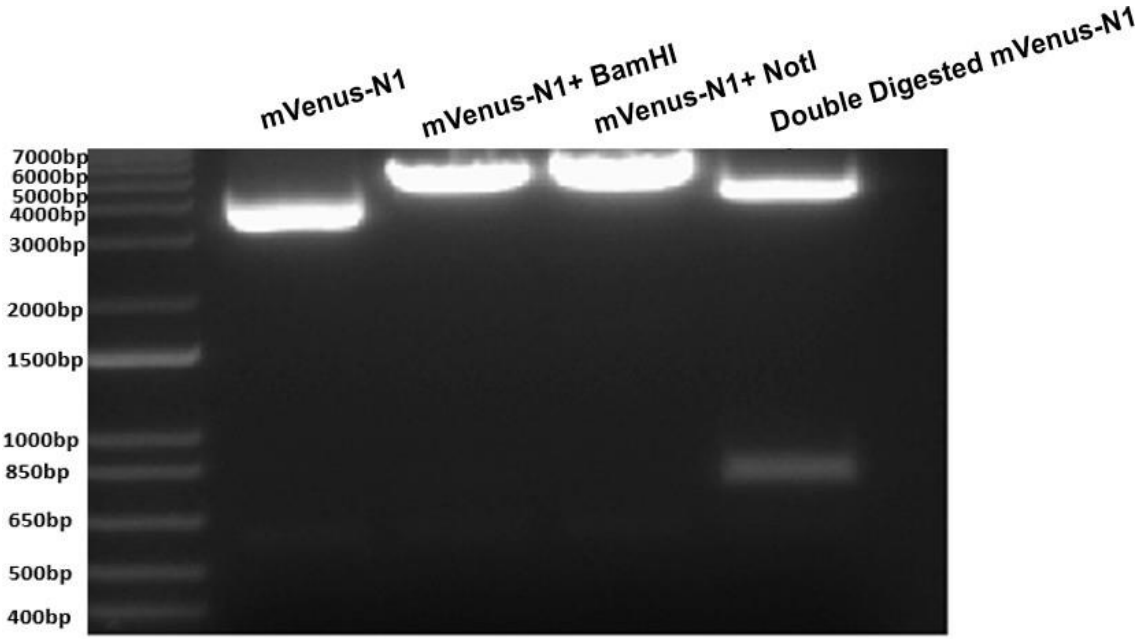

Figure 5.20. Restriction digest of mVenus-N1 with BamHI and NotI restriction enzymes. Double digests with BamHI and NotI restriction enzymes liberated a band at the mass, of ~700bp. The restriction digests of mVenus-N1 and electrophoresis gel image were kindly provided by Dr Chris Roberts.

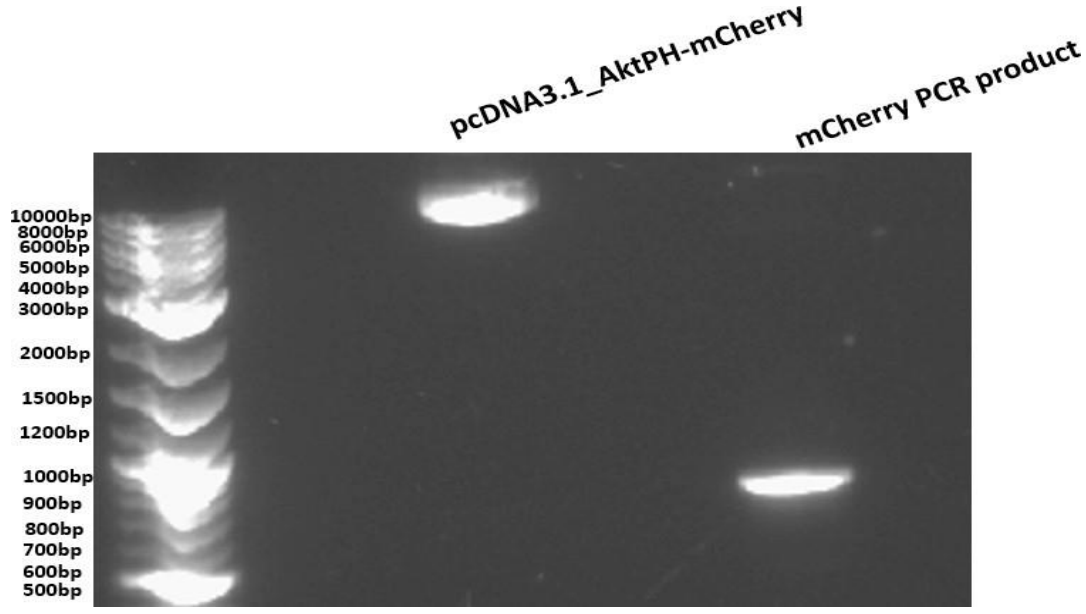

Figure 5.21. PCR amplification of mCherry tag from pCDNA 3.1_AktPH-mCherry. PCR amplification of mCherry was carried out using NEBs Phusion® High Fidelity DNA polymerase with primers *(detailed in Table 5.4).* Gel electrophoresis was used to check whether the mCherry tag could be successfully amplified from pCDNA 3.1_AktPH-mCherry. Products were run on a 0.8% agarose gel.

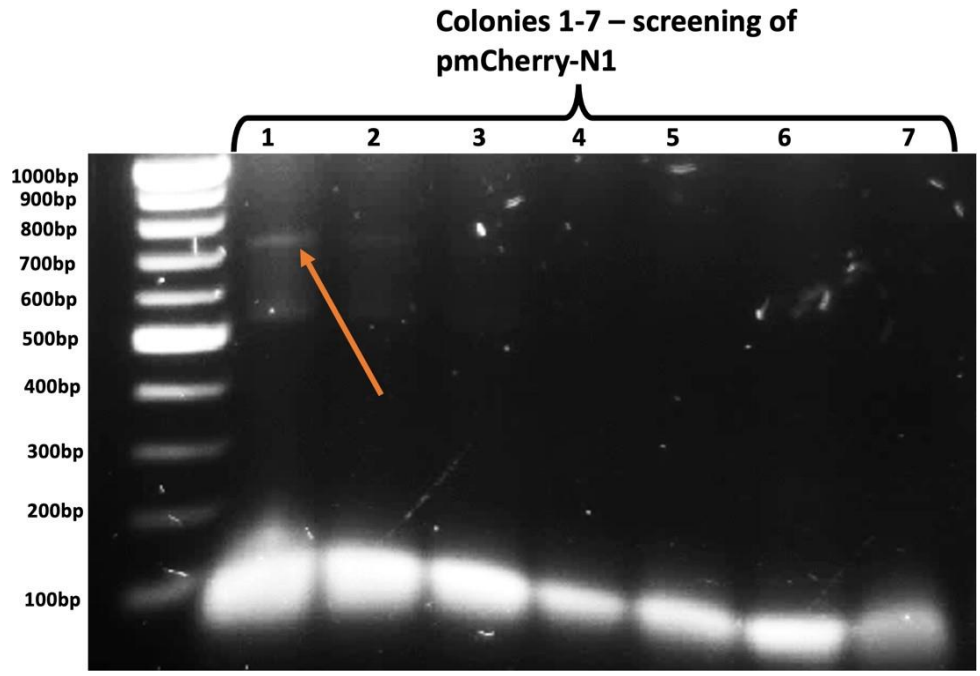

Figure 5.22. Colony PCR screening of mCherry-N1. Screening of positive colonies was carried out using NEBs Taq DNA polymerase, with primers detailed in *Table 5.4.* Gel electrophoresis was used to check whether the mCherry tag could be amplified from positive transformants. Products were run on a 0.8% agarose gel. The mCherry tag (~700bp) could be successfully amplified from colony one (denoted by an orange arrow).

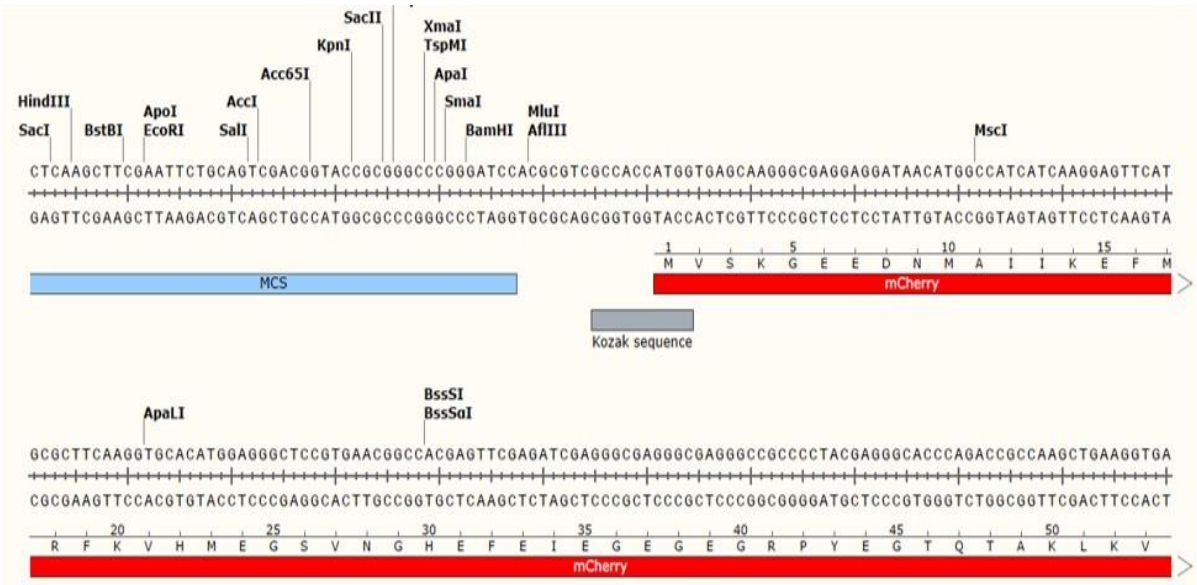

Figure 5.23. Schematic of mCherry-N1. Shown in this schematic is a reconstituted BamHI restriction site, the successful substitution of a MluI site (replacing an AgeI site found in mVenus-N1) and the mCherry tag. Image is from Snapgene Viewer software.

Next molecular cloning was used to generate p85α fluorescent constructs. With both mVenus-N1 and mCherry-N1 containing a nearly identical MCS, inserts generated by PCR could be used in ligation reactions for both vectors. A subcloning strategy was devised for generating fluorescent p85α constructs. In this, PCR primers with EcoRI and BamHI sites *(Table 5.5)* were used to amplify p85α from the PSG5-HA-p85α construct *(Table 2.2).* This construct contains the sequence encoding P85α, fused to a 5' hemagglutinin (HA) tag. P85α could be successfully amplified from PSG5-HA-p85α *(Figure 5.24),* with PCR products (~2200bp in size) then pooled and ethanol precipitated before restriction digests.

Table 5.5. Primers used for amplifying PIK3R1/p85α insert with EcoRI and BamHI restriction sites. PSG5-HA-p85α was used as template in PCR reactions using these primers.

Name	Sequence	Additional Information
P85α Forward	AAAAAGAATTCCACCATGAGTGCTGA GGGGTACCC	EcoRI Restriction Site - GAATTC
P85α Reverse	AAAAGGATCCAATCGCCTCTGCTGTG CATATAC	BamHI Restriction Site – GGATCC

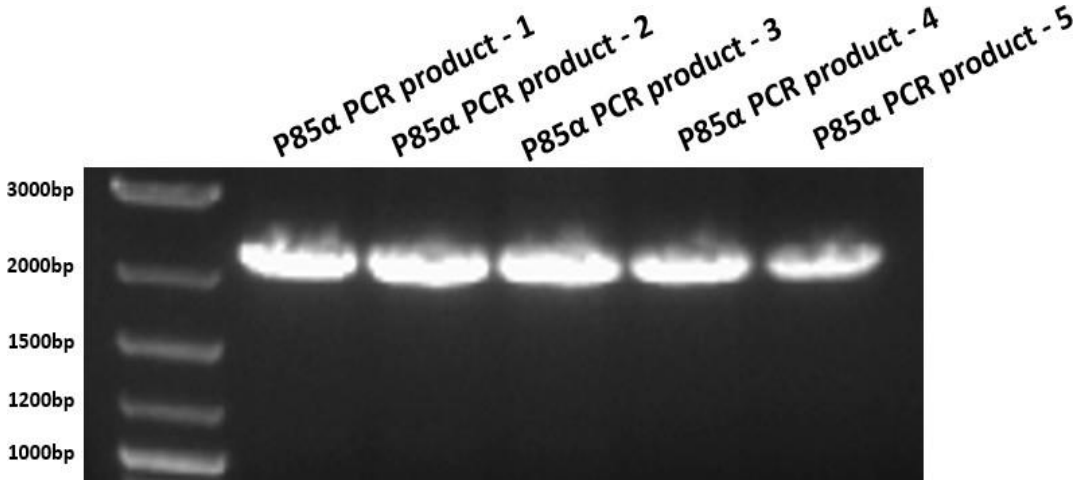

Figure 5.24. PCR amplification of p85α. Five different PCR reactions were conducted using NEBs Phusion® High Fidelity DNA polymerase with primers *(detailed in Table 5.5).* Gel electrophoresis was used to check whether p85α could be successfully amplified from PSG5-HA-p85α. Products were run on a 0.8% agarose gel.

Then, mVenus-N1 and mCherry-N1 vectors were digested with EcoRI and BamHI restriction enzymes *(Figure 5.25)* before ligation and transformation into DH5α competent cells. The primers used to amplify the P85α insert from PSG5-HA-P85α were used to screen positive colonies by colony PCR. Nine colonies were screened for the identification of p85α-mVenus-N1 and p85α-mCherry-N1. Three positive colonies for p85α-mCherry-N1 (colonies 1, 6 and 9) and three positive colonies for p85α-mVenus-N1 (colonies 6, 8 and 9) were identified through colony PCR *(Figure 5.26).* The total number of positive colonies were then miniprepped and sent for sanger sequencing.

The CMV forward primer (CAACGGGACTTTCCAAAATG) was used again in sequencing reactions, as this would allow detection of the 5' HA tag sequence which is fused to p85α. All colonies which underwent sanger sequencing came back positive, an example of the sequencing outputs can be found in *Figure 5.27.* This figure highlights the presence of the HA tag in frame with N terminal p85α sequences. Additionally, sequencing using a reverse mCherry primer (GATCTCGAACTCGTGGCCGT) was conducted. The results from this sequencing highlighted C terminal p85α sequences fused to mCherry sequences (*Figure 5.27).* Finally, diagnostic digests were also performed on p85α-mCherry-N1. Using EcoRI and BamHI restriction enzymes, this released a band of the expected size (~2200bp) *(Figure 5.27)*

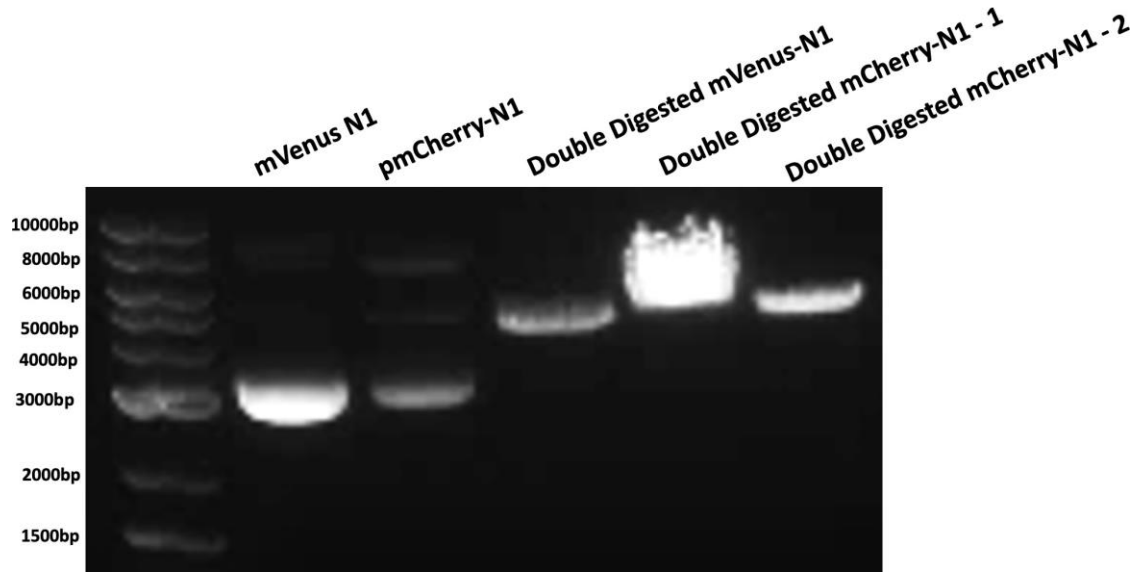

Figure 5.25. Restriction digests of mVenus-N1 and mCherry-N1. Vectors were undigested or double digested with EcoRI and BamHI restriction enzymes in preparation for ligation reactions with double digested p85α inserts.

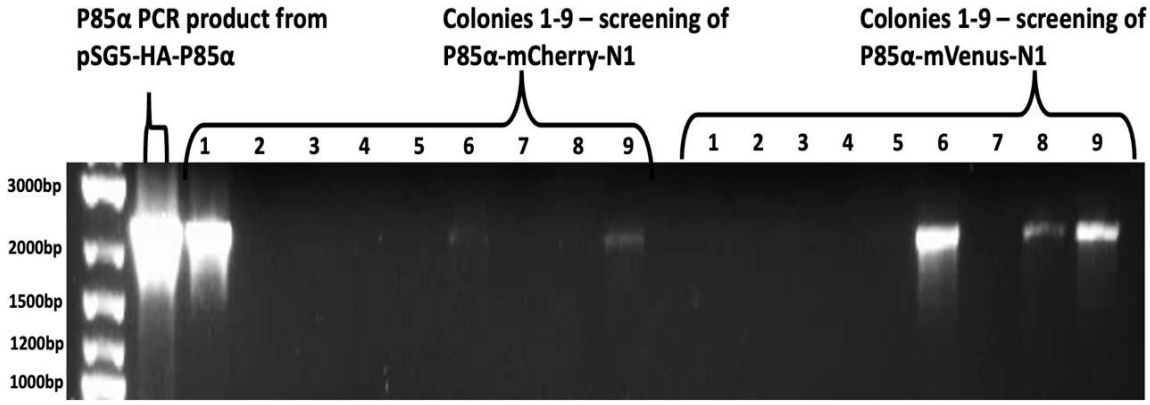

Figure 5.26. Colony PCR screening of p85α-mCherry-N1 and p85α-pmVenus-N1. Screening of positive colonies was carried out using NEBs Taq DNA polymerase, with primers detailed in *Table 5.5*. Gel electrophoresis was used to check whether p85α could be amplified positive transformants. Products were run on a 0.8% agarose gel. Colony PCR detected three positive colonies for p85α-mCherry-N1 (colonies 1, 6 and 9) and three positive colonies for p85α-mVenus-N1 (colonies 6, 8 and 9). A control PCR reaction was run alongside colony PCR reactions, to assess whether p85α could be successfully amplified from PSG5-HA-P85α when using NEBs Taq DNA polymerase.

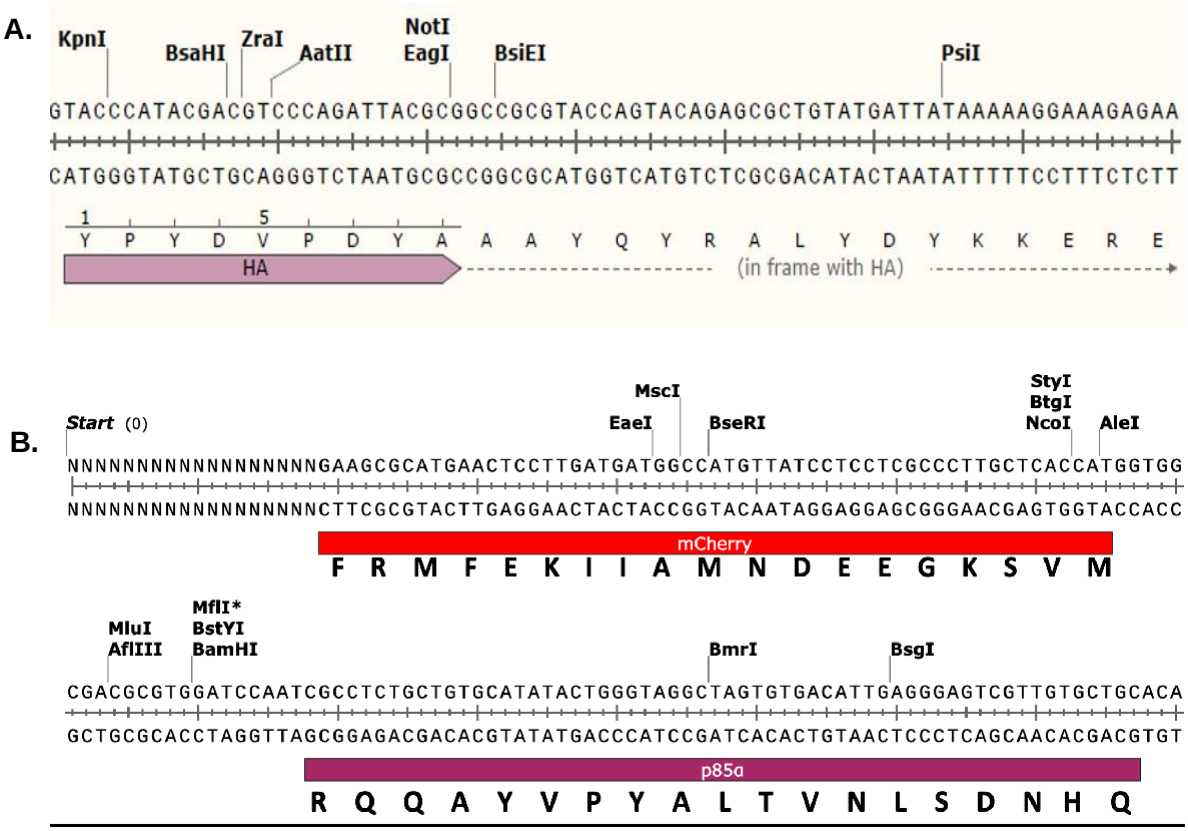

Figure 5.27. Validation of p85α-mCherryN1. A. Sanger sequencing of p85α-mCherryN1 using a CMV forward primer (CAACGGGACTTTCCAAAATG). Shown is the presence of N terminal HA tag, fused in frame to p85α **B.** Sanger sequencing of p85α-mCherryN1 using a reverse mCherry primer (GATCTCGAACTCGTGGCCGT). Shown is the presence of C terminal p85α sequences fused to mCherry. **C.** Diagnostic restriction digests of p85α-mCherryN1. BamHI and EcoRI restriction enzymes were used in this reaction. An expected band of ~2200bp was obtained through BamHI and EcoRI restriction digest. Sequencing shown in **B** and diagnostic digests shown in **C** were performed by Luc Costello Heaven.

5.9. Localisation of mCherryN1 and mCherryN1-PIK3R1 in WT LNCaP C4-2 cells.

To check the localisation of cloned constructs (mCherryN1 and p85α-mCherryN1) these were all transfected into WT LNCaP C4-2 cells. It was previously shown that the localisation of mCherryN1 in U2OS osteosarcoma cells is predominantly nuclear *(McNeill et al., 2013).* Nuclear localisation was observed when WT LNCaP C4-2 cells were transfected with mCherryN1 *(Figure 5.28).* The localisation of p85α-mCherryN1 in WT C4-2 cells was within the cytoplasm and cell membrane, no nuclear localisation was observed for this construct *(Figure 5.28).* This is consistent with previous reports of mCherry and EGFP tagged PIK3R1 constructs, expressed in U2OS and CHO-K1 cell lines respectively *(Luo et al., 2005 ; Zhou et al., 2022).*

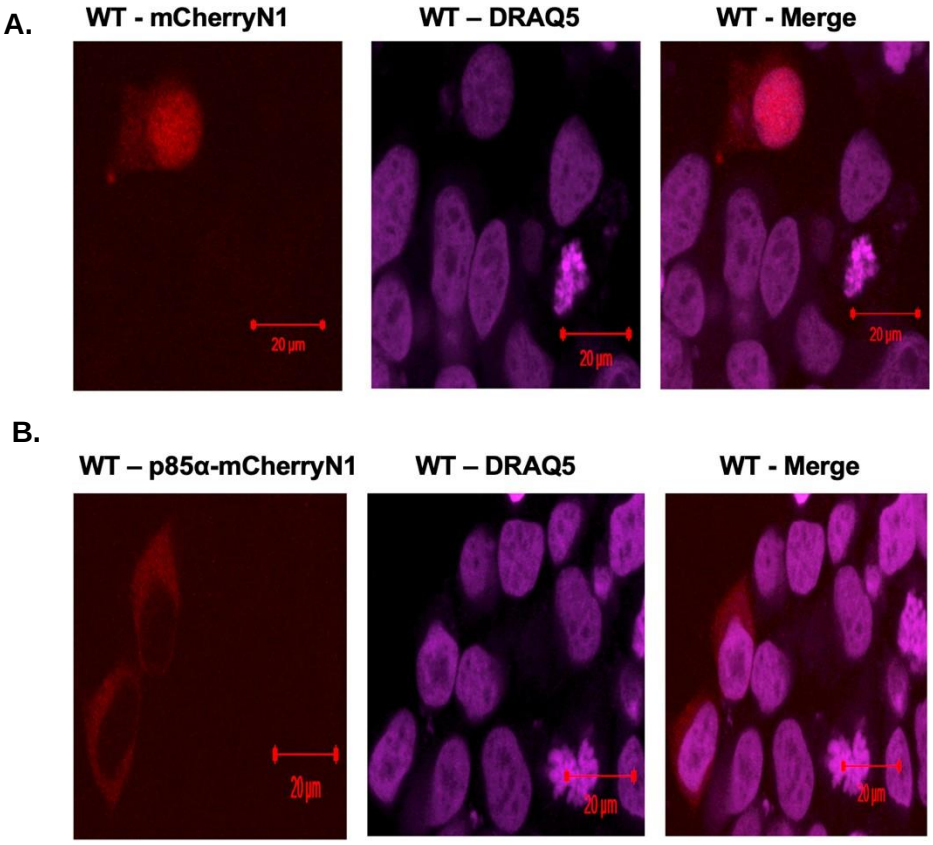

Figure 5.28. Localisation of mCherryN1 and p85α-mCherryN1. WT C4-2 cells were transfected with either mCherryN1 or p85α-mCherryN1 and grown for 48h before being prepared for confocal microscopy. A Zeiss LSM510 Meta confocal microscope was used for image acquisition. **A and B** shows the localisation of mCherryN1 and p85α-mCherryN1 in WT LNCaP C4-2 cells respectively.

5.10. The Effects on phospho-AKT Levels in ΔN C4-2 cells after PIK3R1 Rescue.

To assay whether transfection of p85α-mCherryN1 modulates AKT phosphorylation in ΔN C4-2 cells, flow cytometry was conducted. In these assays ΔN C4-2 cells were transfected with either mCherryN1 or p85α-mCherryN1. After 48h, ΔN C4-2 cells were fixed with PFA, permeabilised with methanol before staining with a phospho-AKT S473 antibody. With mCherry possessing an absorption and emission of 587nm and 610nm respectively, an AlexaFluro 488 secondary antibody was used in these assays. With AlexaFluro 488 possessing an absorption and emission of 495nm and 519nm respectively, this ensured that phospho-AKT levels could be quantified alongside the detection of mCherry positive cells. Ultimately this strategy could be used to see whether reductions in phospho-AKT levels is observed in cells transfected with p85α-mCherryN1. For phospho-AKT flow cytometry experiments conducted in this work, negative controls in the form of WT C4-2 cells either stained with AlexaFluro 488 secondary antibody or transfected with empty mCherryN1 was used when devising the gating strategy *(Figure 5.29).* Additionally experiments which assayed the levels of AKT phosphorylation in untransfected ΔN, KO and WT LNCaP C4-2 cells were run alongside the transfection experiments.

Unfortunately, the data generated from these assays was not statistically significant, and instead the overall results from plotting the median fluorescent intensity (MFI) values/x-med will be discussed. MFI values reflect the “middle” fluorescent intensity value within a sample population. These values are preferred to taking a mean fluorescent intensity value which could be skewed by outliers within a sample population. The MFI values were the greatest in untransfected ΔN LNCaP C4-2 relative to WT and KO cells *(Figure 5.30).* This is in line with previous western blotting data highlighting that the ΔN clone possesses elevated phospho-AKT levels *(Figure 5.1).* The x-med values

for phospho-AKT and mCherry fluorescence show that they are is lower in ΔN cells transfected with p85α-mCherryN1 *(Figures 5.31).* However, the lack of statistical significance in these assays is most likely due to the low transfection efficiencies observed in these assays (~1-2%) *(Figure 5.31)*. Overall, whilst is a suggestion that reductions in phospho-AKT levels were found in ΔN C4-2 transfected with either p85α-mCherryN1 (*Figure 5.31)* further work would be needed to fully validate this observation.

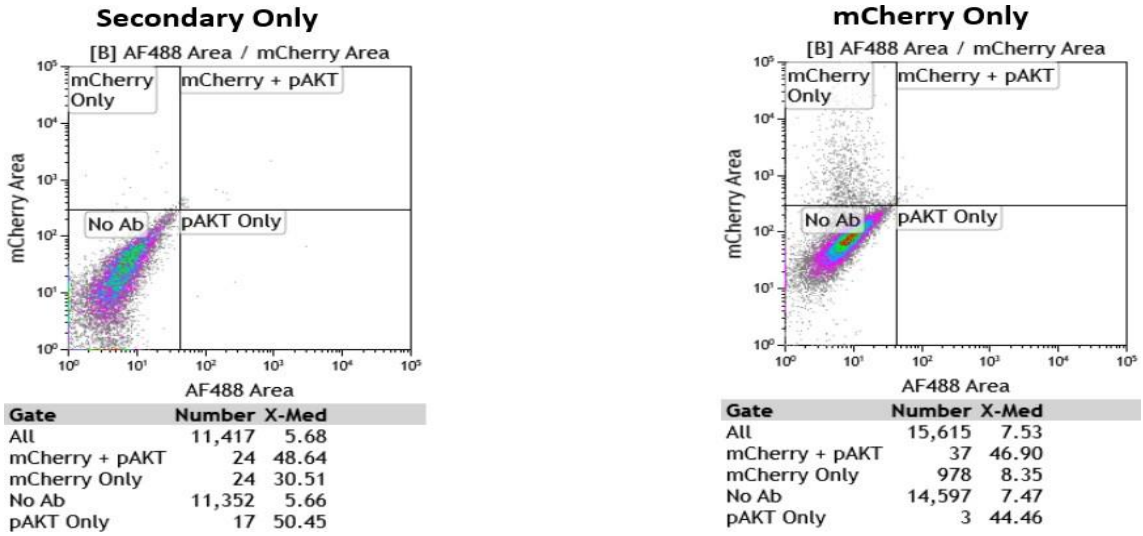

Figure 5.29. Dot plots for secondary only and mCherry only fluorescence. WT C4-2 cells were incubated with just AlexaFluro 488 secondary antibody or transfected with empty mCherryN1. Fluorescent intensities from these dot plots were used to devise the gating strategy used in *Figures 5.30 and 5.31.*

A.

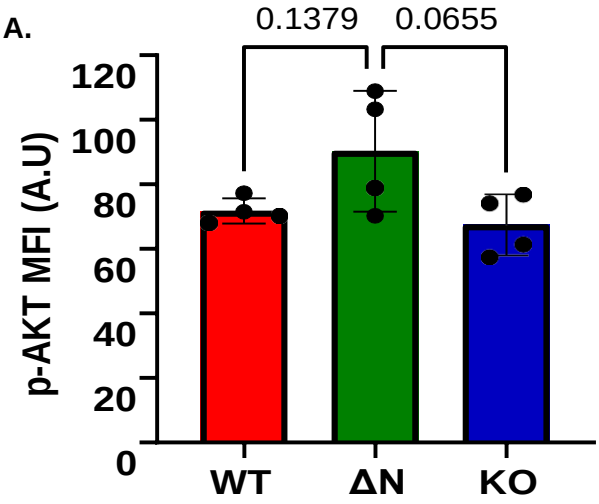

B.

WT - Untransfected

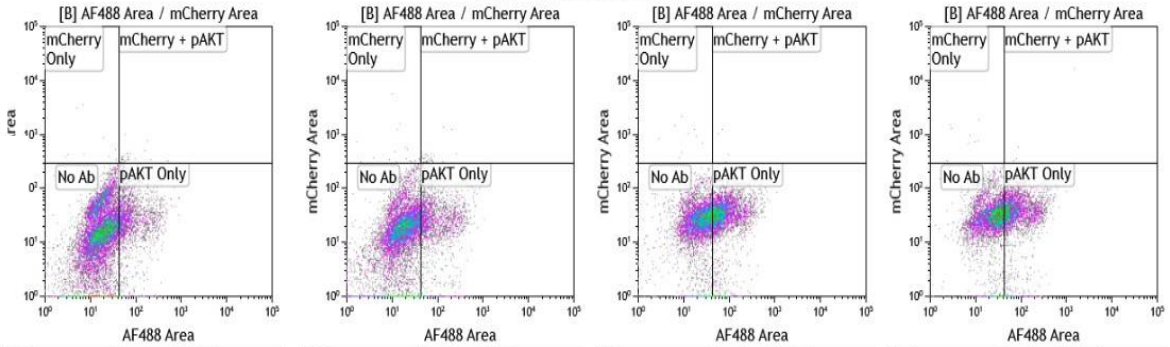

Gate	Number	X-Med
All	11,194	19.99
mCherry + pAKT	31	56.93
mCherry Only	9	7.44
No Ab	9,096	16.68
pAKT Only	2,058	68.17

Gate	Number	X-Med
All	9,287	20.08
mCherry + pAKT	34	59.22
mCherry Only	18	15.36
No Ab	7,237	16.02
pAKT Only	1,998	77.31

Gate	Number	X-Med
All	8,648	38.82
mCherry + pAKT	5	70.49
mCherry Only	10	9.42
No Ab	4,690	22.26
pAKT Only	3,943	70.11

Gate	Number	X-Med
All	7,611	35.83
mCherry + pAKT	5	80.67
mCherry Only	10	9.58
No Ab	4,414	22.97
pAKT Only	3,182	71.51

C.

ΔN - Untransfected

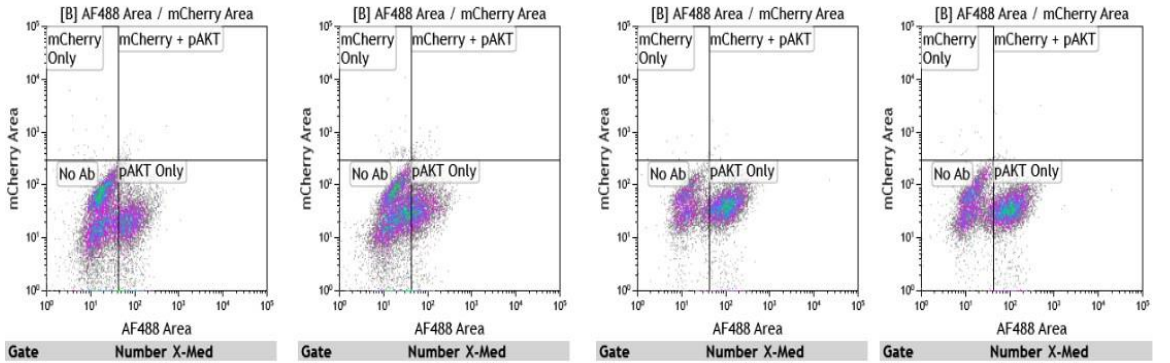

Gate	Number	X-Med
All	13,458	25.78
mCherry + pAKT	39	64.25
mCherry Only	27	8.91
No Ab	8,723	17.22
pAKT Only	4,669	78.78

Gate	Number	X-Med
All	13,116	25.88
mCherry + pAKT	60	57.90
mCherry Only	55	26.51
No Ab	9,032	18.09
pAKT Only	3,969	70.24

Gate	Number	X-Med
All	9,309	60.59
mCherry + pAKT	12	55.36
mCherry Only	10	12.69
No Ab	3,819	14.29
pAKT Only	5,468	108.91

Gate	Number	X-Med
All	10,424	50.66
mCherry + pAKT	23	57.74
mCherry Only	16	16.25
No Ab	4,747	14.51
pAKT Only	5,638	103.28

D.

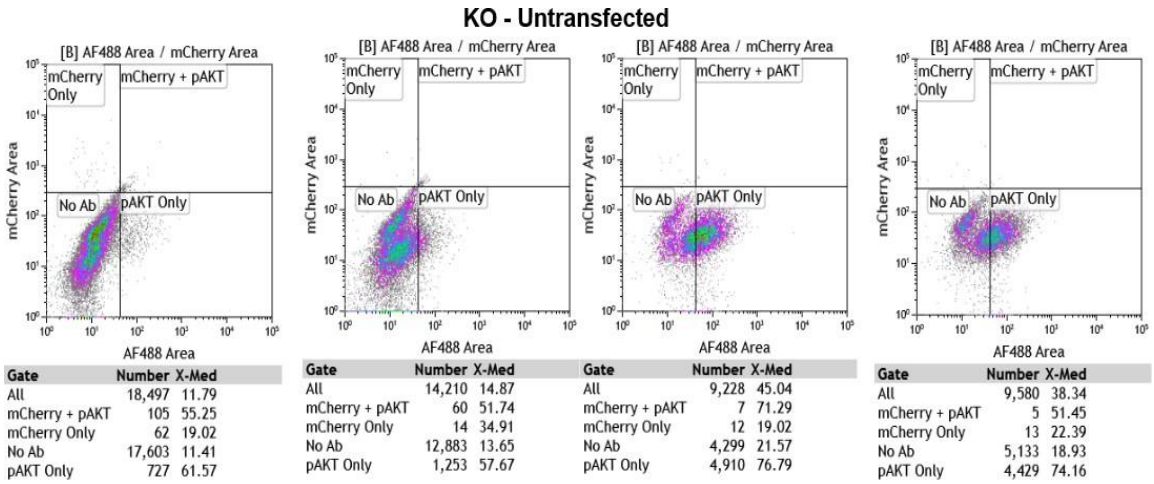

Figure 5.30. Flow cytometry detection of phospho-AKT levels in untransfected WT, ΔN and KO LNCaP C4-2 cells. Cells were stained with a phospho-Akt S473 primary antibody followed by staining with Alexa-Fluor-488 secondary antibody. **A.** The MFI / x-med values for phospho-AKT S473 levels in WT, ΔN and KO. Data is of biological quadruplets (n=4). A one-way ANOVA with a Tukey's multiple comparisons test was calculated, with P values shown

A.

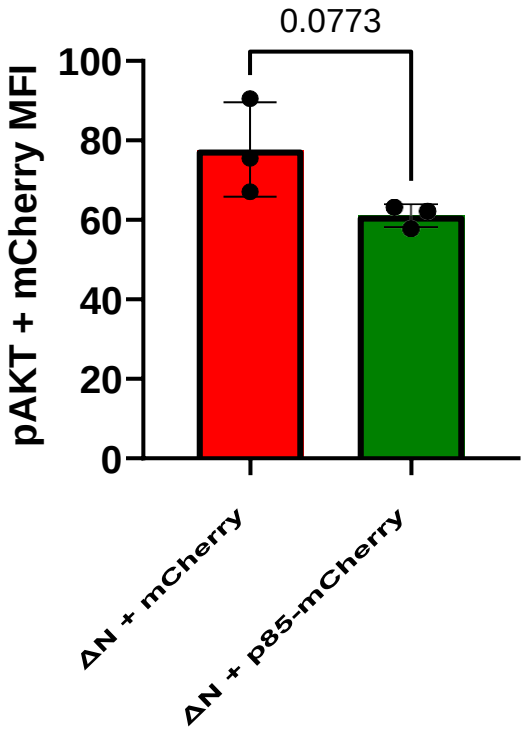

B.

ΔN - pmCherryN1 (p85α-pmCherryN1 Transfection Control)

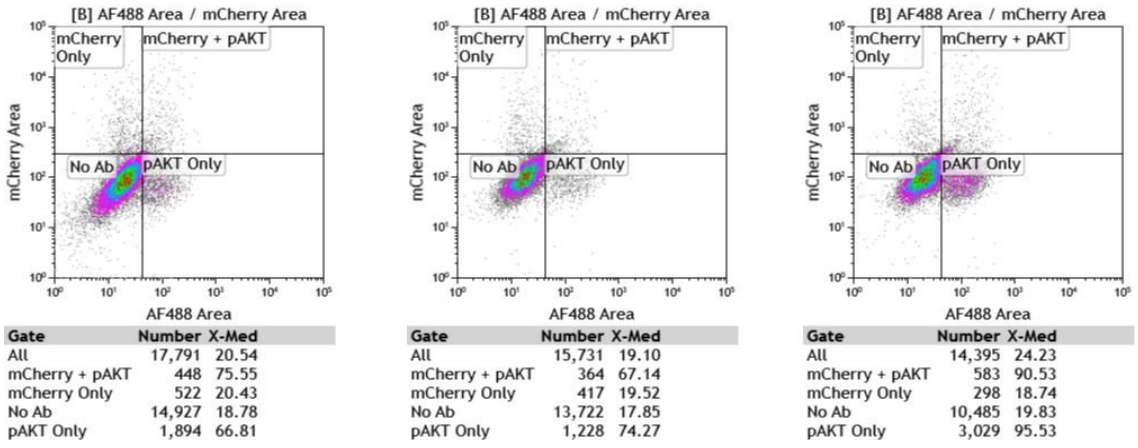

Gate	Number	X-Med
All	17,791	20.54
mCherry + pAKT	448	75.55
mCherry Only	522	20.43
No Ab	14,927	18.78
pAKT Only	1,894	66.81

Gate	Number	X-Med
All	15,731	19.10
mCherry + pAKT	364	67.14
mCherry Only	417	19.52
No Ab	13,722	17.85
pAKT Only	1,228	74.27

Gate	Number	X-Med
All	14,395	24.23
mCherry + pAKT	583	90.53
mCherry Only	298	18.74
No Ab	10,485	19.83
pAKT Only	3,029	95.53

C.

ΔN – p85α-pmCherryN1

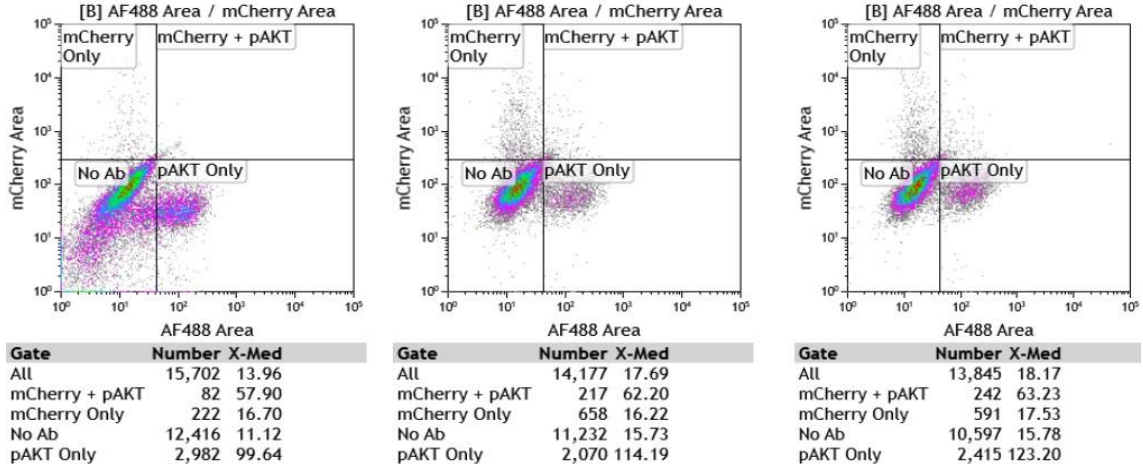

Gate	Number	X-Med
All	15,702	13.96
mCherry + pAKT	82	57.90
mCherry Only	222	16.70
No Ab	12,416	11.12
pAKT Only	2,982	99.64

Gate	Number	X-Med
All	14,177	17.69
mCherry + pAKT	217	62.20
mCherry Only	658	16.22
No Ab	11,232	15.73
pAKT Only	2,070	114.19

Gate	Number	X-Med
All	13,845	18.17
mCherry + pAKT	242	63.23
mCherry Only	591	17.53
No Ab	10,597	15.78
pAKT Only	2,415	123.20

Figure 5.31. Flow cytometry detection of phospho-AKT levels in ΔN C4-2 cells transfected with either mCherryN1 or p85α-mCherryN1. Cells were first before transfected with desired constructs before being stained with a phospho-Akt S473 primary antibody and then an Alexa-Fluor-488 secondary antibody. **A.** The MFI / x-med values for phospho-AKT S473 levels in ΔN cells transfected with either mCherryN1 or p85α-mCherryN1. Data is of biological triplicates (n=3). A one-way ANOVA with a Tukey's multiple comparisons test was calculated, with P values shown on the graph. **B and C.** Dot plots of the biological triplicates used to comprise graph **A**

5.11. Discussion

This chapter has aimed to explore the dysregulation of AKT signalling in ΔN LNCaP C4-2 cells. Western blots conducted in this chapter, align with work previously conducted by *Roberts, (2022)* confirming increased AKT phosphorylation at T308 and S473 residues. The effects of increased phosphorylation of AKT was investigated through confocal microscopy using the AKT reporter, pSBbi-FoxO1_1R_10A_3D. In these assays, the AKT mediated phosphorylation of T24 , S256 and S319 residues would induce cytoplasmic localisation of pSBbi-FoxO1_1R_10A_3D. However from *Figure 5.2* it is apparent that pSBbi-FoxO1_1R_10A_3D undergoes cytoplasmic translocation in WT, ΔN and KO LNCaP C4-2 cells. *Pan et al., (2017)* demonstrated that AKT activity is elevated in PTEN null lines LNCaP, LNCaP C4-2 and LAPC-4 relative to the PTEN positive 22RV1 and DU145 prostate cancer cell lines. Immunofluorescence work by *Pan et al., (2017)* then showed that cells, the basal level of AKT activity in LNCaP cells initiated cytoplasmic localisation of the FOXO1 protein. This would explain why all three cell lines in this work (WT, ΔN and KO) exhibited cytoplasmic localisation of pSBbi-FoxO1_1R_10A_3D. To further investigate downstream effects of dysregulated AKT signalling in ΔN, western blotting to particular AKT substrates (e.g – GSK3β, PRAS40 or TWIST1) or pan western blots to substrates harbouring the phospho-AKT substrate motif (RXRXXS/T) could be conducted.

At the transcriptional level, the effects of dysregulated AKT signalling were investigated *in silico,* by comparing the DEGs from ΔN-WT to other cell systems with dysregulated AKT phosphorylation. These cell systems include MDA-MB-231 breast cancer cells transduced with constitutively active AKT in the form of a myristylated construct or MCF-10A cells expressing constitutively active PI3K (harbouring the hotspot mutation, H1047R). Only a small proportion of genes (~2-3%) were found to be

common within these comparisons *(Figures 5.3 , 5.4, 5.9 and 5.10).* Interestingly however some of the DEGs highlighted in these comparisons (e.g PEG10, SPINK1 and INPP4B) have been implicated with regulating AKT phosphorylation. This suggests several additional mechanisms which could contribute to aberrant AKT activity in these cell models. To explore this further clone ΔN could be treated with AKT inhibitors, with RT-qPCR conducted on a panel of genes identified in these comparisons. This would validate whether AKT activity is necessary for regulating the expression of DEGs identified in these comparisons.

A contributing factor as to why a small pool of genes were identified in this work could be partly explained by the differences in cell types. A lack of suitable prostate cancer models was available for these comparisons meaning RNA-Seq data from breast epithelial cells and breast cancer lines was used instead. For instance, prostate epithelial cell RNA-Seq data published by *Lee et al., (2016)* was available to analyse. However, in these study prostate epithelial cells were transduced with both N-Myc and myristylated AKT. In the context of prostate cancer, overexpression of N-Myc initiates mass transcriptional rewiring which triggers differentiation in neuroendocrine prostate cancer *(Lee et al., 2016 ; Yin et al., 2019).* Due to this, this study was not included in DEG comparisons. Another limitation could be through the manner of which dysregulated AKT signalling was induced in the breast cell lines. In the case of *Hart et al., (2015)* MCF-10A-H1047R cells possess constitutively active p110α, whereas in prostate cancer, dysregulated p110β activity drives disease progression. Knockdown of p110α in PTEN deficient prostate cancer cells does not impede AKT activation, whereas blocking the expression of p110β suppresses downstream AKT phosphorylation *(Wee et al., 2008 ; Hill et al., 2010).* As such, for further work could look to transduce WT LNCaP C4-2 cells with constitutively active p110β and AKT constructs, and through RNA-Seq, compare thetranscriptome to that of clone ΔN.

Prior publications have suggested that reductions in PIK3R1/p85α expression can induce AKT phosphorylation in different cancer cell lines *(Lin et al., 2015 ; Thorpe et al., 2017 ; Li et al., 2019)*. Loss of PIK3R1/p85α was observed in both RNA-Seq data and at the protein level for clone ΔN *(Table 5.1 and Figures 5.11 and 5.13).* This is in contrast to data compiled in *Table 1.5,* which highlights that the expression of Class IA PI3K regulatory and catalytic subunits is largely consistent within a prostate cancer patient cohort.

RNA-Seq data from additional prostate cancer cell models were investigated in this work, include cell lines (LNCaP and VCaP) treated with androgens. This work builds upon a previous publication from *Munkley et al., (2015)* which showed *in vitro*, stimulating LNCaP cells with R1881 reduces PIK3R1 (p85α) and PI3KR3 (p55γ) expression. The LNCaP RNA-Seq data analysed in this work *(Metzger et al., 2016)* not only supported the observation by *Munkley et al., (2015)*, but also highlighted that shorter PIK3R1 transcripts PIK3R1-202 (p55α) and PIK3R1-201 (p50α) expression is also reduced after androgen treatment *(Figure 5.16).* This was particularly interesting, considering that p55α and p50α are shorter PIK3R1 variants, hinting at the presence of AREs or co-factor binding sites throughout the PIK3R1 gene.

Significant reductions of PIK3R1-211 and PIK3R1-202 was also observed in VCaP cells after treatment with R1881 *(Figure 5.17).* In the case of PIK3R1-211 the expression of this transcript could be rescued through administration of the AR antagonist Darolutamide, further highlighting the interplay between AR and PIK3R1*(Figure 5.17).* Whilst reductions of PIK3R3-201 (p55γ) was observed in LNCaP cells after DHT treatment *(Munkely et al., 2015 ; Figure 5.16)* , no statistically significant reductions in expression were observed after VCaP cells were treated with R1881 *(Figure 5.17).*

Whether loss of PIK3R1 expression can induce increases in AKT phosphorylation in prostate cancer cells has been disputed. *In vitro* studies first by *Munkley et al., (2015)* found that knockdown of PIK3R1 expression in LNCaP cells by endoribonuclease-prepared siRNA

(esiRNA) was found to inhibit AKT phosphorylation. More recently however, *Chakraborty et al., (2022)* showed in the PTEN positive prostate cancer cell lines (22RV1 and LAPC4) siRNA knockdown of PIK3R1 induces AKT phosphorylation. The different outcomes in these studies could be explained through the use of different prostate cancer cell models, and how heavily the expression of PIK3R1 has been ablated. Severely disrupting the expression of PIK3R1 would not only impact the pool of monomeric pool of p85 that couples to activated receptors, but also the pool catalytic active p85-p110 dimers.

In this work, ΔN LNCaP C4-2 cells transfected with p85α-mCherryN1 exhibited an (statistically insignificant) reduction in S473 phosphorylation relative to empty vector controls *(Figure 5.31).* In future work, it would be first imperative to improve the transfection efficiencies in the phospho-AKT flow cytometry assays. A greater transfection efficiency would give more insight into whether the PIK3R1 is driving AKT phosphorylation in ΔN C4-2 cells. With this considered, further work could look to transduce PIK3R1 constructs via lentiviral transduction, which has been used previously to achieve transfection efficiencies of over 90% in DU145, PC3 and 22RV1 prostate cancer cell lines *(Lv et al., 2018).* Another mode of optimization could bethrough using phospho-AKT antibodies which are conjugated to a fluorescent dye, such as Alexa Fluor® 488. This would remove the need to use secondary antibody and facilitate direct detection of phospho-AKTlevels in both transfected and untransfected LNCaP C4-2 cell populations.

Chapter 6
Overall Discussion

6.1. Overall Discussion

This project has utilised previously generated CRISPR clones (ΔN and KO) to explore the role PIP5K1α in prostate cancer. In conjunction with small molecule inhibitors, these CRISPR clones can serve as tool to understand how blocking PIP5K1α activity impedes prostate tumorigenesis. The core findings from this work highlight that both CRISPR clones show significantly altered expression of genes associated with androgen signalling and cell cycle progression, KO LNCaP C4-2 cells exhibit defects in $PI(4,5)P_2$ synthesis and surprisingly ΔN LNCaP C4-2 cells show elevated levels of phosphorylated AKT.

In regards to the transcriptional alterations exhibited by both CRISPR clones, both ΔN and KO LNCaP C4-2 cells exhibited upregulation of genes implicated with cell cycle progression *(Tables 3.5 and 3.7).* However, cell proliferation was halted in both ΔN and KO LNCaP C4-2 cells *(Figures 3.12, 3.13 and 3.14).* Oncogene induced replication stress may account for why both CRISPR clones exhibited growth defects, with both ΔN and KO exhibiting increased levels of the DNA damage marker γ-H2AX *(Figure 3.15).* However, there always remains the possibility that when these clones were previously selected for, they already contained elevated levels of DNA damage.

Additionally, both cell lines exhibited a loss of UGT2B expression *(Figures 3.10 and 3.11),* coupled with increases in KLK3/PSA expression *(Figures 3.17 and 3.18).* With UGT2B family members important in the conjugation of androgens, the loss of their expression relieves the negative inhibition this gene family exerts upon androgen signalling. Whilst targeting PIP5K1α caused growth arrest in both CRISPR clones *(Figures 3.12, 3.13 and 3.14)* in a therapeutic setting if blocking PIP5K1α function induces androgen sensitisation, this would be concerning given that prostate cancers can exhibit androgen dependency. Several approaches could be adopted to explore this further.

Firstly, transiently transfecting ΔN and KO LNCaP C4-2 cells with PIP5K1α-mVenus-N1 triggered reductions in KLK3 expression *(Figure 3.19)*. However, a more systematic approach would be to conduct RNA-Seq on ΔN and KO C4-2 cells that have rescued PIP5K1A expression. This would facilitate a more detailed transcriptomic analysis, allowing for changes in genes implicated in androgen signalling (amongst other enriched pathways) to be scrutinised in more detail after rescue. Throughout this work, transient transfections were conducted using lipid based reagents (Lipofectamine 3000). Whilst extremely user friendly, unfortunately very modest transfection efficiencies could only be obtained with these reagents.

To obtain greater transfection efficiencies in subsequent rescue assays, lentiviral based approaches could be used. This has been used previously transduce constructs with great efficiencies (~90%) in DU145, PC3 and 22RV1 prostate cancer cell lines *(Lv et al., 2018).* Alternatively, generating ΔN and KO cell lines with inducible PIP5K1A expression is another strategy for rescuing expression. Whilst this approach would be more technically challenging, the major benefit of this would be the ability to control the duration of PIP5K1A rescue. Ultimately, if this was combined with RNA-Seq, it would be possible to re-express PIP5K1A for different time frames, and the assess the effects this has on the transcriptome. This approach would also be align with the fact that PIP5K1A is overexpressed in prostate cancer *(Semenas et al., 2014)* thus, overexpression models would be able to complement models of PIP5K1A inhibition.

In conjunction with further understanding if loss of PIP5K1A expression induce androgen sensitisation, whether this is also observed after treating prostate cancer cells with PIP5K1α inhibitors is unknown. WT LNCaP C4-2 cells (amongst other prostate cancer cell lines) could be treated with different PIP5K1α inhibitors such as ISA-2011B *(Semenas et al., 2014)* Compound 13 (*Strätker et al., (2020)* and Compound 6 *(Sun et al., 2022)* with RT-qPCR conducted on genes associated with

androgen signalling, such as KLK3 and UGT2B15/17. If results from these assays were comparable to ΔN and KO (upregulated KLK3 expression, loss of UGT2B expression) this would provide further evidence to suggest that antagonising PIP5K1α activity induces androgen sensitisation. If this proved to be the case this would further highlight the requirement in a therapeutic setting to administer AR antagonists/ ADT in conjunction with PIP5K1α inhibitors. This would be to ensure that prostate tumors do not become resensitised to circulating androgens.

KO LNCaP C4-2 cells were generated through CRISPR editing, using guide RNAs targeting Exon 1 and Exon 6, encoding parts of the N terminus and kinase domain respectively. An perturbed kinase domain would ultimately affect kinase activity, which in part explains why LPA stimulation was unable to evoke $PI(4,5)P_2$ in the KO clone.

Another reason as to why PI(4,5)P2 synthesis is effected in clone KO would be the overall loss of expression PIP5K1α. This would ultimately impact the number of PIP5K homodimers and heterodimers which can be formed in KO LNCaP C4-2 cells. This is further compounded by the fact that PIP5K1B is not expressed in LNCaP C4-2 cells *(Table 3.1),* meaning there is less of a PIP5K buffer to compensate for PIP5K1A loss.

ΔN LNCaP C4-2 cells possess elevated levels of phospho-AKT, and much of this work has centered around the mechanisms behind this. A candidate DEG identified as being implicated in AKT phosphorylation was PIK3R1. How loss of PIK3R1 expression drives AKT phosphorylation was first highlighted by the Cantley and Kahn laboratories *(Ueki et al., 2002 ; Mauvais-Jarvis et al., 2002)* where it was suggested that loss of PIK3R1 reduces the levels of monomeric p85 protein, which can antagonise PI3K activity.

Confocal microscopy with $PI(3,4,5)P_3$ and $PI(3,4)P_2$ detecting constructs, pcDNA3.1_AktPH- mCherry, NES-EGFP-cPHx3 and EGFP-Grp1-PH *(Figures 4.5 , 4.6 and4.7)* indicated that the levels of these phosphoinositides were notelevated. As such, the loss of PIK3R1 could be driving AKT phosphorylation in an alternative manner. A possible

mechanism could be through loss of Gab2 phosphorylation, which impairs the recruitmentof 14-3-3 proteins that antagonise AKT activity *(Li et al., 2019).* Further work could look to explore whether reductions of Gab2 S210 phosphorylation is observed in ΔN C4-2 cells, and whether Gab2 S210 phosphorylation can be rescued through overexpressing ΔN C4-2 cells with PIK3R1 expression constructs.

Additionally, rescue experiments assaying the expression of PIK3R1 in PIP5K1α-mVenus-N1 transfected ΔN C4-2 cells was conducted in this work. Preliminary (but statistically insignificant) data showed increases in PIK3R1 expression after ΔN LNCaP C4-2 cells were transfected with PIP5K1α-mVenus-N1 *(Figure 5.14).* If further work demonstrates statistically significant elevations of PI3KR1 expression after PIP5K1α-mVenus-N1 rescue in ΔN C4-2; this would highlight a novel role of PIP5K1α in regulating PI3K/AKT signalling at a transcriptional level. Ultimately however, any future PIK3R1 rescue experiments with CRISPR clones would require improved transfection efficiencies.

In ΔN LNCaP C4-2 cells, translational may be initiating from downstream Exon 1 AUG codons (AUG36 and AUG46). Therefore, another aspect to explore regarding the increases in AKT phosphorylation observed in ΔN C4-2 would be to overexpress the N terminal truncated PIP5K1α variant found in this clone in KO LNCaP C4-2 cells. Whilst this would provide insight as to whether this truncation contributes to AKT activation, in the event that AKT phosphorylation was increased in such assays, detailing a mechanism would be very challenging.

The N terminus of PIP5Ks has been attributed to regulating homo- and heterodimerization which is required for PI(4,5)P_2 synthesis (*Lacalle et al., 2015 ; Hansen et al., 2022).* As such, it is paradoxical that loss of N terminal PIP5K1α residues would induce AKT phosphorylation. Whether the N terminal region (of approximately 30-40 amino acids) has broader roles in regulating expression of genes implicated with regulating AKT activation (e.g PIK3R1) is currently unknown. Also unknown is whether the loss of N terminal residues relives any negative regulation exerted by other kinases on PIP5K1α. For instance four possible PKC

phosphorylation sites (S6, S11,S27 and S31 , as show in *Table 1.11)* would be lost through the N terminal truncation PIP5K1α. Finally, the possibility that the increases in AKT phosphorylation observed in ΔN LNCaP C4-2 cells could be an artifact from clonal selection cannot be avoided.

Overall, this work has highlighted the profound effects that attenuated PIP5K1A expression has upon the transcriptome. ΔN LNCaP C4-2 cells possessed ~2 fold more DEGs than KO C4-2 cells (1675 and 818 DEGs respectively). Compounding factors as to why more DEGs were observed in ΔN LNCaP C4-2 cells includes this the activation of AKT in this clone, along with this clone possessing an unedited PIP5K1α kinase domain. It must be noted that the DEGs recorded in ΔN and KO LNCaP C4-2 were identified by comparing to each CRISPR clone to WT LNCaP C4-2 cells. An additional control to further validate that these genes are affected through loss of PIP5K1α.

Whilst more differentially expressed genes were prominent in ΔN LNCaP C4-2 cells, both CRISPR clones implicated in androgen signalling and cell cycle progression were identified as being dysregulated in It would be worthwhile investigating whether the pathways affected in CRISPR edited LNCaP C4-2 cells would also be differentially regulated after loss of PIP5K1A in other androgen dependent prostate cancer cell lines, such as LNCaP, VCaP and 22RV1. Furthermore, PIP5K1α activity has been implicated with other cancer cell line models such as breast (*Sarwar et al., 2018*), pancreatic (A*dhikari and Counter, 2018*) and liver *(Kawase et al., 2019).* However transcriptomics detailing the pathways effected after attenuating the function of PIP5K1α in these cancer cell line models has yet to be investigate, and could also warrant further investigation.

References

Abida, W., Cyrta, J., Heller, G., Prandi, D., Armenia, J., Coleman, I., Cieslik, M., Benelli, M., Robinson, D., Van Allen, E.M., Sboner, A., Fedrizzi, T., Mosquera, J.M., Robinson, B.D., De Sarkar, N., Kunju, L.P., Tomlins, S., Wu, Y.M., Nava Rodrigues, D. and Loda, M. (2019). Genomic correlates of clinical outcome in advanced prostate cancer. *Proceedings of the National Academy of Sciences,* 116(23), pp.11428–11436.

Adami, A., García-Álvarez, B., Arias-Palomo, E., Barford, D. and Llorca, O., (2007). Structure of TOR and Its Complex with KOG1. *Molecular Cell*, 27(3) pp.509-516.

Adhikari, H. and Counter, C. (2018). Interrogating the protein interactomes of RAS isoforms identifies PIP5K1A as a KRAS-specific vulnerability. *Nature Communications,* 9(1).

Afgan, E., Baker, D., Batut, B., van den Beek, M., Bouvier, D., Čech, M., Chilton, J., Clements, D., Coraor, N., Grüning, B., Guerler, A., Hillman-Jackson, J., Hiltemann, S., Jalili, V., Rasche, H., Soranzo, N., Goecks, J., Taylor, J., Nekrutenko, A. and Blankenberg, D. (2018). The Galaxy platform for accessible, reproducible and collaborative biomedical analyses: 2018 update. *Nucleic Acids Research*. 46(1), pp. 537-544.

Aggarwal, R., Zhang, T., Small, E. and Armstrong, A. (2014). Neuroendocrine Prostate Cancer: Subtypes, Biology, and Clinical Outcomes. *Journal of the National Comprehensive Cancer Network*, 12(5), pp. 719-726.

Agoulnik, I., Hodgson, M., Bowden, W. and Ittmann, M., 2011. INPP4B: the New Kid on the PI3K Block. *Oncotarget*, 2(4), pp.321-328.

Alessi, D., Andjelkovic, M., Caudwel,l B., Cron, P., Morrice, N., Cohen P. and Hemmings BA. (1996). Mechanism of activation of protein kinase B by insulin and IGF-1.*The EMBO Journal,* 15(23), pp. 6541-6551.

Alessi, D., James, S., Downes, C., Holmes, A., Gaffney, P., Reese, C. and Cohen, P. (1997). Characterization of a 3-phosphoinositide-dependent protein kinase which phosphorylates and activates protein kinase Bα. *Current Biology,* 7(4), pp.261-269.

Allen, WE., Jones, GE., Pollard JW. And Ridley AJ. (1997). Rho, Rac and Cdc42 regulate actin organization and cell adhesion in macrophages. *Journal of Cell Science,* (6):707-720

Amzel, L., Huang, C., Mandelker, D., Lengauer, C., Gabelli, S. and Vogelstein, B. (2008). Structural comparisons of class I phosphoinositide 3-kinases. *Nature Reviews Cancer,* 8(9), pp.665-669.

Andrews, S., n.d. FastQC. https://www.bioinformatics.babraham.ac.uk/projects/fastqc/

Antal, Corina E. and Newton, Alexandra C. (2014). Tuning the phosphoinositides output of protein kinase C. *Biochemical Society Transactions*, 42(6), pp.1477–1483.

Ardito, F., Giuliani, M., Perrone, D., Troiano, G. and Muzio, L.L. (2017). The crucial role of protein phosphorylation in cell signalling and its use as targeted therapy (Review). *International Journal of Molecular Medicine*, 40(2), pp.271–280.

Arneth, B. (2009). Clinical Significance of Measuring Prostate-Specific Antigen. *Laboratory Medicine,* 40(8), pp. 487-491.

Ashcroft, M., Kubbutat, M. and Vousden, K. (1999). Regulation of p53 Function and Stability by Phosphorylation. *Molecular and Cellular Biology,* 19(3) pp. 1751-1758.

Barneda, D., Cosulich, S., Stephens, L. and Hawkins, P. (2019). How is the acyl chain composition of phosphoinositides created and does it matter? *Biochemical Society Transactions*, 47(5), pp.1291–1305.

Barr, A.R., Cooper, S., Heldt, F.S., Butera, F., Stoy, H., Mansfeld, J., Novák, B. and Bakal, C. (2017). DNA damage during S-phase mediates the proliferation-quiescence decision in the subsequent G1 via p21 expression. *Nature Communications*, 8(1).

Baumann, B., Weber, C., Troppmair, J., Whiteside, S., Israel, A., Rapp, U. and Wirth, T., 2000. Raf induces NF-κB by membrane shuttle kinase MEKK1, a phosphoinositides pathway critical for transformation. *Proceedings of the National Academy of Sciences*, 97(9), pp.4615-4620.

Baumgart, S.J., Nevedomskaya, E., Lesche, R., Newman, R., Mumberg, D. and Haendler, B. (2020). Darolutamide antagonises androgen signalling by blocking enhancer and super-enhancer activation. *Molecular Oncology*, 14(9), pp.2022–2039.

Bawazir, N., Beshay, M., Ring, A. and Janetopoulos, C. (2018). Plasma Membrane PI(4,5)P_2 Threshold Regulates Chemotactic phosphoinositides pathways and cell morphology. *The FASEB Journal,* 32(S1).

Bayascas, J., Wullschleger, S., Sakamoto, K., Garcia-Martinez, J., Clacher, C., Komander, D., van Aalten, D., Boini, K., Lang, F., Lipina, C., Logie, L., Sutherland, C., Chudek, J., van Diepen, J., Voshol, P., Lucocq, J. and Alessi, D. (2008). Mutation of the PDK1 PH Domain Inhibits Protein Kinase B/Akt, Leading to Small Size and Insulin Resistance. *Molecular and Cellular Biology,* 28(10), pp. 3258-3272.

Bazzi, M.D. and Nelsestuen, G.L. (1990). Protein kinase C interaction with calcium: a phospholipid-dependent process. *Biochemistry*, 29(33), pp.7624–7630.

Bellacosa, A., Testa, J., Moore, R. and Larue, L. (2004). A Portrait of AKT Kinases: Human Cancer and Animal Models Depict a Family with Strong Individualities. *Cancer Biology and Therapy.* 3(3): 268-275.

Benavides-Serrato, A., Lee, J., Holmes, B., Landon, K., Bashir, T., Jung, M., Lichtenstein, A. and Gera, J., (2017). Specific blockade of Rictor-mTOR association inhibits mTORC2 activity and is cytotoxic in glioblastoma. *PLOS ONE*, 12(4).

Benes, C.H., Wu, N., Elia, A.E.H., Dharia, T., Cantley, L.C. and Soltoff, S.P. (2005). The C2 Domain of PKCδ Is a Phosphotyrosine Binding Domain. *Cell*, 121(2), pp.271–280.

Berman, H. M., Westbrook, J., Feng, Z., Gilliland, G., Bhat, T. N., Weissig, H., Shindyalov, I. N., and Bourne, P. E. (2000). The Protein Data Bank. *Nucleic Acids Research,* 28(1), pp. 235–242.

Bethesda Research Laboratories, BRL pUC host: E. coli DH5αTM competent cells. 1986. *Focus,* 8, pp. 9-12.

Bevan, C.L., Hoare, S., Claessens, F., Heery, D.M. and Parker, M.G. (1999). The AF1 and AF2 Domains of the Androgen Receptor Interact with Distinct Regions of SRC1. *Molecular and Cellular Biology,* 19(12), pp.8383–8392.

Bhullar, K.S., Lagarón, N.O., McGowan, E.M., Parmar, I., Jha, A., Hubbard, B.P. and Rupasinghe, H.P.V. (2018). Kinase-targeted *cancer therapies: progress, challenges and future directions. Molecular Cancer,* 17(1).

Bligh, E. and Dyer, W., 1959. A RAPID METHOD OF TOTAL LIPID EXTRACTION AND PURIFICATION. *Canadian Journal of Biochemistry and Physiology*, 37(8), pp.911-917.

Blom, N., Gammeltoft, S. and Brunak, S. (1999). Sequence and structure-based prediction of eukaryotic protein phosphorylation sites. *Journal of Molecular Biology*, 294(5), pp.1351–1362.

Bonkhoff, H., Stein, U. and Remberger, K. (1994). The proliferative function of basal cells in the normal and hyperplastic human prostate. *The Prostate,* 24(3), pp. 114-118.

Boormans, J., Korsten, H., Ziel-van der Made, A., van Leenders, G., Verhagen, P. and Trapman, J. (2010). E17K substitution in AKT1 in prostate cancer. *British Journal of Cancer,* 102(10) pp. 1491-1494.

Boronenkov, I., Loijens, J., Umeda, M. and Anderson, R. (1998). Phosphoinositide Phosphoinositides Pathways in Nuclei Are Associated with Nuclear Speckles Containing Pre-mRNA Processing Factors. *Molecular Biology of the Cell,* 9(12), pp. 3547-3560.

Braun, C., Parks, X., Qudsi, H. and Lopes, C., 2021. Membrane pools of phosphatidylinositol-4-phosphate regulate KCNQ1/KCNE1 membrane expression. *Communications Biology*, 4(1).

Bray, N., Pimentel, H., Melsted, P. and Pachter, L., 2016. Near-optimal probabilistic RNA-seq quantification. *Nature Biotechnology,* 34(5), pp. 525-527.

Breslow, D. and Weissman, J., 2010. Membranes in Balance: Mechanisms of Sphingolipid Homeostasis. *Molecular Cell*, 40(2), pp.267-279.

Brickley, D., Mikosz, C., Hagan, C. and Conzen, S., (2002). Ubiquitin Modification of Serum and Glucocorticoid-induced Protein Kinase-1 (SGK-1). *Journal of Biological Chemistry.* 277(45) pp.43064-43070.

Brodbeck, D., Hill, M. and Hemmings, B. (2001). Two Splice Variants of Protein Kinase Bγ Have Different Regulatory Capacity Depending on the Presence or Absence of the Regulatory Phosphorylation Site Serine 472 in the Carboxyl-terminal Hydrophobic Domain. *Journal of Biological Chemistry,* 276(31), pp. 29550-29558.

Brombacher, E., Urwyler, S., Ragaz, C., Weber, S., Kami, K., Overduin, M. and Hilbi, H., 2009. Rab1 Guanine Nucleotide Exchange Factor SidM Is a Major Phosphatidylinositol 4-Phosphate-binding Effector Protein of Legionella pneumophila. *Journal of Biological Chemistry*, 284(8), pp.4846-4856.

Brown, J.R. and Auger, K.R. (2011). Phylogenomics of phosphoinositide lipid kinases: perspectives on the evolution of second messenger phosphoinositides and drug discovery. *BMC Evolutionary Biology,* 11(1).

Brummer, T., Larance, M., Abreu, M., Lyons, R., Timpson, P., Emmerich, C., Fleuren, E., Lehrbach, G., Schramek, D., Guilhaus, M., James, D. and Daly, R., 2008. Phosphorylation-dependent binding of 14-3-3 terminates phosphoinositides by the Gab2 docking protein. *The EMBO Journal*, 27(17), pp.2305-2316.

Brunet, A., Bonni, A., Zigmond, M., Lin, M., Juo, P., Hu, L., Anderson, M., Arden, K., Blenis, J. and Greenberg, M., 1999. Akt Promotes Cell Survival by Phosphorylating and Inhibiting a Forkhead Transcription Factor. *Cell*, 96(6), pp.857-868.

Brunet, A., Park, J., Tran, H., Hu, L., Hemmings, B. and Greenberg, M., (2001). Protein Kinase SGK Mediates Survival Signals by Phosphorylating the Forkhead Transcription Factor FKHRL1 (FOXO3a). *Molecular and Cellular Biology*, 21(3) pp. 952-965.

Bubb , M., Senderowicz, A., Sausville, E., Duncan, K. and Korn, E., 1994. Jasplakinolide, a cytotoxic natural product, induces actin polymerisation and competitively inhibits the binding of phalloidin to F-actin. *Journal of Biological Chemistry,* 27;269(21), pp.14869-14871.

Buchner, K. (2000). The role of protein kinase C in the regulation of cell growth and in phosphoinositides to the cell nucleus. *Journal of Cancer Research and Clinical Oncology,* 126(1): 1-11.

Burke, J. and Williams, R., 2013. Connecting with an Old Partner in a New Way. *Cancer Cell,* 23(5), pp. 559-561.

Cairns, P., Okami, K., Halachmi, S., Halachmi, N., Esteller, M., Herman, JG., Jen, J., Isaacs, WB., Bova GS. And Sidransky D (1997). Frequent inactivation of PTEN/MMAC1 in primary prostate cancer. *Cancer Research,* 57(22), 4997-5000.

Carpten, J., Faber, A., Horn, C., Donoho, G., Briggs, S., Robbins, C., Hostetter, G., Boguslawski, S., Moses, T., Savage, S., Uhlik, M., Lin, A., Du, J., Qian, Y., Zeckner, D., Tucker-Kellogg, G., Touchman, J., Patel, K., Mousses, S., Bittner, M., Schevitz, R., Lai, M., Blanchard, K. and Thomas, J. (2007). A transforming mutation in the pleckstrin homology domain of AKT1 in cancer. *Nature,* 448(7152) pp. 439-444.

Cato, L., de Tribolet-Hardy, J., Lee, I., Rottenberg, J., Coleman, I., Melchers, D., Houtman, R., Xiao, T., Li, W., Uo, T., Sun, S., Kuznik, N., Göppert, B., Ozgun, F., van Royen, M., Houtsmuller, A., Vadhi, R., Rao, P., Li, L., Balk, S., Den, R., Trock, B., Karnes, R., Jenkins, R., Klein, E., Davicioni, E., Gruhl, F., Long, H., Liu, X., Cato, A., Lack, N., Nelson, P., Plymate, S., Groner, A. and Brown, M. (2019). Arv7 Represses Tumor-Suppressor Genes in Castration-Resistant Prostate Cancer. *Cancer Cell,* 35(3), pp. 401-413

Cervantes, D., Crosby, C. and Xiang, Y., 2010. Arrestin Orchestrates Crosstalk Between G Protein-Coupled Receptors to Modulate the Spatiotemporal Activation of ERK MAPK. *Circulation Research*, 106(1), pp.79-88.

Chakrabarti, R., Bhowmick, D., Bhargava, V., Bhar, K. and Siddhanta, A., 2013. Nuclear pool of phosphatidylinositol 4 phosphate 5 kinase 1α is modified by polySUMO-2 during apoptosis. *Biochemical and Biophysical Research Communications,* 439(2), pp. 209-214.

Chakrabarti, R., Sanyal, S., Ghosh, A., Bhar, K., Das, C. and Siddhanta, A. (2015). Phosphatidylinositol-4-phosphate 5-Kinase 1α Modulates Ribosomal RNA Gene Silencing through Its Interaction with Histone H3 Lysine 9 Trimethylation and Heterochromatin Protein HP1-α. *Journal of Biological Chemistry,* 290(34), pp.20893–20903.

Chakraborty, G., Nandakumar, S., Hirani, R., Nguyen, B., Stopsack, K.H., Kreitzer, C., Rajanala, S.H., Ghale, R., Mazzu, Y.Z., Pillarsetty, N.V.K., Lee, G.-S.M., Scher, H.I., Morris, M.J., Traina, T., Razavi, P., Abida, W., Durack, J.C., Solomon, S.B., Vander Heiden, M.G. and Mucci, L.A. (2022). The Impact of PIK3R1 Mutations and Insulin–PI3K–Glycolytic Pathway Regulation in Prostate Cancer. *Clinical Cancer Research*, 28(16), pp.3603–3617.

Chan, S., Smith, E., Gao, Y., Kwan, J., Blum, B., Tilston-Lunel, A., Turcinovic, I., Varelas, X., Cardamone, M., Monti, S., Emili, A. and Perissi, V., (2021). Loss of G-Protein Pathway Suppressor 2 Promotes Tumor Growth Through Activation of AKT Signalling. *Frontiers in Cell and Developmental Biology*, 8.

Chandra, M., Chin, Y.K.-Y. ., Mas, C., Feathers, J.R., Paul, B., Datta, S., Chen, K.-E., Jia, X., Yang, Z., Norwood, S.J., Mohanty, B., Bugarcic, A., Teasdale, R.D., Henne, W.M., Mobli, M. and Collins, B.M. (2019). Classification of the human phox homology (PX) domains based on their phosphoinositide binding specificities. *Nature Communications*, 10(1).

Chautard, E., Ouédraogo, Z.G., Biau, J. and Verrelle, P. (2014). Role of Akt in human malignant glioma: from oncogenesis to tumour aggressiveness*. Journal of Neuro-Oncology,* 117(2), pp.205–215.

Chen, S., Xu, Y., Yuan, X., Bubley, G.J. and Balk, S.P. (2006). Androgen receptor phosphorylation and stabilization in prostate cancer by cyclin-dependent kinase 1. *Proceedings of the National Academy of Sciences,* 103(43), pp.15969–15974. .

Cheng, L., Luo, S., Jin, C., Ma, H., Zhou, H. and Jia, L. (2013). FUT family mediates the multidrug resistance of human hepatocellular carcinoma via the PI3K/Akt pathway. *Cell Death and Disease*, 4(11).

Choi, N., Zhang, B., Zhang, L., Ittmann, M. and Xin, L. (2012). Adult Murine Prostate Basal and Luminal Cells Are Self-Sustained Lineages that Can Both Serve as Targets for Prostate Cancer Initiation. *Cancer Cell*, 21(2), pp. 253-265.

Choi, S., Chen, M., Cryns, V. and Anderson, R. (2019). A nuclear phosphoinositide kinase complex regulates p53. *Nature Cell Biology,* 21(4), pp.462-475.

Choi, S., Thapa, N., Tan, X., Hedman, A. and Anderson, R. (2015). PIP kinases define PI4,5P2 phosphoinositides specificity by association with effectors. Biochimica et Biophysica Acta (BBA) – *Molecular and Cell Biology of Lipids,* 1851(6), pp.711-723.

Chouinard, S., Barbier, O. and Bélanger, A., (2007). UDP-glucuronosyltransferase 2B15 (UGT2B15) and UGT2B17 Enzymes Are Major Determinants of the Androgen Response in Prostate Cancer LNCaP Cells. *Journal of Biological Chemistry*, 282(46), pp.33466-33474.

Clark, J., Anderson, K., Juvin, V., Smith, T., Karpe, F., Wakelam, M., Stephens, L. and Hawkins, P., 2011. Quantification of PtdInsP3 molecular species in cells and tissues by mass spectrometry. *Nature Methods*, 8(3), pp.267-272.

Clarke, J., Letcher, A., D'santos, C., Halstead, J., Irvine, R. And Divecha, N. (2001). Inositol lipids are regulated during cell cycle progression in the nuclei of murine erythroleukaemia cells. *Biochemical Journal.* 357(3), pp. 905–910.

Clinckemalie, L., Vanderschueren, D., Boonen, S. and Claessens, F. (2012). The hinge region in androgen receptor control. *Molecular and Cellular Endocrinology,* 358(1), pp.1–8.

Cochet, C., Filhol, O., Payrastre, B., Hunter, T. and Gill, G., (1991). Interaction between the epidermal growth factor receptor and phosphoinositide kinases. *Journal of Biological Chemistry*, 266(1), pp.637-644.

Cole, P.A., Chu, N., Salguero, A.L. and Bae, H. (2019). AKTivation mechanisms. *Current Opinion in Structural Biology,* 59, pp.47–53.

Colgan, D. and Manley, J., 1997. Mechanism and regulation of mRNA polyadenylation. *Genes and Development*, 11(21), pp.2755-2766.

Cooke, M., Zhang, X., Zhang, S., Eruslanov, E., Lal, P., Daniel, R.E., Feldman, M.D., Abba, M.C. and Kazanietz, M.G. (2022). Protein Kinase C Alpha is a Central Node for Tumorigenic Transcriptional Networks in Human Prostate Cancer. *Cancer Research Communications*, 2(11), pp.1372–1387.

Coulthard, V.H., Matsuda, S. and Heery, D.M. (2003). An Extended LXXLL Motif Sequence Determines the Nuclear Receptor Binding Specificity of TRAP220*. Journal of Biological Chemistry,* 278(13), pp.10942–10951.

Cowell, C., Döppler, H., Yan, I., Hausser, A., Umezawa, Y. and Storz, P., (2009). Mitochondrial diacylglycerol initiates protein-kinase-D1-mediated ROS phosphoinositides. *Journal of Cell Science*, 122(7), pp.919-928.

Creighton, C., (2007). A gene transcription signature of the Akt/mTOR pathway in clinical breast tumors. *Oncogene*, 26(32), pp.4648-4655.

Danielian, P.S., White, R., Lees, J.A. and Parker, M.G. (1992). Identification of a conserved region required for hormone dependent transcriptional activation by steroid hormone receptors. *The EMBO Journal*, 11(3), pp.1025–1033.

Datlinger, P., Rendeiro, A.F., Schmidl, C., Krausgruber, T., Traxler, P., Klughammer, J., Schuster, L.C., Kuchler, A., Alpar, D. and Bock, C. (2017). Pooled CRISPR screening with single-cell transcriptome readout. *Nature Methods,* 14(3), pp.297–301.

De Camilli, P., Chen, H., Hyman, J., Panepucci, E., Bateman, A., and Brunger, A. T. (2002). The ENTH domain. *FEBS letters*, 513(1), 11–18.

De la Cruz, L., Traynor-Kaplan, A., Vivas, O., Hille, B. and Jensen, J., (2019). Plasma membrane processes differentially regulated by type I phosphatidylinositol phosphate 5-kinases and RASSF4. *Journal of Cell Science*. *133*(2).

De Pascalis, C. and Etienne-Manneville, S., (2017). Single and collective cell migration: the mechanics of adhesions. *Molecular Biology of the Cell*, 28(14), pp.1833-1846.

DePrimo, S.E., Diehn, M., Nelson, J.B., Reiter, R.E., Matese, J., Fero, M., Tibshirani, R., Brown, P.O. and Brooks, J.D. (2002). Transcriptional programs activated by exposure of human prostate cancer cells to androgen. *Genome Biology,* 3(7).

Deslypere, J., Young, M., Wilson, J. and McPhaul, M. (1992). Testosterone and 5α-dihydrotestosterone interact differently with the androgen receptor to enhance transcription of the MMTV-CAT reportergene. *Molecular and Cellular Endocrinology,* 88(1-3), pp.15-22.

Dhand, R., Hiles, I., Panayotou, G., Roche, S., Fry, M.J., Gout, I., Totty, N.F., Truong, O., Vicendo, P. and Yonezawa, K. (1994). PI 3-kinase is a dual specificity enzyme: autoregulation by an intrinsic protein-serine kinase activity. *The EMBO Journal,* 13(3), pp.522–533.

Diaz-Meco, M.T. and Moscat, J. (2012). The atypical PKCs in inflammation: NF-κB and beyond. *Immunological Reviews*, 246(1), pp.154–167.

Dibble, C., Asara, J. and Manning, B., (2009). Characterization of Rictor Phosphorylation Sites Reveals Direct Regulation of mTOR Complex 2 by S6K1. *Molecular and Cellular Biology,* 29(21), pp. 5657-5670.

Dickson, E., Jensen, J. and Hille, B., *2014). Golgi and plasma membrane pools of PI(4)P contribute to plasma membrane PI(4,5)P 2 and maintenance of KCNQ2/3 ion channel current. *Proceedings of the National Academy of Sciences*, 111(22).

Dingjan, T. and Futerman, A., (2021). The fine-tuning of cell membrane lipid bilayers accentuates their compositional complexity. *BioEssays*, 43(5), p.2100021.

Dirican, E. and Akkiprik, M. (2017). Phosphatidylinositol 3-kinase regulatory subunit 1 and phosphatase and tensin homolog as therapeutic targets in breast cancer. *Tumor Biology*, 39(3).

Divecha, N., Banfić, H. and Irvine, R. (1991). The polyphosphoinositide cycle exists in the nuclei of Swiss 3T3 cells under the control of a receptor (for IGF-I) in the plasma membrane, and stimulation of the cycle increases nuclear diacylglycerol and apparently induces translocation of protein kinase. *The EMBO Journal,* 10(11), pp. 3207-3214.

Divecha, N., Roefs, M., Los, A., Halstead, J., Bannister, A. and D'Santos, C. (2002). Type I PIPkinases Interact with and Are Regulated by the Retinoblastoma Susceptibility Gene Product—pRB. *Current Biology,* pp.12(7), 582-587.

Dobin, A., Davis, C., Schlesinger, F., Drenkow, J., Zaleski, C., Jha, S., Batut, P., Chaisson, M. and Gingeras, T., (2013). STAR: ultrafast universal RNA-seq aligner. *Bioinformatics,* 29(1), pp.15-21.

Dobkin-Bekman, M., Ben-Navi, L., Shterntal, B., Sviridonov, L., Przedecki, F., Naidich-Exler, M., Brodie, C., Seger, R. and Naor, Z., (2010). Differential Role of PKC Isoforms in GnRH and Phorbol 12-Myristate 13-Acetate Activation of Extracellular Signal-Regulated Kinase and Jun N-Terminal Kinase. *Endocrinology*, 151(10), pp.4894-4907.

Domart, M., Hobday, T., Peddie, C., Chung, G., Wang, A., Yeh, K., Jethwa, N., Zhang, Q., Wakelam, M., Woscholski, R., Byrne, R., Collinson, L., Poccia, D. and Larijani, B., (2012). Acute Manipulation of Diacylglycerol Reveals Roles in Nuclear Envelope Assembly and Endoplasmic Reticulum Morphology. *PloS ONE*, 7(12), p.e51150.

Dombrosky-Ferlan, P. and Corey, S., (1997). Yeast two-hybrid in vivo association of the Src kinase Lyn with the proto-oncogene product Cbl but not with the p85 subunit of PI 3-kinase. *Oncogene*, 14(17), pp.2019-2024.

Doughman, R., Firestone, A., Wojtasiak, M., Bunce, M. and Anderson, R. (2003). Membrane Ruffling Requires Coordination between Type Iα Phosphatidylinositol Phosphate Kinase and Rac Phosphoinositides. *Journal of Biological Chemistry,* 278(25), pp. 23036-23045.

Dowler, S., Currie, R., Campbell, D., Deak, M., Kular, G., Downes, C. and Alessi, D., (2000). Identification of pleckstrin-homology-domain-containing proteins with novel phosphoinositide-binding specificities. *Biochemical Journal*, 351(1), pp.19-31.

Dries, D.R., Gallegos, L.L. and Newton, A.C. (2006). A Single Residue in the C1 Domain Sensitizes Novel Protein Kinase C Isoforms to Cellular Diacylglycerol Production. *Journal of Biological Chemistry*, 282(2), pp.826–830.

Dubbink, H.J., Hersmus, R., Verma, C.S., van der Korput, H.A.G.M., Berrevoets, C.A., van Tol, J., Ziel-van der Made, A.C.J., Brinkmann, A.O., Pike, A.C.W. and Trapman, J. (2004). Distinct Recognition Modes of FXXLF and LXXLL Motifs by the Androgen Receptor. *Molecular Endocrinology,* 18(9).

Dunn, S., Eberlein, C., Yu, J., Gris-Oliver, A., Swee Hoe Ong, Yelland, U., Cureton, N., Staniszewska, A.D., McEwen, R., Fox, M., Pilling, J., Hopcroft, P., Coker, E.A., Jaaks, P., Garnett, M.J., Isherwood, B., Serra, V., Davies, B.R., Barry, S.T. and Lynch, J.T. (2022). AKT-mTORC1 reactivation is the dominant resistance driver for PI3Kβ/AKT inhibitors in PTEN-null breast cancer and can be overcome by combining with Mcl-1 inhibitors. *Oncogene*, 41(46), pp.5046–5060.

Ebner, M., Lučić, I., Leonard, T. and Yudushkin, I., (2017). PI(3,4,5)P 3Engagement Restricts Akt Activity to Cellular Membranes. *Molecular Cell*, 65(3), pp.416-431

Eisermann, K., Broderick, C.J., Bazarov, A., Moazam, M.M. and Fraizer, G.C. (2013). Androgen up-regulates vascular endothelial growth factor expression in prostate cancer cells via an Sp1 binding site. *Molecular Cancer,* 12(1).

El-Deiry, WS., Tokino, T., Waldman, T., Oliner, J.D., Velculescu, V.E., Burrell, M., Hill D.E, Healy E, Rees, J.L., Hamilton, S.R., Kinzler, K.W. and Vogelstein, B. (1995) Topological control of p21WAF1/CIP1 expression in normal and neoplastic tissues. *Cancer Research* ,55(13), pp.2910-2919.

Eswaran, J., Patnaik, D., Filippakopoulos, P., Wang, F., Stein, R.L., Murray, J.W., Higgins, J.M.G. and Knapp, S. (2009). Structure and functional characterization of the atypical human kinase haspin. *Proceedings of the National Academy of Sciences,* 106(48), pp.20198–20203.

Eyster, C., Duggins, Q. and Olson, A., (2005). Expression of Constitutively Active Akt/Protein Kinase B Signals GLUT4 Translocation in the Absence of an Intact Actin Cytoskeleton. *Journal of Biological Chemistry*, 280(18), pp.17978-17985.

Fancher, A. T., Hua, Y., Camarco, D. P., Close, D. A., Strock, C. J., and Johnston, P. A. (2016). Reconfiguring the AR-TIF2 Protein-Protein Interaction HCS Assay in Prostate Cancer Cells and Characterizing the Hits from a LOPAC Screen. *Assay and Drug Development Technologies,* 14(8), pp. 453–477.

Feng, J. and Mertz, B. (2015). Novel Phosphotidylinositol 4,5-Bisphosphate Binding Sites on Focal Adhesion Kinase. *PLOS ONE*, 10(7), p.e0132833.

Feng, Q. and He, B. (2019). Androgen Receptor Phosphoinositides in the Development of Castration-Resistant Prostate Cancer. *Frontiers in Oncology,* 9.

Fernandes, R.C., Toubia, J., Townley, S., Hanson, A.R., Dredge, B.K., Pillman, K.A., Bert, A.G., Winter, J.M., Iggo, R., Das, R., Obinata, D., Sandhu, S., Risbridger, G.P., Taylor, R.A., Lawrence, M.G., Butler, L.M., Zoubeidi, A., Gregory, P.A., Tilley, W.D. and Hickey, T.E. (2021). Post-transcriptional Gene Regulation by MicroRNA-194 Promotes Neuroendocrine Transdifferentiation in Prostate Cancer. *Cell Reports*, 34(1).

Ferraldeschi, R., Welti, J., Luo, J., Attard, G. and de Bono, J. (2015). Targeting the androgen receptor pathway in castration-resistant prostate cancer: progresses and prospects. *Oncogene,* 34(14), pp.1745-1757.

Ferrero, G., Renner, M., Gil, G., Rodríguez-Berdini, L. and Caputto, B. (2014). C-Fos-activated synthesis of nuclear phosphatidylinositol 4,5-bisphosphate [PtdIns(4,5)P2] promotes global transcriptional changes. *Biochemical Journal,* 461(3) pp.521-530.

Feschenko, M. and Sweadner, K., 1995. Structural Basis for Species-specific Differences in the Phosphorylation of Na,K-ATPase by Protein Kinase C. *Journal of Biological Chemistry*, 270(23), pp.14072-14077.

Fiume, R., Faenza, I., Sheth, B., Poli, A., Vidalle, M., Mazzetti, C., Abdul, S., Campagnoli, F., Fabbrini, M., Kimber, S., Mariani, G., Xian, J., Marvi, M., Mongiorgi, S., Shah, Z. and Divecha, N., 2019. Nuclear Phosphoinositides: Their Regulation and Roles in Nuclear Functions. *International Journal of Molecular Sciences*, 20(12), p.2991.

Fonseca, B., Smith, E., Yelle, N., Alain, T., Bushell, M. and Pause, A., (2014). The ever-evolving role of mTOR in translation. *Seminars in Cell and Developmental Biology*, 36, pp. 102-112.

Fox, M., Mott, H.R. and Owen, D. (2020). Class IA PI3K regulatory subunits: p110-independent roles and structures. *Biochemical Society Transactions,* 48(4), pp.1397–1417.

Fragkos, M., Jurvansuu, J. and Beard, P. (2009). H2AX Is Required for Cell Cycle Arrest via the p53/p21 Pathway. *Molecular and Cellular Biology*, 29(10), pp.2828–2840.

Franke, T.F., Kaplan, D.R., Cantley, L.C. and Toker, A. (1997). Direct Regulation of the Akt Proto-Oncogene Product by Phosphatidylinositol-3,4-bisphosphate. *Science*, 275(5300), pp.665–668.

Frech, M., Andjelkovic, M., Ingley, E., Reddy, K., Falck, J. and Hemmings, B. (1997). High Affinity Binding of Inositol Phosphates and Phosphoinositides to the Pleckstrin Homology Domain of RAC/Protein Kinase B and Their Influence on Kinase Activity. *Journal of Biological Chemistry,* 272(13) pp. 8474-8481

Frigo, Daniel E., Bondesson, M. and Williams, C. (2021). Nuclear receptors: from molecular mechanisms to therapeutics. *Essays in Biochemistry,* 65(6), pp.847–856.

Frønsdal, K., Engedal, N. and Saatcioglu, F., (2000). Efficient DNA-mediated gene transfer into prostate cancer cell line LNCaP. *The Prostate*, 43(2), pp.111-117.

Fruman, D., Meyers, R. and Cantley, L., (1998). Phosphoinositide Kinases. *Annual Review of Biochemistry*. 67(1), pp. 481-507.

Fukami, K., Matsuoka, K., Nakanishi, O., Yamakawa, A., Kawai, S. and Takenawa, T. (1988). Antibody to phosphatidylinositol 4,5-bisphosphate inhibits oncogene-induced mitogenesis. *Proceedings of the National Academy of Sciences*, 85(23), pp.9057–9061.

Funakoshi, Y., Hasegawa, H. and Kanaho, Y., (2011). Regulation of PIP5K activity by Arf6 and its physiological significance. *Journal of Cellular Physiology*, 226(4), pp.888-895.

Fujita, K. and Nonomura, N. (2019). Role of Androgen Receptor in Prostate Cancer: A Review. *The World Journal of Men's Health,* 37(3), pp.288–295.

Ganesan, K., Ivanova, T., Wu, Y., Rajasegaran, V., Wu, J., Lee, M.H., Yu, K., Rha, S.Y., Chung, H.C., Ylstra, B., Meijer, G., Lian, K.O., Grabsch, H. and Tan, P. (2008). Inhibition of Gastric Cancer Invasion and Metastasis by PLA2G2A a Novel β-Catenin/TCF Target Gene. *Cancer Research,* 68(11), pp.4277–4286.

Gao, J., Aksoy, B.A., Dogrusoz, U., Dresdner, G., Gross, B., Sumer, S.O., Sun, Y., Jacobsen, A., Sinha, R., Larsson, E., Cerami, E., Sander, C. and Schultz, N. (2013). Integrative Analysis of Complex Cancer Genomics and Clinical Profiles Using the cBioPortal. *Science Signalling,* 6(269).

Gao, X. and Harris, T.K. (2006). Role of the PH domain in regulating in vitro autophosphorylation events required for reconstitution of PDK1 catalytic activity. *Bioorganic Chemistry*, 34(4), pp.200–223.

Garcia-Garcia, T., Poncet, S., Derouiche, A., Shi, L., Mijakovic, I. and Noirot-Gros, M.-F. (2016). Role of Protein Phosphorylation in the Regulation of Cell Cycle and DNA-Related Processes in Bacteria. *Frontiers in Microbiology*, 7.

Garçon, F., Patton, D., Emery, J., Hirsch, E., Rottapel, R., Sasaki, T. and Okkenhaug, K., (2008). CD28 provides T-cell costimulation and enhances PI3K activity at the immune synapse independently of its capacity to interact with the p85/p110 heterodimer. *Blood*, 111(3), pp.1464-1471.

Gardel, M., Schneider, I., Aratyn-Schaus, Y. and Waterman, C., (2010). Mechanical Integration of Actin and Adhesion Dynamics in Cell Migration. *Annual Review of Cell and Developmental Biology*, 26(1), pp.315-333.

Gawden-Bone, C., Frazer, G., Richard, A., Ma, C., Strege, K. and Griffiths, G., (2018). PIP5 Kinases Regulate Membrane Phosphoinositide and Actin Composition for Targeted Granule Secretion by Cytotoxic Lymphocytes. *Immunity*, 49(3), pp.427-437.

Ge, S., Son, E. and Yao, R. (2018). iDEP: an integrated web application for differential expression and pathway analysis of RNA-Seq data. *BMC Bioinformatics*, 19(534).

Gebäck, T., Schulz, M., Koumoutsakos, P. and Detmar, M., (2009). TScratch: a novel and simple software tool for automated analysis of monolayer wound healing assays. *BioTechniques*, 46(4), pp.265-274.

Gioeli, D. and Paschal, B. (2012). Post-translational modification of the androgen receptor. *Molecular and Cellular Endocrinology,* 352(1-2), pp. 70-78.

Giorgione, J.R., Lin, J.-H., McCammon, J.Andrew. and Newton, A.C. (2006). Increased Membrane Affinity of the C1 Domain of Protein Kinase Cδ Compensates for the Lack of Involvement of Its C2 Domain in Membrane Recruitment. *Journal of Biological Chemistry*, 281(3), pp.1660–1669.

Gkountakos, A., Pilotto, S., Mafficini, A., Vicentini, C., Simbolo, M., Milella, M., Tortora, G., Scarpa, A., Bria, E. and Corbo, V., (2018). Unmasking the impact of Rictor in cancer: novel insights of mTORC2 complex. *Carcinogenesis*, 39(8) pp.971-980.

Gleason, C., Oses-Prieto, J., Li, K., Saha, B., Situ, G., Burlingame, A. and Pearce, D., (2019). Phosphorylation at distinct subcellular locations underlies specificity in mTORC2-mediated activation of SGK1 and Akt. *Journal of Cell Science*, 132 (7).

Gocher, A., Azabdaftari, G., Euscher, L., Dai, S., Karacosta, L., Franke, T. and Edelman, A. (2017). Akt activation by Ca2+/calmodulin-dependent protein kinase kinase 2 (CaMKK2) in ovarian cancer cells. *Journal of Biological Chemistry,* 292(34), pp. 14188-14204.

Goedhart, J. and Luijsterburg, M.S. (2020). VolcaNoseR is a web app for creating, exploring, labeling and sharing volcano plots. *Scientific Reports*, 10(1).

Goñi, G., Epifano, C., Boskovic, J., Camacho-Artacho, M., Zhou, J., Bronowska, A., Martín, M., Eck, M., Kremer, L., Gräter, F., Gervasio, F., Perez-Moreno, M. and Lietha, D., (2014). Phosphatidylinositol 4,5-bisphosphate triggers activation of focal adhesion kinase by inducing clustering and conformational changes. *Proceedings of the National Academy of Sciences*, 111(31).

Goulden, B., Pacheco, J., Dull, A., Zewe, J., Deiters, A. and Hammond, G., (2018). A high-avidity biosensor reveals plasma membrane PI(3,4)P_2 is predominantly a class I PI3K signalling product. *Journal of Cell Biology*, 218(3), pp.1066-1079

Grasso, C.S., Wu, Y.-M., Robinson, D.R., Cao, X., Dhanasekaran, S.M., Khan, A.P., Quist, M.J., Jing, X., Lonigro, R.J., Brenner, J.C., Asangani, I.A., Ateeq, B., Chun, S.Y., Siddiqui, J., Sam, L., Anstett, M., Mehra, R., Prensner, J.R., Palanisamy, N. and Ryslik, G.A. (2012). The mutational landscape of lethal castration-resistant prostate cancer. *Nature,* 487(7406), pp.239–243.

Gross, S., Dane, M., Bucher, E. and Heiser, L., (2019). Individual Cells Can Resolve Variations in Stimulus Intensity along the IGF-PI3K-AKT Signalling Axis. *Cell Systems*, 9(6), pp.580-588.e4.

Guo, T., Feng, Y., Xiao, J., Liu, Q., Sun, X., Xiang, J., Kong, N., Liu, S., Chen, G., Wang, Y., Dong, M., Cai, Z., Lin, H., Cai, X. and Xie, A., (2018). Harnessing accurate non-homologous end joining for efficient precise deletion in CRISPR/Cas9-mediated genome editing. *Genome Biology*, 19(1): 1-20

Guo, W., Liu, R., Bhardwaj, G., Yang, J., Changou, C., Ma, A., Mazloom, A., Chintapalli, S., Xiao, K., Xiao, W., Kumaresan, P., Sanchez, E., Yeh, C., Evans, C., Patterson, R., Lam, K. and Kung, H., (2014). Targeting Btk/Etk of prostate cancer cells by a novel dual inhibitor. *Cell Death and Disease*, 5(9) pp. 1409-1421.

Gustin, J.P., Karakas, B., Weiss, M.B., Abukhdeir, A.M., Lauring, J., Garay, J.P., Cosgrove, D., Tamaki, A., Konishi, H., Konishi, Y., Mohseni, M., Wang, G., Rosen, D.M., Denmeade, S.R., Higgins, M.J., Vitolo, M.I., Bachman, K.E. and Park, B.H. (2009). Knockin of mutant PIK3CA activates multiple oncogenic pathways. *Proceedings of the National Academy of Sciences*, 106(8), pp.2835–2840.

Hagemeier, C., Cook, A. and Kouzarides, T., (1993). The retinoblastoma protein binds E2F residues required for activation in vivo and TBP binding in vitro. *Nucleic Acids Research*, 21(22), pp.4998-5004.

Halliwell, J.A., Gravells, P. and Bryant, H.E. (2020). DNA Fiber Assay for the Analysis of DNA Replication Progression in Human Pluripotent Stem Cells. *Current Protocols in Stem Cell Biology*, 54(1).

Hamada, K., Miyatake, H., Terauchi, A. and Mikoshiba, K. (2017). IP_3-mediated gating mechanism of the IP_3 receptor revealed by mutagenesis and X-ray crystallography. *Proceedings of the NationalAcademy of Sciences*, 114(18), pp.4661–4666.

Hammond, G., Ricci, M., Weckerly, C. and Wills, R., (2022). An update on genetically encoded lipid biosensors. *Molecular Biology of the Cell*, 33(5).

Han, Z., Feng, Y., Gu, B., Li, Y. and Chen, H., (2018). The post-translational modification, SUMOylation, and cancer (Review). *International Journal of Oncology,* 52(4) pp.1081-1094.

Hansen, S.D, Lee, A.A, Duewell, B.R., Groves, J.T., (2022) Membrane-mediated dimerization potentiates PIP5K lipid kinase activity. *eLife.* 11.

Hao, Y., Wang, C., Cao, B., Hirsch, B., Song, J., Markowitz, S., Ewing, R., Sedwick, D., Liu, L., Zheng, W. and Wang, Z. (2013). Gain of Interaction with IRS1 by p110α-Helical Domain Mutants Is Crucial for Their Oncogenic Functions. *Cancer Cell,* 23(5) pp. 583-593.

Harper, J., Elledge, S., Keyomarsi, K., Dynlacht, B., Tsai, L., Zhang, P., Dobrowolski, S., Bai, C., Connell-Crowley, L. and Swindell, E., (1995). Inhibition of cyclin-dependent kinases by p21. *Molecular Biology of the Cell*, 6(4), pp.387-400.

Hart, J.R. and Vogt, P.K. (2011). Phosphorylation of AKT: a Mutational Analysis. *Oncotarget,* 2(6).

Hart, J.R., Zhang, Y., Liao, L., Ueno, L., Du, L., Jonkers, M., Yates, J.R. and Vogt, P.K. (2015). The butterfly effect in cancer: A single base mutation can remodel the cell. *Proceedings of the National Academy of Sciences*, 112(4), pp.1131–1136.

Haynes, J., Srivastava, J., Madson, N., Wittmann, T. and Barber, D., 2011. Dynamic actin remodeling during epithelial–mesenchymal transition depends on increased moesin expression. *Molecular Biology of the Cell*, 22(24), pp.4750-4764.

He, B., Kemppainen, J. and Wilson, E. (2000). FXXLF and WXXLF Sequences Mediate the NH2-terminal Interaction with the Ligand Binding Domain of the Androgen Receptor. *Journal of Biological Chemistry,* 275(30), pp. 22986-22994.

He, J., Haney, R., Vora, M., Verkhusha, V., Stahelin, R. and Kutateladze, T.(2008). Molecular mechanism of membrane targeting by the GRP1 PH domain*. *Journal of Lipid Research*, 49(8), pp.1807-1815.

He, P., Lee, S., Lin, S., Seidler, U., Lang, F., Fejes-Toth, G., Naray-Fejes-Toth, A. and Yun, C. (2011). Serum- and glucocorticoid-induced kinase 3 in recycling endosomes mediates acute activation of Na+/H+exchanger NHE3 by glucocorticoids. *Molecular Biology of the Cell*, 22(20), pp. 3812-3825.

Heery, D., Kalkhoven, E., Hoare, S. and Parker, M. (1997). A signature motif in transcriptional co-activators mediates binding to nuclear receptors. *Nature,* 387(6634), pp. 733-736.

Herberts, C., Murtha, A.J., Fu, S., Wang, G., Schönlau, E., Xue, H., Lin, D., Gleave, A., Yip, S., Angeles, A., Hotte, S., Tran, B., North, S., Taavitsainen, S., Beja, K., Vandekerkhove, G., Ritch, E., Warner, E., Saad, F. and Iqbal, N. (2020). Activating AKT1 and PIK3CA Mutations in Metastatic Castration-Resistant Prostate Cancer. *European Urology*, 78(6), pp.834–844.

Hernandez-Quiles, M. (2016). 'Targeting androgen receptor and PIP5K1A in prostate cancer cells using Crispr-Cas9 genome editing tool.' Msc thesis, University of Nottingham.

Hietakangas, V. and Cohen, S. (2008). TOR complex 2 is needed for cell cycle progression and anchorage-independent growth of MCF7 and PC3 tumor cells, *BMC Cancer*, 8(1).

Hii, C., Huang, Z., Bilney, A., Costabile, M., Murray, A., Rathjen, D., Der, C. and Ferrante, A.(1998). Stimulation of p38 Phosphorylation and Activity by Arachidonic Acid in HeLa Cells, HL60 Promyelocytic Leukemic Cells, and Human Neutrophils. *Journal of Biological Chemistry*, 273(30), pp.19277-19282

Hill, K., Kalifa, S., Das, J., Bhatti, T., Gay, M., Williams, D., Taliferro-Smith, L. and De Marzo, A. (2010). The role of PI 3-kinase p110β in AKT signally, cell survival, and proliferation in human prostate cancer cells. *The Prostate,* 70(7), pp. 755-764.

Hla, T. and Dannenberg, A., (2012). Sphingolipid Signalling in Metabolic Disorders. *Cell Metabolism*, 16(4), pp.420-434.

Hodgson, M., Shao, L., Frolov, A., Li, R., Peterson, L., Ayala, G., Ittmann, M., Weigel, N. and Agoulnik, I. (2011). Decreased Expression and Androgen Regulation of the Tumor Suppressor Gene INPP4B in Prostate Cancer. *Cancer Research,* 71(2), pp. 572-582.

Hoffman, G. and Cerione, R. (2002). Signalling to the Rho GTPases:networking with the DH domain. *FEBS Letters*, 513(1) pp.85-91.

Hong S. K. (2014). Kallikreins as biomarkers for prostate cancer. *BioMed Research International,* 2014, 526341.

Hong, F., Larrea, M., Doughty, C., Kwiatkowski, D., Squillace, R. and Slingerland, J., (2008). mTOR-Raptor Binds and Activates SGK1 to Regulate p27 Phosphorylation. *Molecular Cell*, 30(6) pp. 701-711.

Hoogeboom, D., Essers, M., Polderman, P., Voets, E., Smits, L. and Burgering, B., (2008). Interaction of FOXO with β-Catenin Inhibits β-Catenin/T Cell Factor Activity. *Journal of Biological Chemistry*, 283(14), pp.9224-9230.

Horie-Inoue, K., Bono, H., Okazaki, Y. and Inoue, S. (2004). Identification and functional analysis of consensus androgen response elements in human prostate cancer cells. *Biochemical and Biophysical Research Communications*, 325(4), pp. 1312-1317.

Hornbeck, P., Kornhauser, J., Tkachev, S., Zhang, B., Skrzypek, E., Murray, B., Latham, V. and Sullivan, M., (2011). PhosphoSitePlus: a comprehensive resource for investigating the structure and function of experimentally determined post-translational modifications in man and mouse. *Nucleic Acids Research*, 40(D1), pp.D261-D270.

Hu, J., Yuan, Q., Kang, X., Qin, Y., Li, L., Ha, Y. and Wu, D. (2015). Resolution of structure of PIP5K1A reveals molecular mechanism for its regulation by dimerization and dishevelled. *Nature Communications,* 6(1)

Hu, X.-D., Meng, Q.-H., Xu, J.-Y., Jiao, Y., Ge, C.-M., Jacob, A., Wang, P., Rosen, E.M. and Fan, S. (2011). BTG2 is an LXXLL-dependent co-repressor for androgen receptor transcriptional activity. *Biochemical and Biophysical Research Communications*, 404(4), pp.903–909.

Huang, D., Cao, L., Xiao, L., Song, J., Zhang, Y., Zheng, P. and Zheng, S., (2019). Hypoxia induces actin cytoskeleton remodeling by regulating the binding of CAPZA1 to F-actin via PIP2 to drive EMT in hepatocellular carcinoma. *Cancer Letters*, 448, pp.117-127.

Huang, H., Wu., D. and Ye, Z. (2020) https://www.ncbi.nlm.nih.gov/geo/query/acc.cgi?acc=GSE137200

Hunter, T. and Sefton, B.M. (1980). Transforming gene product of Rous sarcoma virus phosphorylates tyrosine. *Proceedings of the National Academy of Sciences,* 77(3), pp.1311–1315.

Iershov, A., Nemazanyy, I., Alkhoury, C., Girard, M., Barth, E., Cagnard, N., Montagner, A., Chretien, D., Rugarli, E.I., Guillou, H., Pende, M. and Panasyuk, G. (2019). The class 3 PI3K coordinates autophagy and mitochondrial lipid catabolism by controlling nuclear receptor PPARα. *Nature Communications*, 10(1).

Igarashi, M., Wakasaki, H., Takahara, N., Ishii, H., Jiang, Z., Yamauchi,T., Kuboki, K., Meier, M., Rhodes, C. and King, G., (1999). Glucose or diabetes activates p38 mitogen-activated protein kinase via differentpathways. *Journal of Clinical Investigation*, 103(2), pp.185-195.

Ikenoue, T., Inoki, K., Yang, Q., Zhou, X. and Guan, K.-L. (2008). Essential function of TORC2 in PKC and Akt turn motif phosphorylation, maturation and signalling. *The EMBO Journal*, 27(14), pp.1919–1931.

Itoh, T. and Takenawa, T. (2002). Phosphoinositide-binding domains. *Cellular Signalling*, 14(9), pp.733–743.

Itoh, T., Ishihara, H., Shibasaki, Y., Oka, Y. and Takenawa, T. (2000). Autophosphorylation of Type I Phosphatidylinositol Phosphate Kinase Regulates Its Lipid Kinase Activity. *Journal of Biological Chemistry,* 275(25), pp.19389–19394.

Jaamaa, S., Hallstrom, T., Sankila, A., Rantanen, V., Koistinen, H., Stenman, U., Zhang, Z., Yang, Z., De Marzo, A., Taari, K., Ruutu, M., Andersson, L. and Laiho, M. (2010). DNA Damage Recognition via Activated ATM and p53 Pathway in Nonproliferating Human Prostate Tissue. *Cancer Research,* 70(21), pp. 8630-8641.

Jaber, N. and Zong, W.-X. (2013). Class III PI3K Vps34: essential roles in autophagy, endocytosis, and heart and liver function. *Annals of the New York Academy of Sciences*, 1280(1), pp.48–51.

Janiszewska, M., Primi, M. and Izard, T., (2020). Cell adhesion in cancer: Beyond the migration of single cells. *Journal of Biological Chemistry*, 295(8), pp.2495-2505.

Jean, S. and Kiger, A. (2014). Classes of phosphoinositide 3-kinases at a glance. *Journal of Cell Science,* 127(5), pp. 923-928.

Jebali, A. and Dumaz, N., (2018). The role of RICTOR downstream of receptor tyrosine kinase in cancers. *Molecular Cancer*, 17(1).

Jenkins, G. H., Fisette, P. L., and Anderson, R. A. (1994). Type I phosphatidylinositol 4-phosphate 5-kinase isoforms are specifically stimulated by phosphatidic acid. *The Journal of Biological Chemistry,* 269(15), pp.11547–11554.

Jimenez, C., Jones, D., Rodríguez-Viciana, P., Gonzalez-García, A., Leonardo, E., Wennström, S., von Kobbe, C., Toran, J., Borlado, L., Calvo, V., Copin, S., Albar, J., Gaspar, L., Diez, E., Marcos, M., Downward, J., Martinez-A, C., Mérida, I. and Carrera, A. (1998). Identification and characterization of a new oncogene derived from the regulatory subunit of phosphoinositide 3-kinase. *The EMBO Journal,* 17(3), pp.743-753.

Jingwen, B., Yaochen, L. and Guojun, Z. (2017). Cell cycle regulation and anticancer drug discovery. *Cancer Biology and Medicine*, 14(4), p.348.

Joglekar, T., Ku, A., Schollaert, E., Gong, Y., Stewart-Ornstein, J., Urisman, A., and Wang, M. (2022). PKC-alpha promotes phosphorylation of KRAS suppressing its oncogenic properties. *bioRxiv.*

Johnson, L.N. and Barford, D. (1993). The effects of phosphorylation on the structure and function of proteins. *Annual Review of Biophysics and Biomolecular Structure*, 22, pp.199–232.

Joshi, C.J., Ke, W., Drangowska-Way, A., O'Rourke, E.J. and Lewis, N.E. (2022). What are housekeeping genes? *PLOS Computational Biology*, 18(7), p.e1010295.

Kakumoto, T. and Nakata, T., 2013. Optogenetic Control of PIP_3: PIP_3 Is Sufficient to Induce the Actin-Based Active Part of Growth Cones and Is Regulated via Endocytosis. *PLoS ONE*, 8(8), p.e70861.

Kalluri, R. and Weinberg, R. (2009). The basics of epithelial-mesenchymal transition. *Journal of Clinical Investigation*, 119(6), pp.1420-1428.

Karantanos, T., Corn, P. and Thompson, T. (2013). Prostate cancer progression after androgen deprivation therapy: mechanisms of castrate resistance and novel therapeutic approaches. *Oncogene,* 32(49) pp. 5501-5511.

Kaushal, V., Mukunyadzi, P., Dennis, R. A., Siegel, E. R., Johnson, D. E., and Kohli, M. (2005). Stage-specific characterization of the vascular endothelial growth factor axis in prostate cancer: expression of lymphangiogenic markers is associated with advanced-stage disease. *Clinical Cancer Research : an Official Journal of the American Association for Cancer Research*, 11(2 Pt 1), pp. 584–593.

Kawakami, L., Yoon, B., Jackman, J., Knoll, W., Weiss, P. and Cho, N., (2017). Understanding How Sterols Regulate Membrane Remodeling in Supported Lipid Bilayers. *Langmuir*, 33(51), pp.14756-14765.

Kawano, F., Suzuki, H., Furuya, A. and Sato, M., (2015). Engineered pairs of distinct photoswitches for optogenetic control of cellular proteins. *Nature Communications*, 6(1).

Kawase, A., Inoue, Y., Hirosoko, M., Sugihara, Y., Shimada, H. and Iwaki, M. (2019). Decrease in Multidrug Resistance-associated Protein 2 Activities by Knockdown of Phosphatidylinositol 4-phosphate 5-kinase in Hepatocytes and Cancer Cells. *Journal of Pharmacy and Pharmaceutical Sciences,* 22, pp.576–584.

Kennelly, P. J., and Krebs, E. G. (1991). Consensus sequences as substrate specificity determinants for protein kinases and protein phosphatases. *The Journal of Biological Chemistry,* 266(24), pp. 15555–15558.

Khadka, B. and Gupta, R.S. (2019). Novel Molecular Signatures in the PIP4K/PIP5K Family of Proteins Specific for Different Isozymes and Subfamilies Provide Important Insights into the Evolutionary Divergence of this Protein Family. *Genes*, 10(4).

Kielkowska, A., Niewczas, I., Anderson, K., Durrant, T., Clark, J., Stephens, L. and Hawkins, P., (2014). A new approach to measuring phosphoinositides in cells by mass spectrometry. *Advances in Biological Regulation*, 54, pp.131-141.

Kim, D., Sarbassov, D., Ali, S., King, J., Latek, R., Erdjument-Bromage, H., Tempst, P. and Sabatini, D., (2002). mTOR Interacts with Raptor to Form a Nutrient-Sensitive Complex that Signals to the Cell Growth Machinery. *Cell*, 110(2), pp. 163-175.

Kim, L.C., Cook, R.S. and Chen, J. (2016). mTORC1 and mTORC2 in cancer and the tumour microenvironment. *Oncogene,* 36(16), pp.2191–2201.

Kim, M., Jeong, E., Yoo, N. and Lee, S. (2008). Mutational analysis of oncogenic AKT E17K mutation in common solid cancers and acute leukaemias. *British Journal of Cancer,* 98(9) pp. 1533-1535.

Kobayashi, T. and Cohen, P., (1999). Activation of serum- and glucocorticoid-regulated protein kinase by agonists that activate phosphatidylinositide 3-kinase is mediated by 3-phosphoinositide-dependent protein kinase-1 (PDK1) and PDK2. *Biochemical Journal*, 339(2), pp.319-328.

Koch, P.A., Dornan, G.L., Hessenberger, M. and Haucke, V. (2021). The molecular mechanisms mediating class II PI 3-kinase function in cell physiology. *The FEBS Journal*, 288(24), pp.7025–7042.

Kohn, A., Takeuchi, F. and Roth, R. (1996). Akt, a Pleckstrin Homology Domain Containing Kinase, Is Activated Primarily by

Phosphorylation. *Journal of Biological Chemistry*, 271(36), pp.21920-21926.

Koirala, S., Klein., J, Zheng, Y., Glenn, N.O., Eisemann, T., Fon-Tacer, K., Kulak, O., Lu, M., Finkelstein, D.B., Neale, G., Tillman, H., Vogel, P., Strand, D.W., Lum, L., Brautigam, C.A., Pascal, J.M., Clements, W.K., Schulman, B.A. and Potts, P.R. (2020) https://www.ncbi.nlm.nih.gov/geo/query/acc.cgi?acc=GSE141323

Kong, X., Zheng, Z., Song, G., Zhang, Z., Liu, H., Kang, J., Sun, G., Sun, G., Huang, T., Li, X., Rong, D., Wang, K., Tang, W. and Xia, Y. (2022). Over-Expression of GUSB Leads to Primary Resistance of Anti-PD1 Therapy in Hepatocellular Carcinoma. *Frontiers in Immunology,* 13.

Korenchuk, S., Lehr, J. E., MClean, L., Lee, Y. G., Whitney, S., Vessella, R., Lin, D. L., and Pienta, K. J. (2001). VCaP, a cell-based model system of human prostate cancer. *In vivo (Athens, Greece)*, 15(2), pp.163–168.

Koryakina, Y., Ta, H.Q. and Gioeli, D. (2014). Phosphorylation of the Androgen Receptor. *Endocrine-Related Cancer*. 21(4), pp.131–145.

Koshre, G.R., Shaji, F., Mohanan, N.K., Mohan, N., Ali, J. and Laishram, R.S. (2021). Star-PAP RNA Binding Landscape Reveals Novel Role of Star-PAP in mRNA Metabolism That Requires RBM10-RNA Association. *International Journal of Molecular Sciences*, 22(18), p.9980.

Kotsantis, P., Petermann, E. and Boulton, S.J. (2018). Mechanisms of Oncogene-Induced Replication Stress: Jigsaw Falling into Place. *Cancer Discovery,* 8(5), pp.537–555.

Kostich, M., English, J., Madison, V., Gheyas, F., Wang, L., Qiu, P., Greene, J. and Laz, T.M. (2002). Human members of the eukaryotic protein kinase family. *Genome Biology,* 3(9).

Koushik, S.V., Chen, H., Thaler, C., Puhl, H.L. and Vogel, S.S. (2006). Cerulean, Venus, and VenusY67C FRET Reference Standards. *Biophysical Journal,* 91(12), pp.L99–L101.

Kovacina, K., Park, G., Bae, S., Guzzetta, A., Schaefer, E., Birnbaum, M. and Roth, R., (2003). Identification of a Proline-rich Akt Substrate as a 14-3-3 Binding Partner. *Journal of Biological Chemistry*, 278(12), pp. 10189-10194.

Krajnik, A., Brazzo, J., Vaidyanathan, K., Das, T., Redondo-Muñoz, J. and Bae, Y., 2020. Phosphoinositide Signalling and Mechanotransduction in Cardiovascular Biology and Disease. *Frontiers in Cell and Developmental Biology*, 8.

Krijnen, J., Janssen, P., Ruizeveld de Winter, J., van Krimpen, H., Schröder, F. and van der Kwast, T. (1993). Do neuroendocrine cells in human prostate cancer express androgen receptor? *Histochemistry,* 100(5), pp. 393-398.

Krueger, F., n.d. Trim Galore! https://www.bioinformatics.babraham.ac.uk/projects/trim_galore/

Kumar, A., Kasikci, Y., Badredine, A., Azzag, K., Quintyn Ranty, M. L., Zaidi, F., Aragou, N., Mazerolles, C., Malavaud, B., Mendoza-Parra, M. A., Vandel, L., and Gronemeyer, H. (2021). Patient-matched analysis identifies deregulated networks in prostate cancer to guide personalized therapeutic intervention. *American Journal of Cancer Research*, *11*(11), pp.5299–5318.

Kumar, V. and Majumder, P. (1995). Prostate gland: Structure, functions and regulation. *International Urology and Nephrology, 2*7(3), pp. 231-243.

Kunz, J., Wilson, M.P., Kisseleva, M., Hurley, J.H., Majerus, P.W. and Anderson, R.A. (2000). The Activation Loop of Phosphatidylinositol Phosphate Kinases Determines Signalling Specificity. *Molecular Cell,* 5(1), pp.1–11.

Kuo, Y., Huang, K., Yang, C., Yang, Y., Lee, W. and Chiang, C. (2007). Regulation of Phosphorylation of Thr-308 of Akt, Cell Proliferation, and Survival by the B55α Regulatory Subunit Targeting of the Protein Phosphatase 2A Holoenzyme to Akt. *Journal of Biological Chemistry,* 283(4), pp. 1882-1892.

Kwabi-Addo, B., Giri, D., Schmidt, K., Podsypanina, K., Parsons, R., Greenberg, N. and Ittmann, M. (2001). Haploinsufficiency of the Pten tumor suppressor gene promotes prostate cancer progression. *Proceedings of the National Academy of Sciences,* 98(20), pp. 11563-11568.

Kwiatkowska, K. (2010). One lipid, multiple functions: how various pools of PI(4,5)P_2 are created in the plasma membrane. *Cellular and Molecular Life Sciences,* 67(23), pp.3927-3946.

Lacalle, R.A., de Karam, J.C., Martínez-Muñoz, L., Artetxe, I., Peregil, R.M, Sot, J., Rojas, A.M., Goñi, F.M, Mellado, M., and Mañes S. (2015) Type I phosphatidylinositol 4-phosphate 5-kinase homo- and heterodimerization determines its membrane localisation and activity. *FASEB Journal, 2*9(6), pp. 2371-2385.

Laffargue, M., Raynal, P., Yart, A., Peres, C., Wetzker, R., Roche, S., Payrastre, B. and Chap, H. (1999). An Epidermal Growth Factor Receptor/Gab1 Signalling Pathway Is Required for Activation of Phosphoinositide 3-Kinase by Lysophosphatidic Acid. *Journal of Biological Chemistry*, 274(46), pp.32835-32841.

Laplante, M. and Sabatini, D., (2009). mTOR signalling at aglance. *Journal of Cell Science*, 122 (20), pp. 3589-3594.

Larsson, P., Syed Khaja, A., Semenas, J., Wang, T., Sarwar, M., Dizeyi, N., Simoulis, A., Hedblom, A., Wai, S., Ødum, N. and Persson, J. (2019). The functional interlink between AR and MMP9/VEGF signalling axis is mediated through PIP5K1α/pAKT in prostate cancer. *International Journal of Cancer*, 146(6), pp.1686-1699.

Lawrence, M., Stephens, C., Need, E., Lai, J., Buchanan, G. and Clements, J. (2012). Long Terminal Repeats Act as Androgen-Responsive Enhancers for the PSA-Kallikrein Locus. *Endocrinology*, 153(7), pp.3199-3210.

Lee, J.K., Phillips, J.W., Smith, B.A., Park, J.W., Stoyanova, T., McCaffrey, E.F., Baertsch, R., Sokolov, A., Meyerowitz, J.G., Mathis, C., Cheng, D., Stuart, J.M., Shokat, K.M., Gustafson, W.C., Huang, J. and Witte, O.N. (2016). N-Myc Drives Neuroendocrine Prostate Cancer Initiated from Human Prostate Epithelial Cells. *Cancer Cell*, 29(4), pp.536–547.

Lemmon, M.A. (2003). Phosphoinositide Recognition Domains. *Traffic,* 4(4), pp.201–213.

Lempiäinen, H. and Halazonetis, T. (2009). Emerging common themes in regulation of PIKKs and PI3Ks. *The EMBO Journal*, 28(20), pp. 3067-3073.

Lenoir, M., Kufareva, I., Abagyan, R. and Overduin, M. (2015). Membrane and Protein Interactions of the Pleckstrin Homology Domain Superfamily*. Membranes,* 5(4), pp.646–663.

Levina, A., Fleming, K.D., Burke, J.E. and Leonard, T.A. (2022). Activation of the essential kinase PDK1 by phosphoinositide-driven trans-autophosphorylation. *Nature Communications*, 13(1).

Li, L., Han, J., Wang, Z., Liu, J., Wei, J., Xiong, S. and Zhao, Z., (2014). Mass Spectrometry Methodology in Lipid Analysis. *International Journal of Molecular Sciences*, 15(6), pp.10492-10507.

Li, X., Lau, A., Ng, A., Aldehaiman, A., Zhou, Y., Ng, P., Arold, S. and Cheung, L., (2021). Cancer-associated mutations in the p85α N-terminal SH2 domain activate a spectrum of receptor tyrosine kinases. *Proceedings of the National Academy of Sciences*, 118(37).

Li, X., Mak, V., Zhou, Y., Wang, C., Wong, E., Sharma, R., Lu, Y., Cheung, A., Mills, G. and Cheung, L., (2019). Deregulated Gab2 phosphorylation mediates aberrant AKT and STAT3 signalling uponPIK3R1 loss in ovarian cancer. *Nature Communications*, 10(1).

Li, Y. and Araki, H. (2013). Loading and activation of DNA replicative helicases: the key step of initiation of DNA replication. *Genes to Cells,* 18(4), pp.266–277.

Liao, Y., Smyth, G. and Shi, W. (2013). featureCounts: an efficient general purpose program for assigning sequence reads to genomic features. *Bioinformatics,* 30(7), pp. 923-930.

Liberzon, A., Birger, C., Thorvaldsdóttir, H., Ghandi, M., Mesirov, Jill P. and Tamayo, P. (2015). The Molecular Signatures Database Hallmark Gene Set Collection. *Cell Systems*, 1(6), pp.417–425.

Limatola, C., Schaap, D., Moolenaar, W.H. and van Blitterswijk, W.J. (1994). Phosphatidic acid activation of protein kinase C-ζ overexpressed in COS cells: comparison with other protein kinase C isotypes and other acidic lipids. *Biochemical Journal*, 304(3), pp.1001–1008.

Lin, H., Yeh, S., Kang, H. and Chang, C., (2001). Akt suppresses androgen-induced apoptosis by phosphorylating and inhibiting androgen receptor. *Proceedings of the National Academy of Sciences*, 98(13), pp.7200-7205.

Lin, Y., Yang, Z., Xu, A., Dong, P., Huang, Y., Liu, H., Li, F., Wang, H., Xu, Q., Wang, Y., Sun, D., Zou, Y., Zou, X., Wang, Y., Zhang, D., Liu, H., Wu, X., Zhang, M., Fu, Y., Cai, Z., Liu, C. and Wu, S., (2015). PIK3R1 negatively regulates the epithelial-mesenchymal transition and stem-like phenotype of renal cancer cells through the AKT/GSK3β/CTNNB1 signalling pathway. *Scientific Reports*, 5(1).

Ling, K., Schill, N., Wagoner, M., Sun, Y. and Anderson, R., (2006). Movin' on up: the role of PtdIns(4,5)P2 in cell migration. *Trends in Cell Biology*, 16(6), pp.276-284.

Lipp, P. and Reither, G. (2011). Protein Kinase C: The ‘Masters’ of Calcium and Lipid. *Cold Spring Harbor Perspectives in Biology*, 3(7), pp.a004556–a004556.

Liu, A., Sui, D., Wu, D. and Hu, J. (2016). The activation loop of PIP5K functions as a membrane sensor essential for lipid substrate processing. *Science Advances,* 2(11).

Liu, B., Linley, J., Du, X., Zhang, X., Ooi, L., Zhang, H. and Gamper, N., (2010). The acute nociceptive signals induced by bradykinin in rat sensory neurons are mediated by inhibition of M-type K+ channels and activation of Ca2+-activated Cl– channels. *Journal of Clinical Investigation*, 120(4), pp.1240-1252..

Liu, D., Song, H. and Xu, Y. (2009). A common gain of function of p53 cancer mutants in inducing genetic instability. *Oncogene,* 29(7) pp. 949-956.

Liu, M., Clarke, C., Salama, M., Choi, Y., Obeid, L. and Hannun, Y., (2017). Co-ordinated activation of classical and novel PKC isoforms is required for PMA-induced mTORC1 activation. *PLOS ONE*, 12(9), p.e0184818.

Liu, P., Gan, W., Chin, Y., Ogura, K., Guo, J., Zhang, J., Wang, B., Blenis, J., Cantley, L., Toker, A., Su, B. and Wei, W., (2015). PtdIns(3,4,5)P3-Dependent Activation of the mTORC2 Kinase Complex. *Cancer Discovery*, 5(11), pp. 1194-1209.

Liu, S., Knapp, S. and Ahmed, A., (2014). The Structural Basis of PI3K Cancer Mutations: From Mechanism to Therapy. *Cancer Research,* 74(3), pp. 641-646.

Livak, K.J. and Schmittgen, T.D. (2001). Analysis of Relative Gene Expression Data Using Real-Time Quantitative PCR and the 2−ΔΔCT Method. *Methods,* 25(4), pp.402–408.

Loijens, J., Boronenkov, I., Parker, G. and Anderson, R. (1996). The phosphatidylinositol 4-phosphate 5-kinase family. *Advances in Enzyme Regulation*, 36, pp.115-140.

Long, R., Morrissey, C., Fitzpatrick, J. and Watson, R. (2005). Prostate epithelial cell differentiation and its relevance to the understanding of prostate cancer therapies. *Clinical Science,* 108(1).

Love, M., Huber, W. and Anders, S., (2014). Moderated estimation of fold change and dispersion for RNA-seq data with DESeq2. *Genome Biology*, 15(12).

Lu, S., Jenster, G. and Epner, D., (2000). Androgen Induction of Cyclin-Dependent Kinase Inhibitor p21 Gene: Role of Androgen Receptor and Transcription Factor Sp1 Complex. *Molecular Endocrinology*, 14(5), pp.753-760**.**

Lu, S., Liu, M., Epner, D., Tsai, S. and Tsai, M., (1999). Androgen Regulation of the Cyclin-Dependent Kinase Inhibitor p21 Gene through an Androgen Response Element in the Proximal Promoter. *Molecular Endocrinology*, 13(3), pp.376-384.

Lukinavičius, G., Reymond, L., D'Este, E., Masharina, A., Göttfert, F., Ta, H., Güther, A., Fournier, M., Rizzo, S., Waldmann, H., Blaukopf, C., Sommer, C., Gerlich, D., Arndt, H., Hell, S. and Johnsson, K. (2014). Fluorogenic probes for live-cell imaging of the cytoskeleton. *Nature Methods*, 11(7), pp.731-733.

Lund, A.H., Duch, M. and Skou Pedersen, F. (1996). Increased Cloning Efficiency by Temperature-Cycle Ligation. *Nucleic Acids Research*. 24(4), pp.800–801.

Luo, J. (2016). Development of AR-V7 as a putative treatment selection marker for metastatic castration-resistant prostate cancer. *Asian Journal of Andrology*, 18(4), pp. 580-585.

Luo, J., Field, S.J., Lee, J.Y., Engelman, J.A. and Cantley, L.C. (2005). The p85 regulatory subunit of phosphoinositide 3-kinase down-regulates IRS-1 signalling via the formation of a sequestration complex. *Journal of Cell Biology*,170(3), pp.455–464.

Lv, J.-M., Chen, L., Gao, Y., Huang, H., Pan, X.-W., Liu, X., Chen, M., Qu, F.-J., Li, L., Wang, J.-K., Cui, X.-G. and XU, D.-F. (2018). PPP5C promotes cell proliferation and survival in human prostate cancer by regulating of the JNK and ERK1/2 phosphorylation. *OncoTargets and Therapy*, 11, pp.5797–5809.

Ma, X. and Blenis, J., (2009). Molecular mechanisms of mTOR-mediated translational control. *Nature Reviews Molecular Cell Biology*, 10(5) pp.307-318.

Macleod, K.F., Sherry, N., Hannon, G., Beach, D., Tokino, T., Kinzler, K., Vogelstein, B. and Jacks, T. (1995). p53-dependent and independent expression of p21 during cell growth, differentiation, and DNA damage. *Genes and Development*, 9(8), pp.935–944.

Madeira, F., Park, Y. M., Lee, J., Buso, N., Gur, T., Madhusoodanan, N., Basutkar, P., Tivey, A. R. N., Potter, S. C., Finn, R. D., and Lopez, R. (2019). The EMBL-EBI search and sequence analysis tools APIs in 2019. *Nucleic acids research,* 47(W1), pp. W636–W641.

Madsen, R., Vanhaesebroeck, B. and Semple, R. (2018). Cancer-Associated PIK3CA Mutations in Overgrowth Disorders. *Trends in Molecular Medicine,* 24(10), pp. 856-870.

Maestro, I., Boya, P. and Martinez, A., (2020). Serum- and glucocorticoid-induced kinase 1, a new therapeutic target for autophagy modulation in chronic diseases. *Expert Opinion on Therapeutic Targets*. 24(3), pp. 231-243.

Magnuson, B., Ekim, B. and Fingar, D., (2011). Regulation and function of ribosomal protein S6 kinase (S6K) within mTOR signalling networks. *Biochemical Journal*, 441(1).

Mahankali, M., Peng, H., Cox, D. and Gomez-Cambronero, J. (2011). The mechanism of cell membrane ruffling relies on a phospholipase D2 (PLD2), Grb2 and Rac2 association. *Cellular Signalling,* 23(8), pp. 1291-1298.

Malek, M., Kielkowska, A., Chessa, T., Anderson, K., Barneda, D., Pir, P., Nakanishi, H., Eguchi, S., Koizumi, A., Sasaki, J., Juvin, V., Kiselev, V., Niewczas, I., Gray, A., Valayer, A., Spensberger, D., Imbert, M., Felisbino, S., Habuchi, T., Beinke, S., Cosulich, S., Le Novère, N., Sasaki, T., Clark, J., Hawkins, P. and Stephens, L. (2017). PTEN Regulates PI(3,4)P_2 Signalling Downstream of Class I PI3K. *Molecular Cell*, 68(3), pp. 566-580.

Mandal, K., (2020). Review of PIP2 in Cellular Signalling, Functions and Diseases. *International Journal of Molecular Sciences*, 21(21), p.8342.

Mandel, A., Larsson, P., Sarwar, M., Semenas, J., Syed Khaja, A. and Persson, J. (2018). The interplay between AR, EGF receptor and MMP-9 signalling pathways in invasive prostate cancer. *Molecular Medicine,* 24(1).

Mandelker, D., Gabelli, S., Schmidt-Kittler, O., Zhu, J., Cheong, I., Huang, C., Kinzler, K., Vogelstein, B. and Amzel, L. (2009). A frequent kinase domain mutation that changes the interaction between PI3K and the membrane. *Proceedings of the National Academy of Sciences.* 106(40) pp.16996-17001.

Manning, G., Whyte, D. B., Martinez, R., Hunter, T., and Sudarsanam, S. (2002). The protein kinase complement of the human genome. *Science,* 298(5600), pp. 1912–1934.

Mao, Y. and Yin, H. (2007). Regulation of the actin cytoskeleton by phosphatidylinositol 4-phosphate 5 kinases. *Pflügers Archiv - European Journal of Physiology,* 455(1) pp. 5-18.

Martel, V., Racaud-Sultan, C., Dupe, S., Marie, C., Paulhe, F., Galmiche, A., Block, M.R. and Albiges-Rizo, C. (2001). Conformation, Localisation, and Integrin Binding of Talin Depend on Its Interaction with Phosphoinositides. *Journal of Biological Chemistry*, 276(24), pp.21217–21227.

Martelli, A., Evangelisti, C., Nyakern, M. and Manzoli, F. (2006). Nuclear protein kinase C. *Biochimica et Biophysica Acta (BBA).* Molecular and Cell Biology of Lipids. 1761 (5-6), pp. 542-551.

Martelli, A., Gilmour, R., Bertagnolo, V., Neri, L., Manzoli, L. and Cocco, L. (1992). Nuclear localisation and signalling activity of phosphoinositidase Cβ in Swiss 3T3 cells. *Nature,* 358(6383), pp.242-245.

Martin, D.M.A., Miranda-Saavedra, D. and Barton, G.J. (2009). Kinomer v. 1.0: a database of systematically classified eukaryotic protein kinases. *Nucleic Acids Research,* 37(Database), pp.D244–D250.

Massie, C., Lynch, A., Ramos-Montoya, A., Boren, J., Stark, R., Fazli, L., Warren, A., Scott, H., Madhu, B., Sharma, N., Bon, H., Zecchini, V., Smith, D., DeNicola, G., Mathews, N., Osborne, M., Hadfield, J., MacArthur, S., Adryan, B., Lyons, S., Brindle, K., Griffiths, J., Gleave, M., Rennie, P., Neal, D. and Mills, I. (2011). The androgen receptor fuels prostate cancer by regulating central metabolism and biosynthesis. *The EMBO Journal*, 30(13) pp. 2719-2733.

Masuda, K., Shima, H., Katagiri, C. and Kikuchi, K., 2003. Activation of ERK Induces Phosphorylation of MAPK Phosphatase-7, a JNK Specific Phosphatase, at Ser-446. *Journal of Biological Chemistry*, 278(34), pp.32448-32456.

Matheny, R. and Adamo, M. (2009). Current Perspectives on Akt Akt-ivation and Akt-ions. *Experimental Biology and Medicine,* 234(11), pp. 1264-1270.

Mauvais-Jarvis, F., Ueki, K., Fruman, D., Hirshman, M., Sakamoto, K., Goodyear, L., Iannacone, M., Accili, D., Cantley, L. and Kahn, R., (2002). Reduced expression of the murine p85alpha subunit of phosphoinositide 3-kinase improves insulin signalling and ameliorates diabetes. *The Journal of Clinical Investigation*, 109(1), pp.141-149.

McCall, P., Gemmell, L., Mukherjee, R., Bartlett, J. and Edwards, J., (2008). Phosphorylation of the androgen receptor is associated with reduced survival in hormone-refractory prostate cancer patients. *British Journal of Cancer*, 98(6), pp.1094-1101.

McNeill, D.R., Paramasivam, M., Baldwin, J., Huang, J., Vyjayanti, V.N., Seidman, M.M. and Wilson, D.M. (2013). NEIL1 Responds and Binds to Psoralen-induced DNA Interstrand Crosslinks. *Journal of Biological Chemistry*, 288(18), pp.12426–12436.

Mejillano, M., Yamamoto, M., Rozelle, A., Sun, H., Wang, X. and Yin, H., (2001). Regulation of Apoptosis by Phosphatidylinositol 4,5-Bisphosphate Inhibition of Caspases, and Caspase Inactivation of Phosphatidylinositol Phosphate 5-Kinases. *Journal of Biological Chemistry*, 276(3), pp.1865-1872.

Mellman, D., Gonzales, M., Song, C., Barlow, C., Wang, P., Kendziorski, C. and Anderson, R. (2008). A PtdIns4,5P2-regulated nuclear poly(A) polymerase controls expression of select mRNAs. *Nature,* 451(7181), pp.1013-1017.

Merrick, B.A., Phadke, D.P., Bostrom, M.A., Shah, R.R., Wright, G.M., Wang, X., Gordon, O., Pelch, K.E., Auerbach, S.S., Paules, R.S., DeVito, M.J., Waalkes, M.P. and Tokar, E.J. (2019). Arsenite malignantly transforms human prostate epithelial cells in vitro by gene amplification of mutated KRAS. *PLOS ONE*, 14(4).

Meshki, J., Caino, M., von Burstin, V., Griner, E. and Kazanietz, M., (2010). Regulation of Prostate Cancer Cell Survival by Protein Kinase C∈ Involves Bad Phosphorylation and Modulation of the TNFα/JNK Pathway. *Journal of Biological Chemistry*, 285(34), pp.26033-26040.

Metz, H.E. and McGarry Houghton, A. (2010). Insulin Receptor Substrate Regulation of Phosphoinositide 3-Kinase. *Clinical Cancer Research*, 17(2), pp.206–211.

Metzger, E., Willmann, D., McMillan, J., Forne, I., Metzger, P., Gerhardt, S., Petroll, K., von Maessenhausen, A., Urban, S., Schott, A.-K., Espejo, A., Eberlin, A., Wohlwend, D., Schüle, K.M., Schleicher, M., Perner, S., Bedford, M.T., Jung, M., Dengjel, J. and Flaig, R. (2016). Assembly of methylated KDM1A and CHD1 drives androgen receptor–dependent transcription and translocation. *Nature Structural and Molecular Biology*, 23(2), pp.132–139.

Miao, B., Skidan, I., Yang, J., Lugovskoy, A., Reibarkh, M., Long, K., Brazell, T., Durugkar, K., Maki, J., Ramana, C., Schaffhausen, B., Wagner, G., Torchilin, V., Yuan, J. and Degterev, A. (2010). Small molecule inhibition of phosphatidylinositol-3,4,5-triphosphate (PIP_3) binding to pleckstrin homology domains. *Proceedings of the National Academy of Sciences,* 107(46), pp. 20126-20131.

Milne, S., Ivanova, P., DeCamp, D., Hsueh, R. and Brown, H., (2005). A targeted mass spectrometric analysis of phosphatidylinositol phosphate species. *Journal of Lipid Research*, 46(8), pp.1796-1802.

Misteli, T., Cáceres, J. and Spector, D. (1997). The dynamics of a pre-mRNA splicing factor in living cells. *Nature,* 387(6632), pp.523-527.

Mohan, N., AP, S., Francis, N., Anderson, R. and Laishram, R. (2015). Phosphorylation regulates the Star-PAP-PIPKIα interaction and directs specificity toward mRNA targets. *Nucleic Acids Research*, 43(14), pp.7005-7020.

Mohler, J., Titus, M., Bai, S., Kennerley, B., Lih, F., Tomer, K. and Wilson, E. (2011). Activation of the Androgen Receptor by Intratumoral Bioconversion of Androstanediol to Dihydrotestosterone in Prostate Cancer. *Cancer Research,* 71(4), pp. 1486-1496.

Moritz, A., Westerman, J., de Graan, P. N., and Wirtz, K. W. (1992). Phosphatidylinositol 4-kinase and phosphatidylinositol-4-phosphate 5-kinase from bovine brain membranes. *Methods in Enzymology,* 209, pp. 202–211.

Mücksch, F., Citir, M., Lüchtenborg, C., Glass, B., Traynor-Kaplan, A., Schultz, C., Brügger, B. and Kräusslich, H., (2019). Quantification of phosphoinositides reveals strong enrichment of PIP2 in HIV-1 compared to producer cell membranes. *Scientific Reports*, 9(1).

Müller, G., Ayoub, M., Storz, P., Rennecke, J., Fabbro, D. and Pfizenmaier, K. (1995). PKC zeta is a molecular switch in signal transduction of TNF-alpha, bifunctionally regulated by ceramide and arachidonic acid. *The EMBO Journal*, 14(9), pp.1961–1969.

Munkley, J., Livermore, K.E., McClurg, U.L., Kalna, G., Knight, B., McCullagh, P., McGrath, J., Crundwell, M., Leung, H.Y., Robson, C.N., Harries, L.W., Rajan, P. and Elliott, D.J. (2015). The PI3K regulatory subunit gene PIK3R1 is under direct control of androgens and repressed in prostate cancer cells. *Oncoscience*, 2(9), pp.755–764.

Muscolini, M., Camperio, C., Porciello, N., Caristi, S., Capuano, C., Viola, A., Galandrini, R. and Tuosto, L. (2014). Phosphatidylinositol 4–Phosphate 5–Kinase α and Vav1 Mutual Cooperation in CD28-Mediated Actin Remodeling and Signalling Functions. *The Journal of Immunology*, 194(3), pp.1323-1333.

Nakanishi, H., Brewer, K. A., and Exton, J. H. (1993). Activation of the zeta isozyme of protein kinase C by phosphatidylinositol 3,4,5-trisphosphate. *The Journal of Biological Chemistry*, 268(1), 13–16.

Nariai, N., Kojima, K., Mimori, T., Sato, Y., Kawai, Y., Yamaguchi-Kabata, Y. and Nagasaki, M., (2014). TIGAR2: sensitive and accurate estimation of transcript isoform expression with longer RNA-Seq reads. *BMC Genomics*, 15(S10).

Narla, G., Sangodkar, J. and Ryder, C.B. (2018). THE IMPACT OF PHOSPHATASES ON PROLIFERATIVE AND SURVIVAL SIGNALLING
IN CANCER. *Cellular and Molecular Life Sciences,* 75(15), pp.2695–2718.

Nascimento, E., Snel, M., Guigas, B., van der Zon, G., Kriek, J., Maassen, J., Jazet, I., Diamant, M. and Ouwens, D., (2010). Phosphorylation of PRAS40 on Thr246 by PKB/AKT facilitates efficient phosphorylation of Ser183 by mTORC1. *Cellular Signalling*, 22(6) pp. 961-967.

Nickols, N., Nazarian, R., Zhao, S., Tan, V., Uzunangelov, V., Xia, Z., Baertsch, R., Neeman, E., Gao, A., Thomas, G., Howard, L., De Hoedt, A., Stuart, J., Goldstein, T., Chi, K., Gleave, M., Graff, J., Beer, T., Drake, J., Evans, C., Aggarwal, R., Foye, A., Feng, F., Small, E., Aronson, W., Freedland, S., Witte, O., Huang, J., Alumkal, J., Reiter, R. and Rettig, M. (2019). MEK-ERK signalling is a therapeutic target in metastatic castration resistant prostate cancer. *Prostate Cancer and Prostatic Diseases,* 22(4) pp,531-538

Nicotera, T., Schuster, D., Bourhim, M., Chadha, K., Klaich, G. and Corral, D. (2009). Regulation of PSA secretion and survival signallingby calcium-independent phopholipase A2β in prostate cancer cells. *The Prostate,* 69(12), pp. 1270-1280.

Niculescu, A.B., Chen, X., Smeets, M., Hengst, L., Prives, C. and Reed, S.I. (1998). Effects of p21 /Cip1/Waf1 at Both the G1/S and the G2 /M Cell Cycle Transitions: pRb Is a Critical Determinant in Blocking DNA Replication and in Preventing Endoreduplication. *Molecular and Cellular Biology*, 18(1), pp.629–643.

Niemira, M., Borowa-Mazgaj, B., Bader, S.B., Moszyńska, A., Ratajewski, M., Karaś, K., Kwaśniewski, M., Krętowski, A., Mazerska,Z., Hammond, E.M. and Skwarska, A. (2020). Anticancer Imidazoacridinone C-1311 is Effective in Androgen-Dependent and Androgen-Independent Prostate Cancer Cells. *Biomedicines*, 8(9).

Ninomiya, S., Kawahara, T., Iwashita, H., Iwamoto, G., Takamoto, D., Mochizuki, T., Kuroda, S., Takeshima, T., Izumi, K., Teranishi, J., Yumura, Y., Miyoshi, Y., Asai, T. and Uemura, H. (2018). Prostate Basal Cell Carcinoma: A Case Report. *Case Reports in Oncology*, 11(1), pp. 138-142.

Niu, Y., Wang, K., Xing, N., Fan, D. and Jin, S. (2014). Differential expression of 5-alpha reductase isozymes in the prostate and its clinical implications. *Asian Journal of Andrology,*16(2) pp. 274-279

Oancea, E., Bezzerides, V., Greka, A. and Clapham, D., (2003). Mechanism of Persistent Protein Kinase D1 Translocation and Activation. *Developmental Cell*, 4(4), pp.561-574.

Oancea, E., Teruel, M., Quest, A. and Meyer, T. (1998). Green Fluorescent Protein (GFP)-tagged Cysteine-rich Domains from Protein Kinase C as Fluorescent Indicators for Diacylglycerol Signalling in Living Cells. *Journal of Cell Biology*. 140(3), pp.485-498.

Oh, S. (2014). Disturbance in Testosterone Production in Leydig Cells by Polycyclic Aromatic Hydrocarbons. *Development and Reproduction,* 18(4), pp. 187-195.

Ohashi, Y., Tremel, S. and Williams, R.L. (2019). VPS34 complexes from a structural perspective. *Journal of Lipid Research*, 60(2), pp.229–241.

Okano, J., Gaslightwala, I., Birnbaum, M., Rustgi, A. and Nakagawa, H. (2000). Akt/Protein Kinase B Isoforms Are Differentially Regulated by Epidermal Growth Factor Stimulation. *Journal of Biological Chemistry,* 275(40), pp. 30934-30942.

Oliveros, J.C. (2007-2015). Venny. An interactive tool for comparing lists with Venn's diagrams. https://bioinfogp.cnb.csic.es/tools/venny/index.html

Olsen, J., Azeem, W., Hellem, M., Marvyin, K., Hua, Y., Qu, Y., Li, L., Lin, B., Ke, X., Øyan, A. and Kalland, K., (2016). Context dependent regulatory patterns of the androgen receptor and androgen receptor target genes. *BMC Cancer*, 16(1).

Olsen, J.V., Blagoev, B., Gnad, F., Macek, B., Kumar, C., Mortensen, P. and Mann, M. (2006). Global, In Vivo, and Site-Specific Phosphorylation Dynamics in Signalling Networks. *Cell,* 127(3),pp.635–648.

Packer, J. and Maitland, N. (2016). The molecular and cellular origin of human prostate cancer. *Biochimica et Biophysica Acta (BBA) - Molecular Cell Research,* 1863(6), pp. 1238-1260.

Pacold, M.E., Suire, S., Perisic, O., Lara-Gonzalez, S., Davis, C.T., Walker, E.H., Hawkins, P.T., Stephens, L., Eccleston, J.F. and Williams, R.L. (2000). Crystal Structure and Functional Analysis of Ras Binding to Its Effector Phosphoinositide 3-Kinase γ. *Cell*, 103(6), pp.931–944.

Pal Singh, S., Dammeijer, F. and Hendriks, R., (2018). Role of Bruton's tyrosine kinase in B cells and malignancies. *Molecular Cancer*, 17(1).

Pan, C., Jin, X., Zhao, Y., Pan, Y., Yang, J., Karnes, R.J., Zhang, J., Wang, L. and Huang, H. (2017). AKT-phosphorylated FOXO1 suppresses ERK activation and chemoresistance by disrupting IQGAP1-MAPK interaction. *The EMBO Journal*, 36(8), pp.995–1010.

Pandey, P., Seshacharyulu, P., Das, S., Rachagani, S., Ponnusamy, M., Yan, Y., Johansson, S., Datta, K., Fong Lin, M. and Batra, S. (2013). Impaired expression of protein phosphatase 2A subunits enhances metastatic potential of human prostate cancer cells through activation of AKT pathway. *British Journal of Cancer,* 108(12), pp. 2590-2600.

Park, J., Buse, P., Maiyar, A., Firestone, G. and Hemmings, B., (1999). Serum and glucocorticoid-inducible kinase (SGK) is a target of the PI 3-kinase-stimulated signalling pathway. *The EMBO Journal*, 18(11)pp.3024-3033.

Park, S., Kim, Y., Kim, D., So, I. and Jeon, J. (2018). PI3K pathway in prostate cancer: All resistant roads lead to PI3K. *Biochimica et Biophysica Acta (BBA) - Reviews on Cancer*. 1870(2): 198-206.

Park, S.J., Itoh, T. and Takenawa, T. (2001). Phosphatidylinositol 4-Phosphate 5-Kinase Type I Is Regulated through Phosphorylation Response by Extracellular Stimuli. *Journal of Biological Chemistry*, 276(7), pp.4781–4787.

Pearce, L., Komander, D. and Alessi, D., (2010). The nuts and bolts of AGC protein kinases. *Nature Reviews Molecular Cell Biology*, 11(1) pp. 9-22.

Peehl, DM (2001). Basic science of hormonal therapy for prostate cancer. *Reviews in Urology,* 3(S3) pp. 15-22.

Peng, W., Feng, H., Pang, L., Zhang, J., Hao, Y., Wei, X., Xia, Q., Wei, Z., Song, W., Wang, S., Liu, J., Chen, K. and Wang, T. (2023). Downregulation of CAMK2N1 due to DNA Hypermethylation Mediated by DNMT1 that Promotes the Progression of Prostate Cancer. *Journal of Oncology,* 2023, pp.1–15.

Perier, R., Praz, V., Junier, T., Bonnard, C. and Bucher, P., (2000). The Eukaryotic Promoter Database (EPD). *Nucleic Acids Research*, 28(1), pp.302-303.

Pernar, C.H., Ebot, E.M., Wilson, K.M. and Mucci, L.A. (2018). The Epidemiology of Prostate Cancer. Cold Spring Harbor Perspectives in Medicine, 8(12), p.a030361.

Peters, R., Liao, S. and Maniatis, T., (2000). IKKε Is Part of a Novel PMA-Inducible IκB Kinase Complex. *Molecular Cell*, 5(3), pp.513-522.

Pettitt, T., Dove, S., Lubben, A., Calaminus, S. and Wakelam, M., (2006). Analysis of intact phosphoinositides in biological samples. *Journal of Lipid Research*, 47(7), pp.1588-1596.

Pfitzenmaier, J., Quinn, J.E., Odman, A.M., Zhang, J., Keller, E.T., Vessella, R.L. and Corey, E. (2003). Characterization of C4-2 Prostate Cancer Bone Metastases and Their Response to Castration. *Journal of Bone and Mineral Research*, 18(10), pp.1882–1888.

Phin, S., Moore, M. and Cotter, P. (2013). Genomic Rearrangements of PTEN in Prostate Cancer. *Frontiers in Oncology,* 3.

Piccione, E., Case, R.D., Domchek, S.M., Hu, P., Chaudhuri, M., Backer, J.M., Schlessinger, J. and Shoelson, S.E. (1993). Phosphatidylinositol 3-kinase p85 SH2 domain specificity defined by direct phosphopeptide/SH2 domain binding. *Biochemistry*, 32(13), pp.3197–3202.

Pilgrim, C., McCahill, K., Rops, J., Dufour, J., Russell, K. and Koch, T., (2022). A Review of Fetal Bovine Serum in the Culture of Mesenchymal Stromal Cells and Potential Alternatives for Veterinary Medicine. *Frontiers in Veterinary Science*, 9.

Podhorecka, M., Skladanowski, A. and Bozko, P., (2010). H2AX Phosphorylation: Its Role in DNA Damage Response and Cancer Therapy. *Journal of Nucleic Acids*, 2010, pp.1-9.

Porciello, N., Kunkl, M., Viola, A. and Tuosto, L. (2016). Phosphatidylinositol 4-Phosphate 5-Kinases in the Regulation of T Cell Activation. *Frontiers in Immunology,* 7.

Potter, C.J., Pedraza, L.G. and Xu, T. (2002). Akt regulates growth by directly phosphorylating Tsc2. *Nature Cell Biology*, 4(9), pp.658–665.

Qin, X., Jiang, B. and Zhang, Y. (2016). 4E-BP1, a multifactor regulated multifunctional protein. *Cell Cycle*, 15(6) pp.781-786.

Qiu, Y. and Kung, H. (2000). Signalling network of the Btk familykinases. *Oncogene*, 19(49), pp. 5651-5661.

Quinn, K., Behe, P. and Tinker, A. (2008). Monitoring changes in membrane phosphatidylinositol 4,5-bisphosphate in living cells using a domain from the transcription factor tubby. *The Journal of Physiology*, 586(12), pp.2855-2871.

Rada, M., Barlev, N. and Macip, S. (2018). BTK: a two-faced effector in cancer and tumour suppression. *Cell Death and Disease*, 9(11).

Ran, F., Hsu, P., Lin, C., Gootenberg, J., Konermann, S., Trevino, A., Scott, D., Inoue, A., Matoba, S., Zhang, Y. and Zhang, F. (2013). Double Nicking by RNA-Guided CRISPR Cas9 for Enhanced Genome Editing Specificity. *Cell*, 154(6): 1380-1389.

Rao, M., Van Vleet, T., Ciurlionis, R., Buck, W., Mittelstadt, S., Blomme, E. and Liguori, M. (2019). Comparison of RNA-Seq and Microarray Gene Expression Platforms for the Toxicogenomic Evaluation of Liver From Short-Term Rat Toxicity Studies. *Frontiers in Genetics*, 9.

Rathinaswamy, M.K., Dalwadi, U., Fleming, K.D., Adams, C., Stariha, J.T.B., Pardon, E., Baek, M., Vadas, O., DiMaio, F., Steyaert, J., Hansen, S.D., Yip, C.K. and Burke, J.E. (2021). Structure of the phosphoinositide 3-kinase (PI3K) p110γ-p101 complex reveals molecular mechanism of GPCR activation. *Science Advances*, 7(35).

Rawla, P. (2019). Epidemiology of Prostate Cancer. *World Journal of Oncology*, 10(2), pp.63–89.

Reif, K., Okkenhaug, K., Sasaki, T., Penninger, J.M., Vanhaesebroeck, B. and Cyster, J.G. (2004). Cutting Edge: Differential Roles for Phosphoinositide 3-Kinases, p110γ and p110δ, in Lymphocyte Chemotaxis and Homing. *The Journal of Immunology*, 173(4), pp.2236–2240.

Ridley, A., Paterson, H., Johnston, C., Diekmann, D. and Hall, A. (1992). The small GTP-binding protein rac regulates growth factor-induced membrane ruffling. *Cell*, 70(3), pp. 401-410.

Ritchie, M., Phipson, B., Wu, D., Hu, Y., Law, C., Shi, W. and Smyth, G. (2015). limma powers differential expression analyses for RNA-sequencing and microarray studies. *Nucleic Acids Research*, 43(7), pp.e47-e47.

Roberts, C. (2022). 'Characterisation of alternative splice variants of PIP5K1A in the human metastatic prostate cancer cell line, LNCaP C4-2,' PhD thesis, University of Nottingham.

Robinson, D., Van Allen, E., Wu, Y., Schultz, N., Lonigro, R., Mosquera, J., Montgomery, B., Taplin, M., Pritchard, C., Attard, G., Beltran, H., Abida, W., Bradley, R., Vinson, J., Cao, X., Vats, P., Kunju, L., Hussain, M., Feng, F., Tomlins, S., Cooney, K., Smith, D., Brennan, C., Siddiqui, J., Mehra, R., Chen, Y., Rathkopf, D., Morris, M., Solomon, S., Durack, J., Reuter, V., Gopalan, A., Gao, J., Loda, M., Lis, R., Bowden, M., Balk, S., Gaviola, G., Sougnez, C., Gupta, M., Yu, E., Mostaghel, E., Cheng, H., Mulcahy, H., True, L., Plymate, S., Dvinge, H., Ferraldeschi, R., Flohr, P., Miranda, S., Zafeiriou, Z., Tunariu, N., Mateo, J., Perez-Lopez, R., Demichelis, F., Robinson, B., Schiffman, M., Nanus, D., Tagawa, S., Sigaras, A., Eng, K., Elemento, O., Sboner, A., Heath, E., Scher, H., Pienta, K., Kantoff, P., de Bono, J., Rubin, M., Nelson, P., Garraway, L., Sawyers, C. and Chinnaiyan, A. (2015). Integrative Clinical Genomics of Advanced Prostate Cancer. *Cell,* 161(5), pp. 1215-1228.

Robinson, M., McCarthy, D. and Smyth, G.(2009). edgeR: a Bioconductor package for differential expression analysis of digital gene expression data. *Bioinformatics*, 26(1), pp. 139-140.

Rodriguez-Viciana, P., Warne, P., Dhand, R., Vanhaesebroeck, B., Gout, I., Fry, M., Waterfield, M. and Downward, J., (1994). Phosphatidylinositol-3-OH kinase direct target of Ras. *Nature*, 370(6490), pp.527-532.

Romanuik, T.L., Wang, G., Holt, R.A., Jones, S.J., Marra, M.A. and Sadar, M.D. (2009). Identification of novel androgen-responsive genes by sequencing of LongSAGE libraries. *BMC Genomics,* 10(1).

Roskoski, R. (2016). Classification of small molecule protein kinase inhibitors based upon the structures of their drug-enzyme complexes. *Pharmacological Research,* 103, pp.26–48.

Rostislavleva, K., Soler, N., Ohashi, Y., Zhang, L., Pardon, E., Burke, J.E., Masson, G.R., Johnson, C., Steyaert, J., Ktistakis, N.T. and Williams, R.L. (2015). Structure and flexibility of the endosomal Vps34 complex reveals the basis of its function on membranes. *Science*, 350(6257).

Roussev, B., Kosev, P., Hinev, A. and Galunska, B. (2016). Correlation between serum testosterone, biochemical and clinical markers in prostate cancer patients. *Journal of IMAB - Annual Proceeding (Scientific Papers),* 22(3), pp. 1314-1319.

Roux, P., Ballif, B., Anjum, R., Gygi, S. and Blenis, J. (2004). Tumor-promoting phorbol esters and activated Ras inactivate the tuberous sclerosis tumor suppressor complex via p90 ribosomal S6 kinase. *Proceedings of the National Academy of Sciences*, 101(37), pp.13489-13494.

Roy, A. and Levine, T. (2004). Multiple Pools of Phosphatidylinositol 4-Phosphate Detected Using the Pleckstrin Homology Domain of Osh2p. *Journal of Biological Chemistry*, 279(43), pp.44683-44689.

Saarikangas, J., Zhao, H. and Lappalainen, P. (2010). Regulation of the Actin Cytoskeleton-Plasma Membrane Interplay by Phosphoinositides. *Physiological Reviews*, 90(1), pp.259-289.

Sahlberg, S., Gustafsson, A., Pendekanti, P., Glimelius, B. and Stenerlöw, B. (2013). The influence of AKT isoforms on radiation sensitivity and DNA repair in colon cancer cell lines. *Tumor Biology,* 35(4) pp. 3525-3534.

Saito, K., Scharenberg, A. and Kinet, J. (2001). Interaction between the Btk PH Domain and Phosphatidylinositol-3,4,5-trisphosphate Directly Regulates Btk. *Journal of Biological Chemistry*, 276(19), pp. 16201-16206.

Saito, N. and Shirai, Y. (2002). Protein Kinase C (PKC): Function of Neuron Specific Isotype. *Journal of Biochemistry*, 132(5), pp.683-687.

Sakoda, H., Gotoh, Y., Katagiri, H., Kurokawa, M., Ono, H., Onishi, Y., Anai, M., Ogihara, T., Fujishiro, M., Fukushima, Y., Abe, M., Shojima, N., Kikuchi, M., Oka, Y., Hirai, H. and Asano, T., (2003). Differing Rolesof Akt and Serum- and Glucocorticoid-regulated Kinase in Glucose Metabolism, DNA Synthesis, and Oncogenic Activity. *Journal of Biological Chemistry*, 278(28), pp.25802-25807.

Sancak, Y., Thoreen, C., Peterson, T., Lindquist, R., Kang, S., Spooner, E., Carr, S. and Sabatini, D. (2007). PRAS40 Is an Insulin-Regulated Inhibitor of the mTORC1 Protein Kinase, *Molecular Cell*, 25(6), pp.903-915.

Sanmukh, S. and Felisbino, S. (2018). Development of pipette tip gap closure migration assay (s-ARU method) for studying semi-adherent cell lines. *Cytotechnology*, 70(6), pp.1685-1695.

Santos, M., Naal, R., Baird, B. and Holowka, D. (2013). Inhibitors of $PI(4,5)P_2$ Synthesis Reveal Dynamic Regulation of IgE Receptor Signalling by Phosphoinositides in RBL Mast Cells. *Molecular Pharmacology*, 83(4), pp.793-804.

Sarbassov, D., Guertin, D., Ali, S. and Sabatini, D. (2005). Phosphorylation and Regulation of Akt/PKB by the Rictor-mTOR Complex. *Science,* 307(5712), pp.1098-1101.

Sarni, D. and Kerem, B. (2017). Oncogene-Induced Replication Stress Drives Genome Instability and Tumorigenesis. *International Journal of Molecular Sciences*, 18(7), p.1339.

Sarwar, M., Semenas, J., Miftakhova, R., Simoulis, A., Robinson, B., Wingren, A., Mongan, N., Heery, D., Johnsson, H., Abrahamsson, P., Dizeyi, N., Luo, J. and Persson, J. (2016). Targeted suppression of AR-V7 using PIP5K1A; inhibitor overcomes enzalutamide resistance in prostate cancer cells. *Oncotarget,* 7(39).

Sarwar, M., Syed Khaja, A.S., Aleskandarany, M., Karlsson, R., Althobiti, M., Ødum, N., Mongan, N.P., Dizeyi, N., Johnson, H., Green, A.R., Ellis, I.O., Rakha, E.A. and Persson, J.L. (2018). The role of PIP5K1α/pAKT and targeted inhibition of growth of subtypes of breast cancer using PIP5K1α inhibitor. *Oncogene,* 38(3), pp.375–389.

Sattler, M., Salgia, R., Shrikhande, G., Verma, S., Pisick, E., Prasad, K.V.S. and Griffin, J.D. (1997). Steel Factor Induces Tyrosine Phosphorylation of CRKL and Binding of CRKL to a Complex Containing c-Kit, Phosphatidylinositol 3-Kinase, and p120CBL. *Journal of Biological Chemistry*, 272(15), pp.10248–10253.

Saxena, A., Morozov, P., Frank, D., Musalo, R., Lemmon, M., Skolnik, E. and Tycko, B. (2002). Phosphoinositide Binding by the Pleckstrin Homology Domains of Ipl and Tih1. *Journal of Biological Chemistry*, 277(51), pp.49935-49944.

Saxena, P., Trerotola, M., Wang, T., Li, J., Sayeed, A., VanOudenhove, J., Adams, D., FitzGerald, T., Altieri, D. and Languino, L. (2011). PSA regulates androgen receptor expression in prostate cancer cells. *The Prostate,* 72(7), pp. 769-776.

Saxton, R. and Sabatini, D. (2017). mTOR Signalling in Growth,Metabolism, and Disease. *Cell*, 168(6), pp. 960-976.

Schmid, K., Helpap, B., Tötsch, M., Kirchmair, R., Dockhorn-Dworniczak, B., Böcker, W. and Fischer-Colbrie, R. (1994). Immunohistochemical localisation of chromogranins A and B and secretogranin II in normal, hyperplastic and neoplastic prostate. *Histopathology,* 24(3):233-239.

Schmitt, J.M., Smith, S., Hart, B. and Fletcher, L. (2011). CaM Kinase control of AKT and LNCaP cell survival. *Journal of Cellular Biochemistry*, 113(5), pp. 1514-1526

Schmitz-Elbers, M., Lukinavičius, G. and Smit, T. (2021). Live Fluorescence Imaging of F-Actin Organization in Chick Whole Embryo Cultures Using SiR-Actin. *Cells*, 10(7), p.1578.

Schneider, C.A., Rasband, W.S. and Eliceiri, K.W. (2012). NIH Image to ImageJ: 25 years of image analysis. *Nature Methods*, 9(7), pp.671–675.

Schoebel, S., Blankenfeldt, W., Goody, R. and Itzen, A. (2010). High-affinity binding of phosphatidylinositol 4-phosphate by Legionella pneumophila DrrA. *EMBO reports*, 11(8), pp.598-604.

Semenas, J., Hedblom, A., Miftakhova, R., Sarwar, M., Larsson, R., Shcherbina, L., Johansson, M., Harkonen, P., Sterner, O. and Persson, J. (2014). The role of PI3K/AKT-related PIP5K1α and the discovery of its selective inhibitor for treatment of advanced prostate cancer. *Proceedings of the National Academy of Sciences*, 111(35), pp.3689-3698

Semenas, J., Wang, T., Sajid Syed Khaja, A., Firoj Mahmud, A., Simoulis, A., Grundström, T., Fällman, M. and Persson, J., (2020). Targeted inhibition of ERα signalling and PIP5K1α/Akt pathways incastration-resistant prostate cancer. *Molecular Oncology*, 15(4), pp.968-986.

Shambharkar, P., Blonska, M., Pappu, B., Li, H., You, Y., Sakurai, H., Darnay, B., Hara, H., Penninger, J. and Lin, X., 2007. Phosphorylation and ubiquitination of the IκB kinase complex by two distinct signalling pathways. *The EMBO Journal*, 26(7), pp.1794-1805.

Sharifi, N., Gulley, J. and Dahut, W. (2005). Androgen Deprivation Therapy for Prostate Cancer. *JAMA.* 294(2), pp.238-244

Sharp, A., Coleman, I., Yuan, W., Sprenger, C., Dolling, D., Rodrigues, D., Russo, J., Figueiredo, I., Bertan, C., Seed, G., Riisnaes, R., Uo, T., Neeb, A., Welti, J., Morrissey, C., Carreira, S., Luo, J., Nelson, P., Balk, S., True, L., de Bono, J. and Plymate, S. (2019). Androgen receptor splice variant-7 expression emerges with castration resistance in prostate cancer. *Journal of Clinical Investigation,* 129(1), pp. 192-208.

Shaw, R. (2008). Raptor Swoops in on Metabolism. *Cell Metabolism*, 8(5), pp. 343-344.

Sheppard, H.M., Harries, J.C., Hussain, S., Bevan, C. and Heery, D.M. (2001). Analysis of the Steroid Receptor Coactivator 1 (SRC1)-CREB Binding Protein Interaction Interface and Its Importance for the Function of SRC1. *Molecular and Cellular Biology,* 21(1), pp.39–50.

Shiota, M., Yokomizo, A., Takeuchi, A., Imada, K., Kashiwagi, E., Song, Y., Inokuchi, J., Tatsugami, K., Uchiumi, T. and Naito, S. (2013). Inhibition of Protein Kinase C/Twist1 Signalling Augments Anticancer Effects of Androgen Deprivation and Enzalutamide in Prostate Cancer. *Clinical Cancer Research*, 20(4), pp.951–961.

Shiota, M., Yokomizo, A., Takeuchi, A., Kashiwagi, E., Dejima, T., Inokuchi, J., Tatsugami, K., Uchiumi, T. and Eto, M. (2017). Protein kinase C regulates Twist1 expression via NF-κB in prostate cancer. *Endocrine-Related Cancer*, 24(4), pp.171–180.

Shipitsin, M., Small, C., Giladi, E., Siddiqui, S., Choudhury, S., Hussain, S., Huang, Y., Chang, H., Rimm, D., Berman, D., Nifong, T. and Blume-Jensen, P., (2014). Automated quantitative multiplex immunofluorescence in situ imaging identifies phospho-S6 and phospho-PRAS40 as predictive protein biomarkers for prostate cancer lethality. *Proteome Science*, 12(40).

Simonsen, A. and Stenmark, H. (2001). PX domains: attracted by phosphoinositides. *Nature Cell Biology*, 3(8), pp.E179–E181.

Smyth, G. (2005). limma: Linear Models for Microarray Data. *Bioinformatics and Computational Biology Solutions Using R and Bioconductor*, pp.397-420.

Songyang, Z., Shoelson, S., Chaudhurl, M., Gish, G., Pawson, T., Hasser, W., King, F., Ratnofsky, S., Lechleider, R., Neel, B., Birge, R., Fajardo, J., Choi, M., Hanafusa, H., Schaffhausen, B. and Cantley, L. (1993). SH2 domains recognize specific phosphopeptide sequences. *Cell*, 72(5), pp.767-778.

Stahelin, R.V. (2008). Lipid binding domains: more than simple lipid effectors. *Journal of Lipid Research*, 50 (Supplement), pp.S299–S304.

Stallings, J., Tall, E., Pentyala, S. and Rebecchi, M. (2005). Nuclear Translocation of Phospholipase C-δ1Is Linked to the Cell Cycle and Nuclear Phosphatidylinositol 4,5-Bisphosphate. *Journal of Biological Chemistry,* 280(23), pp.22060-22069.

Stebbing, J., Lit, L.C., Zhang, H., Darrington, R.S., Melaiu, O., Rudraraju, B. and Giamas, G. (2014). The regulatory roles of phosphatases in cancer. *Oncogene*, 33(8), pp.939–953.

Stein, C., Hansen, J., Lai, J., Wu, S., Voskresenskiy, A., HØg, A., Worm, J., Hedtjärn, M., Souleimanian, N., Miller, P., Soifer, H., Castanotto, D., Benimetskaya, L., Ørum, H. and Koch, T. (2009). Efficient gene silencing by delivery of locked nucleic acid antisense oligonucleotides, unassisted by transfection reagents. *Nucleic Acids Research*, 38(1), pp.e3-e3.

Stephens, L. and Hawkins, P. (2013). More Paths to PI3Kγ. *PLoS Biology*, 11(6), p.e1001594.

Stoyanova, T., Cooper, A., Drake, J., Liu, X., Armstrong, A., Pienta, K., Zhang, H., Kohn, D., Huang, J., Witte, O. and Goldstein, A. (2013). Prostate cancer originating in basal cells progresses to adenocarcinoma propagated by luminal-like cells. *Proceedings of the National Academy of Sciences,* 110(50), pp. 20111-20116.

Stronach, E., Chen, M., Maginn, E., Agarwal, R., Mills, G., Wasan, H. and Gabra, H. (2011). DNA-PK Mediates AKT Activation and Apoptosis Inhibition in Clinically Acquired Platinum Resistance. *Neoplasia,* 13(11) pp. 1069-1080.

Stuttfeld, E., Aylett, C., Imseng, S., Boehringer, D., Scaiola, A., Sauer, E., Hall, M., Maier, T. and Ban, N., (2018). Architecture of the human mTORC2 core complex. *eLife*, 7.

Su, B. and Jacinto, E. (2011). Mammalian TOR signalling to the AGC kinases. *Critical Reviews In Biochemistry And Molecular Biology*, 46(6), pp.527–547.

Subramanian, A., Tamayo, P., Mootha, V., Mukherjee, S., Ebert, B., Gillette, M., Paulovich, A., Pomeroy, S., Golub, T., Lander, E. and Mesirov, J., (2005). Gene set enrichment analysis: A knowledge-based approach for interpreting genome-wide expression profiles. *Proceedings of the National Academy of Sciences*. 102(43), pp. 5545-15550.

Sui, Y., Yang, Y., Wang, J., Li, Y., Ma, H., Cai, H., Liu, X., Zhang, Y., Wang, S., Li, Z., Zhang, X., Wang, J., Liu, R., Yan, Y., Xue, C., Shi, X., Tan, L. and Ren, J., (2015). Lysophosphatidic Acid Inhibits Apoptosis Induced by Cisplatin in Cervical Cancer Cells. *BioMed Research International*, 2015, pp.1-12.

Suire, S., Hawkins, P. and Stephens, L. (2002). Activation of Phosphoinositide 3-Kinase γ by Ras. *Current Biology*, 12(13), pp.1068–1075.

Sun, Y., Ling, K., Wagoner, M. and Anderson, R. (2007). Type Iγ phosphatidylinositol phosphate kinase is required for EGF-stimulated directional cell migration. *Journal of Cell Biology*, 178(2), pp.297-308.

Sun, M., Zhang, C., Sui, D., Yang, C., Dohun Pyeon, Huang, X. and Hu, J. (2022). Rational Design and Synthesis of D-galactosyl Lysophospholipids as Selective Substrates and non-ATP-competitive Inhibitors of Phosphatidylinositol Phosphate Kinases. *Chemistry – A European Journal,* 29(2).

Suzuki, H., Freije, D., Nusskern, DR., Okami, K., Cairns, P., Sidransky, D., Isaacs WB. and Bova GS (1998). Interfocal heterogeneity of PTEN/MMAC1 gene alterations in multiple metastatic prostate cancer tissues. *Cancer Research,* 58(2), pp. 204-209.

Szabolcs, M., Keniry, M., Simpson, L., Reid, L., Koujak, S., Schiff, S., Davidian, G., Licata, S., Gruvberger-Saal, S., Murty, V., Nandula, S., Efstratiadis, A., Kushner, J., White, M. and Parsons, R. (2009). Irs2 Inactivation Suppresses Tumor Progression in Pten+/− Mice. *The American Journal of Pathology*, 174(1), pp. 276-286.

Szczyrba, J., Niesen, A., Wagner, M., Wandernoth, P., Aumüller, G. and Wennemuth, G. (2016). Neuroendocrine Cells of the Prostate Derive from the Neural Crest. *Journal of Biological Chemistry,* 292(5), pp. 2021-2031.

Szentpetery, Z., Balla, A., Kim, Y., Lemmon, M. and Balla, T., 2009. Live cell imaging with protein domains capable of recognizing phosphatidylinositol 4,5-bisphosphate; a comparative study. *BMC Cell Biology*, 10(1).

T., Waldman, T., Kinzler, K.W. and Vogelstein, B. (1995) p21 is necessary for the p53-mediated G1 arrest in human cancer cells. *Cancer Research* , 55(22), pp.5187-5190

Tang, Q., Cheng, B., Dai, R. and Wang, R. (2021). The Role of Androgen Receptor in Cross Talk Between Stromal Cells and Prostate Cancer Epithelial Cells. *Frontiers in Cell and Developmental Biology*, 9.

Taniguchi, C., Winnay, J., Kondo, T., Bronson, R., Guimaraes, A., Alemán, J., Luo, J., Stephanopoulos, G., Weissleder, R., Cantley, L. and Kahn, C., (2010). The Phosphoinositide 3-Kinase Regulatory Subunit p85α Can Exert Tumor Suppressor Properties through Negative Regulation of Growth Factor Signalling. *Cancer Research*, 70(13), pp.5305-5315.

Tararova, N.D., Narizhneva, N., Krivokrisenko, V., Gudkov, A.V. and Gurova, K.V. (2007). Prostate cancer cells tolerate a narrow range of androgen receptor expression and activity. *The Prostate*, 67(16), pp.1801–1815. doi:https://doi.org/10.1002/pros.20662.

Tcherkezian, J. and Lamarche-Vane, N. (2007). Current knowledge ofthe large RhoGAP family of proteins. *Biology of the Cell*, 99(2), pp.67–86.

Tenbaum, S., Ordóñez-Morán, P., Puig, I., Chicote, I., Arqués, O., Landolfi, S., Fernández, Y., Herance, J., Gispert, J., Mendizabal, L., Aguilar, S., Cajal, S., Schwartz, S., Vivancos, A., Espín, E., Rojas, S., Baselga, J., Tabernero, J., Muñoz, A. and Palmer, H., (2012). β-catenin confers resistance to PI3K and AKT inhibitors and subverts FOXO3a to promote metastasis in colon cancer. *Nature Medicine*, 18(6), pp.892-901.

Tepaamorndech, S., Huang, L. and Kirschke, C. (2011). A null-mutation in the Znt7 gene accelerates prostate tumor formation in a transgenic adenocarcinoma mouse prostate model. *Cancer Letters,* 308(1), pp. 33-42.

Terauchi, Y., Tsuji, Y., Satoh, S., Minoura, H., Murakami, K., Okuno, A., Inukai, K., Asano, T., Kaburagi, Y., Ueki, K., Nakajima, H., Hanafusa, T., Matsuzawa, Y., Sekihara, H., Yin, Y., Barrett, J., Oda, H., Ishikawa, T., Akanuma, Y., Komuro, I., Suzuki, M., Yamamura, K., Kodama, T., Suzuki, H., Koyasu, S., Aizawa, S., Tobe, K., Fukui, Y., Yazaki, Y. and Kadowaki, T. (1999). Increased insulin sensitivity and hypoglycaemia in mice lacking the p85α subunit of phosphoinositide 3–kinase. *Nature Genetics*, 21(2), pp.230-235.

Thomas, P., Jeffery, P., Gahete, M., Whiteside, E., Walpole, C., Maugham, M., Jovanovic, L., Gunter, J., Williams, E., Nelson, C., Herington, A., Luque, R., Veedu, R., Chopin, L. and Seim, I., (2021). The long non-coding RNA GHSROS reprograms prostate cancer cell lines toward a more aggressive phenotype. *PeerJ*, 9, p.e10280.

Thorpe, L., Spangle, J., Ohlson, C., Cheng, H., Roberts, T., Cantley, L. and Zhao, J., 2017. PI3K-p110α mediates the oncogenic activity induced by loss of the novel tumor suppressor PI3K-p85α. *Proceedings of the National Academy of Sciences*, 114(27), pp.7095-7100.

Tiwari, R., Manzar, N., Bhatia, V., Yadav, A., Nengroo, M., Datta, D., Carskadon, S., Gupta, N., Sigouros, M., Khani, F., Poutanen, M., Zoubeidi, A., Beltran, H., Palanisamy, N. and Ateeq, B., 2020. Androgen deprivation upregulates SPINK1 expression and potentiates cellular plasticity in prostate cancer. *Nature Communications*, 11(1).

Tiwari, R., Pandey, S., Goel, S., Bhatia, V., Shukla, S., Jing, X., Dhanasekaran, S. and Ateeq, B., (2021). SPINK1 promotes colorectal cancer progression by downregulating Metallothioneins expression. *Oncogenesis*, 10(2).

Toker, A. (2012). Achieving specificity in Akt signalling in cancer. *Advances in Biological Regulation*, 52(1) pp. 78-87.

Tolias, K., Hartwig, J., Ishihara, H., Shibasaki, Y., Cantley, L. and Carpenter, C. (2000). Type Iα phosphatidylinositol-4-phosphate 5-kinase mediates Rac-dependent actin assembly. *Current Biology,* 10(3): 153-156.

Topacio, B., Zatulovskiy, E., Cristea, S., Xie, S., Tambo, C., Rubin, S., Sage, J., Kõivomägi, M. and Skotheim, J. (2019). Cyclin D-Cdk4,6 Drives Cell-Cycle Progression via the Retinoblastoma Protein's C-Terminal Helix. *Molecular Cell*, 74(4), pp.758-770.e4.

Toulany, M., Schickfluß, T., Fattah, K., Lee, K., Chen, B., Fehrenbacher, B., Schaller, M., Chen, D. and Rodemann, H. (2011). Function of erbB receptors and DNA-PKcs on phosphorylation of cytoplasmic and nuclear Akt at S473 induced by erbB1 ligand and ionizing radiation. *Radiotherapy and Oncology,* 101(1), pp. 140-146.

Tran, M., Seo, E., Min, S., Nguyen, Q., Choi, J., Lee, U., Hong, S., Kang, H., Mansukhani, A., Jou, I. and Lee, S. (2018). NEDD4-induced degradative ubiquitination of phosphatidylinositol 4-phosphate 5-kinase α and its implication in breast cancer cell proliferation. *Journal of Cellular and Molecular Medicine*, 22(9), pp.4117-4129.

Trapnell, C., Williams, B., Pertea, G., Mortazavi, A., Kwan, G., van Baren, M., Salzberg, S., Wold, B. and Pachter, L. (2010). Transcript assembly and quantification by RNA-Seq reveals unannotated transcripts and isoform switching during cell differentiation. *Nature Biotechnology*, 28(5), pp.511-515.

Tsai, M., Katagiri, N., Ohbayashi, N., Iwasaki, K., Ohkohchi, N., Ding, S., Kanaho, Y. and Funakoshi, Y. (2017). Regulation of HGF-induced hepatocyte proliferation by the small GTPase Arf6 through the PIP2-producing enzyme PIP5K1A. *Scientific Reports,* 7(1).

Tsourlakis, M., Khosrawi, P., Weigand, P., Kluth, M., Hube-Magg, C., Minner, S., Koop, C., Graefen, M., Heinzer, H., Wittmer, C., Sauter, G., Krech, T., Wilczak, W., Huland, H., Simon, R., Schlomm, T. and Steurer, S. (2015). VEGFR-1 Overexpression Identifies a Small Subgroup of Aggressive Prostate Cancers in Patients Treated by Prostatectomy. *International Journal of Molecular Sciences,* 16(12), pp.8591–8606.

Ueki, K., Fruman, D., Brachmann, S., Tseng, Y., Cantley, L. and Kahn, C. (2002). Molecular Balance between the Regulatory and Catalytic Subunits of Phosphoinositide 3-Kinase Regulates Cell Signalling andSurvival. *Molecular and Cellular Biology*, 22(3), pp.965-977.

Uhlen, M., Zhang, C., Lee, S., Sjöstedt, E., Fagerberg, L., Bidkhori, G., Benfeitas, R., Arif, M., Liu, Z., Edfors, F., Sanli, K., von Feilitzen, K., Oksvold, P., Lundberg, E., Hober, S., Nilsson, P., Mattsson, J., Schwenk, J.M., Brunnström, H. and Glimelius, B. (2017). A pathology atlas of the human cancer transcriptome. *Science,* 357(6352), p.eaan2507.

van de Wijngaart, D.J., van Royen, M.E., Hersmus, R., Pike, A.C.W., Houtsmuller, A.B., Jenster, G., Trapman, J. and Dubbink, H.J. (2006). Novel FXXFF and FXXMF Motifs in Androgen Receptor Cofactors Mediate High Affinity and Specific Interactions with the Ligand-binding Domain. J*ournal of Biological Chemistry*, 281(28), pp.19407–19416.

van den Bout, I. and Divecha, N. (2009). PIP5K-driven PtdIns(4,5)P2 synthesis: regulation and cellular functions. *Journal of Cell Science,* 122(21), pp.3837-3850.

van den Bout, I., Jones, David R., Shah, Zahid H., Halstead, Jonathan R., Keune, W.-J., Mohammed, S., D'Santos, Clive S. and Divecha, N. (2013). Collaboration of AMPK and PKC to induce phosphorylation of Ser413 on PIP5K1B resulting in decreased kinase activity and reduced PtdIns(4,5)P2 synthesis in response to oxidative stress and energy restriction. *Biochemical Journal,* 455(3), pp.347–358.

van Hennik, P., Klooster, J., Halstead, J., Voermans, C., Anthony, E., Divecha, N. and Hordijk, P. (2003). The C-terminal Domain of Rac1 Contains Two Motifs That Control Targeting and Signalling Specificity. *Journal of Biological Chemistry*, 278(40), pp.39166-39175.

van Horck, F., Lavazais, E., Eickholt, B., Moolenaar, W. and Divecha, N. (2002). Essential Role of Type Iα Phosphatidylinositol 4-Phosphate 5-Kinase in Neurite Remodeling. *Current Biology*, 12(3), pp.241-245.

van Kempen, M., Kim, S., Tumescheit, C., Milot Mirdita, Lee, J., Cameron, Johannes Söding and Steinegger, M. (2023). Fast and accurate protein structure search with Foldseek. *Nature Biotechnology.*

Vanhaesebroeck, B., Higashi, K., Raven, C., Welham, M., Anderson, S., Brennan, P., Ward, S. G., and Waterfield, M. D. (1999). Autophosphorylation of p110delta phosphoinositide 3-kinase: a new paradigm for the regulation of lipid kinases in vitro and in vivo. *The EMBO Journal,* 18(5), pp. 1292–1302.

Varkaris, A., Katsiampoura, A., Araujo, J., Gallick, G. and Corn, P. (2014). Src signalling pathways in prostate cancer. Cancer and Metastasis Reviews. 33(2-3): 595-606.

Várnai, P., Gulyás, G., Tóth, D., Sohn, M., Sengupta, N. and Balla, T., (2017). Quantifying lipid changes in various membrane compartments using lipid binding protein domains. *Cell Calcium*, 64, pp.72-82.

Verze, P., Cai, T. and Lorenzetti, S. (2016). The role of the prostate in male fertility, health and disease. *Nature Reviews Urology*, 13(7), pp. 379-386.

Veveris-Lowe, T., Lawrence, M., Collard, R., Bui, L., Herington, A., Nicol, D. and Clements, J. (2005). Kallikrein 4 (hK4) and prostate-specific antigen (PSA) are associated with the loss of E-cadherin and an epithelial-mesenchymal transition (EMT)-like effect in prostate cancer cells. *Endocrine-Related Cancer,* 12(3), pp. 631-643.

Villar, J., Tsai-Morris, C.-H., Dai, L. and Dufau, M.L. (2012). Androgen-Induced Activation of Gonadotropin-Regulated Testicular RNA Helicase (GRTH/Ddx25) Transcription: Essential Role of a Nonclassical Androgen Response Element Half-Site. *Molecular and Cellular Biology*, 32(8), pp.1566–1580.

Virbasius, J., Song, X., Pomerleau, D., Zhan, Y., Zhou, G. and Czech, M. (2001). Activation of the Akt-related cytokine-independent survival kinase requires interaction of its phox domain with endosomal phosphatidylinositol 3-phosphate. *Proceedings of the National Academy of Sciences*, 98(23), pp.12908-12913.

Vogt, P., Hart, J., Gymnopoulos, M., Jiang, H., Kang, S., Bader, A., Zhao, L. and Denley, A. (2010). Phosphatidylinositol 3-Kinase: The Oncoprotein. *Current Topics in Microbiology and Immunology.* 347, pp. 79-104.

Wada, R., Suto, Y., Kanai, M. and Shibasaki, M. (2002). Dramatic Switching of Protein Kinase C Agonist/Antagonist Activity by Modifying the 12-Ester Side Chain of Phorbol Esters. *Journal of the American Chemical Society*, 124(36), pp.10658-10659.

Wainstein, E., Maik-Rachline, G., Blenis, J. and Seger, R. (2022). AKTs do not translocate to the nucleus upon stimulation but AKT3 can constitutively signal from the nuclear envelope. *Cell Reports,* 41(10), p.111733.

Wander, S., Zhao, D. and Slingerland, J. (2010). p27: A Barometer of Signalling Deregulation and Potential Predictor of Response to Targeted Therapies. *Clinical Cancer Research*, 17(1) pp. 12-18.

Wang, D.G., Paddock, M.N., Lundquist, M.R., Sun, J.Y., Mashadova, O., Amadiume, S., Bumpus, T.W., Hodakoski, C., Hopkins, B.D., Fine, M., Hill, A., Yang, T.J., Baskin, J.M., Dow, L.E. and Cantley, L.C. (2019). PIP4Ks Suppress Insulin Signalling through a Catalytic-Independent Mechanism. *Cell Reports,* 27(7), pp.1991-2001.e5.

Wang, L., Harris, T., Roth, R. and Lawrence, J., (2007). PRAS40 Regulates mTORC1 Kinase Activity by Functioning as a Direct Inhibitor of Substrate Binding. *Journal of Biological Chemistry*, 282(27) pp. 20036-20044.

Wang, Q.J., Fang, T.-W., Nacro, K., Marquez, V.E., Wang, S. and Blumberg, P.M. (2001). Role of Hydrophobic Residues in the C1b Domain of Protein Kinase C δ on Ligand and Phospholipid Interactions. *Journal of Biological Chemistry*, 276(22), pp.19580–19587.

Wang, S. and Basson, M. (2008). Identification of functional domains in AKT responsible for distinct roles of AKT isoforms in pressure-stimulated cancer cell adhesion. *Experimental Cell Research,* 314(2) pp. 286-296.

Wang, S., Yang, S., Nan, C., Wang, Y., He, Y. and Mu, H. (2018). Expression of Androgen Receptor Variant 7 (AR-V7) in Circulated Tumour Cells and Correlation with Drug Resistance of Prostate Cancer Cells. *Medical Science Monitor,* 24, pp. 7051-7056

Wang, T., Sarwar, M., Whitchurch, J. B., Collins, H. M., Green, T., Semenas, J., Ali, A., Roberts, C. J., Morris, R. D., Hubert, M., Chen, S., El-Schich, Z., Wingren, A. G., Grundström, T., Lundmark, R., Mongan, N. P., Gunhaga, L., Heery, D. M., and Persson, J. L. (2022). PIP5K1α is Required for Promoting Tumor Progression in Castration-Resistant Prostate Cancer. *Frontiers in Cell and Developmental Biology,* 10, 798590.

Wang, Y., Zhou, D. and Chen, S. (2014a). SGK3 Is an Androgen-Inducible Kinase Promoting Prostate Cancer Cell Proliferation Through Activation of p70 S6 Kinase and Up-Regulation of Cyclin D1. Molecular Endocrinology, 28(6), pp.935–948.

Wang, Z., Toivanen, R., Bergren, S., Chambon, P. and Shen, M. (2014b). Luminal Cells Are Favored as the Cell of Origin for Prostate Cancer. *Cell Reports,* 8(5), pp. 1339-1346.

Wärnmark, A., Treuter, E., Wright, A. and Gustafsson, J. (2003). Activation Functions 1 and 2 of Nuclear Receptors: Molecular Strategies for Transcriptional Activation. *Molecular Endocrinology,* 17(10), pp. 1901-1909.

Weber, S., Ragaz, C., Reus, K., Nyfeler, Y. and Hilbi, H. (2006). Legionella pneumophila Exploits PI(4)P to Anchor Secreted Effector Proteins to the Replicative Vacuole. *PLoS Pathogens*, 2(5), p.e46.

Wee, S., Wiederschain, D., Maira, S.-M., Loo, A., Miller, C., deBeaumont, R., Stegmeier, F., Yao, Y.-M. and Lengauer, C. (2008). PTEN-deficient cancers depend on PIK3CB. *Proceedings of the National Academy of Sciences*, 105(35), pp.13057–13062.

Weernink, P., Meletiadis, K., Hommeltenberg, S., Hinz, M., Ishihara, H., Schmidt, M. and Jakobs, K. (2003). Activation of Type I Phosphatidylinositol 4-Phosphate 5-Kinase Isoforms by the Rho GTPases, RhoA, Rac1, and Cdc42. *Journal of Biological Chemistry,* 279(9), pp.7840-7849.

Wei, L., Su, Y., Lin, C., Chao, T., Huang, S., Huynh, T., Jan, H., Whang-Peng, J., Chiou, J., Wu, A. and Hsiao, M., (2016). Preclinical investigation of ibrutinib, a Bruton's kinase tyrosine (Btk) inhibitor, in suppressing glioma tumorigenesis and stem cell phenotypes. *Oncotarget*, 7(43) pp.69961-69975.

Weikum, E.R., Liu, X. and Ortlund, E.A. (2018). The nuclear receptor superfamily: A structural perspective. *Protein Science*, 27(11), pp.1876–1892.

Wen, Y., Hu, M. C., Makino, K., Spohn, B., Bartholomeusz, G., Yan, D. H., and Hung, M. C. (2000). HER-2/neu promotes androgen-independent survival and growth of prostate cancer cells through the Akt pathway. *Cancer research*, *60*(24), pp.6841–6845.

Whale, A., Colman, L., Lensun, L., Rogers, H. and Shuttleworth, S. (2017). Functional characterization of a novel somatic oncogenic mutation of PIK3CB. *Signal Transduction and Targeted Therapy,* 2(1).

Widmann, B., Wandrey, F., Badertscher, L., Wyler, E., Pfannstiel, J., Zemp, I. and Kutay, U. (2012). The kinase activity of human Rio1 is required for final steps of cytoplasmic maturation of 40S subunits. *Molecular Biology of the Cell*, 23(1), pp.22–35.

Wilkinson, K. and Henley, J. (2010). Mechanisms, regulation and consequences of protein SUMOylation. *Biochemical Journal.* 428(2), pp.133-145.

Wilson, S., Qi, J. and Filipp, F. (2016). Refinement of the androgen response element based on ChIP-Seq in androgen-insensitive and androgen-responsive prostate cancer cell lines. *Scientific Reports,* 6(1).

Wiza, C., Nascimento, E. and Ouwens, D., (2012). Role of PRAS40 in Akt and mTOR signalling in health and disease. *American Journal of Physiology-Endocrinology and Metabolism*, 302(12), pp.E1453-E1460.

Woods, Y., Rena, G., Morrice, N., Barthel, A., Becker, W., Guo, S., Unterman, T. and Cohen, P. (2001). The kinase DYRK1A phosphorylates the transcription factor FKHR at Ser329 in vitro, a novel in vivo phosphorylation site. *Biochemical Journal*, 355(3), pp.597-607.

Xin, L. (2012). Cells of origin for cancer: an updated view from prostate cancer. *Oncogene,* 32(32), pp. 3655-3663.

Xu, A., Suh, P., Marmy-Conus, N., Pearson, R., Seok, O., Cocco, L. and Gilmour, R. (2001). Phosphorylation of Nuclear Phospholipase C 1 by Extracellular Signal-Regulated Kinase Mediates the Mitogenic Action of Insulin-Like Growth Factor I. *Molecular and Cellular Biology,* 21(9), pp. 2981-2990.

Xu, Y., Xing, Y., Chen, Y., Chao, Y., Lin, Z., Fan, E., Yu, J., Strack, S., Jeffrey, P. and Shi, Y. (2006). Structure of the Protein Phosphatase 2A Holoenzyme. *Cell,* 127(6), pp.1239-1251.

Yahiro, Y., Maeda, S., Shinohara, N., Jokoji, G., Sakuma, D., Setoguchi, T., Ishidou, Y., Nagano, S., Komiya, S. and Taniguchi, N. (2018). PEG10 counteracts signalling pathways of TGF-β and BMP to regulate growth, motility and invasion of SW1353 chondrosarcoma cells. *Journal of Bone and Mineral Metabolism*, 37(3), pp.441–454.

Yamazaki, M., Miyazaki, H., Watanabe, H., Sasaki, T., Maehama, T., Frohman, M. and Kanaho, Y., 2002. Phosphatidylinositol 4-Phosphate 5-Kinase Is Essential for ROCK-mediated Neurite Remodeling. *Journal of Biological Chemistry*, 277(19), pp.17226-17230.

Yang, L., Doshi, D., Morrow, J., Katchman, A., Chen, X. and Marx, S. (2009). Protein Kinase C Isoforms Differentially Phosphorylate Cav1.2 α1c. *Biochemistry*, 48(28), pp.6674-6683.

Yang, Y., He, Y., Wang, X., liang, Z., He, G., Zhang, P., Zhu, H., Xu, N. and Liang, S., 2017. Protein SUMOylation modification and its associations with disease. *Open Biology,* 7(10).

Yao, G., Joswig, J., Keller, B. and Süssmuth, R., 2019. Total Synthesis of the Death Cap Toxin Phalloidin: Atropoisomer Selectivity Explained by Molecular-Dynamics Simulations. *Chemistry – A European Journal*, 25(34), pp.8030-8034.

Yatomi, Y., Ohmori, T., Rile, G., Kazama, F., Okamoto, H., Sano, T., Satoh, K., Kume, S., Tigyi, G., Igarashi, Y. and Ozaki, Y., 2000. Sphingosine 1-phosphate as a major bioactive lysophospholipid that is released from platelets and interacts with endothelial cells. *Blood*, 96(10), pp.3431-3438.

Ye, J., Coulouris, G., Zaretskaya, I., Cutcutache, I., Rozen, S. and Madden, T.L. (2012). Primer-BLAST: A tool to design target-specific primers for polymerase chain reaction. *BMC Bioinformatics*, 13(1).

Yin, H., Glass, J. and Blanchard, K.L. (2007). MOZ-TIF2 repression of nuclear receptor-mediated transcription requires multiple domains in MOZ and in the CID domain of TIF2. *Molecular Cancer, 6*(1).

Yin, Y., Xu, L., Chang, Y., Zeng, T., Chen, X., Wang, A., Groth, J., Foo, W.-C., Liang, C., Hu, H. and Huang, J. (2019). N-Myc promotes therapeutic resistance development of neuroendocrine prostate cancer by differentially regulating miR-421/ATM pathway. *Molecular Cancer*, 18(1).

Yip, S., Eddy, R., Branch, A., Pang, H., Wu, H., Yan, Y., Drees, B., Neilsen, P., Condeelis, J. and Backer, J., (2008). Quantification of PtdIns(3,4,5)P3 dynamics in EGF-stimulated carcinoma cells: a comparison of PH-domain-mediated methods with immunological methods. *Biochemical Journal*, 411(2), pp.441-448.

Young, CY., Andrews, P.E. and Tindall, DJ. (1995). Expression and androgenic regulation of human prostate-specific kallikreins. *Journal of Andrology,* 15(2), pp. 97-99.

Yu, H., Fukami, K., Watanabe, Y., Ozaki, C. and Takenawa, T. (1998). Phosphatidylinositol 4,5-bisphosphate reverses the inhibition of RNA transcription caused by histone H1. *European Journal of Biochemistry,* 251(1-2), pp.281-287.

Yuan, T., Veeramani, S., Lin, F., Kondrikou, D., Zelivianski, S., Igawa, T., Karan, D., Batra, S. and Lin, M. (2006). Androgen deprivation induces human prostate epithelial neuroendocrine differentiation of androgen-sensitive LNCaP cells. *Endocrine-Related Cancer,* 13(1): 151-167.

Zegers, M. and Friedl, P. (2014). Rho GTPases in collective cell migration. *Small GTPases*, 5(3), p.e983869.

Zengerling, F., Streicher, W., Schrader, A., Schrader, M., Nitzsche, B., Cronauer, M. and Höpfner, M. (2012). Effects of Sorafenib on C-Terminally Truncated Androgen Receptor Variants in Human Prostate Cancer Cells. International Journal of Molecular Sciences. 13(9): 11530-11542.

Zewe, J.P., Wills, R.C., Sangappa, S., Goulden, B.D. and Hammond, G.R. (2018). SAC1 degrades its lipid substrate PtdIns4P in the endoplasmic reticulum to maintain a steep chemical gradient with donor membranes. *eLife*, 7.

Zhang, D., Zhao, S., Li, X., Kirk, J.S. and Tang, D.G. (2018). Prostate Luminal Progenitor Cells in Development and Cancer. *Trends in Cancer,* 4(11), pp.769–783.

Zhang, H., Lipovsky, A., Dibble, C., Sahin, M. and Manning, B. (2006). S6K1 Regulates GSK3 under Conditions of mTOR-Dependent Feedback Inhibition of Akt. *Molecular Cell*, 24(2) pp. 185-197.

Zhang, J., Gao, X., Schmit, F., Adelmant, G., Eck, M.J., Marto, J.A., Zhao, J.J. and Roberts, T.M. (2017). CRKL Mediates p110β-Dependent PI3K Signalling in PTEN-Deficient Cancer Cells. *Cell Reports*, 20(3), pp.549–557. doi:10.1016/j.celrep.2017.06.054.

Zhang, J., Luo, R., Wu, H., Wei, S., Han, W. and Li, G., (2008). Role of Type Iα Phosphatidylinositol-4-Phosphate 5-Kinase in Insulin Secretion, Glucose Metabolism, and Membrane Potential in INS-1 β-Cells. *Endocrinology*, 150(5), pp.2127-2135.

Zhang, J., Salojin, K., Gao, J., Cameron, M., Bergerot, K. and Delovitch, T., (1999) p38 mitogen-activated protein kinase mediates signal integration of TCR/CD28 costimulation in primary murine T cells. *The Journal of Immunology*, 162(7), pp.3819-3829

Zhang, X., Loijens, J.C., Boronenkov, I.V., Parker, G.J., Norris, F.A., Chen, J., Thum, O., Prestwich, G.D., Majerus, P.W. and Anderson, R.A. (1997). Phosphatidylinositol-4-phosphate 5-Kinase Isozymes Catalyze the Synthesis of 3-Phosphate-containing Phosphatidylinositol Signalling Molecules. *Journal of Biological Chemistry*, 272(28), pp.17756–17761.

Zhao, Z. and Xu, Y., (2010). An extremely simple method for extraction of lysophospholipids and phospholipids from blood samples. *Journal of Lipid Research*, 51(3), pp.652-659.

Zhong, W., Lin, W., Yang, Y., Chen, D., Cao, X., Xu, M., Pan, G., Chen, H., Zheng, J., Feng, X., Yang, L., Lai, C., Olkkonen, V., Xu, J., Cui, S. and Yan, D. (2022). An acquired phosphatidylinositol 4-phosphate transport initiates T-cell deterioration and leukemogenesis. *Nature Communications*, 13(1).

Zhou, K., Chen, Q., Chen, J., Liang, D., Feng, W., Liu, M., Wang, Q., Wang, R., Ouyang, Q., Quan, C. and Chen, S. (2022). Spatiotemporal regulation of insulin signalling by liquid–liquid phase separation. *Cell Discovery*, 8(1).

Zhou, Y., Bolton, E.C. and Jones, J.O. (2014). Androgens and androgen receptor signalling in prostate tumorigenesis. *Journal ofMolecular Endocrinology*, 54(1), pp.R15–R29.

Zhu, Q., Youn, H., Tang, J., Tawfik, O., Dennis, K., Terranova, P.F., Du, J., Raynal, P., Thrasher, J.B. and Li, B. (2008). Phosphoinositide 3-OH kinase p85α and p110β are essential for androgen receptor transactivation and tumor progression in prostate cancers. *Oncogene*, 27(33), pp.4569–4579.

Zucha, M., Wu, A., Lee, W., Wang, L., Lin, W., Yuan, C. and Yeh, C. (2015). Bruton's tyrosine kinase (Btk) inhibitor ibrutinib suppresses stem-like traits in ovarian cancer. *Oncotarget*, 6(15), pp.13255-13268.

Appendix

PIPS Reflective Statement Template

Note to examiners:

This statement is included as an appendix to the thesis in order that the thesis accurately captures the PhD training experienced by the candidate as a BBSRC Doctoral Training Partnership student.

The Professional Internship for PhD Students is a compulsory 3-month placement which must be undertaken by DTP students. It is usually centred on a specific project and must not be related to the PhD project. This reflective statement is designed to capture the skills development which has taken place during the student's placement and the impact on their career plans it has had.

PIPS Reflective Statement

From January – March 2021 I carried out my PIP in Dr Gareth Evans lab. The Evans's lab is based at the University of York, however due to the coronavirus pandemic, we were able to devise a 3 month project for me which I could do in a remote manner. This origin of this project came about through meeting Gareth at a Biochemical Society members meeting in November 2019 where we discussed his research on SRC kinases, and in particular the neuronal variants of SRC. After getting in contact with Gareth via email in October 2020, we were able to draw up a plan for the work I could do starting in the following year.

The title for this PIP project was "*In silico* Analysis of Neuronal SRC Splice Variants" where we had a particular interest in the role neuronal SRC variants in brain tumours such as neuroblastoma, medulloblastoma and glioblastoma. The "*In silico* Analysis" encompassed a range of computational techniques which we highlighted as skills to develop as part of the project:

The first of which was to develop a greater proficiency in RNA-Seq / Transcriptomics workflows. In this aspect of the project we sought to use computational tools to determine *in silico,* the expression c-SRC andit's neuronal SRC transcripts (denoted as N1-SRC and N2-SRC) in brain tumour cell lines and patient data. Whilst some of the workflows and tools used to do this were familiar with me (such as Kallisto) I was able to develop my understanding of these packages further. One major highlight from this experience was manually curating the N2-SRC splice variant which then allowed me to detect the expression of this transcript in publicly available RNA-Seq datasets. At the time of my project the N2-SRC variant was not an annotated transcript, so manual curation was the only option for trying to deduce its expression. Subsequently, after

getting in touch with Ensembl, they recognised that N2-SRC is a valid transcript, and agreed to add this to their transcriptome annotations. Now that I know how to manually annotate transcripts, I could use these skills again for any other novel transcripts which are yet to be annotated.

The results from this part of the work were consistent with previous work in the field, whilst also offering a novel aspect. For instance, whilst glioblastoma originate in the brain, they arise from non-neuronal glial cells. Acting as a negative control, I analysed the expression pattern of the neuronal SRC variants in both glioblastoma cell lines and tumour data and found that N1 and N2-SRC were not expressed in this type of cancer. On the other hand, we found in medulloblastoma patient tumours that the expression of N1-SRC increased in severity of disease. Upon reading the literature it became apparent that a 2018 *Cancer Cell* publication *(Forget et al., 2018)* linked aberrant SRC activity to medulloblastoma disease progression. Subsequently, the data generated as part of this PIP (to our knowledge) was the first to link N1-SRC expression to medulloblastoma disease progression.

The second component of this project was to understand the workflows used to analyse mass spectrometry datasets. The Evans lab deploys mass spectrometry to understand the phosphorylation events that are initiated by kinases, with the goal to identify novel substrates for kinases of interest. The data which I analysed as part of this project was previously generated by the Evans lab. This data was of a rat brain cell lysate which had been incubated with FSBA, a compound with sequesters endogenous kinase activity. Subsequently, by then reintroducing C-SRC and N1-SRC target proteins specific to both these kinases can then be phosphorylated and identified by mass spectrometry. The aim was to compare the C-SRC and N1-SRC rat brain cell lysate data to published brain tumour datasets, to see whether we could identify any common substrates and phosphorylation sites.

Before doing these comparisons, I needed to filter my datasets and to identify substrates that were statistically significant. This provided me with the opportunity to become more familiar with the R programming package, and I was able to write some basic scripts to help analyse the C-SRC and N1-SRC datasets. Once filtered I could then compare to published phospho-proteomics dataset of neuroblastoma cell lines (*Chen et al., 2016*) and also back to *Forget et al., (2018)*, where this paper contained phospho-proteomics data from 38 medulloblastoma patients. These comparisons proved to be fruitful, where we were able to identify previously unreported SRC phosphorylation sites on ~10-15 different proteins. Additionally, I was able to gain training in using

MaxQuant software, a package which is universally used for the analysis of mass spectrometry datasets.

Prior starting my PIP I felt it was necessary to gain additional training in RNA-Seq and transcriptomics workflows, in conjunction with gaining some experience in analysing mass spectrometry datasets. These are skills that are used extensively in the kinase research, a field I would like to continue to work in after my PhD studies. Overall, this PIP was an enjoyable experience honing these skills and I am extremely grateful for Gareth hosting my project.